COORDINATION COMPLEXES AND NETWORKS WITH CYANO-SUBSTITUTED AZOLATES

Dissertation

zur

Erlangung des Doktorgrades (Dr. rer. nat.)

der

Mathematisch-Naturwissenschaftlichen Fakultät

der

Rheinischen Friedrich-Wilhelms-Universität Bonn

vorgelegt von

M.Sc. Barbara Szafranowska

aus

Wroclaw, Polen

Bonn, 2015

Angefertigt mit Genehmigung der Mathematisch Naturwissenschaftlichen Fakultät der Rheinischen Friedrich-Wilhelms-Universität Bonn.

1. Gutachter: Prof. Dr. Johannes Beck
2. Gutachter: Prof. Dr. Robert Glaum

Tag der Promotion: 28.08.2015

Erscheinungsjahr: 2015

"I've missed more than 9.000 shots in my career. I've lost almost 300 games. 26 times, I've been trusted to take the game winning shot and missed. I've failed over and over and over again in my life. And that is why I succeed."

Michael Jordan

Acknowledgments

I would like to express my sincere gratitude to several people, whose presence and directly or indirectly work became a part in the elaboration of this thesis.

First of all, I would like to express appreciation to my supervisor Prof. Dr. Johannes Beck not only for his valuable support and guidance but also for the chance to work in his research group and for his confidence in my potentials as a scientist. I am also extremely thankful to him for his help during the writing process of the publications and shaping of this thesis.

This thesis would not be possible without the help of several people from the Beck's group, whose contribution was very important for the characterization of the materials. Therefore I am thankful to:

- Dr. Jörg Daniels, Christian Landvogt and Axel Pelka for technical assistance with crystallography and crystallographic measurements
- Norbert Wagner for magnetic measurements
- Klaus Armbruster for DTA/TG thermal investigations
- Dr. Ralf Weisbarth for differential scanning calorimetric measurements
- Prof. Dr. Robert Glaum for the valuable discussion concerning electronic spectra and their interpretation
- Volker Dittrich for single crystal UV/Vis/NIR spectra measurement (AK Glaum)
- Volker Bendisch for crystal photos and technical support
- Marianne Stanko for a good atmosphere and humor in the lab over the years
- all students of the Inorganic Advanced Practical Course for their experimental contributions (Mark Kerzhner, Martin Wickenheisser, Meriam Seddiqzai, Philipp Hegemann, Stephanie Natividad and Juri Ivanov)

My sincere gratitude goes to:

My best friend Kasia Solanko, who has been like a sister to me. She has always believed in me and gave me motivation and strength at times of my self-doubt. My sister Kasia, who was and will be the powerful source of inspiration, energy and motivation. I thank them both from the bottom of my heart for love, encouragement, and concern for me.

Last but not least, I am extremely thankful to Andreas Eich, my partner, who has been endlessly supportive especially at times of my self-doubt, and who inspired me to learn german language. I thank you for your patience, care, love and concern.

Abstract

Cyanoazolates are derivatives of the azolates, in which all of the C–H hydrogen atoms are replaced by the C≡N groups. Their functionality is mainly dominated by the present cyano group(s), which are strongly electron withdrawing. In this way cyanoazolate molecules are electron deficient owing to the extensive negative charge delocalization across the anion's structure and own higher number of coordination sites. Although cyanoazolates have been known for a long time, many structural investigations are still missing.

Consequently, this work provides the first example of a systematic study on the cyanoazolate series $[C_{2n}N_5]^-$ (n = 0, 2, 3, 4) with significant contribution of the crystal structures of 5-cyanotetrazolate, 4,5-dicyano-1,2,3-triazolate, 2,4,5-tricyanoimidazolate and tetracyanopyrrolide obtained as various organic salts used later as a starting materials. The research is completed by the preparation of new cyanoazolate-based coordination materials of first-row transition metal ions (Mn^{2+}, Fe^{2+}, Co^{2+}, Ni^{2+}, Cu^{2+}). The magnetic properties of diverse complexes and coordination polymers are analyzed using magnetic models based on the Heisenberg model principle in order to estimate the strength of magnetic exchange interactions in the magnetic systems. A variety of cooperative phenomena (ferro-, antiferro-, and ferrimagnetism) are detected at low temperatures, whereas mainly isolated ion behavior is observed at high temperatures.
In the presence of water, the C≡N groups of cyanotetrazole and tetracyanopyrrole undergo hydrolytic transformation forming the $C(O)NH_2$ carboxamide yielding tetrazolate-5-carboxamide and 3,4,5-tricyanopyrrole-2-carboxamide trapped in copper(II) complexes.

The project has been extended to a new class of 2D and 3D coordination polymers based on *N,N′,N′′*-tricyanoguanidinate dianion, which serves as triply connecting, trigonal building block with a rare alternating carbon-nitrogen connectivity. Also in this case the magnetic investigations are undertaken to check for a possible magnetic exchanges mediated through the large π-conjugated linkers.

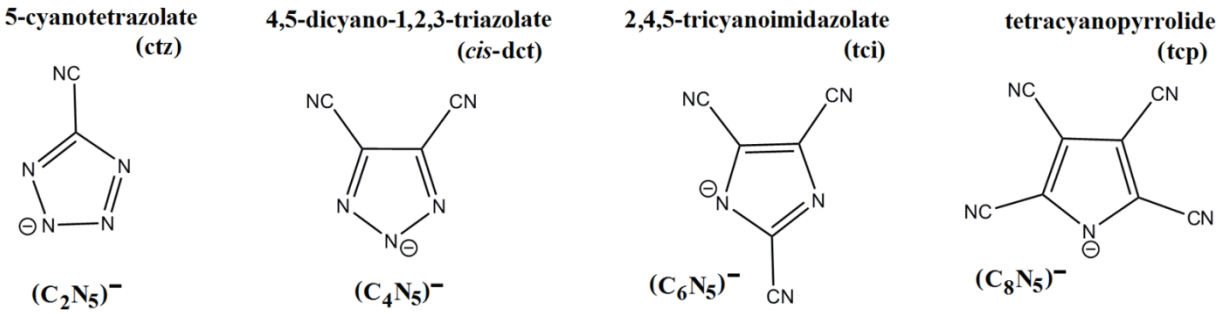

Cyanoazolate mononions investigated in this thesis

List of Abbreviations

C	Curie constant
g	g-factor (Landé factor)
E	energy
H	field
HS	high-spin
LS	low-spin
J	total angular moment, exchange energy coupling constant
L	total orbital angular moment
k_B **or** k	Boltzman constant
$\mathcal{H}$	Heisenberg Hamiltonian operator
M	magnetization, molar magnetization
N	Avogadro number
pK_a / pK_b	dissociation constant
ppm	parts per million
B	Racah parameter of interelectronic repulsion
Dq **or** Δ	crystal field splitting parameter
θ_{MF}	mean-field approximation
S	spin, electronic singlet states
XRD	single-crystal X-ray diffraction
T	temperature
T_C	Curie temperature, critical temperature
T_N	Néel temperature, critical temperature
TGA	thermal gravimetric analysis
DTA	differential thermal analysis
thf	tetrahydrofuran
dmso	dimethyl sulfoxide
VSM	vibrating sample magnetometer
z	number of nearest neighbors around magnetic molecule in the lattice
μ_{eff}	effective Bohr magneton number
μ_B	electronic Bohr magneton
χ	magnetic susceptibility
χ^D	diamagnetic susceptibility
χ^P	paramagnetic susceptibility
χ_{mol}	molar magnetic susceptibility
θ	Curie-Weiss temperature
ϱ	density
ΔH_f	heat of formation
Hctz	5-cyano-*2H*-tetrazole
***cis*-Hdct**	4,5-dicyano-*2H*-1,2,3-triazole
***trans*-Hdct**	3,5-dicyano-*4H*-1,2,4-triazole
Htcpz	3,4,5-tricyano-*1H*-pyrazole
Htci	2,4,5-tricyano-*1H*-imidazole
Htcp	tetracyanopyrrole
ctz	5-cyanotetrazolate
***cis*-dct**	4,5-dicyano-1,2,3-triazolate
***trans*-dct**	3,5-dicyano-1,2,4-triazolate

tcpz	3,4,5-tricyanopyrazolate
tci	2,4,5-tricyanoimidazolate
tcp	tetracyanopyrrolide
TNT	2,4,6-trinitroroluene
RDX	1,3,5-trinitroperhydro-1,3,5-triazine
dca	dicyanamide
tcm	tricyanomethanide
tcg	tricyanoguanidinate
tcpd	2-dicyanomethylene-1,1,3,3-tetracyanopropanediidne
py	pyridine
2,2'-bipy	2,2'-bipyridine
tpm	tris(pyrazol-*1*-yl)methane
IR	Infrared spectroscopy
e	electrons
Oe	Oerstedt
AOM	Angular overlap model
$\boldsymbol{e_{\sigma}, e_{\pi x}, e_{\pi y}}$	Angular overlap parameters
ζ	the spin-orbit coupling

TABLE OF CONTENTS

PART 1

SOME ASPECTS OF MAGNETOCHEMISTRY

1.1 Theoretical Background

1.1.1 Diamagnetism and Paramagnetism

Magnetism has its origin in the motion of charged particles. In the context of atoms magnetism arises from the spin of electrons, from electron orbital motion around the nucleus and in some cases (such as for the hydrogen atom) from a nuclear spin.[1] Therefore, all substances build by atoms interact with an external magnetic field, some of these interactions are strong and others negligible. Substances can be divided according to their manner of interaction with external magnetic field in the two categories: those which are repelled and attracted by magnetic field. The objects from the first group are called diamagnets. **Diamagnetism** is a property of matter and originates from interactions of paired electrons with magnetic fields and it is generally very small in magnitude. The diamagnetic susceptibility χ^D of pure diamagnetic materials is negative and very small, of the order -10^{-6} cm^3/mol and usually independent of the temperature and the strength of magnetic field.

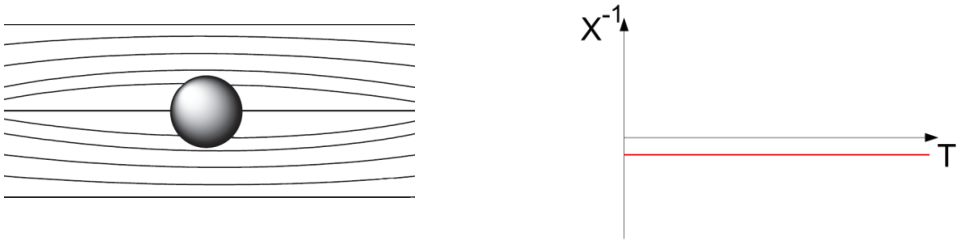

Figure 1.1.1.1 Left - interactions of diamagnetic material (grey ball) with an external magnetic field (flux lines). In this case diamagnetic material is repelled by the field. Right - typical χ^{-1} vs. T plot of a diamagnetic substance.

The group of materials that are attracted by an external magnetic field define paramagnets.[2] **Paramagnetism** is a consequence of the interaction of orbital and/or spin angular moments of one or more unpaired electrons with the applied field. At zero applied field the magnetic dipoles of unpaired electrons are randomly orientated and have no magnetisation. In the field, the dipoles tend to orientate parallel to it, resulting in a positive magnetic moment, but thermal agitation prevents their perfect aligning. Without considering additional interactions, the total magnetic susceptibility of the sample is a sum of paramagnetic and diamagnetic susceptibility:[3]

$$\chi = \chi^D + \chi^P \qquad \textbf{(1.1)}$$

The paramagnetic susceptibility originates from the unequal thermally populated states of a molecule in the applied magnetic field H and follows the fundamental equation[3] (where μ_n - microscopic magnetization, E_n - energy levels):

$$\mu_n = -\frac{\partial E_n}{\partial H} \qquad \textbf{(1.2)}$$

The sum of microscopic magnetisations weighted to the Bolzmann distribution for the occupation of the energy levels E_n gives the macroscopic magnetisation M which is fundamental for molecular magnetism:

$$M = \frac{N\sum n(-\partial E_n/\partial H)\cdot\exp(-E_n/kT)}{\sum n\cdot\exp(-E_n/kT)} \quad \textbf{(1.3)}$$

where N - Avogadro`s number, T - temperature and k - Boltzmann constant. Because this equation is general and difficult to apply, the simplified Van Vleck formula can be derived when the energies E_n are expanded according to the increasing powers of H:

$$E_n = E_n^0 + HE_n^{(1)} + H^2E_n^{(2)} + H^3E_n^{(3)} + \cdots. \quad \textbf{(1.4a)}$$

and by assuming that H/kT is very small (<<1), then the Van Vleck formula follows:

$$\chi = \frac{N\sum n(E_n^{(1)2}/kT - 2E_n^{(2)})\cdot\exp(-E_n^{(0)}/kT)}{\sum n\cdot\exp(-E_n^{(0)}/kT)} \quad \textbf{(1.4b)}$$

where $E_n^{(0)}$ is the energy of level n in zero field. $E_n^{(1)}$ and $E_n^{(2)}$ are called first- and second-order Zeeman coefficients. The Van Vleck equation can be more simplified if the temperature is large and H/kT is small, then $E_n^{(0)} = 0$ and $E_n^{(1)} = m_S g\mu_B$, giving the Curie law written as:

$$\chi = \frac{Ng^2\mu_B^2}{3kT}\, S(S+1) \equiv \frac{C}{T} \quad \textbf{(1.5)}$$

where N — Avogadro`s number, — g-factor (Landé factor), μ_B — electronic Bohr magneton, k — Boltzmann constant, T — temperature and S — spin ground state. Thus, the paramagnetic substances have positive magnetic susceptibilities which follow the Curie law and are temperature dependent (Figure 1.1.1.2).[3] In this reciprocal dependency of the temperature, the parameter C, named the Curie constant, is characteristic for the atomic or molecular species and depends on the spin multiplicity of the ground state.

The Curie constant can be experimentally determined either from the linear plot χ^{-1} vs. T where the slope is $1/C$ or from the spin-only approximation formula:

$$C = \frac{Ng^2\mu_B^2\, S(S+1)}{3k} \quad \textbf{(1.6)}$$

Sometimes the effective magnetic moment (μ_{eff}) or χT of a material is used to describe the magnetic properties. Thus the μ_{eff} can be defined by the following equation:

$$\mu_{eff} = \sqrt{\frac{3kT\chi}{N\mu_B^2}} = 2.828\sqrt{\chi T} \quad \textbf{(1.7)}$$

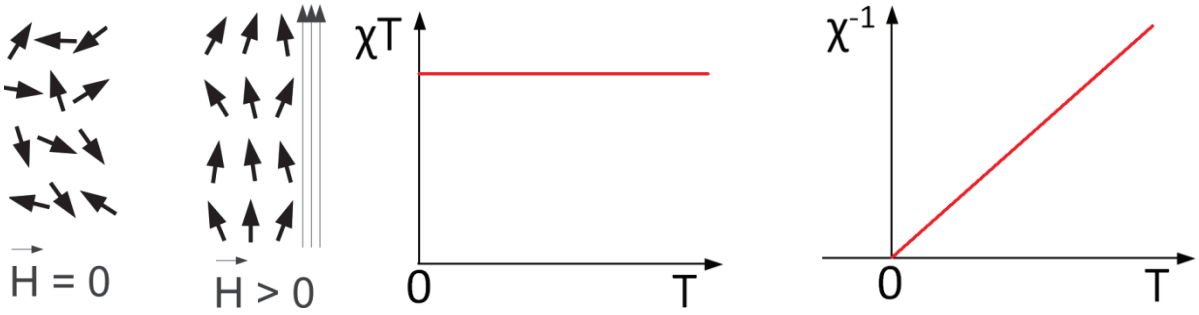

Figure 1.1.1.2 Left - schematic representation of the spin alignment of a paramagnetic substance without and with an applied magnetic field H. Right - typical χT vs. *T* and χ^{-1} vs. *T* plots of an ideal paramagnetic substance described by the Curie law.

1.1.2 The Exchange Interactions

Often the Curie law is not valid because it does not take into account intermolecular interactions between paramagnetic atoms/ions. A simple modification which is known as a Curie-Weiss law includes weak intermolecular interactions:

$$\chi = \frac{C}{T - \Theta} \tag{1.8}$$

where θ is the Curie-Weiss constant defined by:

$$\Theta = \frac{zJS(S+1)}{3k} \tag{1.9}$$

z is the number of nearest neighbors around a magnetic spin and *J* is the interaction parameter between two nearest neighbor spins. If *J* is positive, the spins align parallel (ferromagnetic interactions) or when it is negative the spins align antiparallel (antiferromagnetic interactions).

Sometimes in magnetically diluted substances, independent paramagnetic centers are separated on a quite long distance (some Å) by diamagnetic atoms, which are not able to transmit magnetic information. In such magnetically isolated substances paramagnetism dominates. In some cases there are some interactions (coupling) between spins of paramagnetic centers and cooperative magnetic phenomena like ferromagnetism, antiferromagnetism or ferrimagnetism are observed. The spin-spin interactions lead to an ordering of the spins below a characteristic, critical temperature (T_N or T_C).

Ferromagnetism (FM) occurs when adjacent electron spins tend to align parallel in this same direction below Curie temperature T_C (Figure 1.1.2.1).[4] Typical, above this critical temperature, the ferromagnetic material behaves as a paramagnet due to the thermal activation, which overcomes the strength of ferromagnetic coupling.[5]

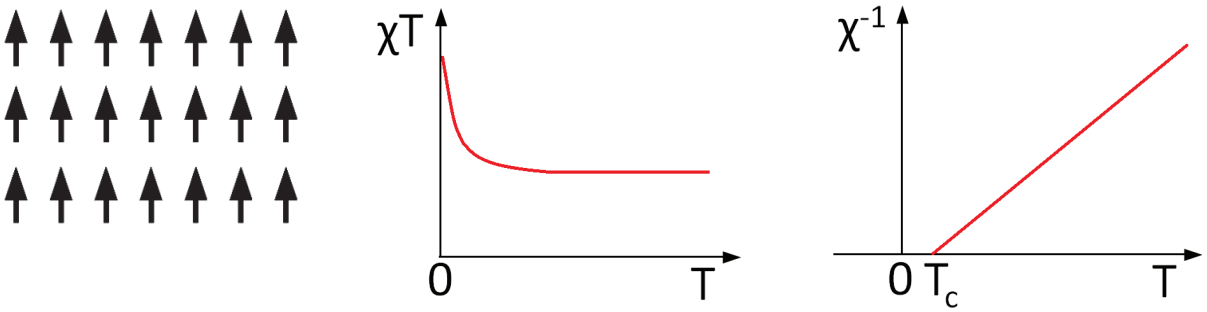

Figure 1.1.2.1 Left - schematic representation of ferromagnetic ordering in solids. Right - typical χT vs. *T* and χ^{-1} vs. *T* plots of a ferromagnetic substance described by the modified Curie-Weiss law. All magnetic moments contribute equally to the spontaneous magnetization, which results in the abrupt, increase of the χT function.

The molecular susceptibility obeys the Curie-Weiss law, giving positive θ and shows an abrupt, very large increase when temperature decreases.

Among **antiferromagnetism** (AFM), below critical Néel temperature (T_N) the spins of unpaired electrons align in antiparallel fashion with vanishing spontaneous magnetization.[6] This results in negative deviation from Curie-Weiss law, yielding negative θ. Above T_N thermal fluctuations dominate, the alignment of the spins is random, leading to a paramagnetic state. AFM can be considered as a system of a two identical interpenetrating ferromagnetic sublattices, which respective magnetizations compensate each other (Figure 1.1.2.2).

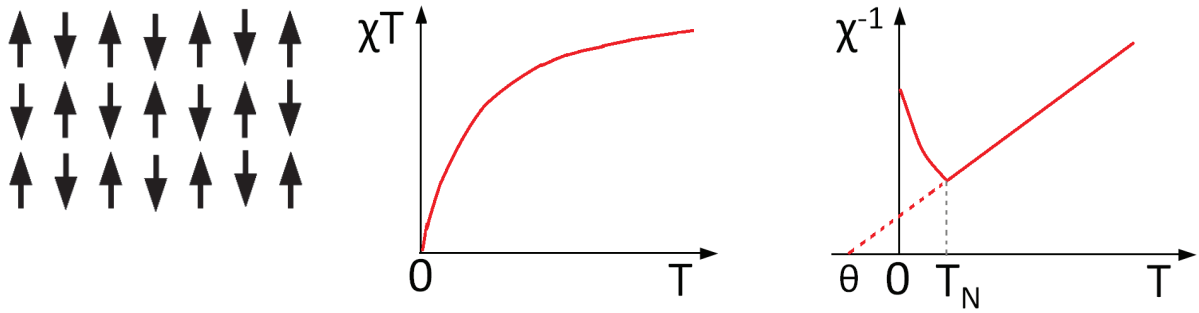

Figure 1.1.2.2 Left - schematic representation of the antiferromagnetic ordering in solids. Right - typical χT vs. T and χ^{-1} vs. T plots of an antiferromagnetic substance described by the modified Curie-Weiss law. Below the critical temperature there is no spontaneous magnetization, which results in a decrease of the χT function.

Ferrimagnetism can be regarded as a special case of antiferromagnetism in which two magnetic sublattices are unequal but still with antiparallel spin alignment. The compensation of magnetic moments is only partial because the magnetization of one sublattice is greater than opposite orientated sublattice, remaining uncompensated, relatively weak spontaneous magnetization.

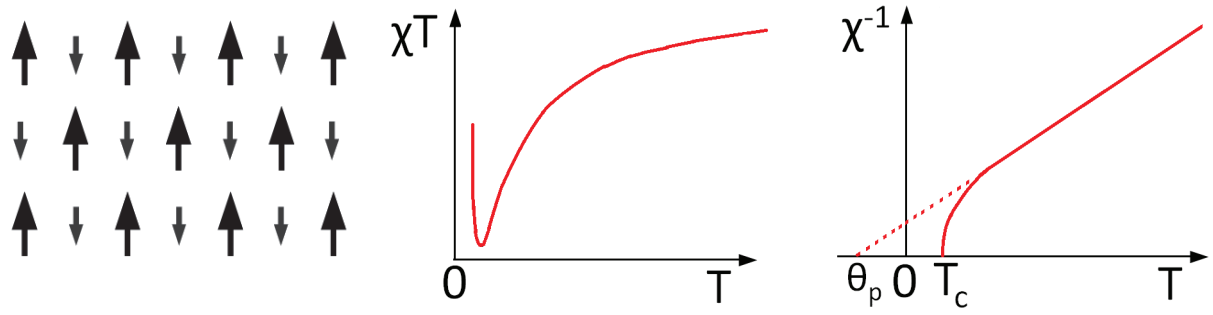

Figure 1.1.2.3 (Left) Schematic drawing of the spin alignment in a typical ferrimagnetic substance reveals unequal moments of different spins. (Right) typical χT vs. *T* and χ^{-1} vs. *T* plots of ferrimagnetic substances described by the Néel law of ferrimagnetism. Below the critical temperature ferrimagnetic substances reveals ferromagnetic order.

As a consequence below the critical temperature (T_C) ferrimagnetic substances order ferromagnetically (Figure 1.1.2.3). Ferrimagnetism was recognized by L. Néel in 1948 and its reciprocal susceptibility follows a hyperbolic law, predicted to be:[7]

$$1/\chi = \frac{T+\theta_P}{C} - \frac{\zeta}{T-\theta'} \qquad \textbf{(1.10)}$$

with the asymptotes θ' and θ_P, which are related to the interactions within and between the magnetic sublattices:

$$\zeta = \frac{\omega^2 C_A C_B [C_A(1+\alpha_A) - C_B(1+\alpha_B)]^2}{(C_A+C_B)^3} \quad \text{where } C = C_A + C_B \qquad \textbf{(1.11)}$$

In the higher temperatures the second term in the Néel law becomes very small and equation 1.10 reduces to the Curie-Weiss law (equation 1.8).

1.1.3. Magnetic Models

Two types of basic models are commonly used in describing the magnetic behavior of matter: one is localized at lattice sites and another is the itinerant electron (band) model. These two models are based on quantum magnetism and illustrate the intrinsic magnetic properties of matter. The localized model essentially describes the exchange interactions which might be mediated by various mechanisms, depending on the structure of the material considered. Generally speaking, within this model there are five types of exchange interactions: direct exchange in metallic systems,[8] indirect exchange in metallic systems through conduction electrons,[9] itinerant exchange through coupling of itinerant electrons in metals,[10] superexchange in magnetic insulators[11] and double exchange through coupling of two localized magnetic moments through an itinerant electron.[12]

In the case of the transition metal complexes investigated in this thesis, the interactions between the paramagnetic centers (Cu^{2+}, Ni^{2+}, Co^{2+}, Fe^{2+}, Mn^{2+}) are mediated by various diamagnetic

linkers described in detail in Part 2. Those superexchange interactions originate from the overlap of the d metal's and p ligand's orbitals resulting in a partial delocalization of involved electrons.

Unfortunately, from the perspective of the classical physics, the dipole-dipole interactions between magnetic moments could not been explained properly due to their small magnitude. This problem was resolved in 1938 by W. Heisenberg,[13] who described quantum mechanical exchange interaction between the magnetic moments and proposed a general and fundamental Heisenberg Hamiltonian given by:

$$\mathcal{H} = -\sum_{i,j} J_{i,j} S_i S_j \qquad \textbf{(1.12)}$$

where $J_{i,j}$ is the exchange integral describing the interactions between the spins S_i and S_j distributed on a regular lattice. Depending on the orbital overlap, the $J_{i,j}$ value can have positive or negative sign, resulting ferromagnetic or antiferromagnetic spin configuration. This quantum mechanics law implied the existence of an effective interaction between electron spins of neighboring atoms with overlapping orbital wave functions.

However, it is difficult to compute the magnetic properties starting from the general equation 1.12. From an experimental point of view, these parameters can by usually obtained by a numerical fit of the measured magnetic susceptibility using Hamiltonian model. A large group of various numerical expressions based on the simplified Van Vleck formula for different spin systems have been developed in the literature.[14] Here, only those which were used in the fitting of magnetic susceptibility data as function of temperature in this thesis are listed:

1) Bleaney–Bowers magnetic model for spin-paring of two S = 1/2[15] derived from the Hamiltonian $\mathcal{H} = -2JS_1S_2$ and given by the numerical expression:

$$\chi = \frac{Ng^2\mu_B^2}{k(T-\theta_{MF})} \cdot \frac{1}{\left[3+\exp\left(\frac{-2J}{kT}\right)\right]} \qquad \textbf{(1.13)}$$

2) FM or AFM Baker 1D model for linear chains for S = 1/2[16] derived from the Hamiltonian $\mathcal{H} = -2J\sum_{N=1}^{\infty} S_1 S_{1+N}$ and given by the numerical expression:

$$\chi = \frac{Ng^2\mu_B^2}{4k(T-\theta_{MF})} \cdot \left[\frac{1+A\cdot\left(\frac{J}{2kT}\right)+B\cdot\left(\frac{J}{2kT}\right)^2+C\cdot\left(\frac{J}{2kT}\right)^3+D\cdot\left(\frac{J}{2kT}\right)^4+E\cdot\left(\frac{J}{2kT}\right)^5}{1++F\cdot\left(\frac{J}{2kT}\right)+G\cdot\left(\frac{J}{2kT}\right)^2+H\cdot\left(\frac{J}{2kT}\right)^3+I\cdot\left(\frac{J}{2kT}\right)^4}\right]^{2/3} \qquad \textbf{(1.14)}$$

where A = 5.7979916, B = 16.902653, C = 29.376885, D = 29.832959, E = 14.036918 and F = 2.7979916, G = 7.0086780 , H = 8.6538644, I = 4.5743114.

3) Van Vleck equation for two interacting spins S = 5/2[17] derived from the Hamiltonian: $\mathcal{H} = -2JS_1S_2$ and given by the numerical expression:

$$\chi = \frac{Ng^2\mu_B^2}{kT} \cdot \left[\frac{\exp(2y)+5\exp(6y)+14\exp(12y)+30\exp(20y)+55\exp(30y)}{1+3\exp(2y)+5\exp(6y)+7\exp(12y)+9\exp(20y)+11\exp(30y)}\right]$$

$$\text{where } y = {}^{J}/_{kT} \qquad \textbf{(1.15)}$$

Some of the basic models were refined by the addition of a mean-field approximation (θ_{MF}):

$$\theta_{MF} = \frac{2zJ_{inter}}{Ng^2\mu_B^2} \qquad \textbf{(1.16)}$$

in which z is the number of nearest-neighbor chains and J_{inter} is the exchange integral for the magnetic interaction between nearest-neighbors chains.

1.2 Treatment of the Experimental Data

The susceptibility is a ratio of magnetization M to the applied external magnetic field H, given by:

$$\chi = {}^{M}/_{H} \qquad \textbf{(1.17)}$$

In all magnetic measurements the molar susceptibility χ_{mol} (cm^3mol^{-1}) have been determined as the experimental data. χ_{mol} can be obtained by dividing χ by the density of the sample ($\chi_{mass} = {}^{\chi}/_{\rho}$) and later multiplying it by a molar mass of the sample (M_{mol}), $\chi_{mol} = \chi_{mass} \cdot M_{mol}$. The data were corrected for the magnetization of the sample holder using the increment method of Haberditzl,[18] and diamagnetic corrections were estimated using Pascal's constants.[19]

During the initial fitting procedure some constants had units in the CSG system and some other in the SI system in order to convert the calculated molar susceptibility in appropriate units. The magnetic properties of measured substances are usually displayed as the thermal dependence of χ_{mol}^{-1} and $\chi_{mol}T$ functions and initially analyzed by the Curie-Weiss law (Equation 1.8). Important steps were determination of the Curie constant given in the unit cm^3Kmol^{-1} and the effective magnetic moment of the substance. The Curie constant could be obtained experimentally from the slope of the function $\chi_{mol}^{-1}=f(T)$ or from the function $\chi_{mol}T=f(T)$ where at high temperatures $\chi_{mol}T \approx C$. Experimental effective magnetic moments μ_{eff} were determined from the experimental data using the equation 1.7 to estimate number of unpaired electrons, oxidation states of the metal ions and the low- or high-spin configuration of the complex. Latter, there were compared to the calculated magnetic effective moments derived from the formulas:

$$\mu_{eff} = 2\sqrt{S(S+1)} \qquad \text{(spin-only formula)} \qquad \textbf{(1.18)}$$

$$\mu_{eff} = \sqrt{4S(S+1)+L(L+1)} \quad \text{(orbital-contribution)} \qquad \textbf{(1.19)}$$

where S - spin angular momentum, L - total orbital angular momentum.

metal ion	d^n configuration	S	μ_{eff} (Eq. 1.18)	μ_{eff} (Eq. 1.19)	μ_{eff} exp[20]
Mn^{2+}	d^5	5/2	5.92	5.92	5.8–5.9
Fe^{2+}	d^6	2	4.90	5.48	5.2–5.5
Co^{2+}	d^7	3/2	3.87	5.20	4.8–5.1
Ni^{2+}	d^8	1	2.83	4.47	2.8–3.3
Cu^{2+}	d^9	1/2	1.73	3.00	1.8–2.0

Table 1.1.5 Calculated and experimental magnetic moments[20] of some transition metal ions for octahedral symmetry given in Bohr magnetons.

At the end of fitting procedures, appropriate numerical expression, that contains a set of fixed (N, g, μ_B, k) and variable parameters (g, J, θ_{MF}) were considered. The parameters g, J, θ_{MF} were found through a fitting with the experimental data taking into account the agreement factor R:

$$R = \sum\left[(\chi_{mol}T)_{exp.} - (\chi_{mol}T)_{calc.}\right]^2 / \sum(\chi_{mol}T)_{exp.}^{\ 2} \qquad \textbf{(1.20)}$$

References

[1] H. Lueken, *Magnetochemie: Eine Einführung in Theorie und Anwendung,* Vieweg & Teubner Verlag, **1999**.

[2] M. Gerloch, E. G. Constable, *Transition Metal Chemistry* **1994**, Wiley-VCH, Weinheim.

[3] O. Kahn, *Molecular Magnetism* **1993**, John Wiley & Sons, Weinheim.

[4] P. Curie, *Ann. Chim. Phys.* **1895**, 289.

[5] K. H. J. Buschow, F. R. de Boer, *Physics of Magnetism and Magnetic Materials,* **2003**, Kluwer Academic/Plenum Publishers, New York.

[6] **(a)** L. Néel, *Ann. de Phys*. **1932**, *17*, 5; **(b)** L. Néel, *Ann. de Phys.* **1936**, *5*, 232; **(c)** L. Néel, *C. R. Acad. Sc.* **1936**, *203*, 304.

[7] **(a)** L. Néel, *Annales de Physique*, **1948**, *3*, 137; **(b)** L. Néel, *Proc. Phys. Soc. A* **1952**, *65*, 869.

[8] W. Heisenberg, Z. Physik **1927**, *44*, 455.

[9] **(a)** M .A. Ruderman C. Kittel, *Phys. Rev.* **1954**, *96*, 99; **(b)** T. Kasuya, *Progr. Theor. Phys*. **1956**, *16*, 45; **(c)** K. Yoshida, *Phys. Rev.* **1957**, *106*, 893.

[10] R. Boča, Current *Methods of Inorganic chemistry, vol. 1, Theoretical Foundations of Molecular Magnetism,* 1st ed. **1999**, Elsevier, Switzerland.

[11] **(a)** J. H. van Vleck, *J. Phys. Radium*, **1951**, *12*, 262 **(b)** P. W. Anderson, *Phys. Rev.* **1959**, *115*, 2

[12] C. Zener, *Phys. Rev*. **1951**, *82*, 403.

[13] W. Heisenberg, *Z. Phys.* **1928**, *49*, 619.

[14] **(a) Spin-Pairing of two S = 2/2 and S=4/2 systems:** R. L. Carlin, *Magnetochemistry* **1986**, Springer-Verlag: Berlin, Germany; **(b) Linear, Isotropic Three-spin System where all S = 1/2:** M. Baskett, P. M. Lahti, F. Palacio, F. *Polyhedron* **2003**, *22*, 2363; **(c) Linear, Isotropic Three-spin System where all S = 1/2:** Y. Ishimaru, M. Kitano, H. Kumada, N. Koga, H. Iwamura, *Inorg. Chem*. **1998**, *37*, 2273; **(d) Linear, Three-spin System, (S1 = 1/2)↔(S2 = 2/2) ↔ (S3 = 1/2), J≠J′ for general case:** C. Stroh,

L. Belorizky, P. Turek, H. Bolvin, R. Ziessel, *Inorg.Chem.* **2003**, *42*, 2938; **(e) Linear, Isotropic Three-spin System, (S=1)(S=1.5)(S=1)**: F. E. Mabbs, D. J. Machin, *Magnetism and Transition Metal Complexes* Wiley **1973**, Chapter 7, New York; **(f) Equilateral Triangle Three-spin System where all S = 1/2 and Isosceles Triangle Three-spin System where all S = 1/2 and Tetrahedron where all S = 1/2:** J. T. Haraldsen, T. Barnes, J. L. Musfeldt, *Phys. Rev. B*, **2005**, *71*, 064403; **(g) Square Four-spin System where all S = 1/2, J=J':** D. Procissi, A. Shastri, I. Rousochatzakis, M. Al Rafai, P. Kögerler, M. Luban, B. J. Suh, F. Borsa, *Phys. Rev. B*, **2004**, *69*, 094436; **(h) Rectangular Four-spin System where all S = 1/2, J' < J:** Y. Ishimaru, M. Kitano, H. Kumada, N. Koga, H. Iwamura, H. *Inorg.Chem.* **1998**, *37*, 2273; **(i) AFM coupled Bonner-Fisher linear chains, S = 1/2 units, all J equal:** J. C. Bonner, M. E. Fisher, *Phys. Rev. A* **1964**, *135*, 650; **(j) AFM coupled alternating linear chains, S = 1/2 units, all J equal:** J. W. Hall, W. E.Marsh, R. R. Weller, W. E. Hatfield, W. E. *Inorg. Chem*., **1981**, *20*, 1033; **(k) Modified 1D Chain Expression (S = 1/2):** L. Li, D. Liao, Z. Jiang, S. Yan, *Inorg. Chem.* **2002**, *41*, 421; L. Li, L. Liao, S. Liu, Z. Jiang, S Yan, *Inorg. Chem. Commun*., **2003**, *6*, 225; Z. Zhu, S. Karasawa, N. Koga, *Inorg. Chem*. **2005**, *44*, 6004; **(l) Spin-Ladder Model, all S = 1/2 units:** Q. Gu, D. K. Yu, J. L. Shen, *Phys. Rev.* **2000**, *B60*, 3009; **(m) Square-planar antiferromagnetic sheet, all S = 1/2 units:** G, Jr. Baker, G., H. E. Gilbert, J. Eve, G. S. Rushbrooke, *Phys. Rev. Lett.* **1967**, *25*, 207; **(n) Interacting Square Planar Bilayers, S = 1/2:** Z. Weihong, *Phys. Rev. B* **1997**, *55*, 12267.

[15] B. Bleaney, K.D. Bowers,. *Proc. R. Soc. London, A*, **1952**, 214.

[16] **(a)** Swank, D. D.; Landee, C. P., Willet, R. D. *Phys. Rev. B*, **1979**, *20*, 2154; **(b)** G.A Baker, G. S. J. Rushbrooke, H. E Gillbert, *Phys. Re*v. **1964**, *135A*, 1272.

[17] C. Baffert, M. N. Collomb, A. Deronzier, S. Kjærgaard-Knudsen, J. M. Latour, K. H. Lund, C. J. McKenzie, M. Mortensen, L. Preuss Nielsenb, N. Thorup, *Dalton Trans.* **2003**, 1765.

[18] W. Haberditzl, *Angew. Chem. Int. Ed.* **1966**, *5*, 288.

[19] G. A. Bain, J. F. Berry, *J. Chem. Educ.* **2008**, *85*, 532.

[20] R. Grinter, *The Quantum in Chemistry: An Experimentalist's View*, Wiley Publishers, **2005**, p. 198.

PART 2

CYANOCARBON CHEMISTRY — INTRODUCTION

Abstract

This part includes a brief literature review and an introduction to the azolates coordination chemistry and different azolates and their cyano derivatives. As an extension a short review about some highly conjugated polynitrile ligands and their coordination chemistry is given.

2.1 Cyano-azolates - Heterocyclic Ligands Bearing a Cyano Group

The simple azoles comprise a class of five-membered heterocycles including at least one nitrogen atom within a ring. Additional presence of non-carbon atoms either sulphur or oxygen leads to thiazole and oxazole derivatives.[1] The replacement of one, two, three or four ring carbon atoms from the parent isoelectronic cyclopentadienyl anion $C_5H_5^-$ by the sp^2 hybridized nitrogen atom leads to the series of *N*-donor ligands: pyrroles, 1,2-diazoles (pyrazoles), 1,3-diazoles (imidazole), 1,2,3-triazole, 1,2,4-triazole and tetrazole (Scheme 2.1.1). This group of compounds belongs to π-electron systems,[2] which follow Hückel's rule. Generally, a N heteroatom possesses a lone electron pair, which contributes together with two double bonds to the aromatic sextet, thus the simple $4n+2$ criterion for aromatic, cyclic and conjugated π-systems is fulfilled. Upon elimination of an azole N–H proton from the ring moiety, an *N*-azolate anion is generated. The new lone pair of electrons, situated in a sp^2 hybrid orbital in the plane of the aromatic ring, does not participate in the sextet, therefore the anion becomes a σ-donor in coordination chemistry.[3]

The most N–H acidic member of the azole family, possessing the lowest pK_a of 4,9 similar to that of acetic acid, is 1-*H*-tetrazole. As the N atom has an electron-withdrawing effect, the acidity of the conjugated acid (neutral molecule) decrease with the lowering of the number of N atoms in the aromatic system[4] (Scheme 2.1.1).

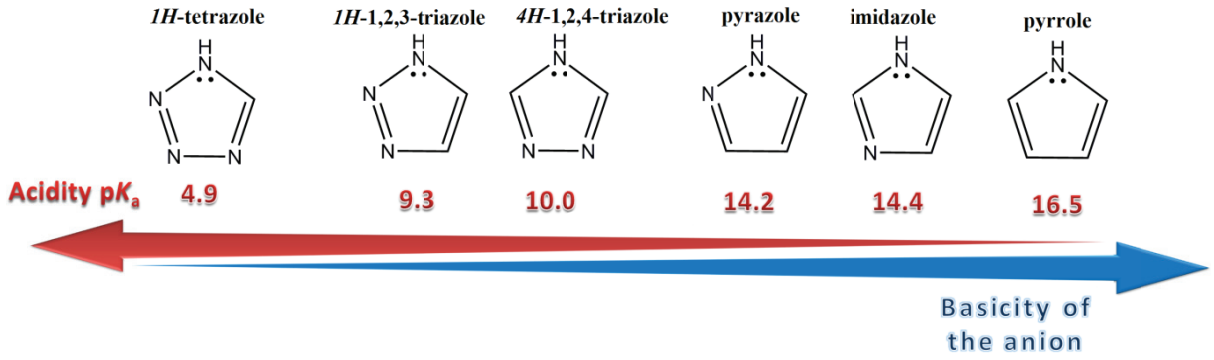

Scheme 2.1.1 Variation of azole pK_a for proton loss with the number of nitrogen atoms (aqueous solution). The basicity of the anions decreases with the increasing number of N atoms.

Systematic replacement of C–H hydrogen atoms in the series of six types of azoles (Scheme 2.1.1) by cyano group(s) leads to new heterocyclic $[C_{2n}N_5H]$ (n = 0, 2, 3, 4) cyano systems shown in the Scheme 2.1.2. With the addition of the groups having an electron-withdrawing effect the overall electron density on the molecule decreases and electron deficiency enhances the acidity. Consequently, Htcp is a medium-strong acid (pK_a = 2.71) and its conjugate anion a weak base (pK_b = 11.29).[5] This same effect can be observed in Htcpz or Hctz where pK_a of the acid is sharply reduced to 2.53[6] and 1.75,[7] with respect to pyrazole and tetrazole. Generally, the substitution with cyano groups reduces the basicity strength and accordingly the tendency to donate an electron pair.

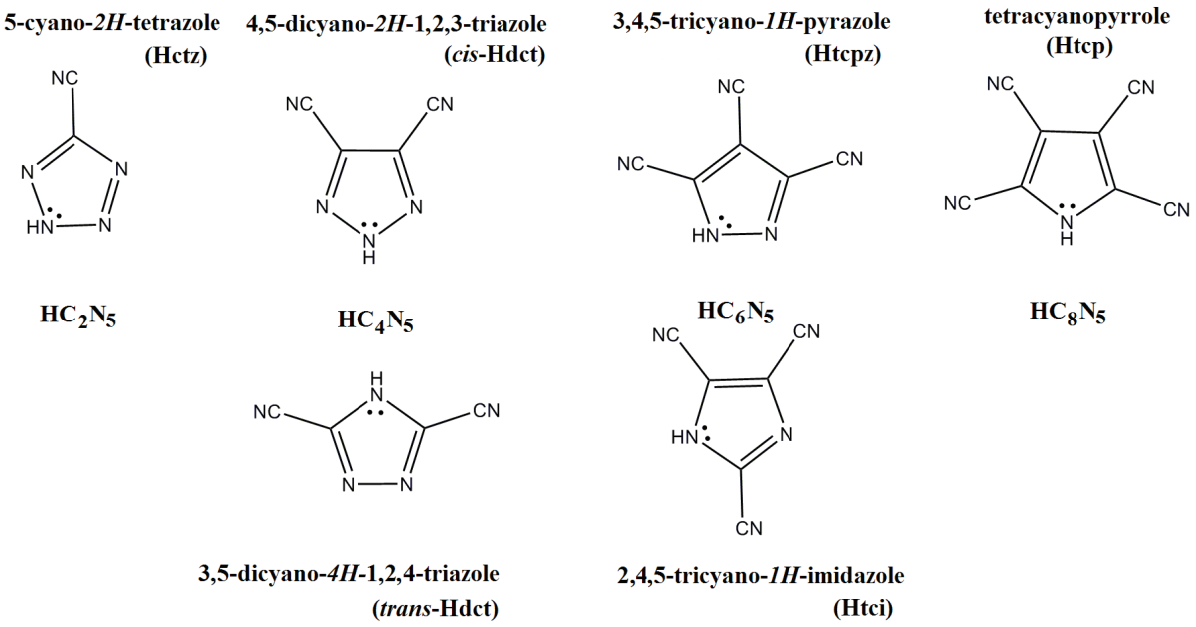

Scheme 2.1.2 Structural formulae of the series of cyano-substituted neutral azoles. The conjugate bases are readily formed upon deprotonation.

Density functional studies on the electronic structures of some cyano derivates give a detailed picture of the charge distribution and support the concept of the inductive effect of cyano substituent's. The electron-withdrawing power of the C≡N groups can be seen by a comparison to the non-substituted anions. The total charge for the tcp anion is more positive (–0.80*e*) as compared to the pyrrolide anion (–1.74*e*) and result in more favorable σ-type interaction in the M–L bonding.[8] A similar charge displacement occurs in the *cis*-dct anion and results in a reduced negative charge of the ring (–0.69*e*) compared to the 1.2.3-triazolate (–1.20*e*).[9] In the tcpz anion three C≡N groups withdraw about 0.62 electrons charge from the ring, which results in more positive charge (–0.38*e*) in the cyclic system.[10] The charge displacement from the ring to the peripheral groups enhances the probability of σ-interaction with Lewis acids but also results in reduction of basicity of the anion. This reduces the coordinating ability of this class of ligands, making them weakly coordinating ligands.

2.1.1 4,5-Dicyano-1,2,3-triazolate- and 5-Cyanotetrazolate-based Energetic Salts

Azole heterocyclic ligands offer a good backbone for the synthesis of energetic salts not only because of the flat structure of the ring, but also because a high nitrogen content and therefore the high density. Generated dinitrogen N_2 gas is the main decomposition/explosion product, substituting CO_2 as the gas product which is undesired in "green" energetic materials research.[11] In this field, much attention is focused on the tetrazole- and triazole-based salts as thermal and chemical stable explosives, since the N–N and N–C bonds in the ring are stabilized by the aromatic character of the five-membered moiety.[12] Moreover, the introduction of cyano groups can up-rate the heats of formation of the energetic materials and keep their relatively

high thermal stabilities.[13] The ctz and dct heterocyclic compounds bearing cyano group were investigated mainly as potentially promising energetic materials (Figure 2.1.1.1).[14]

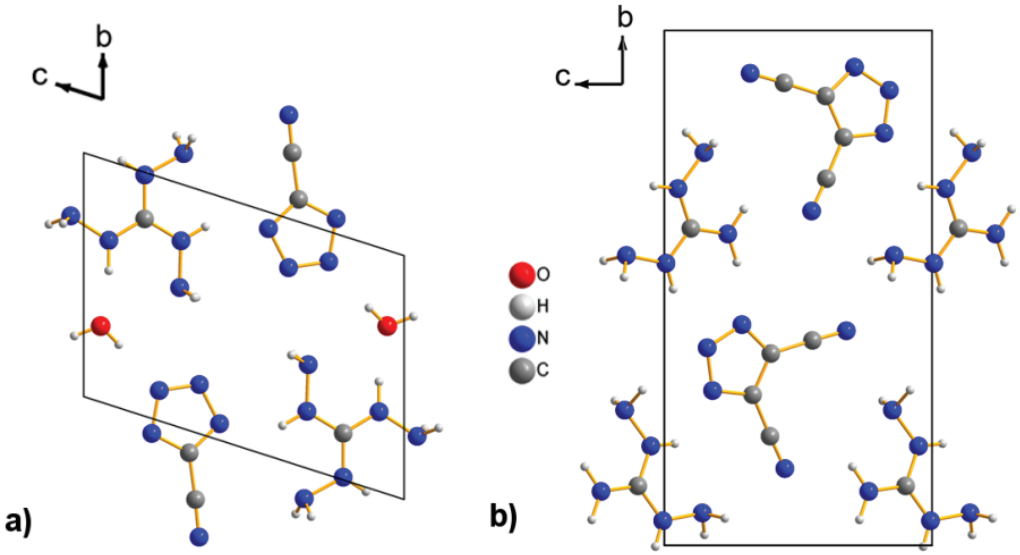

Figure 2.1.1.1 Crystal structures of two energetic salts: **(a)** Triaminoguanidinium 5-cyanotetrazolate monohydrate.[14] **(b)** Diaminoguanidinium 4,5-dicyano-1,2,3 triazolate.[14]

The energetic nitrogen rich salts based on the ctz anion with ammonium, hydrazinium, semicarbazidium, and guanidinium counter-ions have high nitrogen content ranging from 66-77 %, resulting in highly positive heat of formation (ΔH_f) attributed to the number of energetic N–N bonds.[15] The calculated ΔH_f for these energetic materials fall in the range from +1784 to +3665 *kJ*/mol which is higher than TNT (2,4,6-trinitroroluene) and RDX (1,3,5-trinitroperhydro-1,3,5-triazine) often used as explosives for military and industrial applications. The calculated detonation velocities are comparable to those of RDX (D_{RDX} ~ 8800 ms^{-1}).[16] The lower nitrogen content in the dct anion makes its rich nitrogen salts less energetic compare to the ctz explosives with positive heats of formation ranging from +398 to +795 *kJ*/mol. Thus, this class of compounds suffers for a low velocity of detonation and a low detonation pressure.[14]

2.1.2 Coordination Chemistry of Azolates

Besides pharmaceutical and agrochemical aspects,[17] the five-membered binary azolates are most likely used as small and simple organic ligands in the area of coordination chemistry, not only because electron donating nature of their Lewis basic functions, but also due to a short bridging length of the metal sites and superexchange capacity reflected in interesting magnetic properties of their transition metal complexes.[18] However, transition-metal azolates owing to their low solubility and the formation of polycrystalline intractable powders had not been explored widely in the past decade, some of them had been only characterized by powder X-ray diffraction.[19] Later, the combination of hydro(solvo)thermal methods with *in situ* synthesis has

been found to provide suitable single crystals of coordination polymers for X-ray diffraction studies[1].[20]

The pyrrolide anion forms *N*-ligated complexes widely distributed in nature, as found in hemes, chrolophylls, vitamin B_{12}, chlorins, bacteriochlorins[21] and also it occurs in number of naturally occurring antibiotics.[22]

Imidazolate and pyrazolate are sterically and electronically comparable anions, bearing two nitrogen atoms, which have been found to bind metal ions in two coordination modes: in the monodentate mode known for both (pyrazolate and imidazolate anions) or in the bidentate exo-η^1-η^1/endo-η^2 (pyrazolate) mode or exo (imidazolate) mode. Binary metal pyrazolates are known as discrete clusters (mostly cyclic trimers) or as chain-like structures owing to the 1,2-position of the nitrogen atoms in the aromatic ring. The small bridging angle (~ 70 °) of the pyrazolate anion is suitable for the construction of 1D structures. The polymeric chains of transition metal complexes linked by exo-η^1-η^1-pyrazolate bridges are very widely spread as found in [M^{2+}(μ-pz)$_2$] (M^{2+}= Cu, Ni, Co, and Fe) 3d transition metal complexes[23] and in most cases reveal antiferromagnetic exchange between the metal centers in the extended linear chains (Figure 2.1.2.1(b)).[24] Imidazolate anions mainly act as two-coordinated linkers with two nitrogen donors pointing outward of the cyclic ring with an angle of ca. 144 °, which is close to Si–O–Si angle in zeolites. The 1,3-positions of the *N*-donors prevent the formation a double azolate bridge and therefore higher dimensionalities of the networks can be observed (Figure 2.1.2.1(e)).

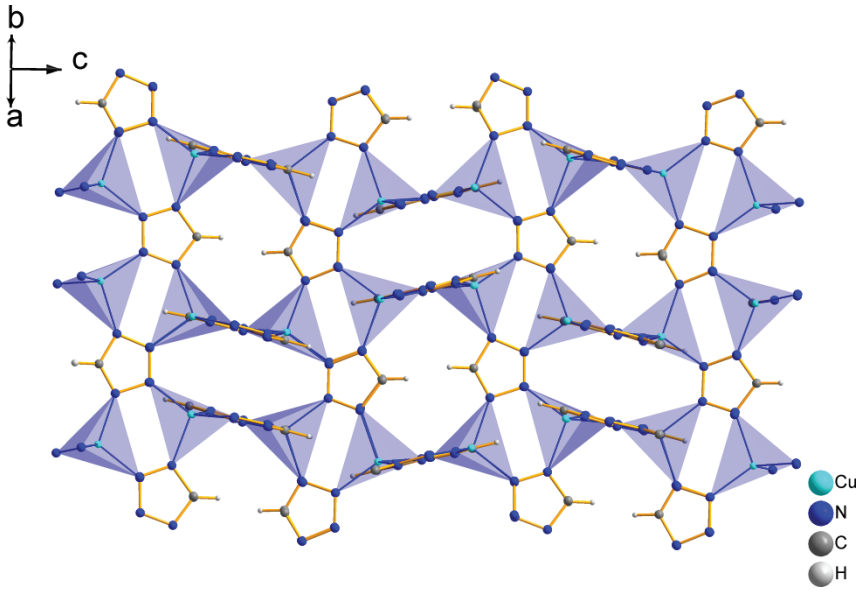

Figure 2.1.2.1 (a) 3D four-connected net of complexes of Cu(I) tetrazolate.[29]

[1] The presentations of crystal structures in this chapter were prepared with the program DIAMOND using crystallographic data from the CSD database. The diagrams of magnetic behavior were taken directly from the respective publications.

Many bivalent imidazolate transition metal complexes have been studied, but only a few of them were structurally characterized, revealing antiferromagnetic interactions between paramagnetic M^{2+} metal centers.[25] As example, the structural[26] and magnetic[27] characterization of $[Fe_3(imid)_6(imidH)_2]_x$ (imidH = imidazole) reveals antiferromagnetic coupling between paramagnetic centres and weak ferromagnetism as a result of long–range order at low temperatures. In related binary cobalt(II) imidazolates similar bridging arrangement leads also to antiferromagnetic exchange (Figure 2.1.2.1(e)).[28] The examples of interesting azolate-transition metal complexes are shown in Figures 2.1.2.1(a-e).

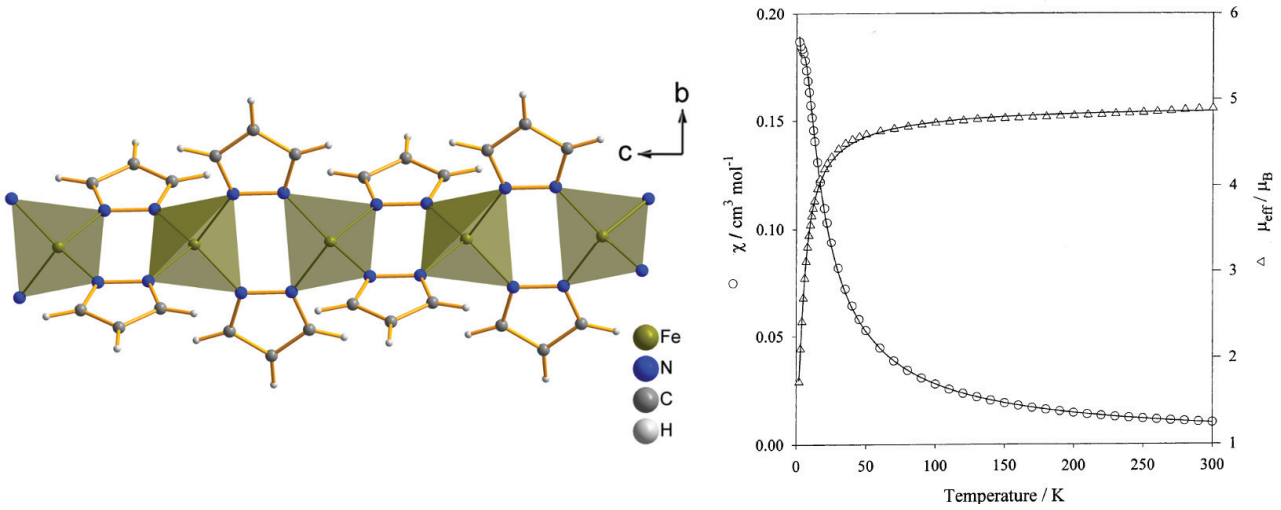

Figure 2.1.2.1 (b) View of a section of the $[Fe(pyrazolate)_2]$ 1D chain with doubly bridged Fe atoms by pyrazolate anions revealing very weak antiferromagnetism (J = –0.59 cm^{-1}).[30]

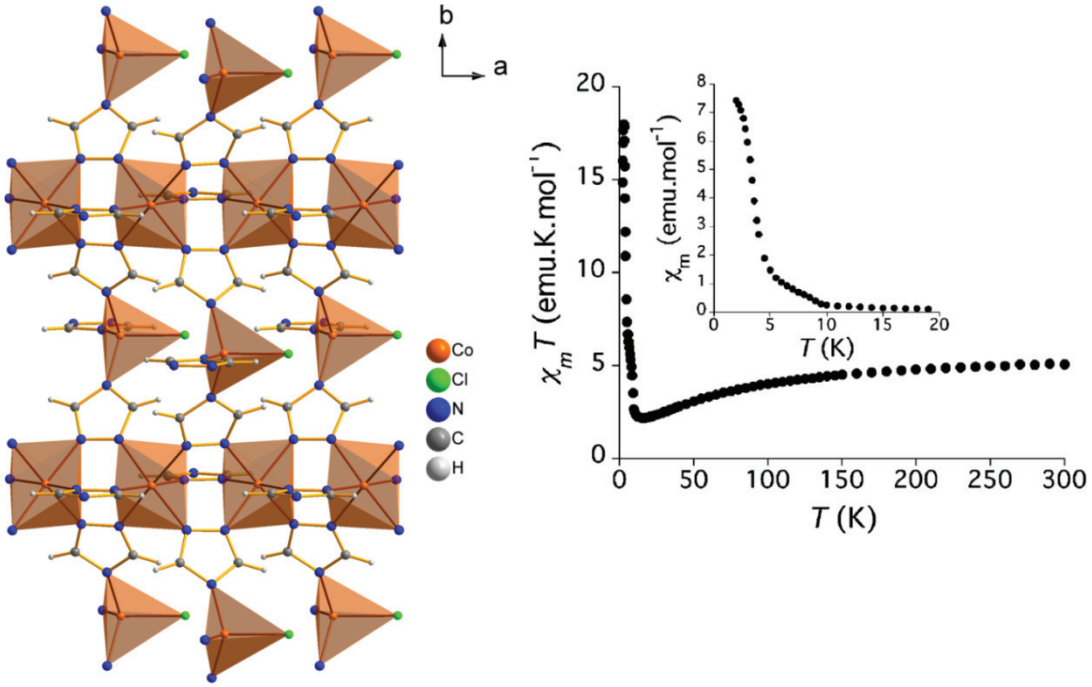

Figure 2.1.2.1 (c) 3D framework of the $[Co_2(1.2.4\text{-triazolate})_3Cl]$ coordination polymer, octahedral and tetrahedral Co^{II} centres give weak ferromagnetic response below Tc = 9 K.[31]

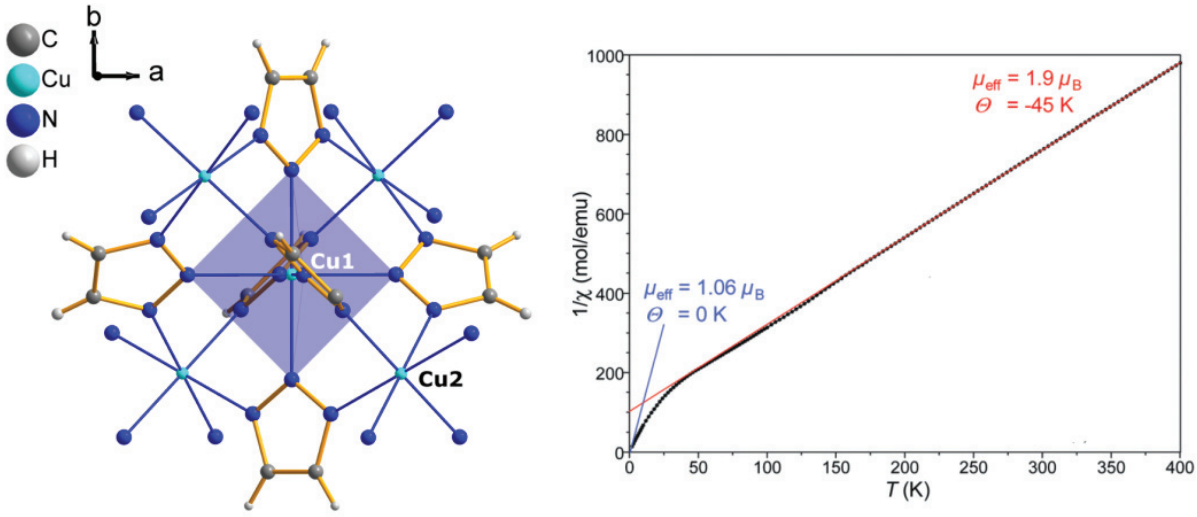

Figure 2.1.2.1 (d) Kuratowski-type pentanuclear $[Cu^{2+}_5(1.2.3\text{-triazolate})_6]^{4+}$ cluster as a part of 3D metal-organic framework revealing weak ferrimagnetism.[32]

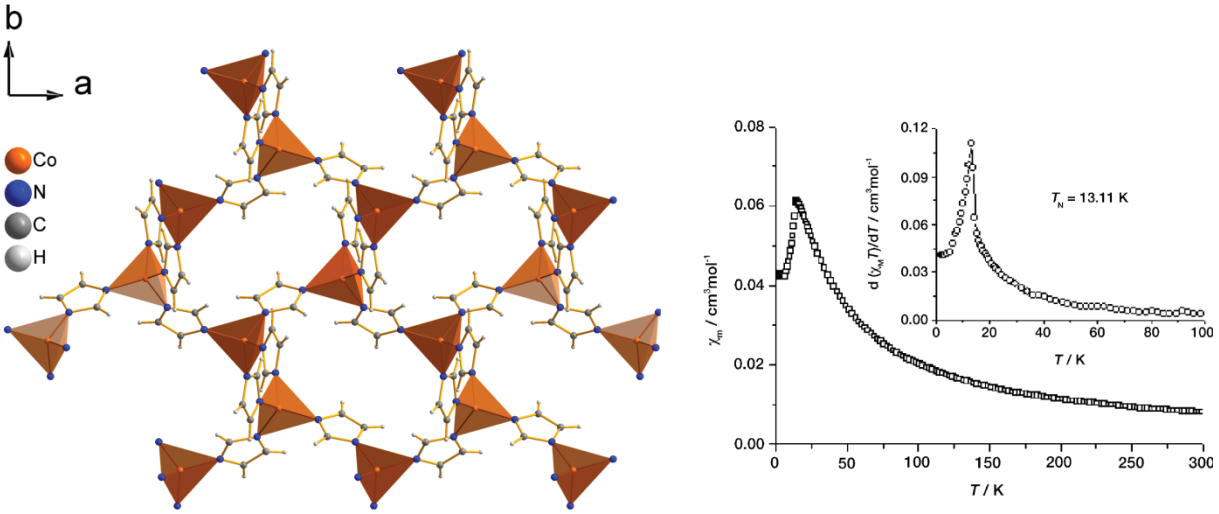

Figure 2.1.2.1 (e) 3D network of [Co(imdazolate)$_2$ · 0.5 py] shows and high-spin tetrahedral Co^{II} ions with the antiferromagnetic behaviour (T_N = 13.11 K).[33]

The triazolate family is represented by an isomeric pair 1,2,3-triazolate or 1,2,4-triazolate with the different position of three N atoms. The N atoms of 1,2,3-triazolate located at the same side of the five-membered ring usually form discrete polynuclear complexes with "Kuratowski-type" pentanuclear $[M^{2+}_5(1,2,3\text{-triazolate})_6]^{4+}$ clusters with divalent metal ions.[34] The 1,2,4-triazolate usually behaves as three-connected ligand with characteristic Y-shape coordination mode, which connects both imizadole and pyrazole binding fashions.[35] Thus, in this bridging capacity 1,2,4-pyrazolates reveal great coordination abilities specially when triazolate moiety is substituted with additional donor groups.[36] As a example Cu(II)-triazolate-based complexes show different magnetic behavior, very often antiferromagnetism or rarely ferromagnetism are observed.[37]

Compared to the other azoles, tetrazoles possess the highest number of *N*-donor atoms in the aromatic ring and therefore the highest number of coordination modes, but suffer from low basicity and weak coordination ability. Very often due to their instability, substituted tetrazoles are used instead, which form various one-, two- and three dimensional coordination polymers together with other species present in solution (solvents, counter-ions or co-ligands). The magnetic investigations on numerous tetrazolate-containing complexes including Fe^{2+}, Cu^{2+}, Co^{2+} and Mn^{2+} systems were described in the literature, in which various magnetic behaviors like antiferromagnetism, ferromagnetism, spin crossover, spin canting and ferrimagnetism were observed.[38]

2.2 The Chemistry of *N′*,*N″*,*N‴*-tricyanoguanidinate

Multidimensional coordination polymers composed of transition metals and polydentate organic nitrile-donor ligands have been an active area of research interest for many years (Scheme 2.2.1).[39] The solids that contain transition metal cations and polynitrile units can be divided into two main categories: in the first category the ligand is σ-bonded to the metal cation, in the second unsaturated polynitriles (electron acceptors) and electron donors are organized into stacked systems.[40] Generally, cyano-containing organic linkers are useful as they feature a good Lewis basicity and provide efficient superexchange pathways between metal centers.[41] The association of the π electron system of the CN groups with the π electron system of the central skeleton induces electron delocalization that facilitates transmission of electronic effects between the metal centers.[42] Despite the presence of various CN units, their special geometries preclude the chelating coordination mode, forcing them to act as either terminal or (poly)bridging ligands.[43]

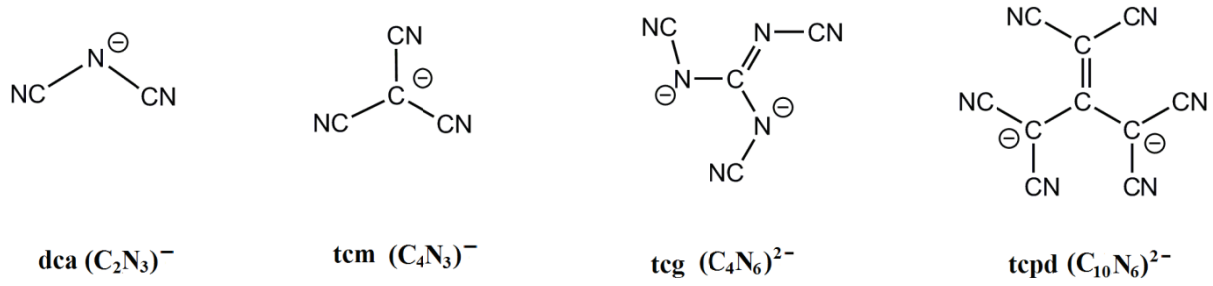

Scheme 2.2.1 Some polycyanoanions as closed shell ligands: dca - dicyanamide, tcm - tricyanomethanide, tcg - tricyanoguanidinate and tcpd 2-dicyanomethylene-1,1,3,3-tetracyanopropanediidne anions represent different point group symmetries (dca C_{2v}, tcm, tcpd D_{3h} and tcg C_{3v}). Only one tautomeric form is shown.

Among the binary carbon-nitrogen compounds, which have been reported, the coordination polymers of pseudohalide ligands possessing alternating carbon-nitrogen connectivity such as dicyanamide (dca, $[N(CN)_2]^-$) or trigonal, 3-connecting tricyanomethanide (tcm, $[C(CN)_3]^-$)

ligands have been extensively studied, partly due to the discovery of long-range magnetic order in the α-M(dca)$_2$ compounds.[44]

Owing to the highly conjugated nature of polycyano molecules they can provide spin coupling between paramagnetic metal centres. For example, the isostructural complexes of the dca series (M^{2+} = Cr, Mn, Fe, Co, Ni, Cu) display diverse types of magnetic order such as canted-spin antiferromagnetism (Cr^{2+}, Mn^{2+}, Fe^{2+}) or ferromagntism (Co^{2+}, Ni^{2+}, Cu^{2+}).[45] In the tricyanomethanide-based complexes, the larger size of the tcm ligand compared to the dca makes coordination networks more spacious, and thus such materials show mainly weak spin coupling via the five atom *–NCCCN–* bridges, as shown in Figure 2.2.3.

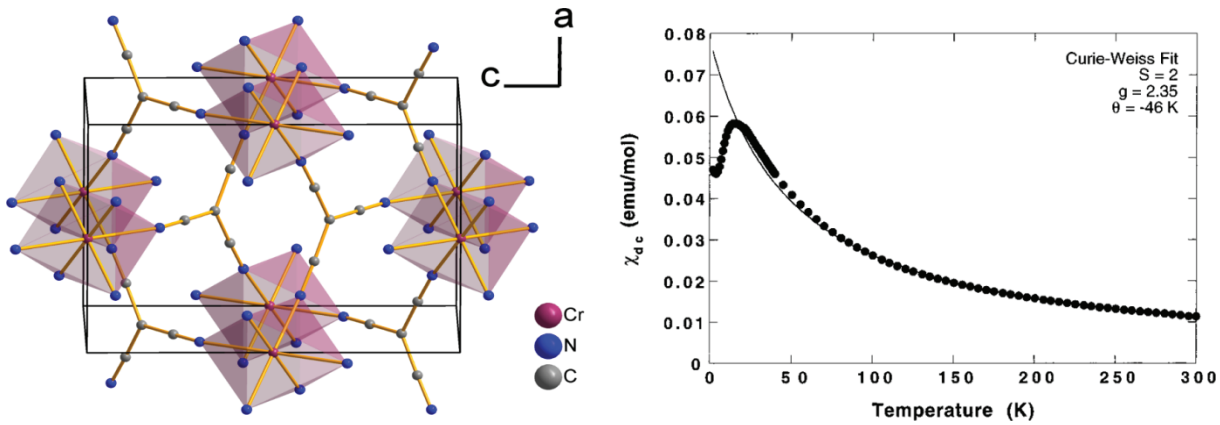

Figure 2.2.2 Three dimensional rutile-like coordination network of high-spin $Cr^{II}(tcm)_2$ complex reveals strong antiferromagnetism Θ= −46 K).[47]

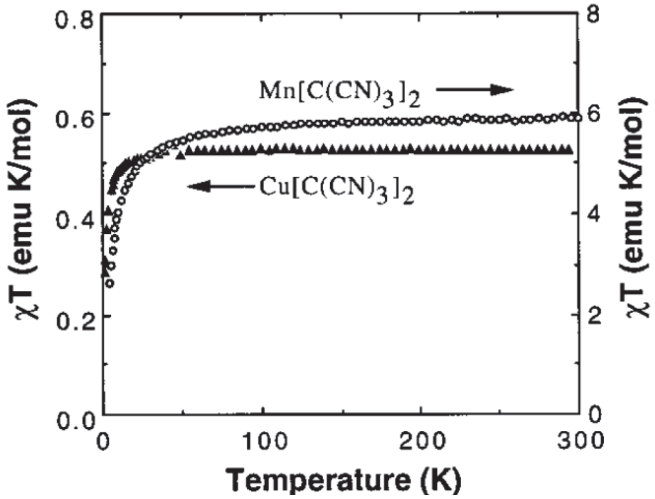

Figure 2.2.3 The high-spin Mn(II) and Cu(II) analogues isostructural to $Cr^{II}(tcm)_2$ complex reveal a weak antiferromagnetic coupling (Θ_{Mn}= −4.8 K and Θ_{Cu}= −1.4 K).[48]

These compounds with the general formula M(tcm)$_2$ (M^{2+}= V, Cr, Mn, Fe, Co, Ni) crystallize as 3D structures similar to that of rutile TiO_2, in which the tcm ligands bind three different metal centers.[46] In contrast, the stronger antiferromagnetic coupling of Θ = −46 K is observed in Cr(tcm)$_2$ complex (Figure 2.2.2), which is additionally stabilized by the Jahn-Teller effect.[47]

Also large polynitrile molecules are interesting ligands for the preparation of variety different structural motifs, however magnetic exchange mediated through π-conjugated linking ligands decreases with the elongation of the bridges connecting the metal atoms. As example, the related large polynitrile tcpd ligand gives only very weak magnetic coupling, estimated to have the exchange constant of J = +0.6 cm^{-1} when bridging Cu(II) metal ions (Figure 2.2.4).[49]

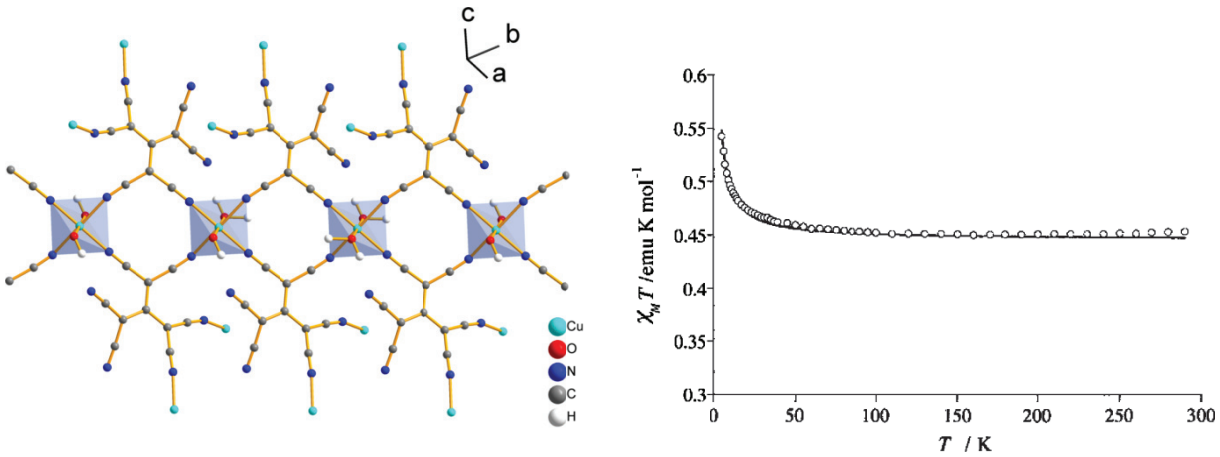

Figure 2.2.4 Crystal structure of 3D [Cu(tcpd)$_2$(H$_2$O)$_2$] coordination polymer containing the symmetrical tcpd dianion. Weak ferromagnetic interactions (J= +0.6 cm^{-1}) are present between neighbouring Cu(II) centres.[49]

The interesting high-spin magnetic properties of rutile-like network in the M(tcm)$_2$ complexes and weak ferromagnetic exchange in the large tcpd copper(II) complex prompted us to make up new coordination polymers using the long forgotten and poorly characterized *N,N´,N´´*-tricyanoguanidinate dianion (tcg) (Scheme 2.2.1), which serves as triply connectcing, trigonal building block with a rare alternating carbon-nitrogen connectivity.

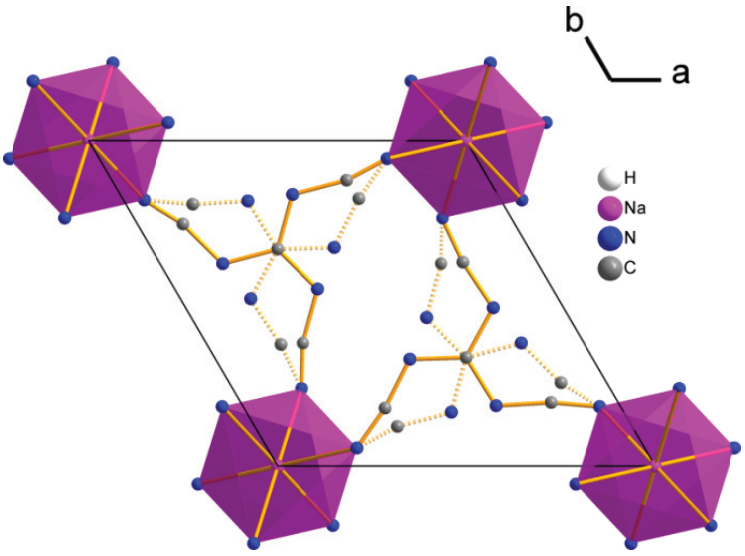

Figure 2.2.5 Crystal structure of the guanidinium sodium [Na(tcg)][C(NH$_2$)$_3$] salt refined in the trigonal space group $P\bar{3}$. The sodium atoms and the tcg dianions are situated at 3-fold symmetry sites, thus imply a complicated local structure with the tcg dianions in two different orientations (dashed lines). The guanidinium cations are omitted for clarity.[50]

The first chemical and structural characterization of tcg ligand has been done by Subrayan *et al.* in 1995. He reported a new, improved synthesis of the tcg dianion, which was isolated as disodium Na$_2$(tcg) · H$_2$O salt and later structurally characterized as the monoguanidinium

monosodium [Na(tcg)][C(NH$_2$)$_3$] salt (Figure 2.2.5). Despite the crystal structure of disodium salt Na$_2$(tcg) · H$_2$O was unsolved, it revealed a strong second harmonic generation optical effect.[50]

2.3 Aim and Scope of the Thesis

The coordination chemistry of cyano-substituted azoles could give promising results with respect to the deeply investigated parent azolate-based coordination materials, reviling widespread applications. Surprisingly little is known about binding abilities of cyanoazolates to 3d transition metal ions. A possible reason could be the assumption of their weak coordination abilities by the progressive substitution of electron-withdrawing cyano groups and enhanced acidity of the [C$_{2n}$N$_5$]$^-$ ions. However, even "non-nucleophilic" ligands like the pentacyanocyclopentadienide [C$_5$(CN)$_5$]$^-$ anion,[51] whose conjugate acid is as strong as perchloric acid, has recently been recognized as a σ-ligand in coordination chemistry with some transition metals.[58] Until now, the chemistry of the cyanoazolate series has not been the subject of systematic investigations. Some of the [C$_{2n}$N$_5$]$^-$ ions have been synthesized long ago (ctz 1912,[52] *cis*-dct 1923,[53] tcpz 1962,[54] tci 1988[55] and tpc 1980,[51] *trans*-dct still undiscovered) but only a few reports about their structural chemistry have been published to date (see next chapters – in the respective Introduction Part). The attention has been mainly referred to non-coordinating behaviour of those cyano anions in lithium polymer electrolytes[56] or they were considered as component of possible new energetic materials as described in subchapter 2.1.1. Later, the investigation of their explosive properties were extended to alkali and alkaline earth metal salts.[57]

Within this project, systematic studies of the cyanoazolate series (ctz, *cis*-dct, tci and tcp) with the emphasis on the coordination chemistry towards the first-row transition metals and on the structures and magnetic properties of new obtained compounds were undertaken. For this purpose, some magnetic models based on the Heisenberg model principle (see Part 1, Equation 1.12) will be applied to calculate the exchange interactions in the presented magnetic systems. Moreover, the detailed, reproducible syntheses of the ligands including their analytical characterization will be given. The project is additionally extended to the long forgotten and poorly characterized polycyano *N*,*N*´,*N*´´-tricyanoguanidinate (C$_4$N$_6$)$^{2-}$ anion, which gives interesting polymeric complexes with ions that have unpaired spin(s), as described in detail in Part 7.

References

[1] K. Schofield, M.R Grimmett, B. R. T. Keene, *Heteroaromatic Nitrogen Compounds: The Azoles*, Cambridge University Press, Cambridge, England **1976**.

[2] A.R Katritzky, C. A. Ramsden, E. F. V. Scriven, R. J. K. Taylor, *Comprehensive Heterocyclic Chemistry III*, vol. 3-6, Elsevier Oxford, **2008**.

[3] J. A. Joule, K. Mills, *Heterocyclic Chemistry*, John Wiley & Sons, 5th Edition **2010**.

[4] A. R. Katritzky, C. A. Ramsden, J. A. Joule, V. V. Zhdankin, *Handbook of Heterocyclic Chemistry*, 3th Edition Elsevier, **2010**.

[5] **(a)** H. E. Simmons,Du Pont de Nemours & Co. patent, US3221024, **1962**; (b) R. D. Vest S. A. Vladuchick, O. W. Webster, *J. Org. Chem.* **1980**, *45*, 5113.

[6] R. C. Storr, T. L. Gilchrist, R. A. Aitken, *Science of Synthesis: Houben-Weyl Methods of Molecular Transformations Vol. 13*, Stuttgart Thieme, **2006**.

[7] J. E. Womelsduff, V. M. Loyola, *High Pressure Liquid Chromatographic Method for CP Amide Analysis, 1981 Explosive Materials Division 2516*, Sandia National Laboratories. Albuquerque, NM 87185.

[8] M. Becker, J. Harloff, T. Jantz, A. Schulz, A. Villinger, *Eur. J. Inorg. Chem.* **2012**, *34*, 5658.

[9] P. Johansson, S. Beranger, M. Armand, H. Nilsson, P. Jacobsson, *Solid State Ionics* **2003**, *156*, 129.

[10] H. Markusson, S. Beranger, P. Johansson, M. Armand, P. Jacobsson, *J. Phys. Chem. A* **2003**, *107*, 10177.

[11] H. Gao, J. M. Shreeve, *Chem. Rev.* **2011**, *111*, 7377.

[12] **(a)** T. M. Klapäotke, C. M. Sabaté, *Chem. Mater.* **2008**, *20*, 3629; **(b)** V. A. Ostrovskii, M. S. Pevzner, T. P. Kofman, M. B. Shcherbinin, I. V. Tselinskii, *Targets Heterocycl. Syst.* **1999**, *3*, 467; (c) A. I. Lesnikovich, O. A. Ivashkevich, S. V. Levchik, A. I. Balabanovich, P. N. Gaponik, A. A. Kulak, *Thermochim. Acta* **2002**, *388*, 233.

[13] H. Gao, Z. Zeng, B. Twamley, J. M. Shreeve, *Chem. Eur. J.* **2008**, *14*, 1282.

[14] **(a)** M. J. Crawford, T. M. Klapötke, F. A. Martin, C. M. Sabaté, M. Rusan, *Chem. Eur. J.* **2011**, *17*, 1683; **(b)** M. J. Crawford, K. Karaghiosoff, T. M. Klapötke, F. A. Martin, *Inorg. Chem.* **2009**, *48*, 1731.

[15] H. Muthurajan, R. Sivabalan, M. B. Talawar, M. Anniyappan, S. Venugopalan, *Journal of Hazardous Materials* **2006**, *A133*, 30.

[16] Y. Huang, H. Gao, B. Twamley, J. M. Shreeve, *Eur. J. Inorg. Chem.* **2007**, *14*, 2025.

[17] **(a)** E. Abele, R. Abele, E. Lukevics, *Chem. Heterocycl. Compd.* **2008**, *44*, 769; **(b)** L. V. Myznikov, A. Hrabalek, G. I. Koldobskii, *Chem. Heterocycl. Compd.* **2007**, *43*, 1; **(c)** R. Kharb, Pr. C. Sharma, M. S. Yar, *J. Enzym. Inhib. Med. Chem.* **2011**, *26*, 1; **(d)** S. Cronin, P. H. Chandrasekar, *J. Antimicrob. Chemother.* **2010**, *65*, 410.

[18] J. P. Zhang, Y. B. Zhang, J. B. Lin, X. M.Chen, *Chem. Rev.* **2012**, *112*, 1001.

[19] N. Masciocchi, S. Galli, A. Sironi, *Comments Inorg. Chem.* **2005**, *26*, 1.

[20] (a) Z. P. Demko, K. B. Sharpless, *J. Org. Chem.* **2001**, *66*, 7945; (b) Z. P. Demko, K. B. Sharpless, *Angew. Chem. Int. Ed.* **2002**, *41*, 2110.

[21] J. Jusélius D. Sundholm. *Phys. Chem* **2000**, *2*, 2145.

[22] Ch. T. Walsh, S. Garneau-Tsodikova, A. R. Howard-Jones, *Nat. Prod. Rep*. **2006**, *23*, 517.

[23] **(a)** M. K. Ehlert, A. Storr, R. C. Thompson, *Can. J. Chem.* **1993**, *71*, 1412; **(b)** N. Masciocchi, G. A. Ardizzoia, S. Brenna, G. La Monica, A. Maspero, S. Galli, A. Sironi, *Inorg. Chem.* **2002**, *41*, 6080; **(c)** M. K Ehlert, A. Storr, R. C. Thompson, F. W. B Einstein, R. J. Batchelor, *Can. J. Chem.* **1993**, *71*, 331; **(d)** T. L. Hu, J. J. Wang, J. R Li, X H. Bu, *J. Mol. Struct.* **2006**, *796*, 18; **(e)** C. C. Quitmann, K. Z. Müller-Buschbaum, *Anorg. Allg. Chem.* **2005**, *631*, 1191; **(f)** A. Cingolani, S. Galli, N. Masciocchi, L.

Pandolfo, C. Pettinari, A. Sironi, *J. Am. Chem. Soc.* **2005**, *127*, 6144; **(g)** N. Masciocchi, G. A. Ardizzoia, A. Maspero, G. LaMonica, A. Sironi, *Inorg. Chem.* **1999**, *38*, 3657.

[24] **(a)** M. K. Ehlert, S. J. Rettig, A. Storr, R. C. Thompson, J. Trotter, *Can. J. Chem.* **1989**, *67*, 1970; **(b)** M. K. Ehlert, S. J. Rettig, A. Storr, R.C. Thompson, J. Trotter, *Can. J. Chem.* **1991**, *69*, 432.

[25] **(a)** S. J. Rettig, A. Storr, D. A. Summers, R. C. Thompson J. Trotter, *Can. J. Chem.* **1999**, *77*, 425; **(b)** S. J. Rettig, V. Sanchez, A. Storr, R. C. Thompson and J. Trotter, *J. Chem. Soc., Dalton Trans.* **2000**, 3931; (c) V. Sanchez, A. Storr, R. C. Thompson, *Can. J. Chem.* **2002**, *80*, 133.

[26] R. Lehnert, F. Seel, *Z. Anorg. Allg. Chem* **1978**, *444*, 91.

[27] S. J. Rettig, A. Storr, D.A. Summers, R.C. Thompson, J. Trotter, *J. Am. Chem. Soc.* **1997**, *119*, 8675.

[28] V. Sánchez, A. Storr, R. C. Thompson, *Can. J. Chem* **2002**, *80*, 133.

[29] X. M. Zhang, Y. F. Zhao, H. S. Wu, S. R. Batten, S. Weng Ng, Dalton Trans. **2006**, 3170.

[30] B. O. Patrick, W. M. Reiff, V. Sanchez, A. Storr, R. C. Thompson, *Polyhedron* **2001,** *20*, 1577.

[31] W. Ouellette, J. R. Galán-Mascarós, K. R. Dunbar, J. Zubieta, *Inorg. Chem.* **2006**, *45*, 1909.

[32] M. Grzywa, D. Denysenko, J. Hanss, Ernst-Wilhelm Scheidt, W. Scherer, M. Weil, D. Volkmer, *Dalton Trans.* **2012**, *41*, 4239.

[33] Y. Q. Tian, C. X. Cai, X. M. Ren, C. Y. Duan, Y. Xu, S. Gao, X. Z. You, *Chem. Eur. J.* **2003**, *9*, 5673.

[34] J. P. Zhang, Y. B. Zhang, J. B. Lin, X. M. Chen, *Chem. Rev.* **2012**, *112*, 1001.

[35] W. Ouellette, S. Jones, J. Zubieta, *Cryst. Eng. Comm.* **2011**, *13*, 4457.

[36] J. G. Haasnoot, *Coord. Chem. Rev.* **2000**, 200.

[37] **(a)** W. Ouellette, M. H. Yu, C. J. O'Connor, D. Hagrman, J. Zubieta, *Angew. Chem., Int. Ed.* **2006**, *45*, 3497; **(b)** W. Ouellette, A. V. Prosvirin, J. Valeich, K. R. Dunbar, J. Zubieta, *Inorg. Chem.* **2007**, *46*, 9067; **(c)** W. Ouellette, A. V. Prosvirin, V. Chieffo, K. R. Dunbar, B. Hudson, J. Zubieta, *Inorg. Chem.* **2006**, *45*, 9346.

[38] **(a)** H. Kooijman, A. L. Spek, J.G Haasnoot, J. Moscovici, K. Provost, A. Michalowicz, F. Renz, P. Gütlich, *Inorg. Chem.* **2000**, *39*, 1891; **(b)** A. F. Stassen, M. Grunert, E. Dova, M. Müller, P. Weinberger, G. Wiesinger, H. Schenk, W. Linert, J. G.Haasnoot, J. Reedijk, *Eur. J. Inorg. Chem.* **2003**, 2273.; **(c)** C. M. Grunert, J. Schweifer, P. Weinberger, W. Linert, *Inorg. Chem.* **2004**, *43*, 155.

[39] **(a)** S. R. Batten, S. M Neville, D. R. Turner, *Coordination Polymers: Design, Analysis and Applications*, Royal Cambridge, U.K., **2008**. **(b)** F. Herren, P. Fischer, A. Ludi, W. Hälg, *Inorg. Chem.* **1908**, *19*, 956; **(c)** A. Ludi, H.U. Gudel, *Struct. Bonding* **1973**, *14*, 1; **(d)** R. M. Bozorth, H. J. Williams, D. E. Walsh, *Phys. Rev.* **1956**, *103*, 572; **(e)** A. Ito, M. Suenaga, K. J. Ono, *Chem. Phys.* **1968,** *48*, 3597; **(f)** A. Goujon, F. Varret, V. Escax, A. Bleuzen, M. Verdaguer, *Polyhedron* **2001**, *20*, 1339; **(h)** V. Gadet, T. Mallah, I. Castro, M. J. Verdaguer, *Am. Chem. Soc.* **1992**, *114*, 9213; **(i)** W. D. Greibler, D. Babel, *Z. Naturforsch., Teil B* **1982**, *87*, 832.

[40] K. R. Dunbar, *Angew. Chem., Int. Ed.* **1996**, *35*, 1659.

[41] **(a)** S. Ferlay, T. Mallah, R. Ouahes, P. Veillet, M. Verdaguer, *Nature* **1995**, *378*, 701; **(b)** H. Miyasaka, N. Matsumoto, H. Okawa, N. Re, E. Gallo, C. Floriani, *Angew. Chem., Int. Ed. Engl.* **1995**, *34*, 1446; **(c)** W. R. Entley, G.S. Girolami, *Science* **1995**, *268*, 397; **(d)** J. S. Miller, A. J. Epstein, *Chem. Commun.* **1998**, 1319.

[42] J. S. Miller, J. L. Manson, *Acc. Chem. Res.* **2001**, *34*, 563.

[43] F. Thetiot, S. Triki, J. Sala Pala, *Polyhedron* **2003**, *22*, 1837.

[44] **(a)** S. R. Batten, P. Jensen, B. Moubaraki, K. S. Murray, R. Robson, *Chem. Commun*. **1998**, 439; **(b)** M. Kurmoo, C. J. Kepert, *New J. Chem.* **1998**, *22*, 1515; **(c)** J. L. Manson, C. R. Kmety, Q. Z. Huang, J. W. Lynn, G. M. Bendele, S. Pagola, P. W. Stephens, L. M. Liable Sands, A. L. Rheingold, A. J. Epstein, J. S. Miller, *Chem. Mater.* **1998**, *10*, 2552.

[45] S. R. Batten, K. S. Murray, *Coord. Chem. Rev*. **2003**, *246*, 103.

[46] S. R. Batten, B. F. Hoskins, B. Moubaraki, K. S. Murray, R. Robson, *J. Chem. Soc., Dalton Trans.* **1999**, 2977.

[47] J. L. Manson, E. Ressouche, J. S. Miller, *Inorg. Chem.* **2000**, *39*, 1135.

[48] H. Hoshino, K. Iida, T. Kawamoto, T. Mori, *Inorg. Chem.* **1999**, *38*, 4229.

[49] S. Triki, J. Sala Pala, M. Decoster, P. Molinie, L. Toupet, *Angew. Chem. Int. Ed.* **1999**, *38*, 113.

[50] R. P. Subrayan, A. H. Francis, J. W. Kampf, P. G. Rasmussen, *Chem. Mater.* **1995**, *7*, 2213.

[51] **(a)** O. W. Webster, *J. Am. Chem. Soc.* **1966**, *88*, 4055; **(b)** E. Simmons, R. D. Vest, S. A. Vladuchick, O. W. Webster, *J. Org. Chem.* **1980**, *45*, 5113.

[52] E. Oliveri-Mandala, T. Passalaqua, *Gazz. Chim. Ital.* **1912**, *41*, 430.

[53] G. Gryszkiewicz-Trochimowski, *Chem. Zentral Bl.* **1923**, *94*, 1366.

[54] C. D. Weis, *J. Org. Chem.* **1962**, *27*, 3695.

[55] D. S. Allan, D. F. Bergstrom, P. G. Rasmussen, *Synthetic Metals* **1988**, *25*, 139.

[56] **(a)** P. Johansson, S. Beranger, M. Armand, H. Nilsson, P. Jacobsson, *Solid State Ionics* **2003**, *156*, 129; **(b)** H. Markusson, S. Beranger, P. Johansson, M. Armand, P. Jacobsson, *J. Phys. Chem. A* **2003**, *107*, 10177.

[57] C. M. Sabaté, E. Jeanneau, H. Delalu, *Dalton Trans.* **2012**, *41*, 3817.

[58] **(a)** R. J. Less, M. McPartlin, J. M. Rawson, P. T. Wood, D. S. Wright, *Chem. Eur. J.* **2010**, *16*, 13723; **(b)** R. J. Less, T. C. Wilson, M. McPartlin, P. T. Wood, D. S. Wright, *Chem. Commun.* **2011**, *47*, 10007; **(c)** R. J. Less, B. Guan, N. M. Muresan, M. McPartlin, E. Reisner, T. C. Wilson, D. S. Wright, *Dalton Trans.* **2012**, *41*, 5919. **(d)** R. J. Less, T. C. Wilson, B. Guan, M. McPartlin, A. Steiner, P.T. Wood, D. S. Wright, *Eur. J. Inorg. Chem.* **2013**, *7*, 1161.

PART 3

5-CYANOTETRAZOLATE AS A LIGAND TOWARDS DIVALENT Cu(II) IONS

Abstract

A series of copper(II) complexes and coordination polymers incorporating the 5-cyanotetrazolate anion ($C_2N_5^-$) **(ctz)**, pyridine (**py**), 2,2′-bipyridine (**bipy**) and tris(pyrazol-*1*-yl)methane (**tpm**) have been characterized in the solid state. This part provides detailed crystal structure analyses and some magnetic investigations of the compounds $PPh_4[Cu(ctz)_3]$ **(1ctz)**, $[Cu(ctz)_2(bipy)]$ (**2ctz**), $[CuCl(py)_4](ctz) \cdot 2py$ **(3ctz)**, **[**$Cu_2(ctz)_6Cu(CH_3CN)_2(H_2O)_2] \cdot 2CH_3CN$ **(4a-ctz)**, $[Cu_2(ctz)_6Cu(H_2O)_3\{(CH_3)_2CO\}] \cdot 3(CH_3)_2CO$ **(4b-ctz)**, $[Cu(ctz)_2(py)_4]$ (**5ctz**), $[Cu_2(ctz)_4(bipy)_2]$ (**6ctz**), $[Cu_2(ctz)_2(tpm)_2(NO_3)]NO_3$ (**7ctz**). In the presence of water, the CN group undergoes hydrolytic transformation forming the $C(O)NH_2$ carboxamide. This copper-mediated process leads to tetrazolate-5-carboxamide $(N_4C_2(O)NH_2)^-$ (**tca**) observed as a ligand in the compounds $[Cu(tca)_2(bipy)] \cdot H_2O$ **(8tca)**, its mixed crystal of $[Cu_2(ctz)_2(tca)_2(bipy)_2]_{0.5}[Cu_2(ctz)_4(bipy)_2]_{0.5}$ **8a-tca** and $Cu(tca)_2 \cdot 2H_2O$ **(9tca)**.

3.1 Introduction

Tetrazole and its 5-substituted derivatives are in the focus of research owing to their diverse properties. The biological activity of the acidic tetrazole group (CN_4H) is investigated, as it acts as a surrogate for carboxylic groups (CO_2H) and found its way into pharmacologically active compounds.[1] Their high nitrogen content also makes tetrazolates good candidates for energetic materials like rocket propellants,[2,3] or energetic polymers.[4] A new family of energetic salts containing the tetrazolate anion and nitrogen-rich cations has been extensively investigated by Shreeve[5] and by Klapötke and co-workers.[2] The functionality of tetrazoles is based on the five-membered CN_4H heterocyclic system with four concatenated N atoms and on a moderately N–H acidic character.[1] 5-Cyanotetrazole HN_4CCN (Hctz), classified as a mixed ligand possessing a functional cyano group,[6] was fully characterized by X-ray single diffraction in 2012,[7] although it was prepared a century ago by Passalaqua and Oliveri-Mandala[8] through [2+3] dipolar cycloaddition[9] between hydrazoic acid HN_3 and cyanogen $(CN)_2$. There are only a few structural reports of the cyanotetrazolate anion $(C_2N_5)^-$ (ctz). In addition to the salts of ctz with nitrogen-rich bases,[2] these include the complex salt $[Co(ctz)(NH_3)_5](ClO_4)_2$,[10] phenylcyanotetrazole $H_5C_6–N_4C–CN$,[11] cesium, potassium, sodium, and silver cyanotetrazolate Cs(ctz),[12] K(ctz),[2] Na(ctz) · $1.5H_2O$,[2] Ag(ctz).[7] Some transition metal salts (Mn^{2+}, Fe^{2+}, Co^{2+}, Ni^{2+}, Cu^{2+}) have been only characterized by spectroscopic methods,[13] therefore they represent an almost unexplored area of coordination chemistry.

3.2 Results and Discussion

Hctz, is known to be formed readily from cyanogen $(CN)_2$ and aqueous hydrazoic acid HN_3. The cyclization occurs when HN_3 reacts as a dipole with an activated nitrile, yielding a five-membered heterocyclic ring system of four nitrogen atoms and one carbon atom. Two tautomeric forms are possible: 5-cyano-1*H*-tetrazole and 5-cyano-2*H*-tetrazole (Scheme 3.2.1). The DFT calculated gas phase energy shows that the 2-*H* form is 15.77 kJ/mol more stable with regard to the 1-*H* tautomer.[14] The ctz anion possesses four lone electron pairs on the N atoms of the aromatic ring system and one lone electron pair on the nitrogen atom of the cyano group and can, therefore, be considered as a multidentate *N*-donor ligand. Thus, the ctz is a good candidate for preparation of mononuclear, dinuclear, and oligonuclear complexes as well as for coordination networks of different dimensionalities. Moreover, the negatively charged ctz can compensate for the repulsive electrostatic forces between metals, resulting in short M···M contacts in the range 3.5 – 4 Å.[23] The aromatic heterocyclic ring of tetrazole possesses also a weak π-donor ability for the formation of charge-transfer complexes with π-acids.[24,25] The high versatility of the ctz anion opens a route for the synthesis of transition metal complexes of d-block metal ions with interesting structural and magnetic properties.

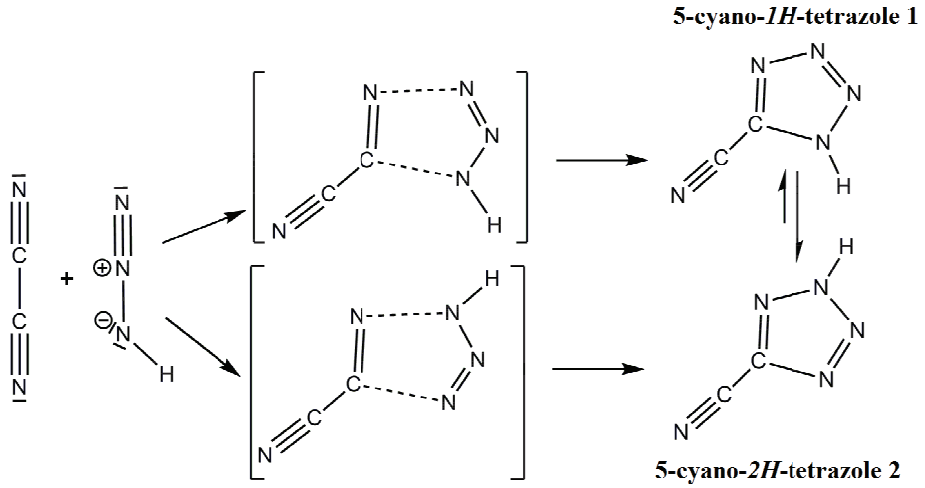

Scheme 3.2.1 The mechanism of the [2+3] dipolar cycloadditio between $(CN)_2$ and NH_3.

Under suitable conditions, ctz forms complexes and coordination polymers with Cu(II) ions. Owing to manifold of coordination modes, there is a tendency to form $Cu(ctz)_2$ polymers, which are sparingly soluble and difficult to characterize. We applied the principle of blocking coordination sites at the transition metal ion by additional neutral co-ligands like py, bidentate 2,2'-bipy, and tridentate tpm. Applying different methods of crystallization (see Experimental Part) a series of Cu(II) cyanotetrazolates could be obtained, which contain besides ctz other ligands attached to Cu(II). The exception is $PPh_4[Cu(ctz)_3]$ (**1ctz**), which is built from chains $[(Cu(ctz)_3)^-]_n$.

3.2.1 Coordination Modes of ctz in the Cu(II) Complexes

Several types of azolate ligands, like pyrazoles, imidazoles, triazoles and tetrazoles provide a large palette of coordination modes towards transition metals of the d-block with remarkable structural features and interesting magnetic properties.[6,23,26-28] Among these cyclic *N*-donor ligands, the tetrazolate ion exhibits the highest number of coordination modes due to the presence of four nitrogen atoms with lone electron pairs and therefore allows for various binding modes. In principle, all four N atoms of the five-membered ring are able to bind towards a transition metal ion, since the basicities of the individual N atoms are comparable.[23,25] Consequently, the deprotonated tetrazolate unit of Hctz is found in the structures of the compounds **1ctz**-**7ctz** in various coordination modes as a terminal, monodentate ligand, coordinating via *N*(1) and *N*(2) ($\kappa^1N(1)$ and $\kappa^1N(2)$), as a bidentate ligand in three of the four possible coordination modes ($\kappa^2N(1,2)$, $\kappa^2N(1,3)$, $\kappa^2N(2,3)$, but not $\kappa^2N(1,4)$) and as a tridentate ligand in one of the two possibilities ($\kappa^3N(1,2,4)$, but not $\kappa^3N(1,2,3)$). The conceivable tetradentate function $\kappa^4N(1,2,3,4)$ was not observed. The binding modes are summarized in Scheme 3.2.1.1. Moreover, the lone electron pair on the N atom of the cyano group of the ctz ion can coordinate and duplicate the number of possible coordination modes

from nine to eighteen. In the structures of Cs(ctz),[12] K(ctz)[2] and Ag(ctz),[7] ctz binds through all tetrazolate N atoms and the CN group is engaged in the coordination sphere around the M^+ cations.

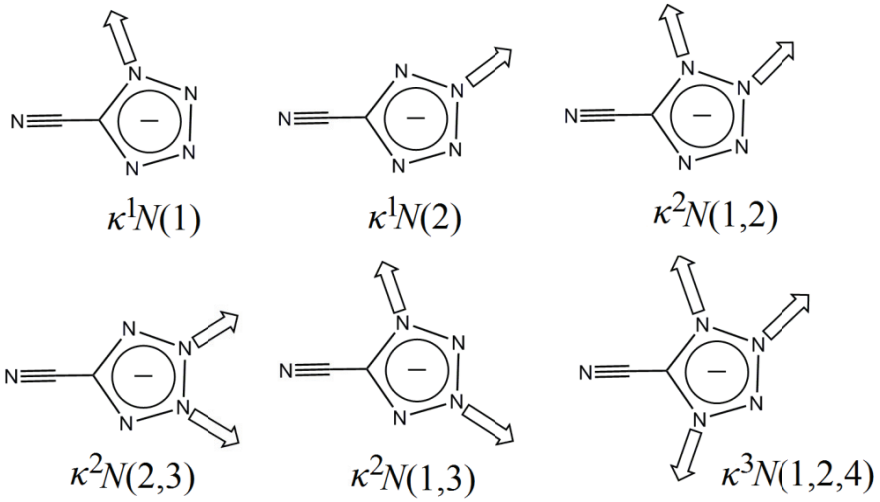

Scheme 3.2.1.1 The various binding modes of the tetrazolate unit of ctz observed in the structures of **1ctz**-**7ctz** compounds.

The proximity of the N atoms ensures the tetrazolate anion is preferably a bridging ligand. The structure analyses of the Cu(II) 5-cyanotetrazolate compounds **1ctz**-**7ctz** revealed the specific bridging functions of ctz. The $\kappa^2N(1,2)$ and the $\kappa^2N(2,3)$ modes are found as the most common in the structures of **1ctz**, **4a-ctz**, **4b-ctz**, **6ctz,** and **7ctz** and allow the formation of 1D chains or dinuclear entities as in **6ctz** or **7ctz**. The $\kappa^2N(1,3)$ coordination mode appears only in the structure of the coordination polymer **2ctz**. In the layered 2D structures of **4a-ctz** and **4b-ctz**, ctz acts as a tridentate ligand, bridging two Cu ions in both, the $\kappa^2N(2,3)$ and the $\kappa^2N(1,2)$ fashion and additionally coordinates to a third Cu ion through $N(4)$. In the structures of the mononuclear and dinuclear complexes **5ctz** and **6ctz**, as well as in the coordination polymer **2ctz**, ctz is present as a terminal monodentate ligand in the $\kappa^1N(2)$ or $\kappa^1N(1)$ fashion. Finally, in the structure of **3ctz**, ctz is not coordinated to the transition metal ion and acts only as a counter-ion for the positively charged $[CuCl(py)_4]^+$ complex. In all examined cases, the cyano group remains uncoordinated.

3.2.2 Molecular Geometry of ctz in the Cu(II) Complexes

The structures of the ctz anions in all characterized compounds deviate only to a small extent. The bond lengths C–N and N–N and the angles C–N–N, N–N–N and N–C–N within the heterocyclic rings are similar and found in the range between 1.308(4)–1.355(4) Å and 102.0(3)–114.0(4)°. They are comparable with the calculated structure of ctz[12] (Appendix E). The approximately equal N–N (sp^2-sp^2) and C–N (sp^2-sp^2) bond lengths within the ring indicate that

the bonds have an intermediate character between a double and a single bond within the delocalized π-electron system of the aromatic ring.[29] The five-membered N_4C rings in the structures of **1ctz-7ctz** are almost planar, the torsion angles N–N–N–N in the rings are close to 0° with maximal deviation of 1.1(3)°. The exocyclic C–C bond lengths are in the range of 1.417(8)–1.446(8) Å and reflect the mixed sp^2-sp hybridization type of the two C atoms connected by a shortened single bond.[30] The electron withdrawing cyano groups at the 5-position of the tetrazolate units generally deviate slightly from the plane of the aromatic ring systems with maximal deviation from planarity of less than 5°. The C–C≡N angles vary between 175.6(5) and 179.3(8) °. The short C≡N distances of those of cyano groups (1.130(8)–1.153(6) Å) correspond to bond order three and are comparable with other nitriles.[31] Generally, in the structures of the compounds **1ctz-7ctz**, the ideal C_{2v} symmetry of the ctz anion is slightly deformed due to the coordination to the copper(II) centres. Other effects like the packing arrangement of the molecules or non-covalent interactions between molecules may also play also a role.

3.2.3 1D Chains

The compounds **1ctz**, **2ctz** and **3ctz** represent novel 1D coordination polymers with ctz anions and copper(II) cations as the main structural components. Blocking of the coordination sites on the Cu ions with additional mono and bidentate ligands (py, 2,2'-bipy) or by using an excess of ctz in the presence of counterions (Cl^-, PPh_4^+) effectively restricts the connection of the concatenated complexes in the structures to one dimension. Different crystallization techniques using various solvents also have a significant influence on the crystal structures. The crystal structures of **1ctz**, **2ctz**, and **3ctz** are dominated by 1D-connected coordination units of ctz and Cu(II) ions. The blue needle-shaped crystals of **1ctz** and **2ctz** are both centrosymetric, whereas the structure of dark blue block-shaped crystals of **3ctz** is best described in the non-centrosymetric space group *Cc*. In the structure of $PPh_4[Cu(ctz)_3]$ **(1ctz)** the two crystallographically independent cations Cu1 and Cu2 are located at inversion centres (Figure 3.2.3.1). Each Cu centre is surrounded by six N atoms of six ctz anions in octahedral fashion with a significant axial elongation of two Cu–N bonds. In both independent CuN_6 octahedra, two *trans*-positioned Cu–N bonds are longer (Cu1–N11 2.365(3) Å, Cu2–$N1^i$ 2.327(3) Å) than those in the equatorial planes (Cu1–$N_{(equat)}$ 2.001(3) – 2.044(3) Å, Cu2–$N_{(equat)}$ 2.012(3) – 2.036(3) Å), which gives the coordination polyhedron shape of an elongated octahedron with idealized D_{4h} point symmetry, typical for the Jahn-Teller effect of the divalent Cu ion. The three independent ctz ions link the Cu ions through the $\kappa^2N(1,2)$ and $\kappa^2N(2,3)$ bridging mode to a linear chain $[(Cu(ctz)_3)^-]_n$ along the crystallographic *a*-axis. The Cu1···Cu2 distances within the chain are uniform and amount to 3.769(1) Å. The tetraphenylphosphonium cations are located between the $[(Cu(ctz)_3)^-]_n$ chains and separate them widely. The overall arrangement of anionic chains and cations stacks has a hexagonal rod packing motif (Figure. 3.2.3.1).[32]

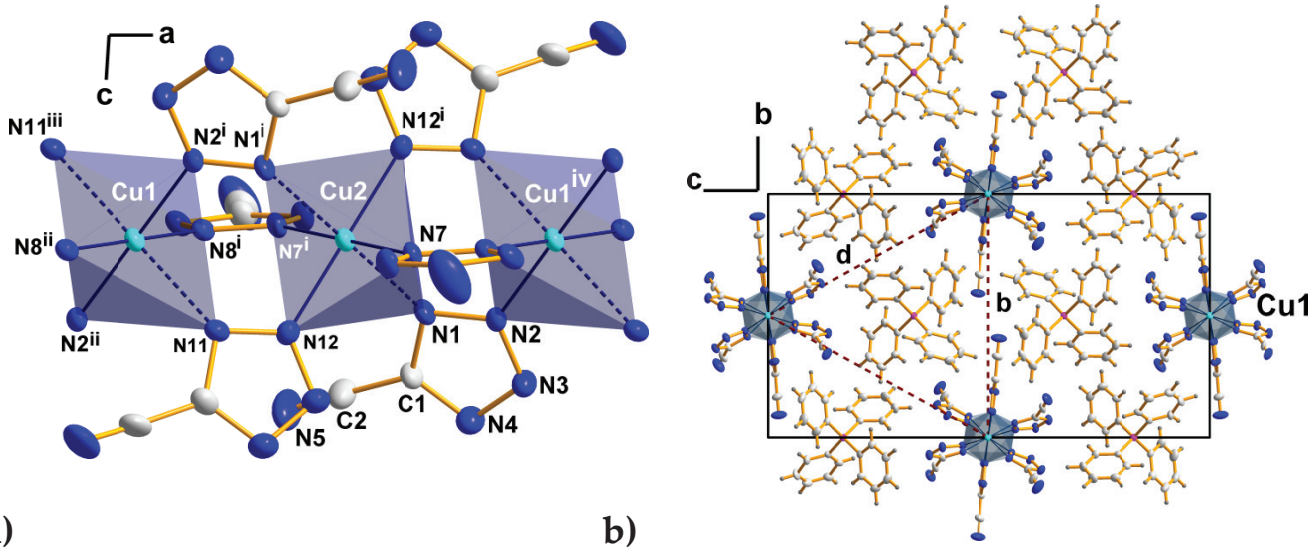

Figure 3.2.3.1 The crystal structure of $PPh_4[Cu(ctz)_3]$ (**1ctz**). **(a)** The section of the linear chain of $[(Cu(ctz)_3)^-]_n$. Dashed lines indicate the elongated Cu–N bonds within the CuN_6 polyhedra. Displacement ellipsoids are drawn at the 50% probability level. H atoms are drawn with arbitrary radii. **(b)** The view of the unit cell along *a*-axis is depicted showing the hexagonal rod packing of the $[(Cu(ctz)_3)^-]_n$ chains and the stacked PPh_4^+ ions. Dashed lines indicate the distances between the Cu ions of neighboured chains (b = 15.09 Å, d = 15.61 Å). Symmetry codes: (i) $-x+2, -y+1, -z$; (ii) $x-1, y, z$; (iii) $-x+1, -y+1, -z$; (iv) $x+1, y, z$.

In the presence of the chelating 2,2'-bipyridine ligand, $[Cu(ctz)_2(bipy)]$ (**2ctz**) crystallizes as a second variant of a chainlike structure with bridging ctz ligands. $[Cu_2(ctz)_4(bipy)_2]$ (**6ctz**) is an isomer of **2ctz** with a molecular structure of dinuclear complexes, see below. In the structure of **2ctz**, only one independent Cu ion is present, which is coordinated by three ctz anions and one 2,2'-bipy ligand, resulting in a distorted CuN_5 square pyramidal coordination environment with idealized C_{4v} symmetry. The basal plane of the coordination polyhedron is a slightly distorted square with Cu–N bond lengths of 2.000(3) to 2.023(3) Å, the apical Cu–N bond length is longer and amounts to 2.279(3) Å (Figure. 3.2.3.2). The four basal coordinating N atoms (N12, N11, $N3^i$, and N6) deviate from the least-squares plane by approximately 0.09 Å, the copper ion is displaced out of this plane by 0.184 Å in direction of the apical nitrogen atom. One basal position is occupied by a N atom of a terminal ctz ion, which coordinates in the $\kappa^1N(1)$ fashion. The axial and one basal positions are occupied by two $\kappa^2N(1,3)$ bridging ctz ligands, which link the coordination polyhedra to infinite chains, that propagate along the 2_1 screw axes in the crystallographic *b* direction. The Cu atoms in the chain are arranged in a plane zigzag motif and are separated by 6.105(1) Å (Figure. 3.2.3.2).

$[CuCl(py)_4](ctz) \cdot 2py$ (**3ctz**) was obtained from $CuCl_2$ and Hctz in pyridine as solvent. The crystal structure also represents a chain motif, which is, however, distinct from the chains in the structures of **1ctz** and **2ctz**. The crystal structure of **3ctz** consists of concatenated $\{CuCl_2(py)_4\}$ octahedral complexes, mono-bridged by Cl^- ligands to form almost linear $[(CuCl(py)_4)^+]_n$ chains. In the strongly distorted $\{CuCl_2(py)_4\}$ octahedra, the bridging Cl^- ions are in the *trans* positions. The $[\cdots Cu–Cl\cdots Cu–Cl\cdots]_n$ chains are asymmetric with respect to the Cu–Cl bond lengths, which differ substantially (2.6226(4) Å and 3.1075(4) Å).

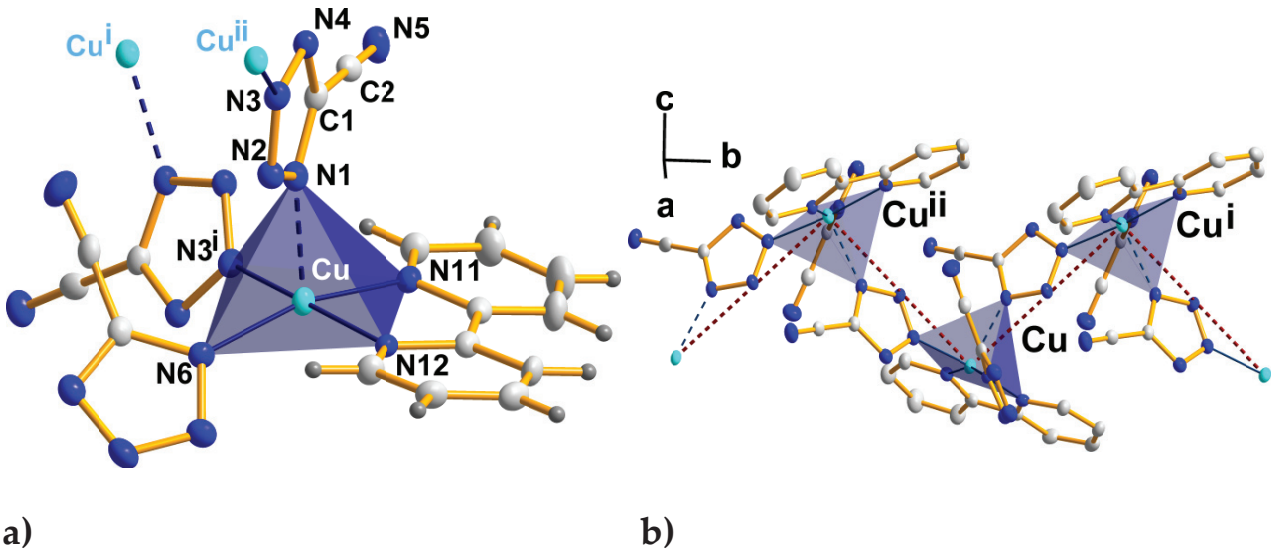

Figure 3.2.3.2 The crystal structure of $[Cu(ctz)_2(bipy)]$ (**2ctz**). **(a)** The square pyramidal coordination environment of the Cu ion. **(b)** The section of the $[Cu(ctz)_2(bipy)]_n$ chain with the zigzag motif of the Cu ions (dotted line). The CuN_5 coordination polyhedra are represented by transparent square pyramids around the metal centres. Displacement ellipsoids are drawn at the 50% probability level. H atoms are omitted for clarity. Symmetry codes: (i) $-x+1$, $y-1/2$, $-z+3/2$; (ii) $-x+1$, $y+1/2$, $-z+3/2$.

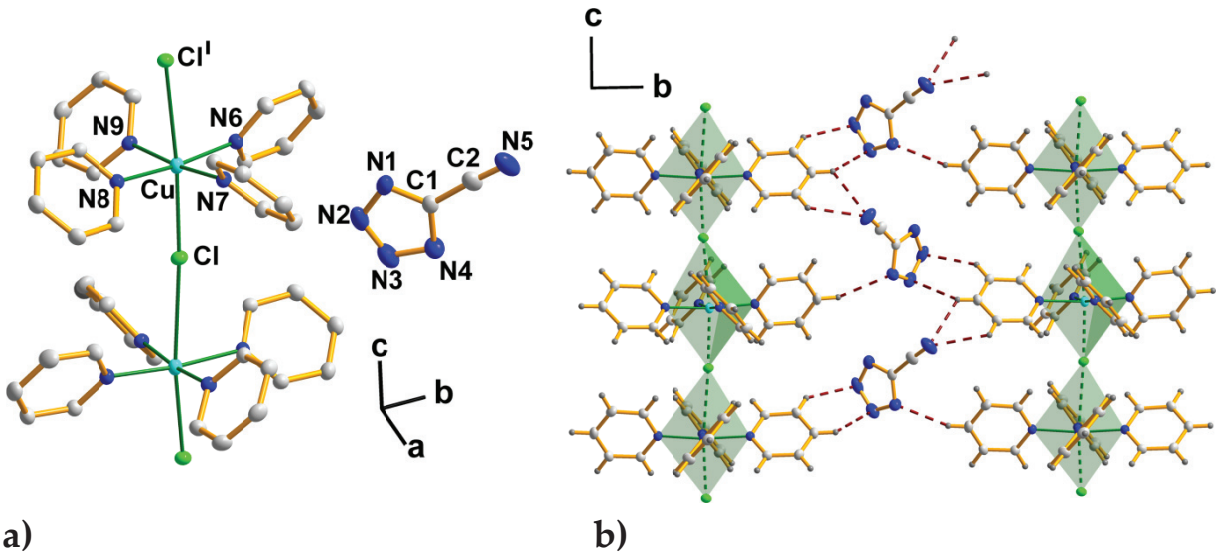

Figure 3.2.3.3 The crystal structure of $[CuCl(py)_4](ctz) \cdot 2py$ (**3ctz**). **(a)** A section of the $[(CuCl(py)_4)^+]_n$ chain and the isolated ctz anion. **(b)** Larger section of structure including the C–H···N short contacts (C···N 3.290(3)-3.475(2) Å) (thick dashed lines)). Solvate pyridine molecules are omitted for clarity. Displacement ellipsoids are drawn at the 50% probability level. H atoms are drawn with arbitrary radii. Symmetry code: (i) x, −y+1, z−1/2.

This asymmetry has already been observed for halo-bridged copper(II) complexes.[33] The equatorial plane is defined by four N atoms of pyridine ligands with Cu–N lengths of 2.026(1)–2.040(1) Å. The structure of the cationic chain is thus dominated by a very pronounced Jahn-Teller effect. The ctz is not coordinated to the metal ions and plays only the role of isolated counterion in the lattice (Figure 3.2.3.3). The crystals contain additionally two molecules of pyridine as solvate. The uncoordinated ctz anions and the solvate pyridine molecules reside in

the inter-chain space. A series of C–H···N short contacts occur between the nitrogen atoms of ctz and the carbon atoms of the coordinated pyridine ligands (Figure 3.2.3.3).

3.2.4 2D Layer Motifs

The absence of strong donor co-ligands allows expanded catenation among the structures of Cu(II) cyanotetrazolates to two dimensions. The presence of weakly coordinating ligands such as acetone, acetonitrile and water, which were used as solvents, is essential for the formation of the layered structures **4a-ctz** and **4b-ctz** (Figure 3.2.4.1 and Figure 3.2.4.2). The blue crystals of both, $[Cu_2(ctz)_6Cu(CH_3CN)_2(H_2O)_2] \cdot 2CH_3CN$ (**4a-ctz**) and $[Cu_2(ctz)_6Cu(H_2O)_3\{(CH_3)_2CO\}] \cdot 3(CH_3)_2CO$ **(4b-ctz)** are triclinic but with different unit-cell contents. The basic unit of **4a-ctz** is made up by three crystallographically independent Cu atoms located in the inversion centres. Three ctz, two acetonitrile molecules and one water molecule are located in the general positions. The crystal structure of **4b-ctz** represents a very similar structural motif and is build analogously to **4a-ctz**. In contrast to the acetonitrile solvate **4a-ctz**, the basic unit of the acetone solvate **4b-ctz** is characterized by four crystallographically independent Cu atoms, two of which are located in inversion centres, six ctz anions, three water and four acetone molecules. The structures of **4a-ctz** and **4b-ctz** both contain two different kinds of Cu coordination polyhedra, CuN_6 for **4a-ctz** and **4b-ctz**, CuN_4O_2 for **4a-ctz** and CuO_4N_2 for **4b-ctz**, all of which represent octahedra with strong Jahn-Teller distortions. The CuN_6 sites of **4a-ctz** and **4b-ctz** are defined by six nitrogen atoms of the ctz ligands with axial elongation of two Cu–N bond lengths to ca 2.35 Å, which are significantly longer than those from the equatorial bonds (average 2.03 Å). The Cu atoms in the CuN_6 octahedra are interlinked through three ctz bridging ligands with κ^2N(1,2) and κ^2N(2,3) donor functions, to generate the $[(Cu(ctz)_3)^-]_n$ chains, which are analogous to those in the structure of **1ctz**. Within the chains, the Cu(II) centres are separated by 3.848(1) Å in the acetonitrile solvate **4a-ctz** and 3.889(1) Å for Cu1···Cu2 and 3.798(1) Å for Cu2···Cu3 in the acetone solvate **4b-ctz**. The chains form layers through a presence of the second kind of Cu complexes. The octahedral CuN_4O_2 units of the **4a-ctz** involve two aqua and two ctz ligands in the equatorial plane, whereas the strong axial elongation is present at the two acetonitrile ligands (Cu1–N1 2.353(3) Å). The CuO_4N_2 units of **4b-ctz** are built by two N atoms of two ctz ligands, four O atoms of three coordinated water molecules and one acetone molecule. Two oxygen atoms of one acetone and one aqua ligand occupy the axial positions and the respective Cu–O bonds are strongly elongated (Cu4–O4 2.388(1) Å and Cu4–O2W 2.265(1) Å). The connectivity between the CuN_6 and the CuN_4O_2 units in the structure of **4a-ctz** and the CuN_6 and CuO_4N_2 units of **4b-ctz** is achieved through the sharing of two crystallographically related ctz ligands. These anions act as bidentate donor ligands through the atoms N1 and N2 within the chains, but coordinate with atom N4 of the tetrazole ring to the Cu atom, which is located between the chains, and thus gain the function of trinucleating κ^3N(1,2,4) linkers.

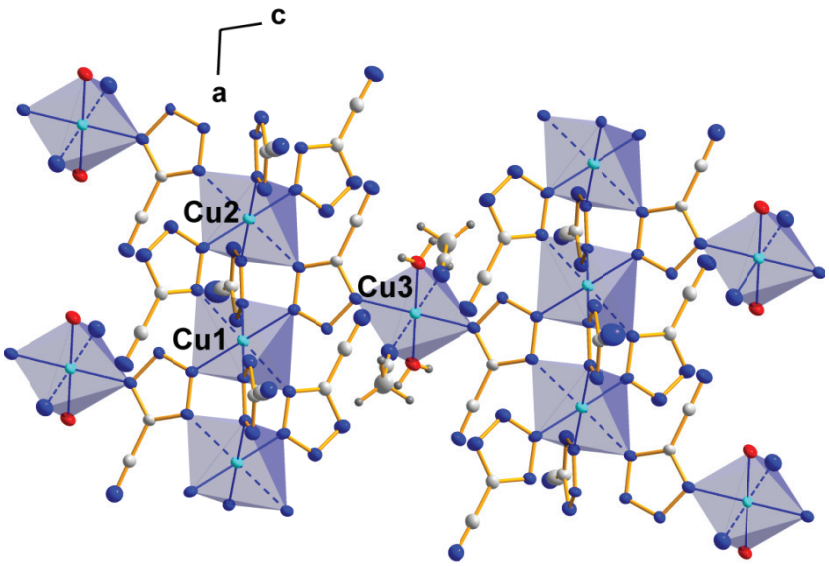

Figure 3.2.4.1 The crystal structure of $[Cu_2(ctz)_6Cu(CH_3CN)_2(H_2O)_2] \cdot 2CH_3CN$ (**4a-ctz**). The view perpendicular to the layer along the [010] is given. The solvate molecules, which are embedded between the layers, are not included. Dashed lines indicate the long Cu–N bonds within the Jahn-Teller distorted coordination octahedra. Displacement ellipsoids are drawn at the 50% probability level. H atoms are drawn with arbitrary radii.

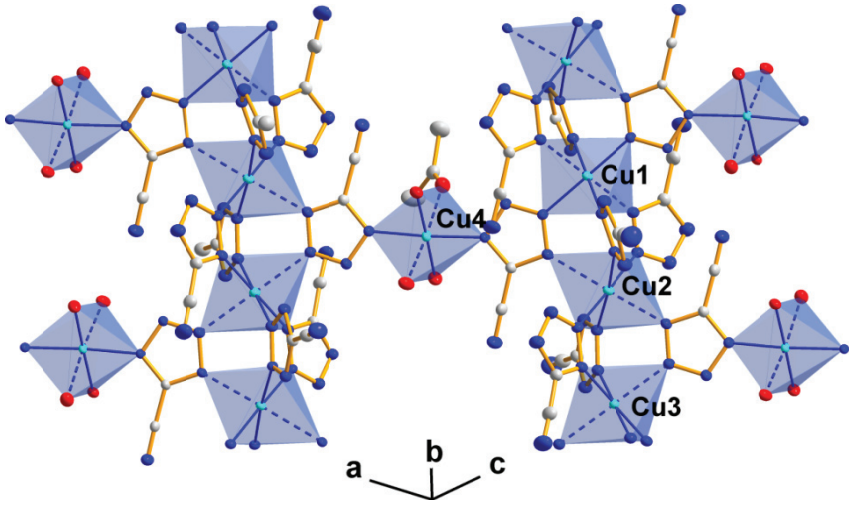

Figure 3.2.4.2 The crystal structure of $[Cu_2(ctz)_6Cu(H_2O)_3\{(CH_3)_2CO\}] \cdot 3(CH_3)_2CO$ (**4b-ctz**). Dashed lines indicate the long Cu–N bonds within the Jahn-Teller distorted coordination octahedra. Displacement ellipsoids are drawn at the 60% probability level. H atoms are omitted for clarity.

Accordingly, for **4a-ctz,** the shortest distances between the copper ions Cu3···Cu1 and Cu3···Cu2 in the *ac*-plane are 5.892(1) Å and 6.447(1) Å, respectively. In the structure of **4b-ctz**, the respective distances between Cu4···Cu1 and Cu4···Cu2 in the [111] plane are 5.951(1) Å and 6.496 (1) Å, respectively. Some H bonding is present in both structures. The polar O–H bonds of the aqua ligands attract the nitrogen atoms of acetonitrile solvate molecules in **4a-ctz** and acetone solvate molecules of **4b-ctz** (Appendix E). Additionally, the CN groups of neighbouring ctz ligands are involved in O–H····N bonding with H····N distances close to 2.0 Å (Appendix E).

3.2.5 Mononuclear and Dinuclear Complexes

The formation of the polymeric cationic chain $[(CuCl(py)_4)^+]_n$ involving Cu–Cl···Cu bridges from $CuCl_2$ and Hctz in the presence of pyridine as solvent encouraged us to repeat this synthesis in the absence of coordinating Cl^- anions. The replacement of $CuCl_2$ by the polymeric copper 5-cyanotetrazolate of tentative composition $Cu(ctz)_2$ produces dark blue crystals of $[Cu(ctz)_2(py)_4]$ (**5ctz**). The triclinic unit cell of **5ctz** contains two discrete molecular complexes. The Cu(II) central atom has a distorted octahedral [2+4] coordination. The equatorial plane is defined by four nitrogen atoms of the pyridine donor ligands with similar Cu–N distances (2.027(1) – 2.045(1) Å). The axial positions are occupied by the N atoms of two ctz anions with a significant elongation of two Cu–N bonds (averaged 2.62 Å), typical for the Jahn-Teller distortion. The ctz anions are coordinated to the metal centre only by one donor atom of the five-membered tetrazole ring in the $\kappa^1N(2)$ fashion. These terminal ligands are bound in a 'bend' way relative to the axial direction, which shows the high conformational flexibility of the ctz ligand (Figure 3.2.5.1). A similar mononuclear structure of $[Mn(ctz)_2(bipy)_2]$ **5a-ctz** is isolated if manganese(II) acetate, Hctz and the sterically more demanding 2,2'-bipy are used. Interestingly, the orientation of two crystallographically independent ctz ions differs from the **5ctz** complex. In the slightly distorted octahedral sphere around the manganese(II) cations, ctz ligands adopt the *cis*-configuration with $\kappa^1N(2)$ fashion, so the coordination is established by 2,2'-bipy bidentate ligands.

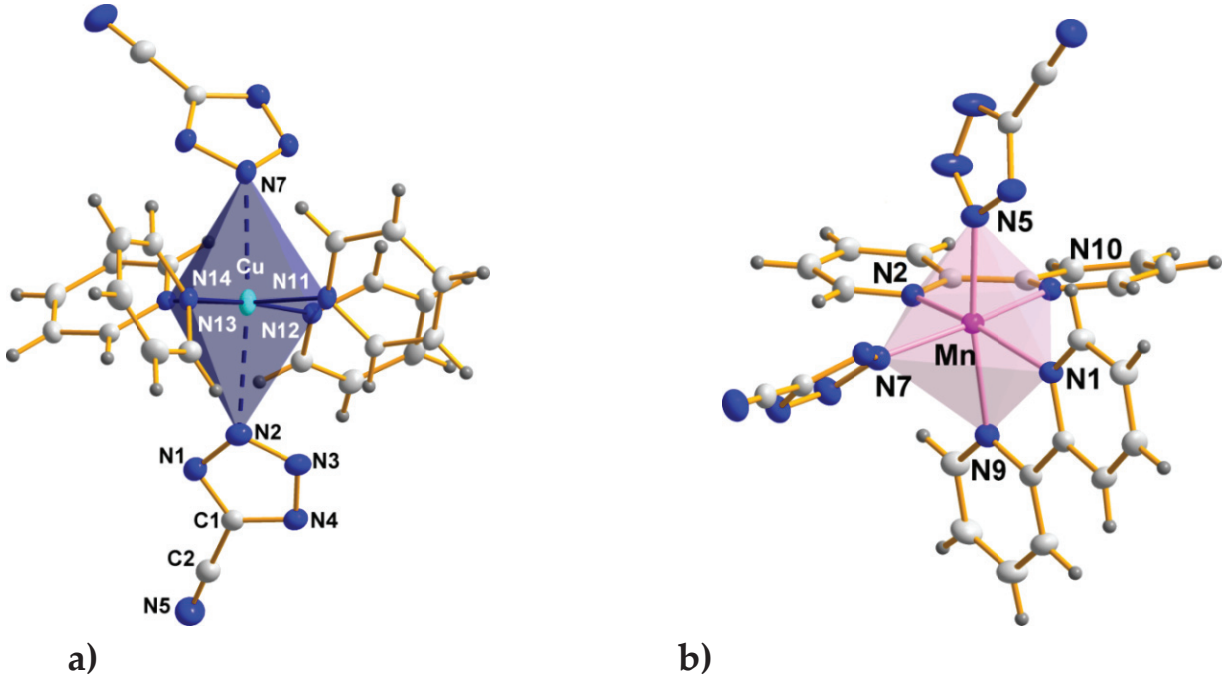

Figure 3.2.5.1 The structure of the molecular complex $[Cu(ctz)_2(py)_4]$ (**5ctz**) **(a)** and the structure of $[Mn(ctz)_2(bipy)_2]$ (**5a-ctz) (b)** as an example of *cis* and *trans* coordination of the ctz ligand. Dashed lines indicate the elongated Cu–N bonds within the CuN_6 coordination polyhedron. Displacement ellipsoids are drawn at the 50% probability level. H atoms are drawn with arbitrary radii.

The dinuclear copper complex $[Cu_2(ctz)_4(bipy)_2]$ (**6ctz**) shows a close structural relationship to the 1D coordination polymer $[Cu(ctz)_2(bipy)]$ (**2ctz**). Both are isomers with identical formula but different structure. In the dinuclear complex **6ctz**, two independent Cu atoms, denoted as CuA and CuB, have analogous square-pyramidal coordination spheres with one 2,2'-bipy ligand and three ctz anions (Figure 3.2.5.2). The Cu–N distances are uniform in the basal plane (ca. 2.01 Å), whereas the Cu–N distances to the apical position are much longer (ca. 2.26 Å), as observed in the structure of **2ctz**. The difference between the two structures lies in the linking of the coordination polyhedra by bridging ctz anions. In the structure of **2ctz**, the one bridging ctz coordinates to two Cu atoms in a $\kappa^2N(1,3)$ fashion, in contrast to the structure of **6ctz**, in which two bridging ctz ligands connect two Cu atoms in a $\kappa^2N(2,3)$ fashion. The centrosymmetry of **6ctz** causes two pentagonal pyramids, which are directed in the opposite orientations with the respect to the pseudo-fourfold axes. The Cu(II) ions are 4.034(1) Å apart for CuA···CuA^{i} and 4.180(1) Å for CuB···CuB^{i}.

The reaction between $Cu(NO_3)_2 \cdot 3H_2O$, tpm and Hctz in a 1 : 1 : 1 molar ratio with the support of a solution layering technique yields the crystals of $[Cu_2(ctz)_2(tpm)_2(NO_3)]NO_3$ (**7ctz**). The crystal structure belongs to the orthorhombic system and consists of dinuclear complexes. Each complex is bisected by two crystallographic mirror planes and by a two-fold rotation axis, to give the C_{2v} point symmetry. The Cu atoms are coordinated by the chelating tpm ligands, which block three positions in the coordinating sphere. The remaining three positions are occupied by two nitrogen atoms of two ctz anions and one O atom of the nitrate ion. The average Cu–N bond length in the equatorial plane of the coordination octahedron is 2.02 Å. The *trans*-positioned axial bonds are longer (Cu–N4 2.376(3) Å and Cu–O1 2.335(4) Å).

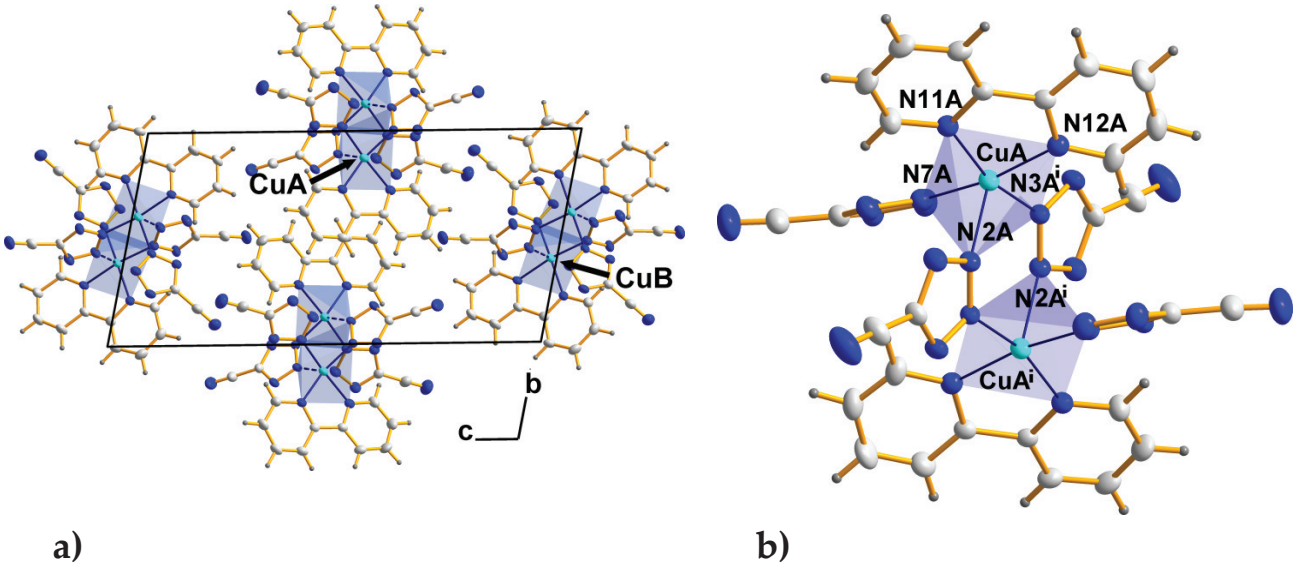

Figure 3.2.5.2 The structure **6ctz** is built of two independent dinuclear complexes $[Cu_2(ctz)_4(bipy)_2]$, denoted as A and B. **(a)** The projection of the unit cell along the *a*-axis. **(b)** The dinuclear complex A. Displacement ellipsoids are drawn at the 50% probability level. H atoms are drawn with arbitrary radii. Symmetry code: (i) $-x+1, -y+2, -z+1$.

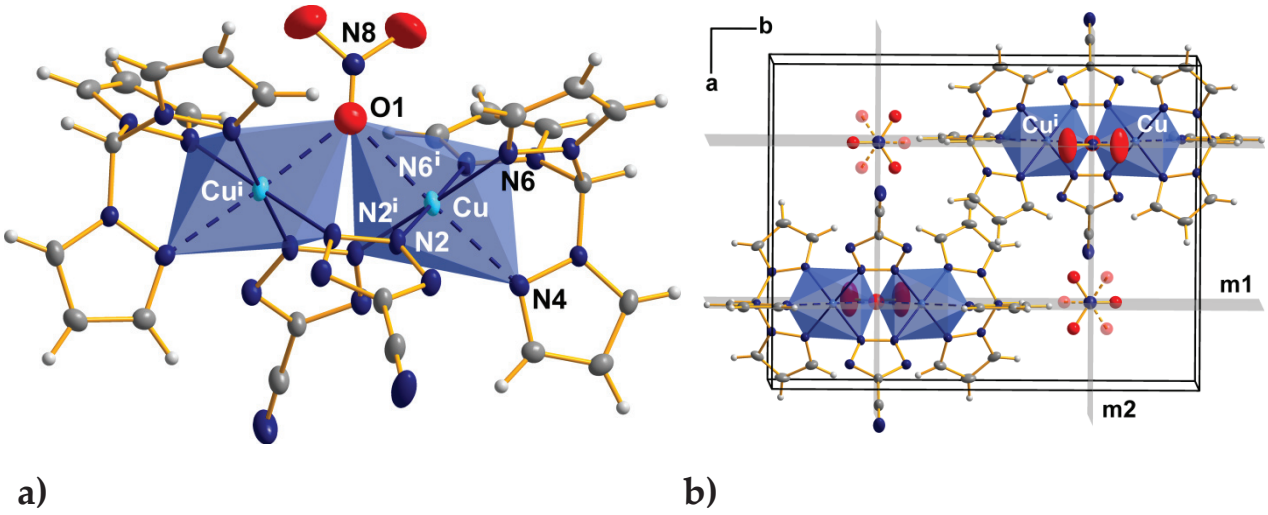

Figure 3.2.5.3 Crystal structure of $[Cu_2(ctz)_2(tpm)_2(NO_3)]NO_3$ (**7ctz**). **(a)** The individual complex. The atoms O1 and N8 have been refined with isotropic displacement parameters and are depicted as spheres. **(b)** The view of the unit cell along the *c* direction. The mirror planes that bisect the orthorhombic cell are marked as *m1* and *m2*. Displacement ellipsoids are drawn at the 50% probably level. H atoms are drawn with arbitrary radii. The atoms of the free nitrate ions are drawn as spheres. Symmetry code: (i) $-x+1/2, y, z$.

Two elongated $\{CuN_5O\}$ octahedra share one common corner at the position of the O atom. Two ctz anions connect the Cu ions in the $\kappa^2N(2,3)$ bridging fashion and separate them on the relatively short distance of 3.517(1) Å. To compensate the positive charge of the dinuclear complexes $[Cu_2(ctz)_2(tpm)_2(NO_3)]^+$, additional nitrate ions are present in the crystal structure, located in the *mm2* (C_{2v}) special positions (Figure 3.2.5.3).

3.2.6 Crystal Structures of Tetrazole-5-carboxamide Complexes of Divalent Cu(II)

The carboxamide group $C(O)NH_2$ offers two potentially binding atoms (oxygen and nitrogen) that can form a variety of coordination complexes upon isomerisation, tautomerization or deprotonation. The pure amide character of the NH_2 group in the neutral state makes the N atom a poor ligand, thus coordination through O as the donor is more frequent. Formation of nitrogen-bound metal carboxamide complexes requires the deprotonation of the amide nitrogen atom.[33,34] This occurs mainly in chelate rings (glycinamide, picolinamide and oxalamide) and very rarely for monodentate amide ligands.[36] The product of the copper-mediated hydration of ctz, namely tetrazole-5-carboxamide **(tca)** additionally offers four potentially metal binding sites from the deprotonated tetrazole ring. The structure analyses of compounds **8tca**, **8a-tca** and **9tca** revealed only three types of bridging modes, where the tca acts mainly as a tridentate ligand that coordinates through $\kappa^3N(1,3)O(7)$ or $\kappa^3N(1,2)O(7)$ or more rarely as a terminal monodentate $\kappa^1N(2)$ ligand. The investigations of their crystal structures show no significant structural changes in the average C=O and C–N bond lengths of the carboxamide group upon the cooper(II) coordination compared to free carboxamides.[36] The

binding to Cu ions always occurs through the carbonyl oxygen atom or through the tetrazolatate N atom with significant elongation of some *trans*-positioned Cu–$O_{(carbox)}$ or Cu–$N_{(tet)}$ bonds lengths typical for the Jahn-Teller effect (averaged 2.44 Å). Upon coordination to the metal centre the average C–N bond length of 1.32 Å gains a partial double bond character between a single aliphatic amine (1.45–1.47 Å)[37] and a double imine C=N bond (1.23–1.24 A).

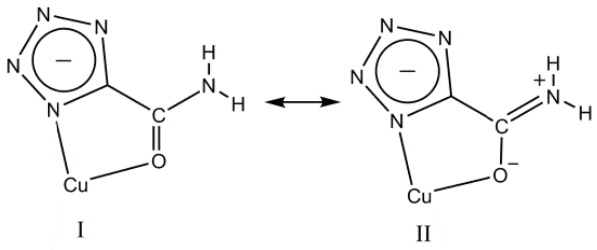

Scheme 3.2.6.1 A carboxamide resonance model of coordinated tca ligand in crystal structures **8tca** and **9tca**. The nitrogen bonds are arranged in a trigonal planar configuration as a result of sp^2 hybridization.

The observed lengthening of the C=O bonds (1.24 Å, compared with the typical C=O bonds for ketones (1.21–1.23 Å.[38])) and shortening of the C–N bonds for complexes **8tca**, **8a-tca** and **9tca** appoints to a hybrid structure of two resonance forms I and II and therefore explains the planarity and stability (Figure 3.2.6.1).[39]

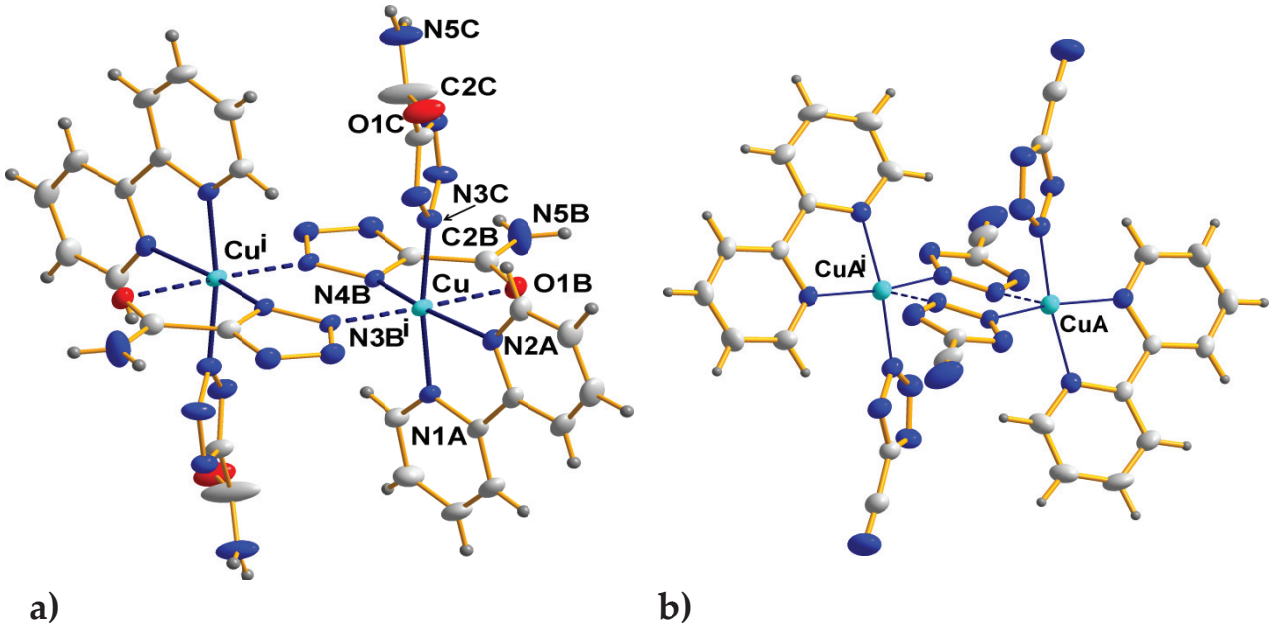

Figure 3.2.6.1 (a) The structure of dinuclear complex **8tca**. Symmetry code: (i) −x+1, −y+1, −z+1. **(b)** The structure of dinuclear complex **6ctz.** Symmetry code: (i) −*x*+1, −*y*+2, −*z*+1. In the both complexes two copper atoms are bridged by the tetrazolate moiety, but in the different fashion ($\kappa^3N(1,2)O(7)$ for **8tca** and $\kappa^2N(2,3)$ for **6ctz**). The dashed lines indicate the elongated Cu–N bonds. The molecule is drawn in the displacement ellipsoids at the 50 % probability level.

The ctz as a free ligand is stable in the presence of water, however the crystallization process with $Cu(NO_3)_2$ for more than 2 days at ambient temperature results in the copper-mediated hydration and yields mixed crystals of **8a-tca** complex with both the tetrazole-5-carboxamide (tca) and the 5-cyanotetrazolate (ctz) ligands present. Elongation of this time to 7 days leads to complex **8tca** where all CN groups are converted to $C(O)NH_2$ (Figrure 3.2.6.1).

The crystal structure analysis of **8tca** shows that the complex is dinuclear with $\kappa^3N(1,2)O(7)$-bridging by two nitrogen atoms of the tetrazolate ring. Each Cu atom is six-fold coordinated by three tca ligands and one 2,2'-bipy ligand, with two symmetry related, equatorially bridging tca ligands separating two metal ions in the distance of 4.085 Å. The axial positions in the complex are occupied by the terminal monodentate $\kappa^1N(2)$ tca ligands, in which the carbonyl group is disordered over two positions (site-occupancy factors 0.5 of each oxygen atom). When the time of crystallization is shorter, the new complex **8a-tca** crystallizes as a mixed-crystal compound that contains two different components (Figure 3.2.6.2). The asymmetric unit cell of **8a-tca** contains half on the dinuclear complex that means one divalent Cu ion, one bipy molecule and two ctz anions. However, during refinement, there were two significant residual electron density maxima (2.28 and 1.59 electrons per $Å^3$) near to the CN group of the bridging ligands indicating a compositional disorder between the ctz ligand and another moiety (Figure 3.2.6.2).

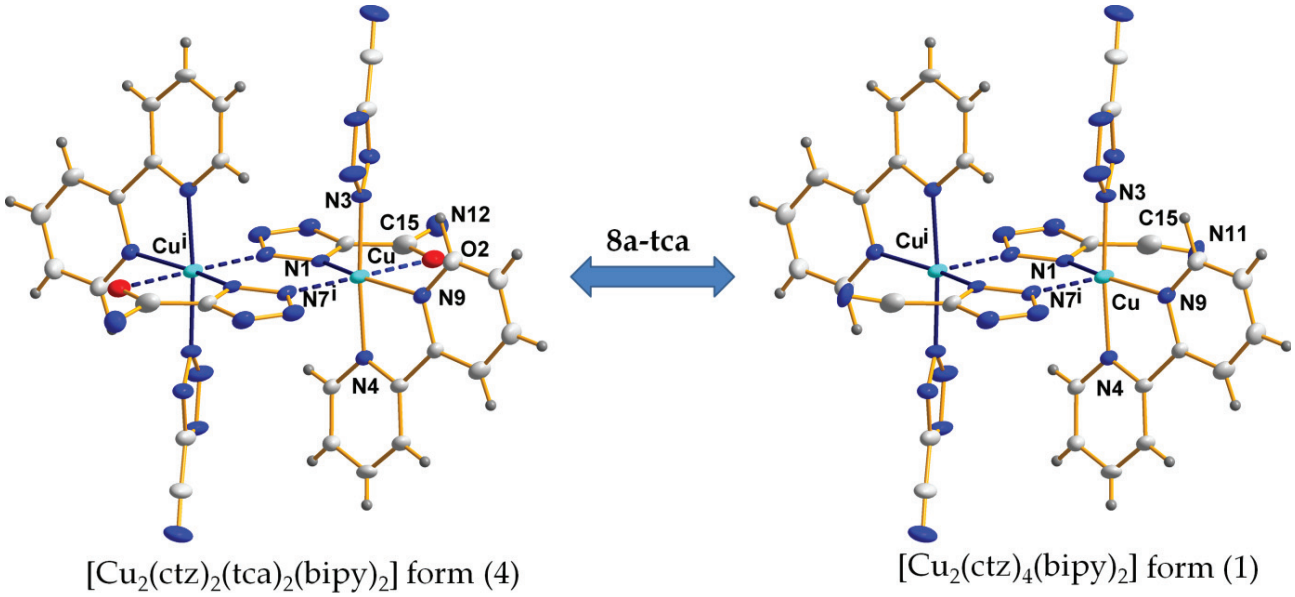

Figure 3.2.6.2 The crystal structure of the mixed crystal **8a-tca** reveals the positional disorder of two moieties. The molecules are drawn in the displacement ellipsoids at the 50 % probability level. The dashed lines indicate the elongated Cu–N bonds. It was assumed that form **1** and **4** are involved in the copper-mediated hydration of cyano group. For the detailed description see Scheme 3.2.7.2. Symmetry code: (i) $-x, -y, -z+2$.

Based on the geometry and chemical knowledge, the density maxima were identified as the oxygen and nitrogen atoms, which potentially belonged to the carboxamide substituent of the tca species. Thus, the single crystal of **8a-tca**, contains two related dinuclear complexes $[Cu_2(ctz)_4(bipy)_2]$ (form **1**) and $[Cu_2(ctz)_2(tca)_2(bipy)_2]$ (form **4**) mixed together in the one crystal. Both structures differ only slightly. In the form **1** the copper atoms have a square-pyramidal

coordination, very similar to the **6ctz** complex, but the bridging ctz anions coordinate to two Cu atoms in the $\kappa^2N(1,2)$ instead of the $\kappa^2N(2,3)$ fashion.
In the form **4,** six-fold coordination of each Cu atoms is fulfilled by the bridging tca ligand, which coordinates to the metal centers in the $\kappa^3N(1,2)O(7)$ fashion like in the structure of **8tca**. It is noteworthy to add, that the terminal ctz ligands in the form **1** and **4** stay unaffected.

Usually, the reaction between $Cu(NO_3)_2$ and $PPh_4(ctz)$ leads to crystalline coordination polymer **1ctz**, but elongation of the process to about two weeks gives a second sort of crystals of composition $Cu(tca)_2 \cdot 2H_2O$ (**9tca**). Single-crystal X-ray analysis reveals that compound **9tca** had formed, crystallizing in the orthorhombic crystal system in the space group *Iba*2. **9tca** contains a 2D coordination network, in which copper atoms are interlinked by the tca ligands. Each copper ion, residing in a general position, is surrounded by four tca ligands that ligate neighboring symmetry-related Cu atoms through the carboxamide and the tetrazolate moiety in the $\kappa^3N(1,3)O(7)$ fashion. The coordination geometry around Cu resembles a distorted octahedron with axial Cu–O bond lengths of 2.362(5) Å and 2.547(2) Å. Those bonds are significantly longer than from equatorial plane (averaged Cu–N 1.99 Å) and consistent with a strong Jahn-Teller effect in an octahedral ligand field. Each trinucleating tca ligand binds two metal centers on the distance of 5.971 Å and 6.009 Å generating a 2D coordination network spread out in the *ac*-plane (Figure 3.2.6.4). The layers are joined through moderately N–H···O and N–H···N hydrogen bonds,[42] with $R_2^2(9)$ ring motifs[43] and also through the H-bonds between crystallization water and the adjacent NH_2 groups (Figure 3.2.6.3) (Appendix E).

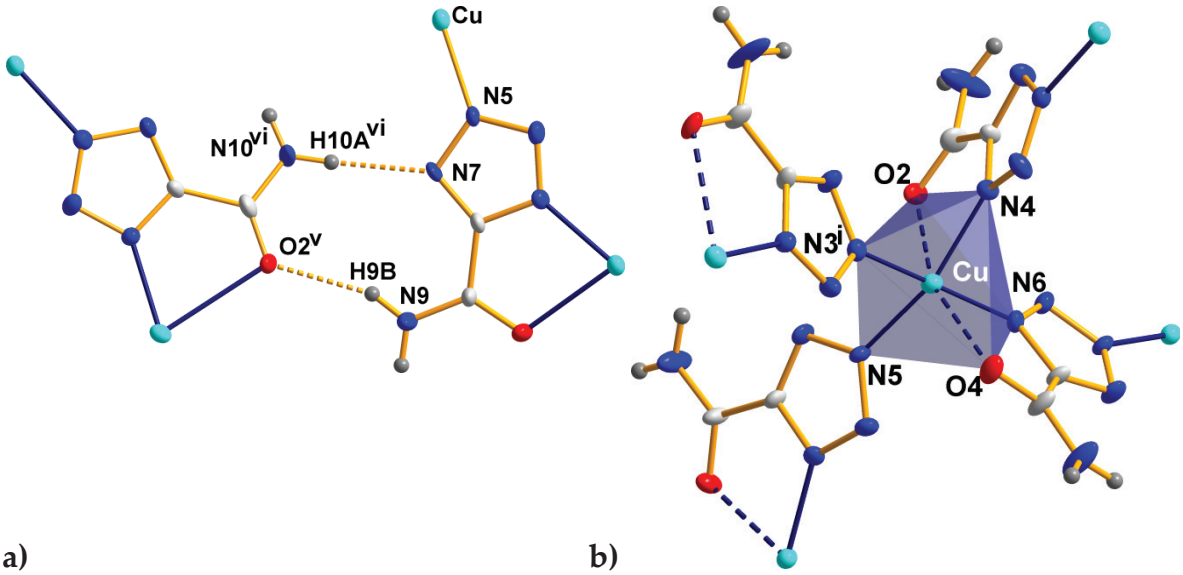

Figure 3.2.6.3 **(a)** The dimeric hydrogen bonds that join the layers in the **9tca**. **(b)** Coordination environment of the Cu atom in the **9tca** complex. Dashed lines indicate Jahn-Teller distortion. Displacement ellipsoids are drawn at the 50% probably level. H atoms are drawn with arbitrary radii. Symmetry codes: (i) $x, -y-1, z+1/2$; (v) $x, y-1/2, -z+3/2$; (vi) $x-1/2, -y+2, z$.

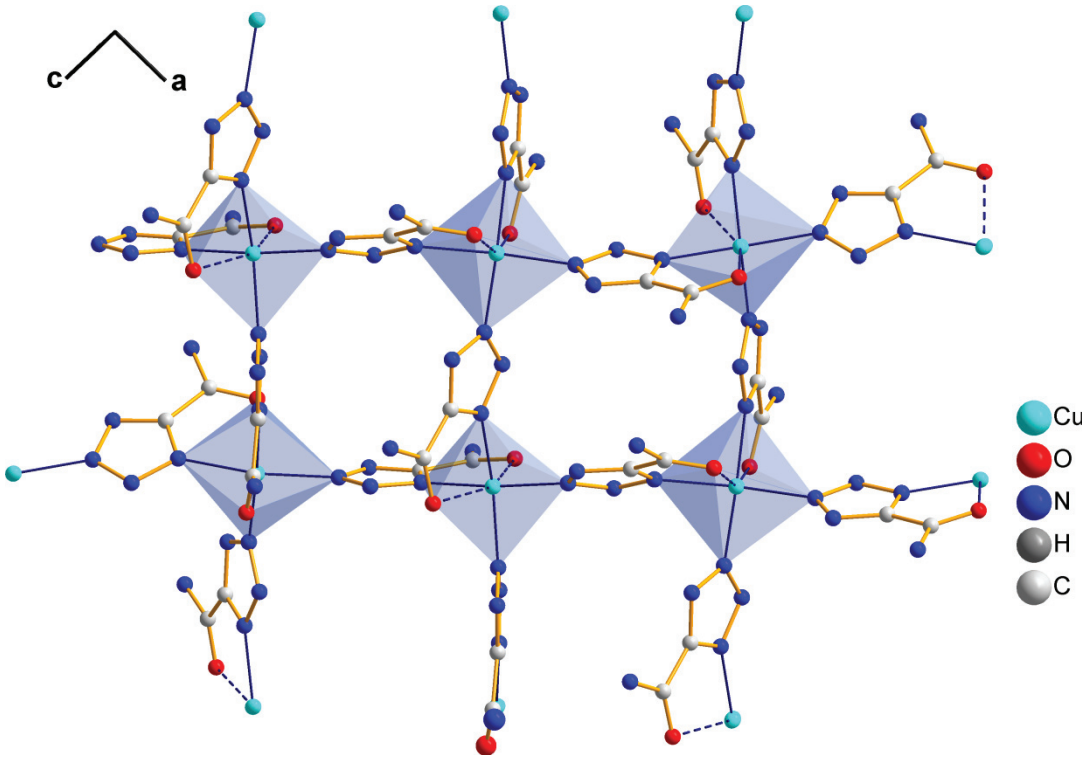

Figure 3.2.6.4 Section of the 2D layer of **9tca**. Hydrogen atoms are omitted for clarity.

3.2.7 Copper-Mediated Hydration of Cyano Group

During some crystallization processes performed in this thesis work, hydration of the cyano group was commonly observed, showing that the substituted group of ctz is sensitive towards the presence of water. Very recently, T. M. Klapötke and co-workers reported the reactivity of Hctz towards water under harsh conditions (6 M HNO_3, 80 °C) and studied the energetic character of the product tetrazole-5-carboxamide and its derivatives.[7] The common mechanism implies an acid-catalyzed hydration of the nitrile to the corresponding carboxamide. Like a carbonyl group, the CN group is polarized and has a slightly positive charged electrophilic carbon atom. Since water is only a weak nucleophile, the activation of the CN group is done by initial protonation of its nitrogen atom. In this situation, the slightly positive charged electrophilic carbon atom is attacked by the water molecule, one of the π bond breaks, which leads to a transition product – hydroxyimine, rapidly isomerising to a carboxamide $C(O)NH_2$ (Scheme 3.2.7.1).[15]

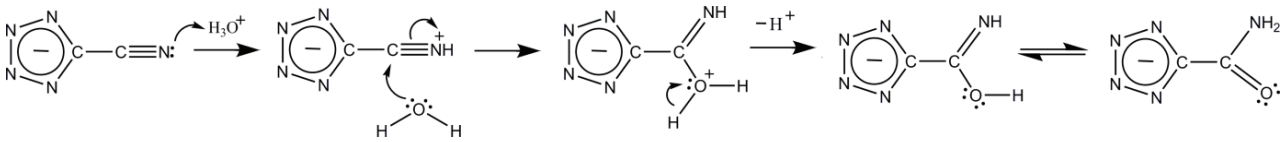

Scheme 3.2.7.1 The mechanism of the acid-catalyzed hydration of the ctz to the corresponding carboxamide under harsh conditions reported by T. M. Klapötke.[7]

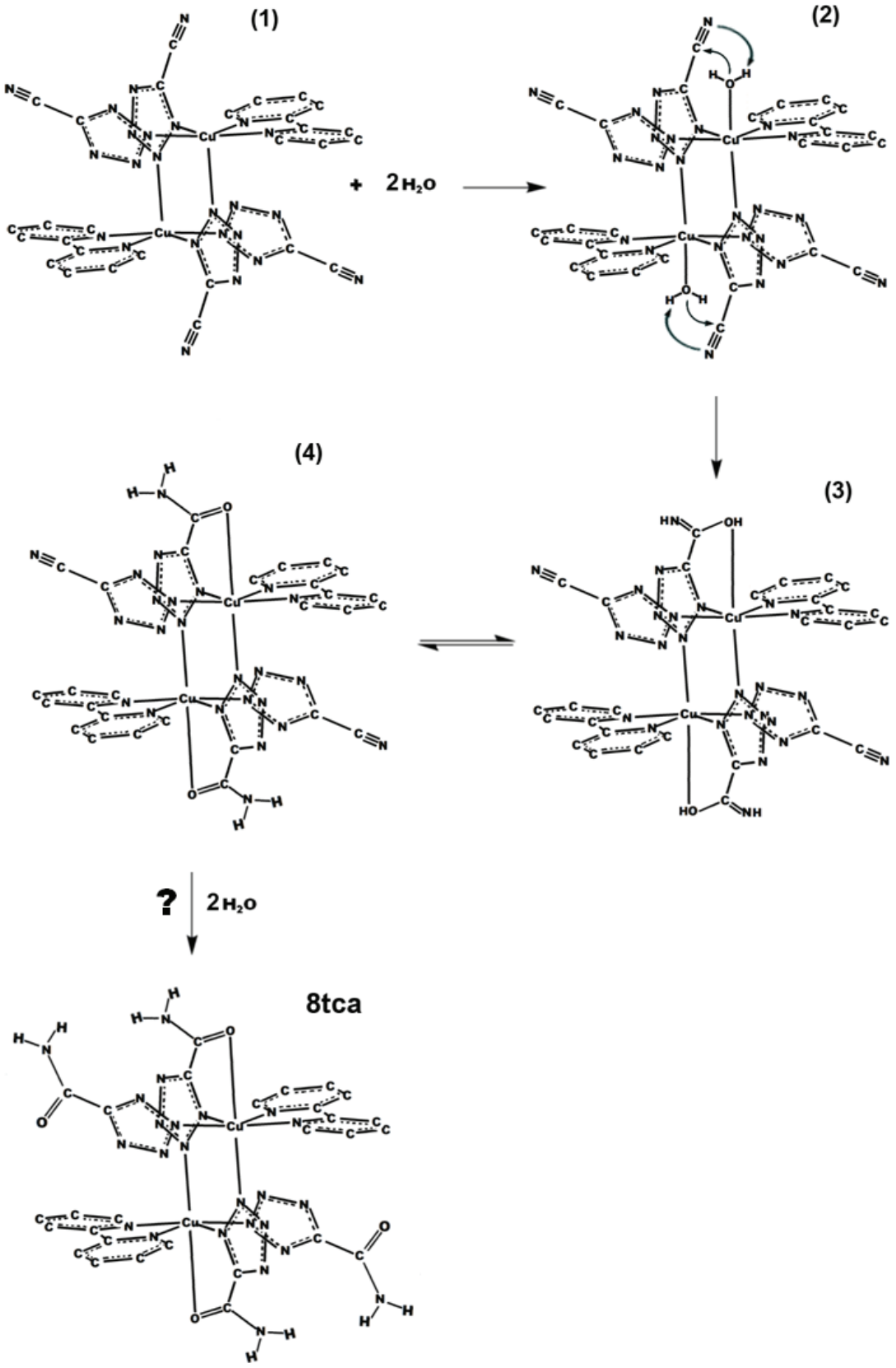

Scheme 3.2.7.2 Proposed mechanism for the the first step for the copper-mediated reaction of carboxamide formation in the complex **8tca.** For a crystallographic description see subchapter 3.2.6.

The crystallization of the Cu-cyanotetrazolate complexes was always performed under mild conditions (lack of external acid/base or high temperatures) (see Experimental Part). When water was present, the crystallization process did not give the compounds described in the previous subchapters, but yielded a new series of: $[Cu(tca)_2(bipy)] \cdot H_2O$ **(8tca),** its transition product $([Cu_2(ctz)_2(tca)_2(bipy)_2]_{0.5}[Cu_2(ctz)_4(bipy)_2]_{0.5}$ **8a-tca** and $Cu(tca)_2 \cdot 2H_2O$ **(9tca)** described in the previous 3.2.6 subchapter. In this case, the hydration process (from CN to $C(O)NH_2$) was based on the well known metal-mediated hydration of nitrile, that usually yields the carboxamide metal complexes.[53] On these terms, the electrophilic nature of the nitrile's carbon atom was enhanced by the Cu mediator, making the active group more susceptible to the H_2O nucleophile. Unfortunately, the mechanism of the metal-mediated hydration is not completely understood, especially the question as whether a water molecule or the nitrile, or both, coordinate to the metal in order to be activated.

However, in the literature a few examples show that the nitrile group is not coordinated directly to metal centre ([M←N≡C–R]) to react with water, the activation can occur in the vicinity of the metal ion centre.[17-22] The crystal structures described in the previous sub-chapters clearly show that the ctz ligand usually binds to Cu(II) centres from the tetrazolate site leaving the CN group uncoordinated. Thus, on this basic information and, with the support from the literature,[22] the proposed hydration of $[Cu_2(tca)_4(bipy)_2] \cdot H_2O$ **(8tca)** is shown in the Scheme 3.2.7.2.

It is noteworthy to add that the similar dinuclear complexes $[Cu_2(ctz)_4(bipy)_2]$ **(6ctz)** and $[Cu_2(tca)_4(bipy)_2] \cdot H_2O$ **(8tca)** can be crystallized from this same solution, but the time and presence of water have a key role in this transformation (see Experimental Part). The proposed pathway begins with an incoming water molecule to the "open" 6th coordination copper site of species **1**. This arrangement favors the nucleophilic attack of the hydroxide on the nitrile carbon atom, leading to the new C=O bond formation, which results in formation of a metal complex **4**. The intermediate carboxamide product is trapped in the complex, thus protected towards further nucleophilic attack of the water on the carboxamide's carbonyl group, which finally leads to carboxylate. However, this mechanism explains only reactions in the vicinity of the metal ion centre (i.e. **1** → **2** → **3, 4**), the explanation how metal-mediated hydration works on the uncoordinated CN groups (i.e. **4** → **8tca**) is still ambiguous. In order to support the hypothetic copper-mediated hydration of **8tca**, the respective IR spectra were recorded. As can be seen in Figure 3.2.7.3, the spectra of **8tca** and its transition state, (which can be mixture of **6ctz** and **8cta** or the it can be the pure **8a-tca**) are almost identical in the carbonyl absorption region around 1680 cm^{-1} due to the C=O stretching vibrations,[41] which are not observed in the pure dinuclear **6ctz** complex. A characteristic major amide band can be also observed in **8tca** as doublet, which involves NH_2 deformation and C=O stretching vibration in the region of 1650–1695 cm^{-1}. The appearance of an additional strong band at 2257 cm^{-1} in the spectrum of the transition state can be attributed to the remaining C≡N group, which is still present in the mixture or **8a-tca** compound and later hydrated, to give the final **8tca** complex.

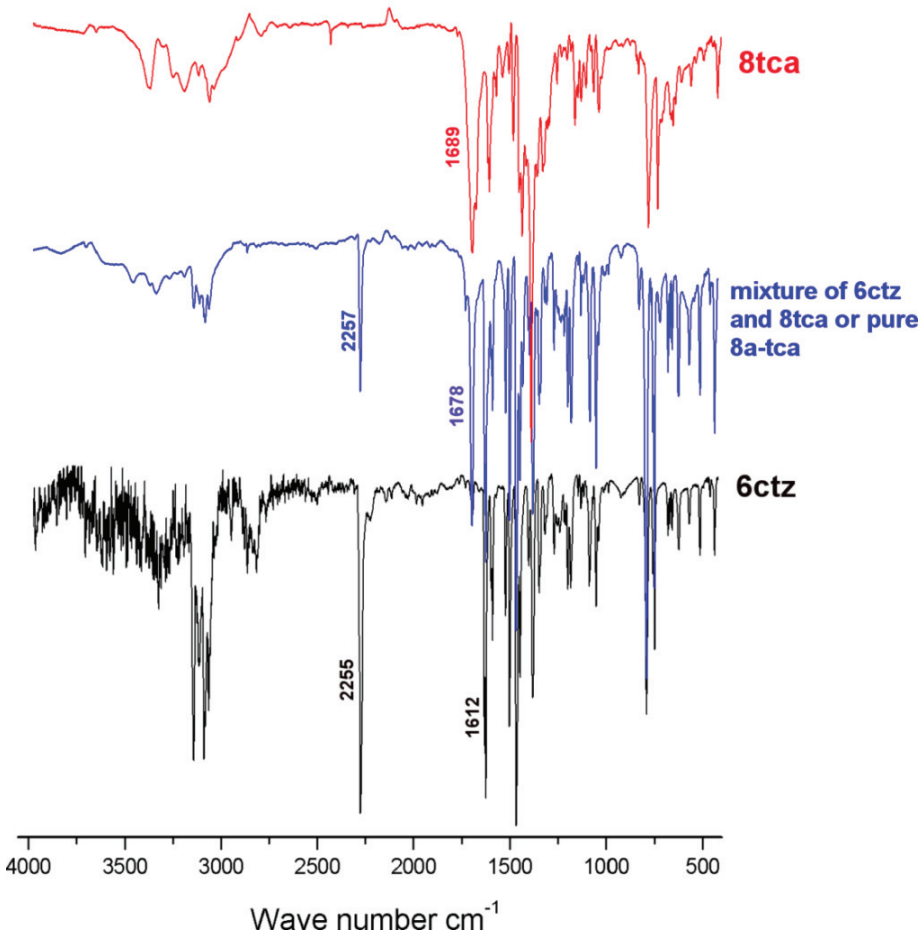

Figure 3.2.7.3 IR spectra of **8tca**, **8a-tca** (or mixture of **8a-tca** and **6ctz**) and **6ctz** with the characteristic stretching vibrations for cyano and carboxamide groups. Due to presence of water and aromatic groups (ν(O–H) and ν(C–H)) N–H stretching vibrations in the region of 3400–3500 cm^{-1} are unresolved.

3.2.8 Magnetic Interactions in the Cu(II) Complexes and Coordination Polymers

For **6ctz,** Curie-Weiss paramagnetism is mainly present, although the Cu^{2+} ions are bridged by ctz anions. The $\chi^{-1}(T)$ function is essentially linear in the full range of temperature and obeys the Curie-Weiss law (Eqn. 1.8, Part 1) with C = 0.41 cm^3 K mol^{-1} and Θ = –0.47 K, giving a paramagnetic moment of 1.83 μ_B at 298 K per Cu(II) ion. The best fit to equation $\chi = g^2\mu_B^2NS(S+1)/kT$ over the full temperature range gives the parameters S = 1/2 and g = 2.10.

The decrease of $\chi T(T)$ at low temperatures and the small negative Curie-Weiss constant indicates for a weak antiferromagnetism in the sample. Application of the modified Bleaney-Bowers magnetic model (Eqn.1.1 3 Part 1) allows for the calculation of the magnetic coupling parameter. The best fit results in a small exchange constant (J = −0.53 cm^{-1}) with Landé g factor of 2.10 (Figure 3.2.8.1). The weak antiferomagnetic interaction is consistent with other structurally similar double-bridged dicopper tetrazolate complexes like $Cu_2(TzC)_2(H_2O)_6 \cdot nH_2O$ [TzC = tetrazole-5-carboxilic acid] with a corresponding magnetic exchange constant of J close to –9.1 cm^{-1}.[44]

Above 6 K, the magnetic susceptibility data for compound **7ctz** shows isolated spin behaviour and therefore can be fit to the Curie-Weiss law (Eqn. 1.8, Part 1) as shown in Figure 3.2.8.2. The linear regression of the $\chi^{-1}(T)$ function gives a negative Curie-Weiss temperature (Θ = −3.61 K) and a Curie constant C = 0.44 cm³ Kmol⁻¹. The calculated effective magnetic moment at room temperature using Eqn. 1.7 for one Cu^{2+} ion equals 1.88 μ_B and it is slightly higher than the value for a single unpaired electron (1.73 μ_B, S = 1/2) but still within the typical range for divalent Cu. The best fit to the equation $\chi = g^2\mu_B^2 NS(S+1)/kT$ over the full temperature range gives S=1/2 and g = 2.03. However, the $\chi T(T)$ function shows a decrease of the magnetic moment at low temperatures, indicating a weak antiferromagnetic coupling between the two Cu(II) ions, which are 3.517(1) Å apart from each other.

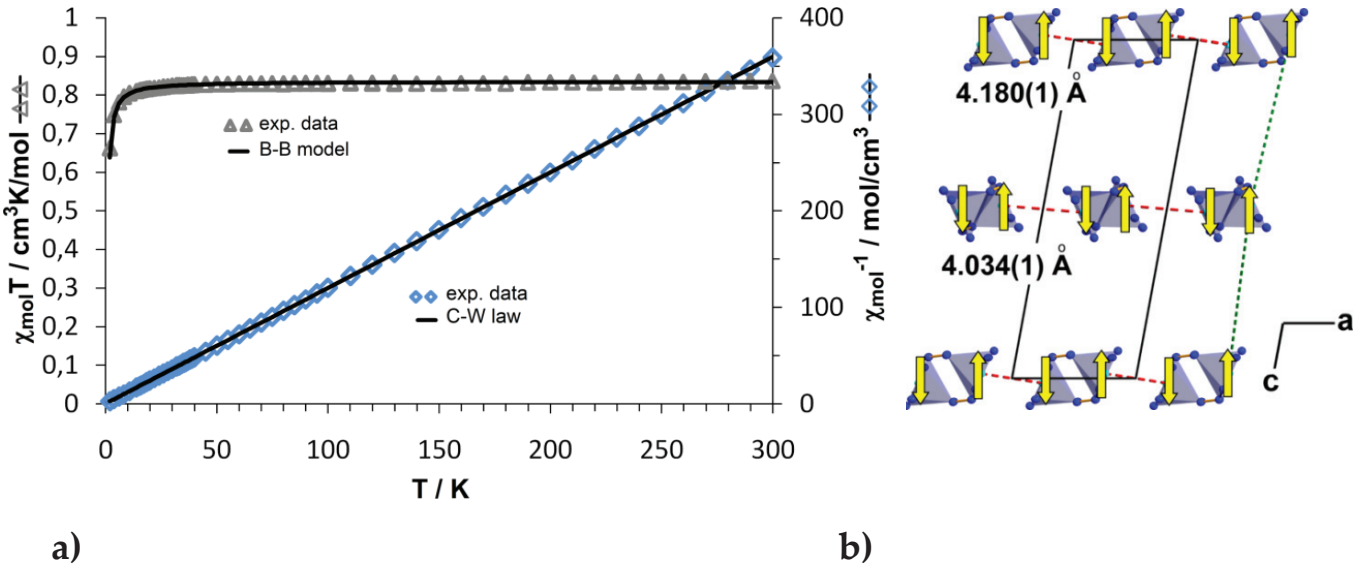

Figure 3.2.8.1 (a) Plot of $\chi T(T)$ and $\chi^{-1}(T)$ of **6ctz** in a field of 10 kOe. Empty triangles and squares represent an experimental data, the solid lines represent the best fit to the Bleaney-Bowers magnetic model (see the text description and Eqn. 1.13, Part 1). Agreement factor for the least-square fit: $R = 8.44 \cdot 10^{-6}$.

The best fit to the experimental data was obtained according to the modified Bleaney-Bowers equation (Eqn. 1.13. Part 1) which resulted in an exchange constant J = −2.91 cm⁻¹ with the Landé g factor of 2.14. The calculated mean-field correction temperature (Θ_{MF}) equals 0 and indicates that inter-dimer interactions should most likely be excluded. A correspondent magnetic exchange, but with the higher magnetic exchange parameter (J = –94.3 (2) cm⁻¹) has been found within the dinuclear complex $[Cu_2(Hdatrz)_2(\mu\text{-}OH_2)(H_2O)_4(SO_4)](SO_4) \cdot 3.5H_2O$ [Hdatrz = 3,5-diamino-1,2,4-triazole].[45]

The 1D coordination polymer **1ctz** shows a different linear dependence of $\chi T(T)$. Taking into account the Curie-Weiss relationship, the equation $\chi_{mol} = C/(T-\Theta)$ yields a positive Curie-Weiss temperature of θ = + 4.7 K and C = 0.39 cm³ K mol⁻¹. The positive θ indicates a presence of a weak ferromagnetic exchange interaction between copper(II) ions in low temperatures (Figure

3.2.8.3). When temperature is lowered, $\chi_{mol}T$ slowly increases to reach a maximum at 5.5 K (0.62 cm^3K/mol). However, below this temperature $\chi_{mol}T$ value decreases to 1.9 K to reach values of 0.48 cm^3K/mol.

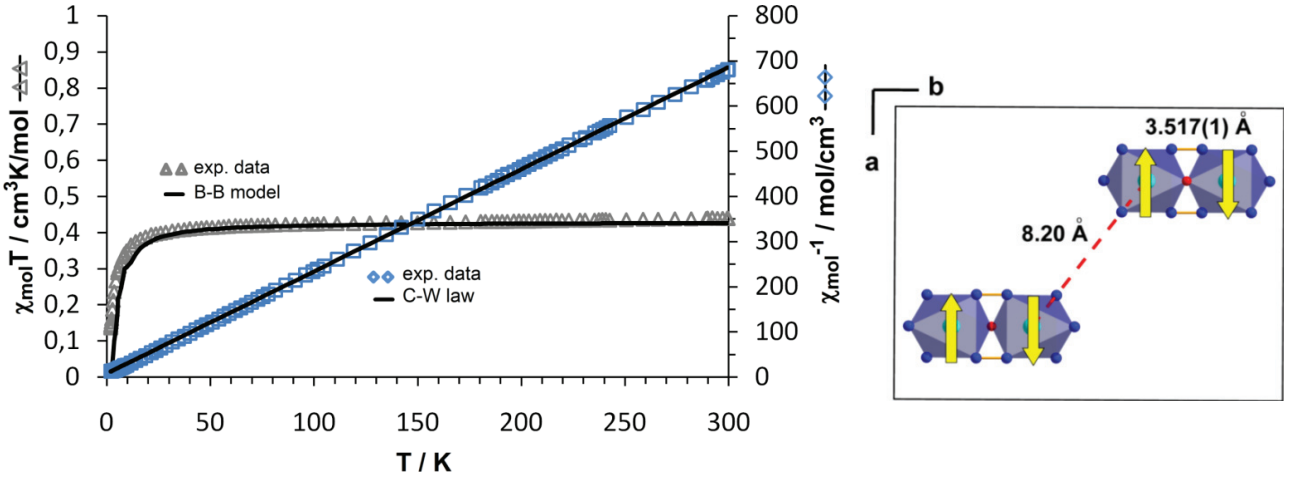

a) b)

Figure 3.2.8.2 (a) Plot of $\chi T(T)$ and $\chi^{-1}(T)$ of **7ctz** in a field of 20 kOe. Empty squares and triangles represent an experimental data, the solid lines represent the best fit to the Bleaney-Bowers magnetic model (see the text description). Agreement factor for the least-square fit: R = $9.99 \cdot 10^{-3}$. **(b)** The schematic representation of the spin coupling model.

This behavior is typical for ferromagnetic coupling between copper(II) ions. The decrease in $\chi_{mol}T$ at low temperatures could be attributed to either inter-chain antifferomagnetic interactions and/or to the zero-field splitting effect (ZFS) of the ground state.[45a] The experimental effective magnetic moment at room temperature (298 K) equals 1.79 μ_B.

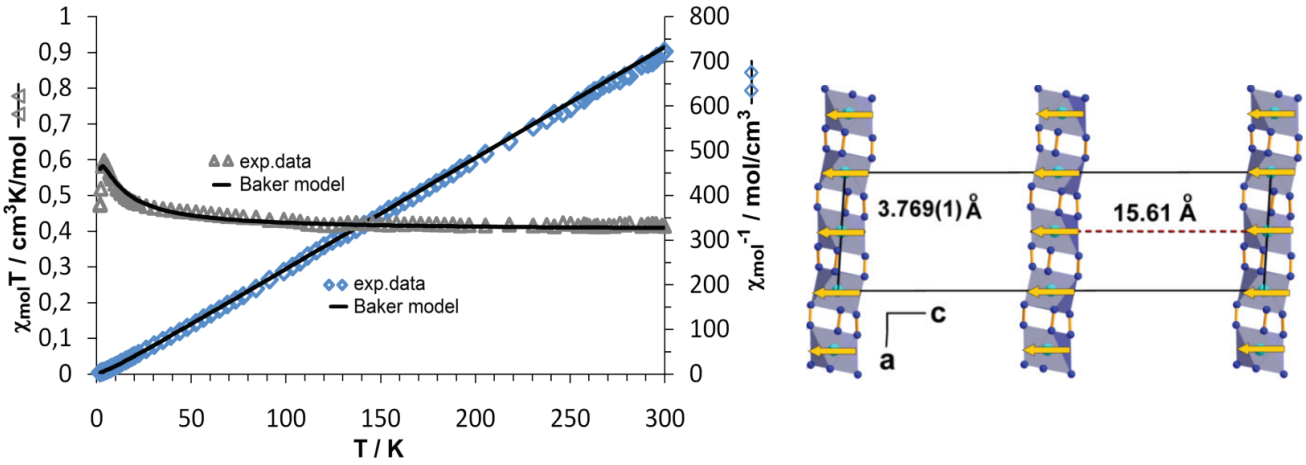

a) b)

Figure 3.2.8.3 (a) Plot of $\chi T(T)$ and $\chi^{-1}(T)$ of **1ctz** in a field of 20 kOe**.** Empty squares and triangles represent an experimental data, the solid lines represent the best fit to the Baker 1D model modified including inter-chain interactions (see the text description). Agreement factor for the least-square fit: $R = 3.21 \cdot 10^{-7}$. **(b)** The schematic representation of the spin coupling model.

The analysis of the susceptibility data in the temperature region between 1.9 and 300 K was performed by using the Baker 1D (S = 1/2) chain model (Eqn. 1.14, Part 1) including the Θ_{MF} term for inter-chain effects. The best fit to the experimental data was achieved with J = +6.5 cm^{-1}, Θ_{MF} = -3.6 cm^{-1} and g = 2.07.

Above 30 K the susceptibility of the 2D layered compound **4a-ctz** follows the Curie-Weiss law (Eqn. 1.8 Part 1) with the linear function of $\chi^{-1}(T)$ and the parameters C = 0.51 cm^3 K mol^{-1} and a negative characteristic temperature of θ_P = –27.71 K with g = 1.93 (Figure 3.2.8.4). The experimental effective moment over the full temperature range was estimated to be 1.68 μ_B per Cu(II) ion, somewhat lower than the spin only value for the d^9 electronic configuration. Below 30 K there is a characteristic change in the $\chi^{-1}(T)$ experimental data seen as a nonlinear slope, recognized as ferrimagnetic ordering. According to the Néel theory of ferrimagnetism, the relationship between χ_{mol} and C constant can be described by the Equation 1.10 in Part 1. The temperature function of the experimental susceptibility can be fitted quite accurately with the following parameters: C = 0.51 cm^3 K mol^{-1}, θ_P = –27.71 K, θ' = –2 K and ζ = 149 K. The relation of the parameters (negative θ_P and positive ζ) to the crystal structure of **4a-ctz** allows for the set up of the model of two magnetic sublattices of different weight with ferromagnetic coupling within the chains and antiferromagnetic coupling between them.

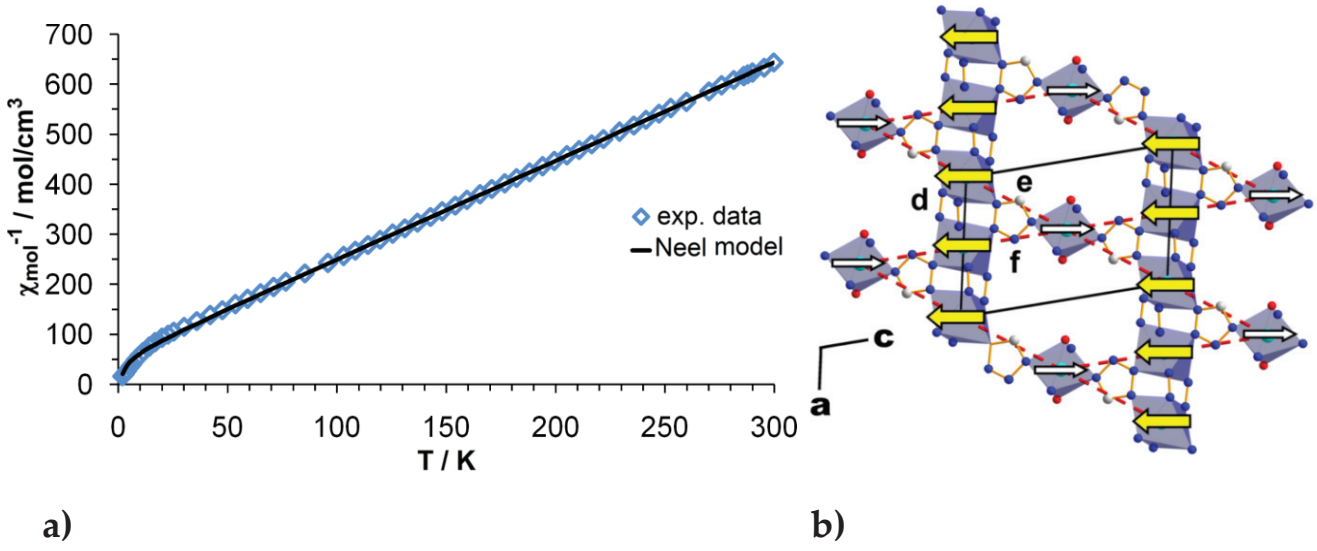

Figure 3.2.8.4 (a) Plot of $\chi T(T)$ and $\chi^{-1}(T)$ of **4a-ctz** in a field of 20 kOe. **(b)** The schematic representation of the spin coupling model. Empty squares and triangles represent an experimental data, the solid lines represent the best fit to the ferrimagnetic Néel magnetic model (see the text description). Cu···Cu distances: d = Cu1···Cu2 3.848(1) Å, e = Cu2···Cu3 6.447(1) Å and f = Cu1···Cu3 5.892(1) Å. Agreement factor for the least-square fit: R= 1.08·10^{-3}. **(b)** The schematic representation of the spin coupling model.

A comparison of the structure of **4a-ctz** with the very similar compound **1ctz** shows that the $[(Cu(ctz)_3)^-]_n$ chains are a common feature, for which ferromagnetic ordering was found in **1ctz**. The Cu···Cu distances within the chains amount to 3.848(1) in **4a-ctz** and 3.769(1) Å in **1ctz**. Therefore, an analogous ferromagnetic behaviour can be assumed to be present for **4a-ctz**. In the

structure of **4a-ctz**, the independent atoms Cu1 and Cu2 make up the chains, which are connected by trinucleating κ^3N(1,2,4) ctz ligands coordinating to the Cu3 in the *ac*-planes to layers (Figure 3.2.4.1). Assuming ferromagnetic ordering for Cu1 and Cu2 within the chains and antiferromagnetic ordering between the Cu3 ions gives two magnetic sublattices of weight 2 : 1. The antiferromagnetic coupling between them explains the weak ferrimagnetic behaviour of **4a-ctz**.

Generally, magnetic behaviour is a result of the competition between antiferromagnetic (AF) and ferromagnetic (F) exchange interactions.[46] In chainlike coordination polymers the domination of AF or F coupling is interrelated with the coordination geometry around the Cu^{2+} centres. All Cu(II) ions exhibit the typical coordination environment of elongated CuN_6 octahedra caused by the Jahn-Teller effect. The $d_{x^2-y^2}$ orbitals are located perpendicular to the long octahedron axes. These orbitals on the copper(II) ions overlap with σ orbitals of the nitrogen atoms of the bridging ligands in the equatorial CuN_4 plane. For the magnetic behaviour the connection of these magnetic orbitals through the ligands is essential. Within the concatenated coordination polyhedra, there is one continuous N–N–Cu–N–N chain made up of only short Cu–N bonds. Since only in the short Cu–N bonds the orbitals are involved, the geometry of these chains is of importance. In the structures of **1ctz**, **4a-ctz** and $[Cu(hyetrz)_3](CF_3SO_3)_2{\cdot}H_2O$ [hyetrz = 4-(2-hydroxyethyl)-1,2,4-triazole],[47] this particular $[N–N–Cu–]_n$ chain is made of planar zigzag shape, the two N atoms are in *trans* position at the CuN_6 coordination octahedra (Figure 3.2.8.5). For these compounds, ferromagnetic interactions are observed. In the structure of $[Cu(hyetrz)_3](ClO_4)_2{\cdot}3H_2O$[48] these chains are observed as well, but a sequence of alternating *cis* and *trans* conformations at the Cu(II) ions is observed. Here, antiferromagnetic exchange dominates (Figure 3.2.8.5). These relationships are apparently limited to infinite chains with Cu(II) ions μ(*N*1,*N*2)-bridged solely by triazoles and tetrazoles. Introduction of a monoatomic bridge as present in $\{[Cu(\mu\text{-}OH)(\mu\text{-}ClPhtrz)](H_2O)(BF_4)\}_n$ [ClPhtrz = ((4-chlorophenyl)methylidene)-1,2,4-triazole-4-amine][49] changes the magnetic interactions dramatically and leads to the antiferromagnetic coupling of two to three orders of magnitude stronger than observed for the compounds presented in this study.

a)

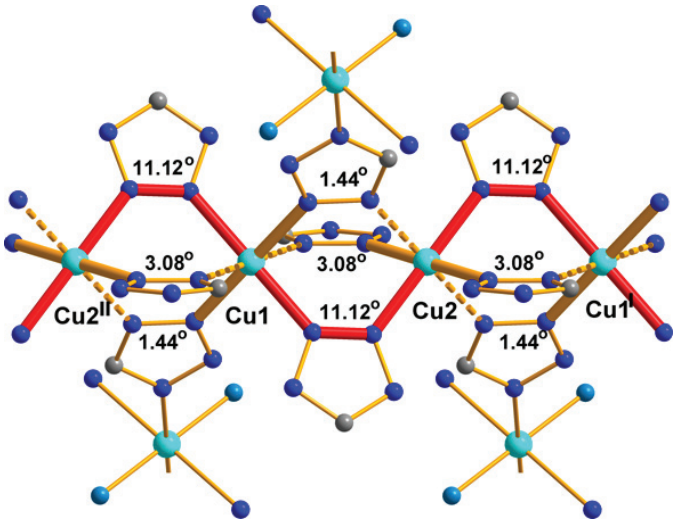

b)

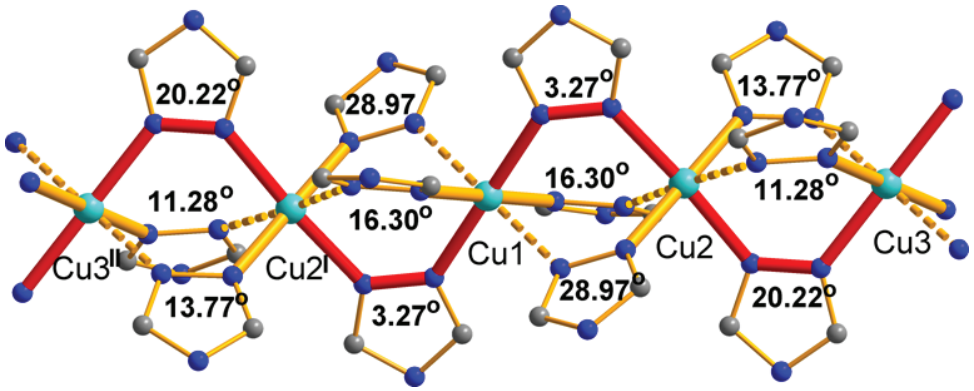

c)

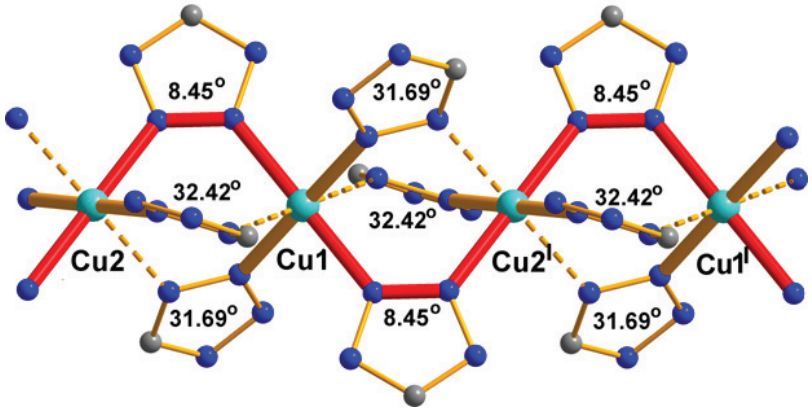

d)

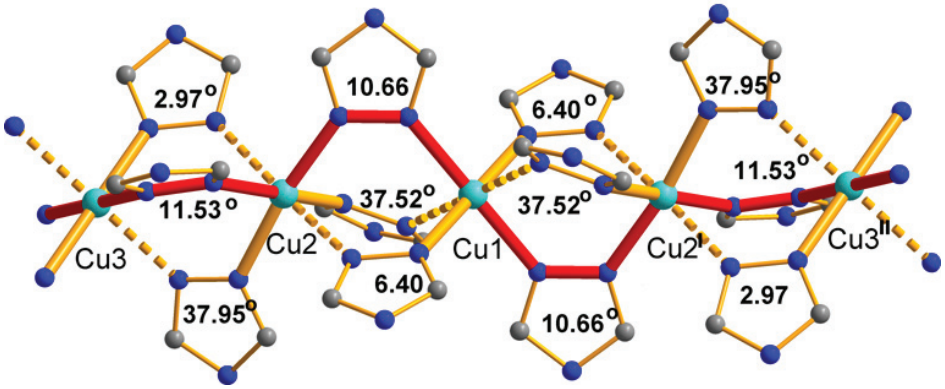

Figure 3.2.8.5 The geometries of the **4a-ctz (a)**, **1ctz (c)** linear chains and other literature examples of the 1D copper-triazolate chains (**(b)** $[Cu(hyetrz)_3](CF_3SO_3)_2 \cdot H_2O$ [hyetrz = 4-(2-hydroxyethyl)-1,2,4-triazole][47] and **(d)** $[Cu(hyetrz)_3](ClO_4)_2 \cdot 3H_2O$ ((hyetrz) = 4-(2-hydroxyethyl)-1,2,4-triazole][48]). The figures are simplified for clarity by omitting substituents on the tetrazole and triazole rings. In all figures the Cu–N–N–Cu angles are given. The dotted Cu···N bonds represent the two long bonds within the CuN_6 coordination octahedra. Short $[N–N–Cu–]_n$ bonds running parallel to the chain are depicted by thick lines. **(a)** The **4a-ctz** complex reveals ferromagnetic coupling. The intrachain coupling constant J is unknown due to antiferromagnetic coupling with Cu3 (see text). Symmetry codes: (i) −x+1, −y, −z; (ii) −x, −y, −z; **(b)** The complex shows ferromagnetic coupling, J = +1,45 cm^{-1}. Symmetry codes: (i) -x+1, -y+1, -z; (ii) x, y, z-1. **(c)** The **1ctz** compound reveals ferromagnetic coupling with J = +6.5 cm^{-1}. Symmetry code: (i) $-x+2, -y+1, -z$. **(d)** The complex shows the antiferromagnetic coupling with J = –1.18(2) cm^{-1}. Symmetry codes: (i) -x+1, -y+1, -z+1; (i) x, y, z+1.

3.3 Conclusions

The purpose of presented work was to examine the coordination abilities of the multidentate linker ligand 5-cyanotetrazolate towards the paramagnetic Cu^{2+} ion and to study the magnetic interactions between the Cu ions mediated by the ctz ligand. Through different methods of synthesis and the use of mono-, bi-, and tridentate co-ligands, a series of mono and dinuclear complexes and 1D and 2D coordination polymers could be obtained and characterized by structure determinations and magnetic measurements. 5-cyanotetrazolate turns out as a highly versatile ligand with various coordination modes towards the transition metal ion, ranging from monodentate terminal function to triple bridging of three Cu ions. Jahn-Teller distorted polyhedra around Cu^{2+} are always observed. A variety of cooperative magnetic effects were observed: ferro-, antiferro-, and ferrimagnetism mediated by the ctz anions are present at low temperature, whereas mainly isolated ion behaviour is observed at high temperatures. In the course of the experimental work, a copper-mediated hydration reaction, which converted 5-cyanotetrazolate to tetrazole-5-carboxamide was frequently observed. Direct coordination of the cyano group to the metal centre was not necessarily required for this reaction, since ctz binds to the copper ion through the tetrazolate moiety. The formation of oxygen-bound carboxamide complexes ensured their stability and protected carboxamide group towards further hydrolysis to tetrazole-5-carboxylate.

3.4 Experimental Section

Safety note: Although 5-cyanotetrazole and all complexes are stable at room temperature and turned out as insensitive to friction and impact, they should be handled with care. The high nitrogen content makes them energetic materials and suitable safety precautions need to be taken. Hydrazoic acid (HN_3) is shock sensitive and highly toxic in concentrated form. Sodium cyanide is highly poisonous and liberates volatile HCN when mixed with acids. Because of the poisonous character of the compounds involved in the synthesis of cyanotetrazole including the poisonous cyanogen gas, all operations should be performed in a well-ventilated fume hood.

Syntheses

Tris(pyrazol-*1*-yl)methane, $HC(C_3H_3N_2)_3$ (tpm) was synthesised according to published procedures,[50] unreacted pyrazole was removed by sublimation under vacuum ($4 \cdot 10^{-3}$ mbar) at 90-95 °C; pale yellow solid. M.p.: found 98–99 °C, lit.[50] 102–104 °C. $C_{10}H_{10}N_6$ (tpm): Elemental analysis (%) $HC(C_3H_3N_2)_3$ (214.23) calc: C 56.07, H 4.70, N 39.23; found C 56.48, H 5.23, N 38.70; NMR: ^{13}C ppm in ($CDCl_3$): 141.4 (3-C(pz)), 129.2 (5-C(pz)), 106.9 (4-C(pz)), 82.9 (CH); ^{1}H ppm in ($CDCl_3$): 6.3 (dd, 3*H*, 4-C*H* J_{HH}= 2.5 Hz, 1.8 Hz 4-H(pz)), 7.5 (d, *3H*, J_{HH} = 2.5 Hz 5-H (pz)), 7.6 (d, *3H*, J_{HH} = 1.4 Hz 3-H (pz)), 8.4 (s,1*H*, C*H*).

5-Cyanotetrazole (Hctz): Hctz was prepared in high yield by the *in-situ* [3+2] cycloaddition reaction of hydrazoic acid HN_3 in aqueous solution with gaseous cyanogen $(CN)_2$ according to the reported procedure.[8] HN_3 was prepared by passing 20 mL of an aqueous solution of NaN_3 (7.28 g, 0.11 mol) through freshly acidic loaded column of ion exchange resin (Amberlite IR 120 H). The obtained diluted solution of HN_3 was collected in a 500 mL round bottom flask and cooled with an ice bath. $(CN)_2$ was produced by adding 100 mL of an aqueous solution of NaCN (22.0 g, 0.45 mol) dropwise on solid $CuSO_4$ (35.8 g, 0.22 mol) within 60 min. The released $(CN)_2$ gas was directly passed through the solution of HN_3. After the gas evolution of $(CN)_2$ had ceased, argon gas was passed through the aqueous solution to remove all traces of excess $(CN)_2$ or HN_3. The water was distilled off at 30 °C and 35 mbar until a slightly red coloured oil remained, which spontaneously solidified to a light red, crystalline raw product. This solid was purified by sublimation under vacuum ($3 \cdot 10^{-3}$ mbar) at 90-98 °C to give white crystals of pure Hctz. Yield: 3.396 g (35.72 mmol, 32% based on NaN_3). M.p: 98 °C, lit.[8] 99 °C. (KBr disc): 3163 (s), 2279 (m), 1616 (w), 1467 (m), 1416 (m), 1296 (m), 1223 (w), 1171 (m), 1114 (m), 1045 (m), 1024 (m), 843 (m), 741 (w), 541 (w), 487 (w) cm^{-1}. Elemental analysis (%) C_2HN_5 (95.064 g/mol): calc: C 25.27, N 73.67, H 1.06, found C 25.12, N 74.50, H 1.29; ^{1}H NMR (DMSO-d_6): δ = 11.5 ppm (s, 1*H*, N*H*); ^{13}C NMR (DMSO-d_6): δ = 138.5 (s, 1*C*, *C*-CN), 112.2 ppm (s, 1*C*, *C*N).

Tetraphenylphosphonium 5-cyanotetrazolate PPh_4(ctz) was prepared by combining aqueous solutions with equimolar amounts of PPh_4Cl and Hctz. PPh_4(ctz) precipitated as a white crystalline solid, which was filtered and dried in vacuo. M.p: 172-174 °C. IR (KBr disc): 3420, 3054, 1627, 1585, 1486, 1436, 1316, 1104, 997, 763, 724, 691, 528 cm^{-1}. Elemental analysis (%) $C_{26}H_{20}N_5P$ (433.45 g/mol) calcd: C 72.05, H 4.65, N 16.16, P 7.15; found, C 71.71, H 4.79, N 16.05, P 7.31; ^{1}H NMR (DMSO-d_6): δ = 8.0-7.7 ppm (m, 20*H*, Ar*H*); ^{13}C NMR (DMSO-d_6): δ = 137.7 ppm (s, 1*C*, *C*-CN), 135.5 (d, $^4J_{PC}$ = 2.6 Hz, Ph_{para}), 134.5 (d, $^2J_{PC}$ = 10.3 Hz, Ph_{ortho}), 130.4 (d, $^3J_{PC}$ = 12.9 Hz, Ph_{meta}), 117.7 (d, $^1J_{PC}$ = 89.2 Hz, Ph_{ipso}), 115.2 ppm (s, 1*C*, *C*N).

Crystallization of 1ctz: The technique of diffusion of reacting solutions was applied.[51] PPh_4(ctz) (8.5 mg, 0.020 mmol) was dissolved in 3 mL of chloroform and placed in a test tube. $Cu(NO_3)_2 \cdot 3H_2O$ (2.4 mg, 0.01 mmol) was dissolved in 3 mL of acetone and this solution was carefully layered above the chloroform solution with the aid of a syringe. The tube was closed and left to stand at room temperature undisturbed for 7 days. Blue long needle shaped crystals, which were suitable for X-ray analysis appeared at the boundary between the two solutions. Yield: 2.53 mg (37%). M.p.: decomposition starting at 201 °C to a grey solid, leaving a grey-black liquid at 260 °C. Elemental analysis (%) $C_{30}H_{20}CuN_{15}P$ (685.12 g/mol): calc. C 52.59, H 2.94, N 30.66; found C 51.74, H 3.11, N 30.30. IR (KBr disc): 3172 (w), 3080 (w), 3054 (w), 3024 (w), 2254 (s), 1682 (w), 1588 (m), 1485 (m), 1442 (s),1437 (s), 1366 (m), 1361 (m), 1315 (w), 1227 (w), 1171 (w), 1110 (s), 1071 (w), 996 (m), 759 (m) 726 (s), 690 (s), 607 (w), 528 (s), 494 (w) cm^{-1}.

Crystallization of 2ctz and 6ctz: Crystals suitable for X-ray analysis were obtained by slow solvent evaporation and seeding crystals.[51,52] $CuNO_3 \cdot 3H_2O$ (163.5 mg, 0.68 mmol) was

dissolved in 3 mL of water, Hctz (129.1 mg, 1.36 mmol) was dissolved in 4 mL of water, 2,2'-bipy (106.1 mg, 0.68 mmol) was dissolved in 2 mL of EtOH. These solutions were mixed in a small crystallization dish, covered by a perforated plastic paraffin coated film. After 5 days two kinds of crystals appeared, dark blue blocks of **6ctz** and long, light blue needles of **2ctz**, which were separated mechanically. Crystals of **2ctz** could also be obtained in pure form by nucleation using a seed of crystals of **2ctz** from a mixture of $CuNO_3 \cdot 3H_2O$ (127.5 mg, 0.53 mmol) dissolved in 2 mL of water, Hctz (100.5 mg 1.06 mmol) in 2 mL of water and 2,2'-bipy (84.3 mg, 0.54 mmol) in 1 mL of EtOH. The solutions were combined and 10 mL of ethanol were added. The solution was then divided in two parts. To the first part, a small amount of crystals of **2ctz** were added. After 15 min., the precipitated crystals were collected, washed with 5 mL of water and 2 mL of diethyl ether and dried in air. Yield: 19 mg (17.2%). M.p.: decomposition starting at 210 °C to a grey solid, leaving a grey-black liquid at 230 °C. Elemental analysis (%) $C_{14}H_8CuN_{12}$ (407.86 g/mol): calc. C 41.23, H 1.98, N 41.21; found C 41.26, H 2.09, N 40.89.

The purity of the compound was checked by comparison of the X-ray powder diffraction pattern with a simulated pattern based on the crystallographic parameters of **2ctz** obtained by single crystal diffraction. The observed and the calculated powder diffraction pattern show the presence of some additional reflections indicating that the precipitated material contains minor amounts of other phases (Figure 3.4.1).

Evaporation of the second part of solution gave after approx. 75 min. dark blue crystals of **6ctz**. They were washed with 5 mL of water and 2 mL of diethyl ether and dried in air. Yield: 69 mg (62.7%). M.p.: decomposition starting at 218 °C to a grey solid, leaving a grey-black liquid at 230 °C. Elemental analysis (%) $C_{28}H_{16}Cu_2N_{24}$ (815.73 g/mol): calc. C 41.23, H 1.98, N 41.21; found C 40.99, H 2.18, N 40.47. The purity of the compound was confirmed by X-ray powder diffraction.

Crystallization of 3ctz, 4b-ctz and 5ctz

Crystals of **3ctz**: $CuCl_2 \cdot 2H_2O$ (8.1 mg, 0.048 mmol) and Hctz (9.8 mg, 0.10 mmol) were transferred into a 10 mL glass vial and 5 mL of pyridine were added. The glass vial was covered by a perforated plastic paraffin coated film. Very slow evaporation of the solvent gave dark blue crystals after 14 days. The crystals were sensitive when exposed to air and decomposed after one day in air. M.p.: decomposition starting at 120 °C to a grey solid, leaving a grey-black liquid at 182 °C. Elemental analysis $C_{32}H_{20}ClCuN_{11}$ (%) (667.66 g/mol): calc. C 57.58, H 2.53, N 23.08; found C 56.14, H 4.46, N 22.70. IR (KBr disc): 3135 (m), 3110 (m), 3067 (m), 3041 (m), 2256 (s), 1636 (w), 1607 (m), 1533 (m), 1487 (m), 1450 (m), 1376 (w), 1361 (w), 1251 (w), 1220 (w), 1080 (w), 1043 (w), 758 (m), 691 (m) cm^{-1}.

Crystals of **4b-ctz** were prepared applying the same technique as described above. $Cu(OH)_2$ (22.1 mg, 0.23 mmol) and Hctz (48.4 mg, 0.51 mmol) were transferred into a 10 mL glass vial

and 5 mL of acetone were added. The glass vial was closed and heated for 10 min. up to 45 °C in order to dissolve all reagents. Light blue, block shaped crystals of **4a-ctz** appeared after 4 days at room temperature in a closed class vial. Crystals were very sensitive and decomposed when exposed to air within 10 min.

Crystals of **5ctz**: $Cu(NO_3)_2 \cdot 3H_2O$ (90 mg, 0.37 mmol) and Hctz (71 mg, 0.75 mmol) were both dissolved in a small amount of water and the two solutions were mixed. The light blue precipitated crystalline solid was collected and dried in air. The 5.62 mg of freshly produced solid was transferred into a 10 mL glass vial and 5 mL of pyridine was added. The glass vial was covered by a perforated plastic paraffin coated film. Very slow evaporation of the solvents gave dark blue crystals after 7 days. M.p.: decomposition starting at 200 °C to a grey solid, leaving a grey-black liquid at 230 °C. Elemental analysis $C_{24}H_{20}CuN_{14}$ (%) (568.08 g/mol): calc. C 50.75, H 3.55, N 34.52; found C 50.08, H 3.61, N 34.52.

Crystallization of 4a-ctz: Suitable crystals for X-ray analysis were obtained by slow cooling and slow evaporation of the solvent as the crystallization technique.[51,52] Hctz (111 mg, 1.17 mmol) was dissolved in 17 mL of hot acetonitrile, $Cu(NO_3)_2 \cdot 3H_2O$ (47 mg, 0.19 mmol) was dissolved in 2 mL of water and then added to the hot solution of Hctz. The combined solutions were transferred to a test tube, which was covered by means of a perforated plastic paraffin coated film and allowed to cool slowly in a Dewar vessel filled with hot water (ca. 70 °C) over period of 24 hours. Light blue block shaped crystals were formed, which were stable at 20 °C. Yield: 30 mg (49%). M.p.: decomposition starting at 230 °C to a grey solid, explosion at 290 °C. Elemental analysis (%) $C_{16}H_{10}Cu_3N_{32}O_2 \cdot 2(C_2H_3N)$ (955.29 g/mol): calc. C 25.15, H 1.69 N 49.86; found C 24.43, H 1.82, N 49.87. IR (KBr disc): 3343 (m), 2935 (w), 2283 (w) 2265 (s), 1638 (s), 1617 (m) 1528 (w), 1434 (m), 1419 (w), 1396 (m) 1371 (s), 1245 (m),1234 (m) 1181 (w), 1098 (w), 1047 (w), 734 (m) 713 (w), 610 (m), 551 (w) 487 (w) cm^{-1}. DTA/TG: 2 stages over the temperature range 24 °C to 235 °C; first mass loss of 8.5% at 36 °C (two molecules of CH_3CN (calculated amount 7.88%)), second mass loss of 16.7% at 150 °C with mass loss of 16.65% (three molecules of acetonitrile and two molecules of water (calculated amount 15.28%)).

Crystallization of 7ctz: Suitable crystals for X-ray analysis were obtained by applying diffusion of reacting solutions as the crystallization technique.[51,52] Tris(pyrazol-*1*-yl)methane (14 mg, 0.065 mmol) was dissolved in 3 mL of chloroform in a test tube. $Cu(NO_3)_2 \cdot 3H_2O$ (16 mg, 0.065 mmol) and Hctz (6.2 mg, 0.065 mmol) were dissolved in 3 mL of acetone. This solution was layered carefully by means of syringe over the chloroform solution. The test tube was covered by means of a perforated plastic paraffin coated film and left to stand at room temperature undisturbed for 3 days. Yield: 19 mg blue crystals (67.1%). M.p.: decomposition at 230 °C to a grey solid, explosion at 267 °C. Elemental analysis (%) $C_{24}H_{20}Cu_2N_{23}O_3 \cdot NO_3$ (867.72): calc. C 33.22, H 2.32, N 38.74; found C 33.60, H 2.72, N 38.67. IR (KBr disc): 3532 (w), 3123 (m), 3006 (m), 2258 (m), 1699 (m), 1631 (w), 1517 (m), 1411 (s), 1368 (s), 1299 (s), 1286 (m), 1257 (w), 1224 (w), 1111 (w), 1092 (m), 1076 (m), 1050 (m), 1004 (w), 969 (w), 916 (w), 818 (m), 803 (m), 792 (s), 776 (s), 607 (m), 553 (m) cm^{-1}.

Crystallization of 5a-ctz: $Mn(CH_3COO)_2 \cdot 4H_2O$ 48 mg (0.2 mmol) and Hctz 37.2 mg (0.4 mmol) were disolved in 20 mL of water and then heated for 3h at 80 °C to remove CH_3COOH. After this time, an ethanolic solution of 46 mg (0.3 mmol) bipy was slowly added to aqueous mixture. Slow evaporation of the solvent during two days gave yellow blocks. Yield: 70 %.

Crystallization of 8a-tca and 8tca: Crystals of **8a-tca** and **8tca** were prepared applying the same technique as described for **6ctz.** Expanding the crystallization time from 75 min. to two days was achieved by diluting the components. Reducing the concentration of Hctz to 2 % ((6:1 H_2O : EtOH), elongated the crystallization time to two days, which gave the blue **8a-tca** complex. After the reduction of concentration of Hctz to 0.1 % and slow evaporation of the solvent, blue crystals of **8cta** appeared after seven days.

Crystallization of 9tca: Crystals of **9tca** were prepared applying the same technique as described in **1ctz.** A 8 mL of aqueous solution of $Cu(NO_3)_2 \cdot 3H_2O$ (40 mg (0.17 mmol)) was layered in a test tube on the solution that contains: 47 mg (0.11 mmol) of PPh_4ctz dissolved in 8 mL of $CHCl_3$, then the test tube was closed. After 2 weeks blue long needles of **9tca** crystallized together with the **1ctz** complex.

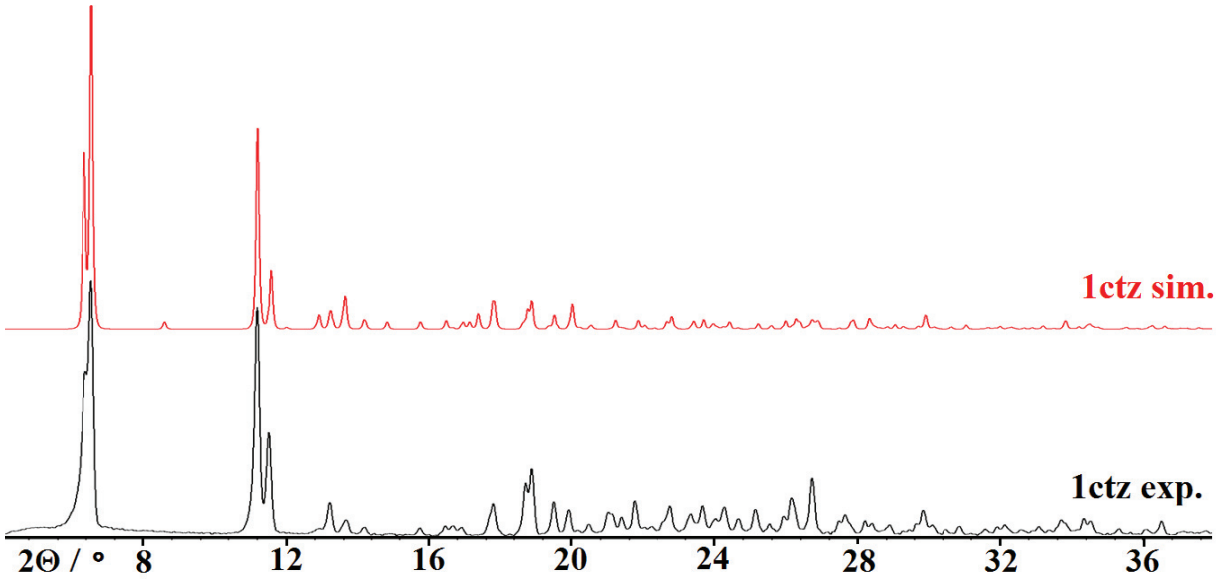

Figure 3.4.1 The simulated and experimental X-ray powder diffraction patterns of **1ctz** are shown (Cu-Kα radiation).

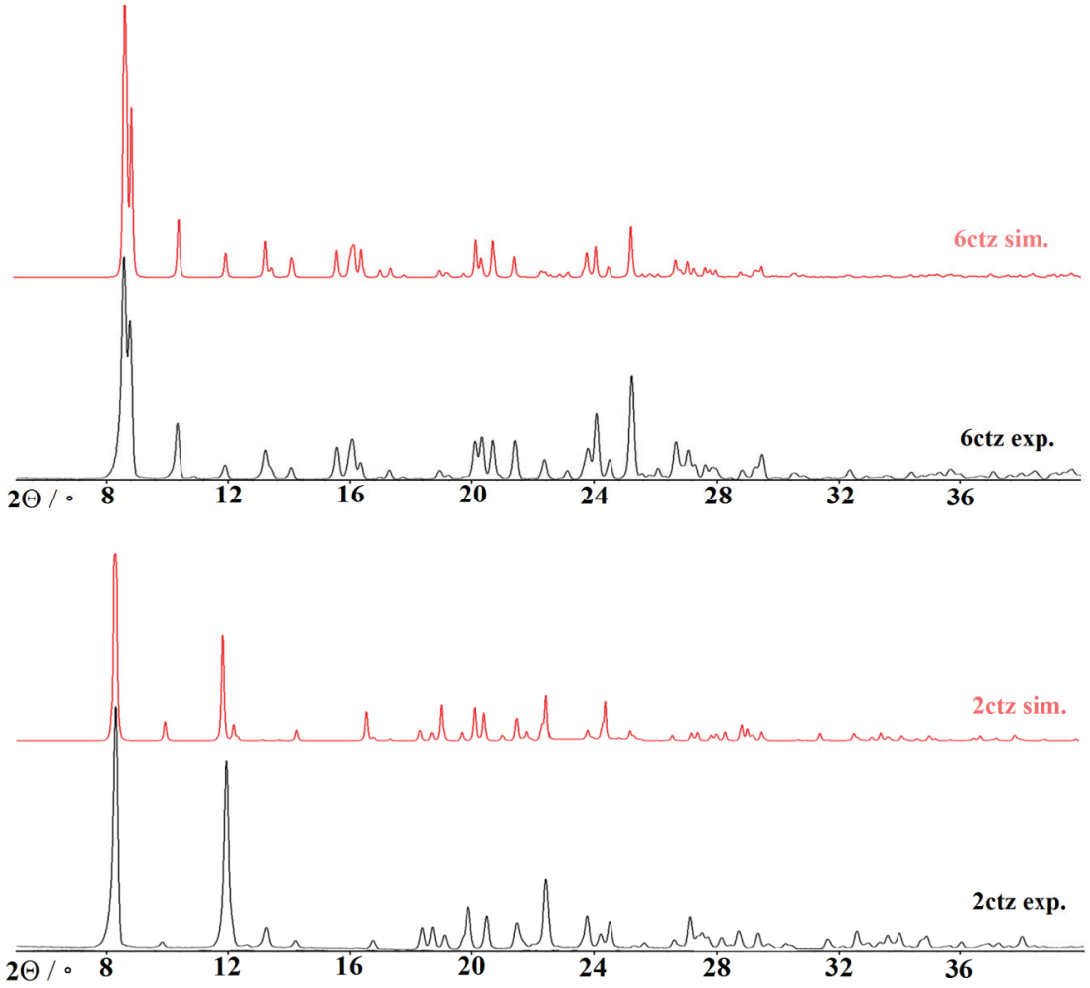

Figure 3.4.2 The simulated and experimental X-ray powder diffraction patterns of **4a-ctz** and **2ctz** are compared, showing that the complexes were isolated as a pure phase (Cu-Kα radiation).

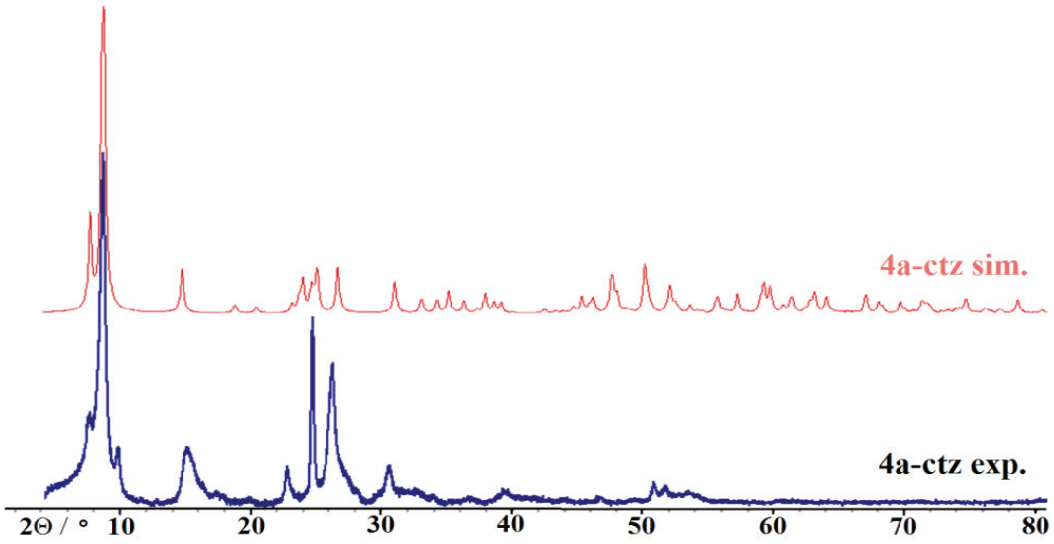

Figure 3.4.3 The simulated and experimental X-ray powder diffraction patterns of partly decomposed **4a-ctz** (Cu-Kα radiation).

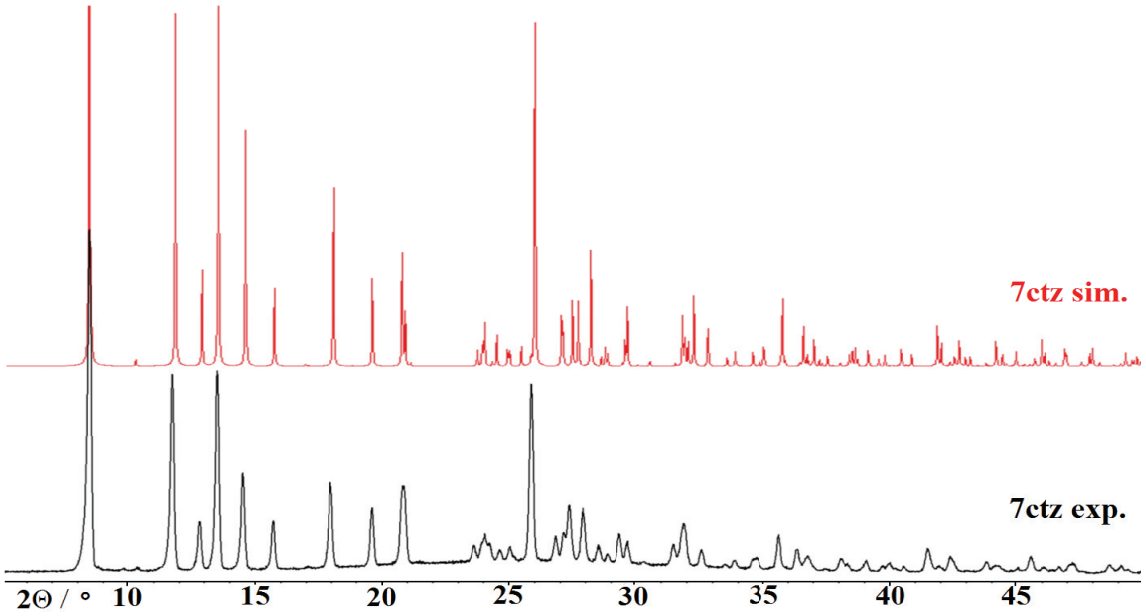

Figure 3.4.4 The simulated and experimental X-ray powder diffraction patterns of **7ctz** (Cu-Kα radiation).

References

[1] R. J. Herr, *Bioorg. Med. Chem.* **2002**, *10*, 3379.
[2] M. J. Crawford, T. M. Klapötke, F. A. Martin, C. M. Sabaté, M. Rusan, *Chem. Eur. J.* **2011**, *17*, 1683.
[3] C. G. Miller, G. K. Williams, US7667045, **2005**.
[4] T. M. Klapötke, S. M. Sproll, *J. Polym. Sci., Part A* **2010**, *48*,122.
[5] (a) R. P. Singh, R. D. Verma, D. T. Meshri, J. M. Shreeve, *Angew. Chem.* **2006**, *118*, 3664; (b) *Angew. Chem. Int. Ed.* **2006**, *45*, 3584–3601.
[6] G. Aromi, L. A. Barrios, O. Roubeau, P. Gamez, *Coord. Chem.Rev.* **2011**, *255*, 485.
[7] N. Fischer, T. M. Klapötke, S. Rappenglück, J. Stierstorfer, *ChemPlusChem* **2012**, *77*, 877.
[8] E. Oliveri-Mandala, T. Passalaqua, *Gazz. Chim. Ital.* **1912**, *41*, 430.
[9] (a) F. Himo, Z. P. Demko, L. Noodleman, K. B. Sharpless, *J. Am. Chem. Soc.* **2002**, *124*, 12210; (b) A. Hantzsch, A. Vagt, *JustusLiebigs Ann. Chem.* **1901**, *314*, 339; (c) H. Zhao, Z. R. Qu, H. Y. Ye, R. G. Xiong, *Chem. Soc. Rev.* **2008**, *37*, 84.
[10] E. J. Graeber, B. Morosin, *Acta Crystallogr. Sect. C* **1983**, *39*, 567.
[11] K. Yamaguchi, A. Ohsawa, T. Kaihoh, T. Itoh, *Acta Crystallogr. Sect. C* **1990**, *46*, 1161.
[12] P. Hans, H. Arp, A. Decken, J. Passmore, D. J. Wood, *Inorg.Chem.* **2000**, *39*, 1840.
[13] P. L. Franke, W. L. Groeneveld, *Trans. Met. Chem.* **1980**, *5*,240.
[14] A. N. Chermahini, H. A. Dabbagh, A. Teimouri, *J.Mol. Struc-Theochem* **2007**, *822*, 33.
[15] (a) J. March, *Advanced Organic Chemistry*, 3rd Edition. Wiley-Interscience: New York, **1985**; p. 788, (b) F. C. Schaefer, *The Chemistry of the Cyano Group*, Interscience: New York, **1970**, p. 239.
[16] V. Y. Kukushkin, A. J. L. Pombeiro, *Inorg. Chim. Acta* **2005**, *358*, 1.
[17] C.R. Clarke, R.W. Hay, *J. Chem. Soc., Dalton Trans.* **1974**, 2148.
[18] R. Breslow, R. Fairweather, J. Keana, *J. Am. Chem. Soc.* **1967**, 89, 2135.
[19] S. G. Kang, J. Song, J. H. Jeong, *Bull. Korean Chem. Soc.* **2002**, 23, 824.
[20] S.G. Kang, J. Song, J. H. Jeong, *Chem. Abstr*. **2002**, *137*, 256.

[21] R. Breslow, M. Schmir, *J. Am. Chem. Soc.* **1971**, *93*, 4960.
[22] K. Nasser, J. Thallaj, R. Przybilla, W. D. Mandon, *J. Am. Chem.Soc.* **2008**, *130*, 2414.
[23] W. Ouellette, S. Jones, J. Zubieta, *Cryst. Eng. Comm.* **2011**, *13*, 4457.
[24] T. C. Wehmann, A. I. Popov, *J. Phys. Chem.* **1966**, *70*, 3688.
[25] R. N. Butler, *Comprehensive Heterocyclic Chem. II*, Pergamon, New York, **1996**, vol. 4, p. 621.
[26] M. Inoue, M. Kubo, *J. Coord. Chem.* **1977**, *6*, 157.
[27] J. G. Haasnoot, *Coord. Chem. Rev.* **2000**, *200*, 131.
[28] J. Goslar, P. B. Sczaniecki, *Trans. Met. Chem.* **1988**, *13*, 81.
[29] P. J. Eulgem, A. Klein, N. Maggiarosa, D. Naumann, R. W. H. Pohl, *Chem. Eur. J.* **2008**, *14*, 3727.
[30] A. H. Bent, *Chem. Rev.* **1961**, *61*, 275.
[31] D. A. Dixon, P. A. Charlier, P. G. Gassman, *J. Am. Chem. Soc.***1980**, *102*, 3957.
[32] M. O'Keeffe, S. Andersson, *Acta Crystallogr. Sect. A* **1977**, *33*, 914.
[33] A. Ray, D. Maiti, W. S. Sheldrick, H. Mayer-Figge, S. Mondal, M. Mukherjee, S. Gao, M. Ali, *Inorg. Chim. Acta* **2005**, *358*, 3471.
[34] A. Rajput, R. Mukherjee, *Coord. Chem. Rev.* **2013**, *257*, 350.
[35] H. Sigel, R.B. Martin, *Chem. Rev.* **1982**, 82, 385.
[36] O. Clement, B. M. Rapko, B. P. Hay, *Coord. Chem. Rev.* **1998**, *170*, 203.
[37] L. R. Schmitz, N. L. Allinger, *J. Am. Chem. Soc.* **1990**, 112, 8307.
[38] N. L. Allinger, K. Chen, M. Raman, A. Pathiaseril, *J. Am. Chem. Soc.* **1991**, *113*, 4505.
[39] C. R. Kemnitz M. J. Loewen, *J. Am. Chem. Soc.* **2007**, 129, 2521.
[40] P. Müller, P. *Crystal Structure Refinement*. 1st Ed. New York, NY: Oxford University Press, **2006**
[41] G. Socrates, *Infrared and Raman Characteristic Group Frequencies – Tables and Charts*, 3rd ed., John Wiley & Sons Ltd., England **2001**.
[42] C. B. Aakeröy, B. M. T. Scott, J. Desper, *New. J. Chem.* **2007**, *31*, 2044.
[43] J. Bernstein, R. E. Davis, L. Shimoni, N. L. Chang, *Angew. Chem. Int. Ed. Engl.* **1995**, *34*, 1555.
[44] A. Rodríguez-Diéguez, A. J. Mota, J. Cano, J. Ruiz, D. Choquesillo-Lazarte, E. Colacio, *Dalton Trans.* **2009**, 6335.
[45] A. Aznar, S. Ferrer, J. Borrás, F. Lloret, M. Liu-González, H. Rodríguez-Prieto, S. García-Granda, *Eur. J. Inorg. Chem.* **2006**, 5115.
[45a] (a) E. Gungor, H. Kara, E. Colacio, A. J. Mota, *Eur. J. Inorg. Chem.* 2014, 1552; **(b)** M. Fondo, N. Ocampo, A. M. Garcıa-Deibe,a M. Corbella, M. R. Bermejo, J. Sanmartin, *Dalton Trans*. **2005**, 3785; **(c)** M. Fondo, A. M. García-Deibe, M. Corbella, J. Ribas, A. Llamas-Saiz, M. R. Bermejo, J. Sanmartin, *Dalton Trans.* **2004**, 3503.
[46] O. Kahn, *Molecular Magnetism*, **1993**, New York.
[47] Y. Garcia, P. J. Koningsbruggen, G. Bravic, D. Chasseau, O. Kahn, *Eur. J. Inorg. Chem.* **2003**, 356.
[48] Y. Garcia, P. J. van Koningsbruggen, G. Bravic, P. Guionneau, D. Chasseau, G. L. Cascarano, J. Moscovici, K. Lambert, A. Michalowicz, O. Kahn, *Inorg. Chem.* **1997**, *36*, 6357.
[49] K. Drabent, Z. Ciunik, A. Ozarowski, *Inorg. Chem.* **2008**, *47*, 3358.
[50] D. L. Reger, T. C Grattan, K. J. Brown, C. A. Little, J. J. S. Lamba, A. L. Rheingold, R. D. Sommer, *J. Organomet. Chem.***2000**, *607*, 120.
[51] P. G. Jones, *Chem. Brit.* **1981**, *17*, 222.
[52] A. Clegg, A. J. Blake, R. O. Gould, P. Main, *Crystal StructureAnalysis: Principles and Practice*, Oxford University Press, Oxford, UK, **2001**, p. 27.
[53] V. Yu. Kukushkin, A. J. L. Pombeiro, *Inorg. Chim. Acta* **2005**, *358*, 1.

PART 4

THE TETRACYANOPYRROLIDE ANION AS A LIGAND IN TRANSITION METAL COMPLEXES

Abstract

The coordination chemistry of the tetracyanopyrrolide anion $[C_4(CN)_4N]^-$ **(tcp)** was explored and its simple compounds Htcp **(10tcp)**, $[Na(tcp)H_2O] \cdot H_2O$ **(11tcp)**, $[Me_4N]tcp$ **(12tcp)** have been prepared and characterized in the solid state. Two isotypic mononuclear discrete complexes $[Co(MeCN)_4(tcp)_2] \cdot 2$ MeCN **(13tcp),** $[Ni(MeCN)_4(tcp)_2] \cdot 2$ MeCN **(14tcp)** were synthesized from **12tcp** and the respective metal perchlorates in acetone/acetonitrile. The tcp ligand in the presence of water and Cu(II) transition metal ions is hydrated to the respective carboxamide isolated as $[Cu(tcpc)_2(H_2O)_2] \cdot H_2O$ **(16tcpc)** and $[Cu(tcpc)_2(dmf)_2]$ **(17tcpc)** complexes, which incorporate a mononegative 3,4,5-tricyanopyrrole-2-carboxamide **(tcpc)** monoanions as a chelating ligand.

4.1 Introduction

Cyanocarbons are a class of compounds that consist solely of C and N, known as neutral species and as anions. The functionality is mainly dominated by the large number of present cyano groups, which are strongly electron withdrawing and participate by resonance with the π system of the underlying carbon ring or chain. Cyanocarbon molecules are highly electron deficient and the respective anions weakly basic and weakly coordinating.[1] Azole ring based polynitriles[2] and cyano-substituted pyrroles[3] have been in the focus of theoretical investigations, showing the aromaticity, the stability vs. oxidation and decreasing basicity with increasing number of CN groups. The pentacyanocyclopentadienide anion $[C_5(CN)_5]^-$ is a prominent member due to its high symmetry. The coordination chemistry of $[C_5(CN)_5]^-$ has received substantial attention during the last years for the preparation of metal-organic coordination polymers.[4-7] In contrast, the chemistry of its congener, in which a nitrogen atom replaces one ring carbon atom, namely the tetracyanopyrrolide anion (**tcp**) is still scarcely explored. Although the tcp anion was prepared already in 1980 by Webster *et al.* only one report about its structural chemistry has been published, which includes H(tcp), Me(tcp), $[Me_4N]$tcp, Na(tcp) · 2.33thf, and EMIM(tcp) (EMIM = 1-ethyl-3-methylimidazolium) compounds characterized by the single crystal X-ray diffraction.[9] This cyanocarbon ion attracted our attention because it has the potential for metal coordination, which maintain a classical σ coordination behaviour either through CN groups, as has been found in the structure of Na(tcp)[9] or via the N atom of the pyrrole ring. Substitution of all H atoms of the underlying pyrrolide $[C_4H_4N]^-$ anion with four electron-withdrawing CN groups leads to dispersion of the negative charge towards the peripheral cyano groups. Thus, the tcp may behave as a multifunctional ligand that gains particular interest in constructing metal-organic hybrid systems.

4.2 Results and Discussion

The tetracyanopyrrolide anion is a weak base in aqueous solution (pK_b = 11.29) and in the gas phase (proton affinity 1215 $kJmol^{-1}$).[3] Substitution of all C–H bonds in the parent pyrrolide anion by four C–C≡N groups dramatically decreases basicity of the anion making its conjuncted acid medium-strong (pK_a = 2.71). The tcp classified as a resonance binary C/N planar monoanion, can be synthesized in four steps as a sodium salt from commercially available carbon disulfide (CS_2) and sodium cyanide (NaCN) (see Appendix H). It can be easily isolated as the tetramethylammonium salt[2] $[Me_4N]$tcp **(12tcp)** in 37 % yield by adding an equimolar amount of $[Me_4N]Cl$ to the aqueous solution of Na(tcp) · H_2O. **10tcp** can be obtained by passing an acetonitrile solution of **12tcp** through a column filled with a with H^+ loaded cation exchange resin.

[2] Crystal structures recently published by M. Becker, J. Harloff, T. Jantz, A. Schulz, A. Villinger, *Eur. J. Inorg. Chem.* **2012**, *34*, 5658.

The synthetic method employed for the formation of the complexes **13tcp** and **14tcp** is the metathesis reaction of $[Me_4N]tcp$ with the perchlorates of Co^{2+} and Ni^{2+} as summarized in Scheme 4.2.2. If water is not strictly excluded, tcp undergoes hydration under transformation of one cyano substituent to a carboxamide group, transforming tcp into 3,4,5-tricyanopyrrole-2-carboxamide, which yields in the complexes **16tcpc** and **17tcpc**.

$$M(ClO_4)_2 + 2\,[Me_4N]tcp \xrightarrow{\text{acetone}} M(tcp)_2 + 2\,[Me_4N]ClO_4$$

$$M(tcp)_2 \xrightarrow{\text{MeCN}} [M(NCMe)_4(tcp)_2] \cdot 2\,MeCN$$

$$M = Co^{2+}, Ni^{2+}$$

Scheme 4.2.2 The synthetic route for the formation of complexes **13tcp** and **14tcp**.

The experiments show that the coordination ability of tcp is rather weak. It turned out as essential to use a weakly coordinating anion in transition metal salts for the successful synthesis. Water-free metal perchlorates $Co(ClO_4)_2$ and $Ni(ClO_4)_2$ dissolved in dry acetone were therefore used. During crystallization, the perchlorate residues could be precipitated out as the white $[Me_4N]ClO_4$ solid, when mixed with $[Me_4N]tcp$, mainly leaving the M^{2+} (M = Ni, Co) cations and the tcp anions in the solution. The recrystallization of the residues from acetonitrile yielded two new complexes **13tcp** and **14tcp**, deeply investigated.

4.2.1 Thermal Behaviour of Mononuclear Complexes with tcp as Ligand

The thermal decomposition of the air stable complex **14tcp** occurs in two stages in the temperature range of 25 - 420 °C. The first mass loss of 12.6 % occurs between 90 - 130 °C with the DTA peak at 110.3 °C and is assigned to the release of two solvate acetonitrile molecules (calculated weight loss 12.9 %) (Figure 4.2.1.1). The second mass loss of 22.0 %, occurring between 140 - 190 °C (DTA peak at 176.1 °C), is attributed to the release of four coordinated MeCN molecules (calculated mass loss 25.8 %), which leads to $Ni(tcp)_2$. The crystals of **13tcp** have a pronounced tendency to lose the incorporated solvate molecules. Just on exposure to air, freshly prepared orange crystals of **13tcp** become opaque after some minutes. This limited stability of the **13tcp** complex in air results in the low accuracy in the thermal and elemental analyses in comparison to the nickel **14tcp** complex. Thermal decomposition occurs in two stages with the first mass loss of 16.4 % beginning as low as 25 °C (DTA peak at 73.1 °C). The second detected mass loss of approx. 17 % can be contributed to the formation of $Co(tcp)_2$ (Figure 4.2.1.1).

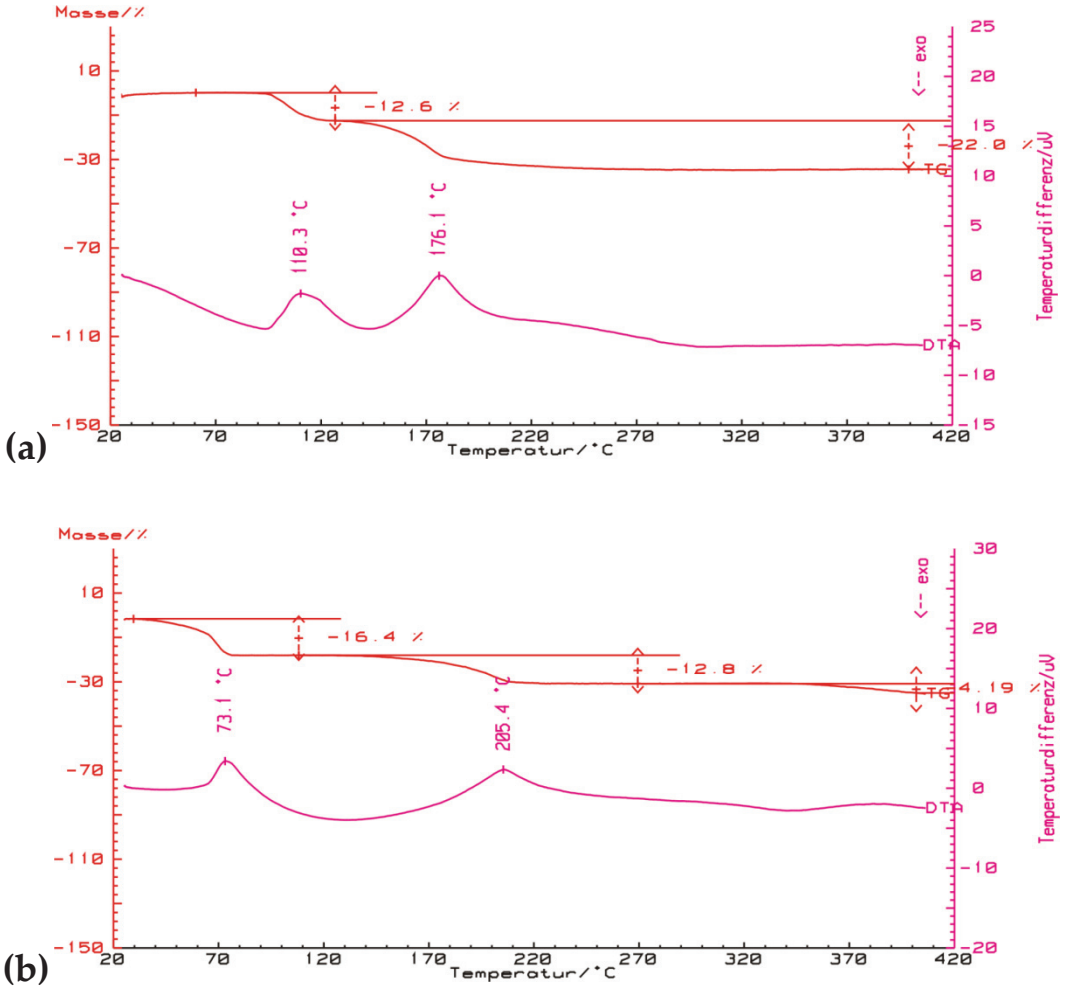

Figure 4.2.1.1 TG/DTA curves of **14tcp (a)** and **13tcp (b)** measured under argon-gas flow at the heating rate of 7 °C/min. Red - TG curve, pink - DTA curve.

4.2.2 Cyclic Voltammetric Investigation of [Me$_4$N]tcp

In the current study, the electrochemical behavior of **12tcp,** investigated by cyclic voltammetry, suggests an irreversible redox process with single electron transfer (Figure 4.2.2). During the anodic scan, an oxidation wave for the tcp was observed at + 1.20 *V* (E_{pa}), whereas a reduction wave at –0.25 *V* (E_{pc}) was observed during the reverse scan. The average of two peak potentials does not afford the half-wave potential for the corresponding couple ($E_{1/2}$ = (E_{pa} + E_{pc})/2) like in the case of redox process of ferrocene (Figure 4.2.1).[11] Moreover, the peaks are reduced in size and they are widely separated, indicating an irreversible process. Usually, a reversible couple potential follows: $\Delta E_p = E_{pa} - E_{pc} = 0.059/n$, but this equation not fulfilled for **12tcp**. As a result, the slow electron transfer and the reduction rate constant results in an 'elongated shape' in the cyclic voltammogram. The most reasonable identity of the produced transient species can be attributed to the unstable neutral radical of **12tcp**.

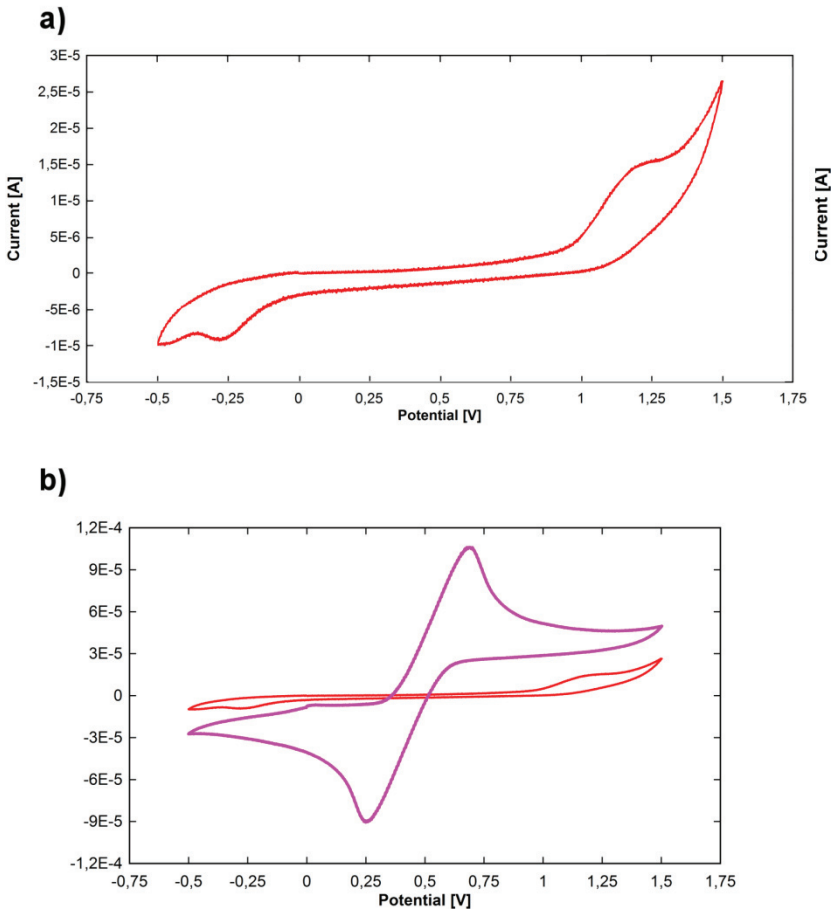

Figure 4.2.2 (a) The cyclic voltammogram of **12tcp** (5 mM) in CH_2Cl_2 at 25 °C ((0.1 M) [N(*n*-Bu_4)]BF_4 supporting electrolyte; scan rate 400 mVs^{-1}; glassy carbon working electrode, $Ag/AgNO_3$ reference electrode). **(b)** The cyclic voltammogram of **12tcp** vs. ferrocene Fc^0/Fc^+ as a reference.

4.2.3 Molecular Geometry of the tcp Ligand in its Simple Salts and in the Mononuclear Complexes

The tcp anions are planar (**12tcp**) or almost planar (**10tcp**, **11tcp**, **13tcp**, **14tcp**, **15tcp**), the maximal deviation from the least square planes through all 13 atoms amounts to 0.09 Å for tcp anion. The functionality of the anion is based on the five-membered C_4N heterocyclic system with four cyano groups attached to the pyrrolide moiety. The C–N and C–C bond lengths within the rings (1.362–1.409 Å), the exocyclic C–C bond lengths (1.423–1.436 Å) and the C≡N triple bond lengths (1.144–1.150 Å) reveal a good agreement with previously determined crystal structures involving this anion and the optimized structure obtained on the basis of DFT calculations.[9] The charge of C_4N-ring unit in the tcp ion is dispersed towards four cyano groups, which results in a reduced negative charge compared to the $[H_4C_4N]^-$ pyrrolide ion (from −1.74*e* to −0.80*e*). Upon substitution with four cyano groups the basicity of the N pyrrole atom is slightly reduced from −0.63*e* to −0.45*e*.[9] This results in the more favourable σ-type interaction with metal ions than in the π-type. The tendency for delocalization of the π-electron

system towards the peripheral groups is displayed in the exocyclic C–C bond lengths, which are only slightly longer than those within the aromatic ring. The ideal C_{2v} symmetry of the tcp anion is disturbed by the packing arrangement or by non-covalent interactions between molecules.

4.2.4 The Simple Salts with tcp Anion

The single-crystal X-ray diffraction study was undertaken on yellowish crystals of Htcp (**10tcp**),[3] produced using a strongly acidic cation exchange resin. Recrystallization from CH_2Cl_2 gave unsolvated crystals. The crystal structure was refined in the orthorhombic space group *Pna*2$_1$. The protonation occurs at the N pyrrole atom of the five membered ring, thus gaining an sp^2 hybridization. The Htcp as neutral molecules are organized in hydrogen-bonded chains extended along the crystallographic *b*-direction (Figure 4.2.4.1). The packing of the structure is influenced by the interaction between pyrrole N–H donor groups and the corresponding adjacent cyano acceptors at the 3 position of the five-membered ring. The chain motif can be referred to a graph-set notation $C_1^1(6)$[13] with N···N distance of 2.894 Å and N–H bond length of ca. 0.89 Å (Appendix E). The chains form an *ABAB* array in the crystallographic *c*-direction.

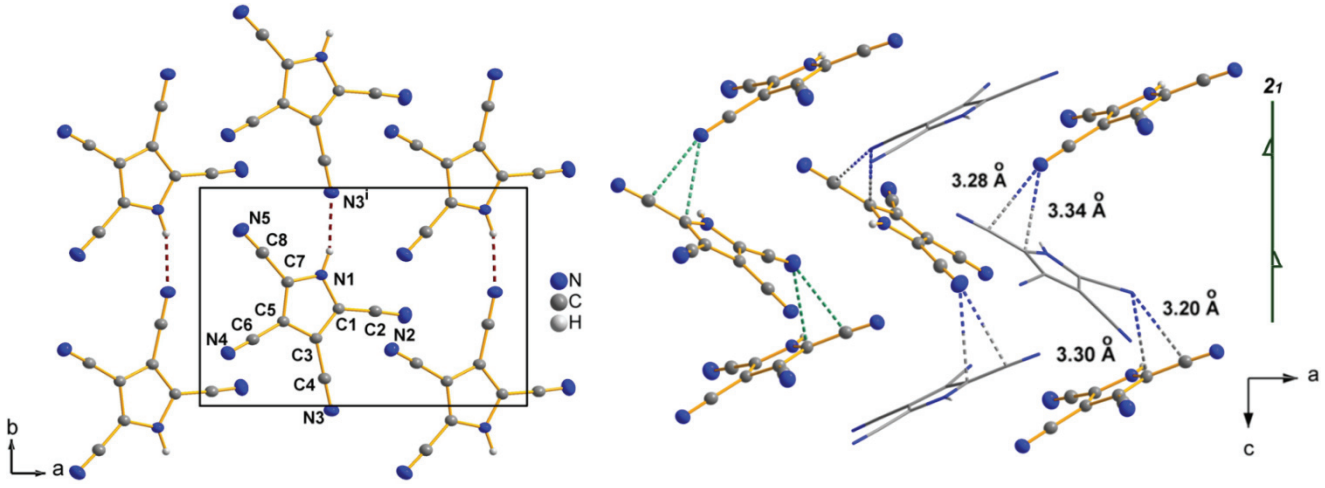

a) **b)**

Figure 4.2.4.1 (a) Hydrogen bonding in the unit cell of **10tcp. (b)** The *ABAB* arrangement of the Htcp molecules of **10tcp**. The short intermolecular distances are indicated by the dotted lines. The wireframe-styled molecules are twisted with respect to the 2$_1$ screw axis. Symmetry code: (i) *x*-0.5, *y*, -*z*+1.

Slow crystallization of Na(tcp) from a $CHCl_3$-MeOH mixture provided yellowish long crystalline needles of sodium salt [Na(tcp)H_2O] · H_2O **(11tcp)**. The crystal structure was refined in the monoclinic centrosymmetric space group *C*2/*c*.

[3] In the course of this thesis work, the crystal structure of Htcp was determined. Independently, A. S. Schulz and co-workers published this crystal structure in 2012. The structure will be described here anyway.

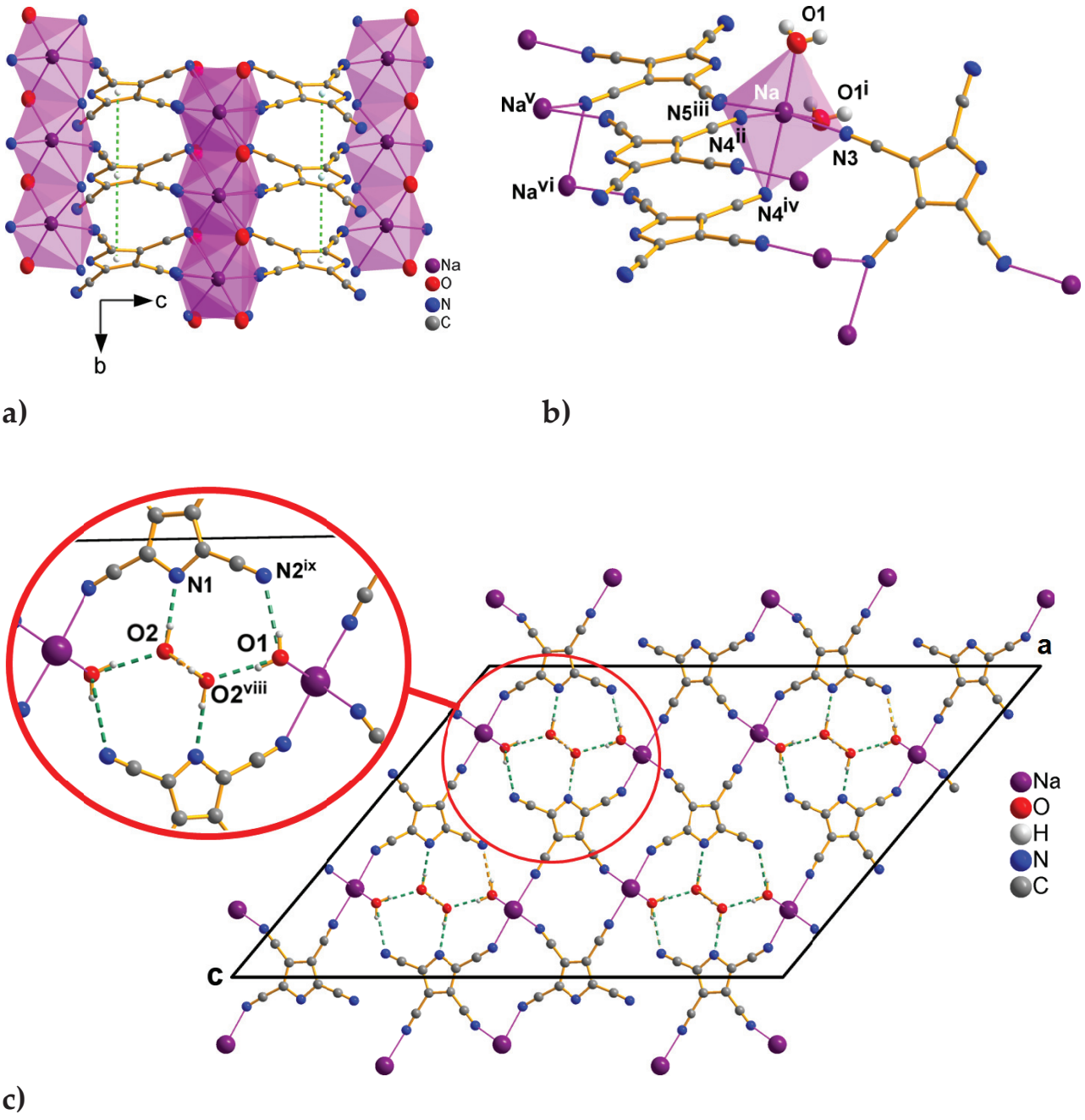

Figure 4.2.4.2 **(a)** The crystal structure of **11tcp** reveals the π···π interactions of the tcp anions (centroid···centroid distance 3.74 Å). **(b)** Coordination environment of the Na^+ ion in the **11tcp,** tcp acts as four-connecting ligand. Symmetry codes: (i) *x*, *y*−1, *z*; (ii) −*x*, *y*+1, −*z*−1/2; (iii) *x*, −*y*, *z*−1/2; (iv) −*x*, *y*, −*z*−1/2; (v) *x*, *y*+1, *z*; (vi) −*x*, *y*−1, −*z*−1/2. **(c)** View of the unit cell of the structure of **11tcp** along the *b*-axis. The three-dimensional network is made up by intermolecular hydrogen bonding interactions (green dotted lines). Symmetry codes: (viii) *x*, −*y*+1, *z*−1/2; (ix) −*x*+1/2, −*y*+3/2, −*z*.

The large *a* and *c* lattice parameters (31.859(3) Å and 23.376(1) Å, respectively) in contrast to the short *b* constant (3.743(1) Å) are affected by a 2D network formed in the *ac*-plane. The symmetry equivalent Na ions have a slightly distorted *cis*-[NaO_2N_4] environment with approximately C_{2v} point symmetry.

Each sodium atom is surrounded by two crystallographically related water molecules and also by four crystallographically related tcp donor ligands, which are σ-bound to the metal ion (Figure 4.2.4.2). Three out of the four CN groups coordinate to the Na^+ ion, of which two are forming single σ-bonds with the metal ions and one is bridging two sodium atoms in the distance of 3.74 Å. In such way, tcp acts as a four-connecting ligand with one cyano group unbound. The dense packing of **11tcp** is facilitated by weak π···π interactions between the aromatic rings and again by the sodium chains extended along the crystallographic *b*-direction (Figure 4.2.4.2). The Na–N and Na–O bond lengths fall in the range of 2.370 – 2.802 Å. Together with the coordinated water tcp anions join the edge-shared *cis*-[NaO_2N_4] octahedra in the chains, further connecting them to 2D layers parallel to the *ac*-plane. The three dimensional network is formed when taking into account the hydrogen bonds between the lattice and hydrated water molecules, uncoordinated cyano groups and the pyrrolide N atoms (Figure 4.2.4.2). The described structure reveals an interesting comparison with the similar salt Na(tcp) · 2.33thf[9] and shows the variability of the coordination. In contrast to the **11tcp**, the thf solvated salt crystallizes in the triclinic $P\bar{1}$ space group as a 3D coordination polymer, in which the pyrrolide nitrogen atoms always take part in the Na^+ coordination, either one or two CN groups remain uncoordinated.

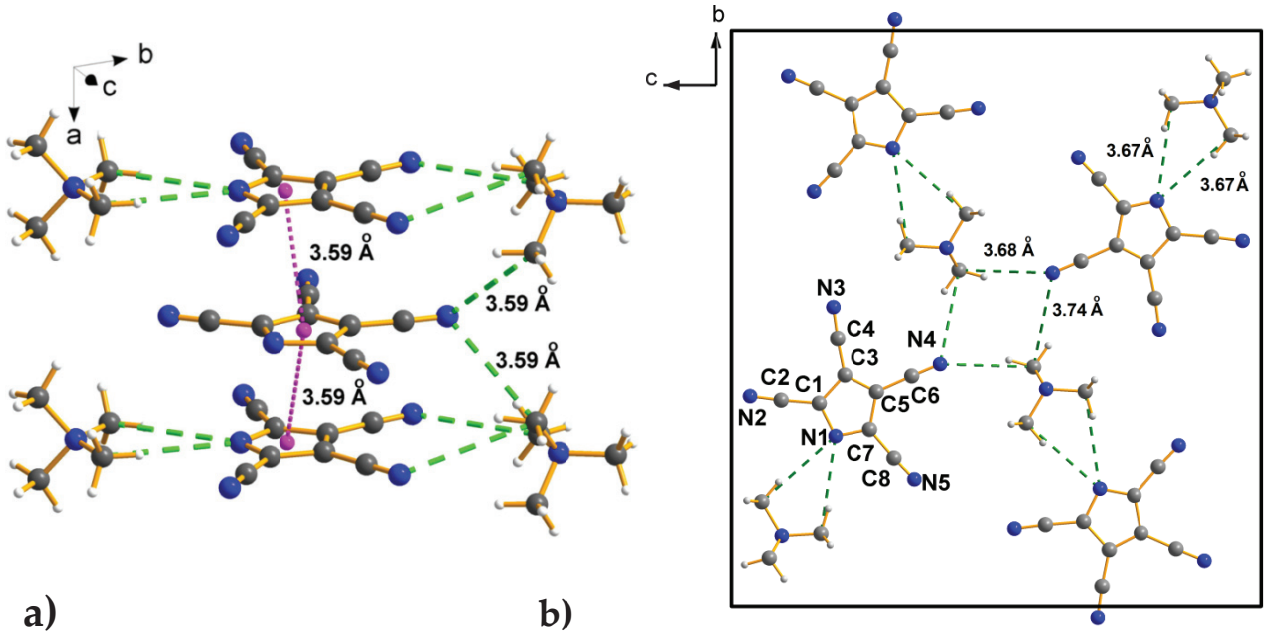

Figure 4.2.4.3 (a) The π···π interactions between planar molecules with respect distance of 3.59 Å in **12tcp**. **(b)** The *C*-centered unit cell of **12tcp**, dotted green lines – short intermolecular interactions between the cations and the anions.

The crystal structure of the salt [Me_4N]tcp **(12tcp)**, refined in the centrosymetric space group *Cmca* consists of tcp anions, which are balanced by the positively charged tetramethylammonium ions. The ion pairs are associated by weak electrostatic interactions between the H atoms of the methyl groups and the N pyrrolide atoms, which function as bifurcated acceptors. The significant intermolecular short C···N contacts are close to the sum of their van der Waals radii (3.25 Å)[14] (Figure 4.2.4.3). Both, cations and anions are located in

crystallographic mirror planes. Therefore, the tcp ligands are completely planar. The tcp anions are stacked parallel to the *bc*-plane and separated by the distance of 3.59 Å. These non-covalent π interactions between the centroids of five-membered rings are similar to those in the lattice of organic pentacyanocylcopentadiene salts.[4]

4.2.5 Transition Metal Complexes with tcp as Ligand

Two isotypic mononuclear discrete complexes $[Co(MeCN)_4(tcp)_2] \cdot 2\ MeCN$ **(13tcp)** and $[Ni(MeCN)_4(tcp)_2] \cdot 2\ MeCN$ (**14tcp**) containing the tcp ligand were synthesized in metathesis reactions shown in Scheme 4.2.2. Both structures contain mononuclear complexes with the central metal ions Co^{2+} and Ni^{2+} located at inversion centres. The metal atoms are six-fold coordinated each in a slightly distorted octahedral shape by two *trans*-positioned tcp ligands and four molecules of acetonitrile in the equatorial plane (Figure 4.2.5.1). Two axially bound tcp ligands are coordinated via their N atoms of the pyrrole rings in the η^1-fashion.

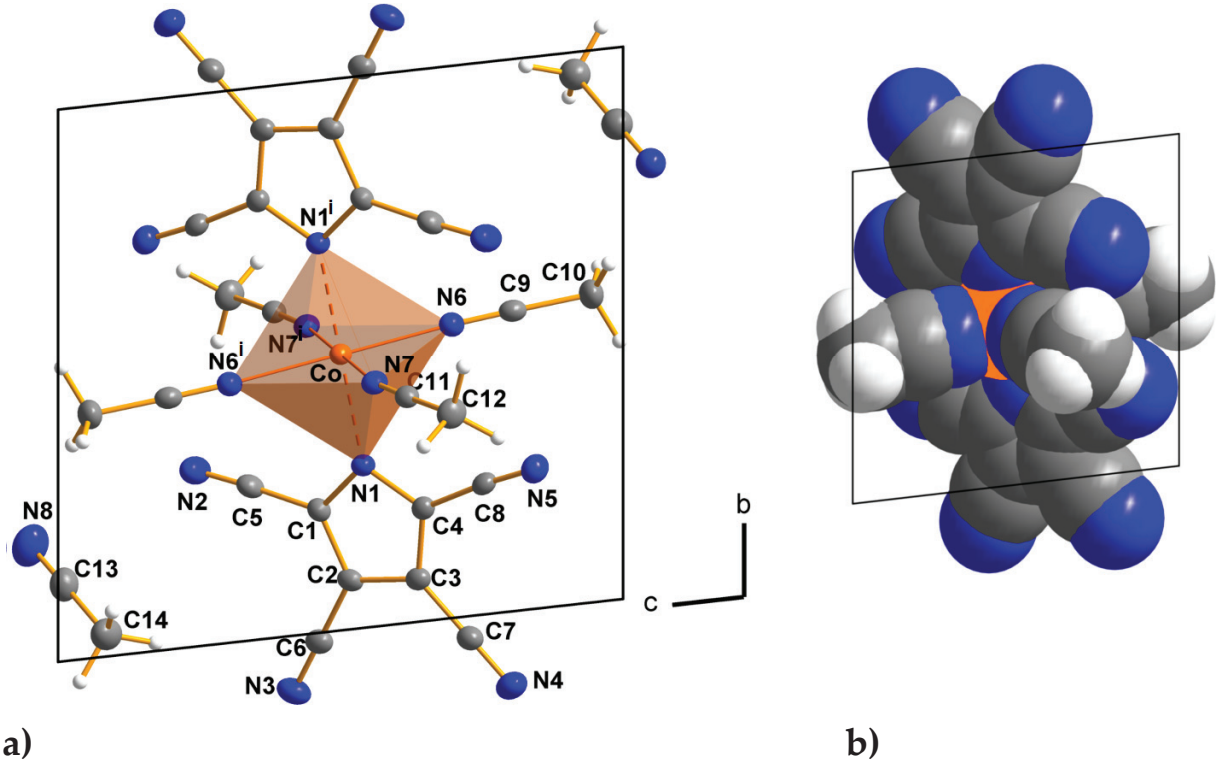

Figure 4.2.5.1 (a) The crystal structure of $[Co(MeCN)_4(tcp)_2] \cdot 2\ MeCN$ (**13tcp**) in a view of the unit cell along the *a*-axis. Displacement ellipsoids are drawn to enclose a 50 % probability. **(b)** Space filling model of the complex is given to depict the high sterical demand of the tcp ligand. The solvate CH_3CN molecules have been omitted for clarity. Symmetry code: (i) $-x, -y, -z+2$.

A sandwich structure with η^5-pyrrolide ligands as characteristic for the bis(η^5-pyrrolide)cobalt or bis(η^5-pyrrolide)nickel complexes [15,16] is not present, which is obviously caused by the low electron density in the central C_4N ring due to the strong electron-withdrawing effect of the

nitrile substituents. The average angle M−N−centroid (tcp ring) equals 178 °, indicating that the metal atoms are essentially in the plane of the C_4N ring, which is expected for a σ-bonding situation. The bonds M−N(pyrrole) amount to ca. 2.15 Å for **13tcp** and 2.11 Å for **14tcp** and are shorter than previously observed in $[Na(tcp)H_2O] \cdot H_2O$ but slightly longer than those of the bonds M−$NCCH_3$ in the equatorial planes (average M−N 2.12 Å for **13tcp** and 2.07 Å for **14tcp**). Two nitrile substituents at the 2 and 5 positions of the pyrrole ring cause a high sterical demand of this molecule when bound in the η^1-*N* mode, which becomes apparent in the space filling representation of the molecular structure (Figure 4.2.5.1). Complexes **13tcp** and **14tcp** adopt a similar structural arrangement as found for the complex $[Co\{C_5(CN)_5\}_2(H_2O)_2(thf)_2]$ ($C_5(CN)_5^-$ = pentacyanocyclopentadienide anion), where the Co(II) atom is coordinated by the N atoms of nitrile groups of two *trans*-positioned $C_5(CN)_5$ ligands.[5] In the crystal of **13tcp** and **14tcp** complexes, the shortest distance between the centroids of each two closest neighboured tcp ligands amounts to 4.36 Å, which excludes any π-stacking interactions.

4.2.6 Bis-chelate Copper(II) Complexes of 3,4,5-tricyanopyrrole-2-carboxamide

The single X-ray crystal structures of copper(II) complexes **16tcpc** and **17tcpc** complexes shown in Figure 4.2.6.1 are based on the ligand 3,4,5-tricyanopyrrole-2-carboxamide (tcpc), binding to the central atom with two atoms. Both complexes are closely related, although **16tcpc** compound crystallizes in monoclinic space group $P2_1/c$ whereas **17tcpc** is described in $P\bar{1}$. In both crystal structures, the copper(II) central atoms are in inversion centres and adopt an octahedral coordination. The equatorial positions are occupied by two symmetry-related tcpc ligands to form a five-membered planar chelate ring. The binding to the Cu atoms occurs through the carbonyl oxygen atom and through the N atom of the aromatic ring.

The six-fold coordination if fulfilled by two *trans*-positioned dmf molecules, which coordinate via their oxygen atoms (**17tcpc**) or by *trans*-positioned water molecules (**16tcpc**) to give an elongated octahedron. A pronounced Jahn-Teller effect is present, manifested in largely differing bond lengths Cu−N(equat) = Cu−O(equat) = 1.96 Å and $Cu-O_{(axial)}$ = 2.56 Å for **17tcpc** or $Cu-N_{(equat)}$ = $Cu-O_{(equat)}$ = 1.97 Å and $Cu-O_{(axial)}$ = 2.50 Å for **16tcpc**. The tcpc ligands are essentially planar, the largest deviation from the plane through all 16 atoms amounts to 0.14 Å. Moderately strong amide-amide hydrogen bonds interlink the mononuclear $[Cu(tcpc)_2(H_2O)_2]$ (**16tcpc)** or $[Cu(tcpc)_2(dmf)_2]$ (**17tcpc**) entities (e.g. a moderately H-bonds $N2\cdots N3^{i}$ = 3.04 Å in the **16tcpc**), which further propagate to form chains. Moreover, in the **16tcpc** complex, the *trans*-positioned water together with the crystallization water molecules (residing between mononuclear complexes) take also part in H-bonding interactions ($O3^{iv}\cdots O2$ = 2.94 Å and $N5\cdots O3^{iv}$= 2.94 Å) to ensure the connectivity between the chains.

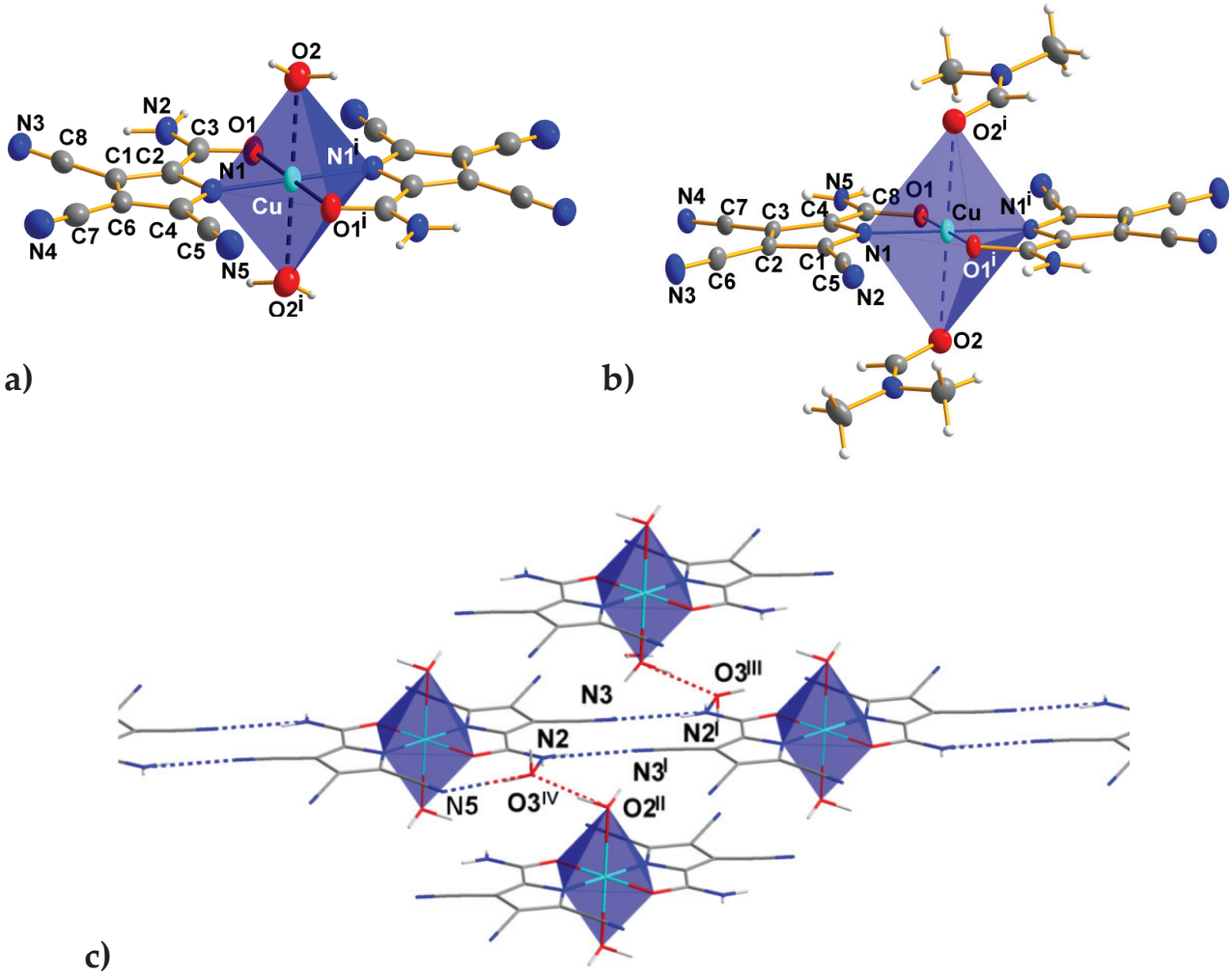

Figure 4.2.6.1 Coordination environment of the mononuclear complexes of **16tcpc (a)** and **17tcpc (b).** The chelation results in the formation of five membered rings. **(c)** A view of the structure of **16tcpc** complex, showing a section of the polymeric structure formed by intermolecular H-bonds (N–H···N and water-mediated amide hydrogen bonds)**.** Displacement ellipsoids are drawn to enclose a 40 % probability. Symmetry codes: (i) −x, −y, −z+1; (ii) −x+1,y+1/2, −z+1/2; (iii) −x+1, −y, −z; (iv) x ,y, 1−z.

In the **17tcpc** complex, this function is attributed to the carbonyl oxygen atoms of *trans*-positioned dmf molecules, which are further bound to adjacent carboxamide NH_2 groups. The combination of those two kinds of hydrogen bonds results in 3D hydrogen polymeric network shown in the Figure 4.2.6.1.

4.2.7 Copper Mediated Mono-Hydration of Cyano Group

Crystallization of copper complexes with tcp ligand in the presence of traces of water yielded a new series of complexes $[Cu(tcpc)_2(H_2O)_2] \cdot H_2O$ **(16tcpc)** and $[Cu(tcpc)_2(dmf)_2]$ **(17tcpc),** containing the product of hydration 3.4.5-tricyanopyrrole-2-carboxamide (tcpc). The mechanistic considerations of the transformation of tcp to tcpc were based on the metal-

mediated mono-hydration of a cyano to the carboxamide group under mild conditions, which are very similar to the process extensively described in the subchapter 3.2.7. Taking into account the crystal structures of **13tcp**, $[Co\{C_5(CN)_5\}_2(H_2O)_2(thf)_2]$ $(C_5(CN)_5)^-$ = pentacyanocyclopentadienide anion)[5] and **16tcpc** a reasonable mechanism of tcp to tcpc formation in the complex **16tcp** could be concluded (Figure 4.2.7.1). So far, only the η^1-*N*-σ-coordination mode in the complexes was found. The proposed hydration mechanism shown in Scheme 4.2.7.1 is based on this structural feature. It is assumed that in initial step water approaches to the equatorial plane of the metal site. Thus, the mononegative tcp anions bind to the copper ion through the N atom of the pyrrolide rings in the *trans*-position, leaving all CN groups unbound.

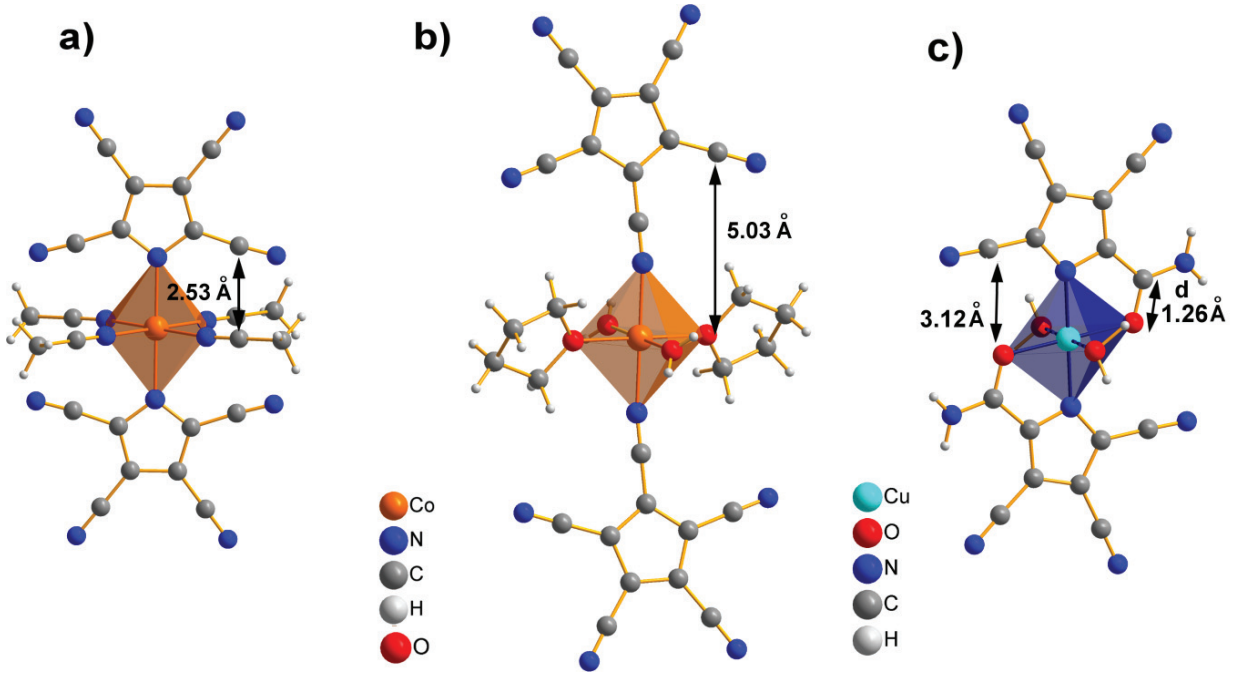

Figure 4.2.7.1 Coordination environment of the molecular complexes **13tcp (a)**, the complex $[Co\{C_5(CN)_5\}_2(H_2O)_2(thf)_2]$ $(C_5(CN)_5)^-$ = pentacyanocyclopentadienide anion)[5] **(b)** and **16tcpc (c)** with the marked distance between the cyano groups and equatorial planes. Coordination through N pyrrolide atom shortens the distance equatorial plane···CN groups from ca. 5.03 Å to 2.53Å, which creates a suitable prerequisites for the nucleophilic attack when water is present. Detailed description of the crystal structures of **13ctz** and **16tcpc** complexes are given in sub-chapters 4.2.5 and 4.2.6.

The η^1-coordination drastically shortens the distance of cyano groups to the equatorial plane of the complex. This close approach of the cyano groups at the positions 2 and 5 (Figure 4.2.7.1) favors the nucleophilic attack of the hydroxide to the cyano carbon atom, which leads to the new C=O bond formation. The transformation of cyano groups only in the 2 position of the tcp ions is interrelated with the distance of the *trans*-coordinated water. Just two CN groups are present in the vicinity of two water molecules. In other words only two water molecules are placed near the plane of the tcp ion and only there the nucleophile attacks. The remaining two

water molecules located in the equatorial plane are too far away from the CN groups at 5 position to attack them.

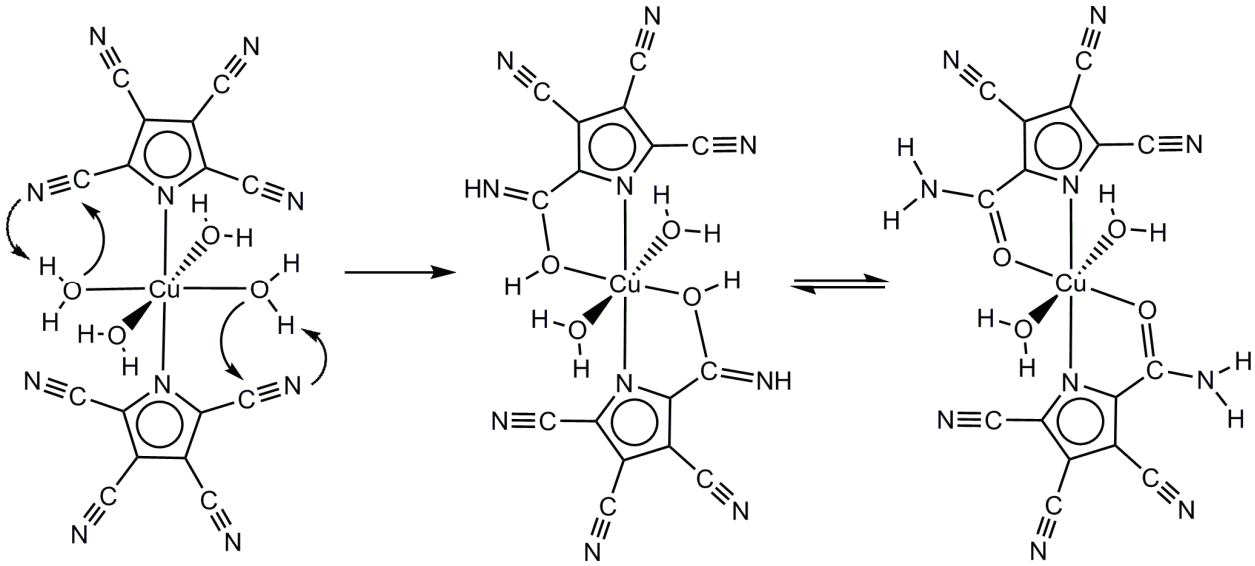

Scheme 4.2.7.1 Proposed mechanism for the metal-mediated mono-hydration of the tcpc ligand in the **16tcpc** complex.

4.2.8 Magnetic Interactions in the Transition Metal Complexes with tcp as Ligand

Magnetic susceptibility data of $[Ni(MeCN)_4(tcp)_2]\cdot 2MeCN$ (**14tcp**) and, due to its sensitivity of $[Co(MeCN)_4(tcp)_2] \cdot 2MeCN$ (**13tcp**) with some loss of incorporated MeCN were recorded in the range of 1.9 K – 300 K. Both complexes show nearly ideal Curie behaviour in the full temperature range and therefore display regular paramagnetism. From the equation $\mu_{eff} = 2.828(\chi_{mol}T)^{1/2}$ the calculated effective magnetic moment per Ni^{2+} ion in **14tcp** complex at 300 K is 3.09 μ_B, which fits well with the free Ni^{2+} ion spin-only value for a $S = 1$ system ($\mu_{eff} = 2.83\ \mu_B$).[17] According to the linear regression of the $\chi^{-1} = f(T)$ function for the cobalt(II) **13tcp** complex (Figure 4.2.8.1) the susceptibility is consistent with a high-spin complex of a magnetically isolated Co^{2+} ion in octahedral coordination. The experimental moment μ_{eff} at 300 K amounts to 4.98 μ_B, which is substantially higher than the spin only value of $\mu_{eff} = 3.87\ \mu_B$ calculated for a $S = 3/2$ system. The enlarged effective magnetic moment is typical for Co^{2+} and is explained by the contribution of the orbital angular momentum to the magnetic moment.[18] The large M···M separation between the discrete complexes in the crystals excludes any significant metal-metal magnetic interactions and pure paramagnetism is present.

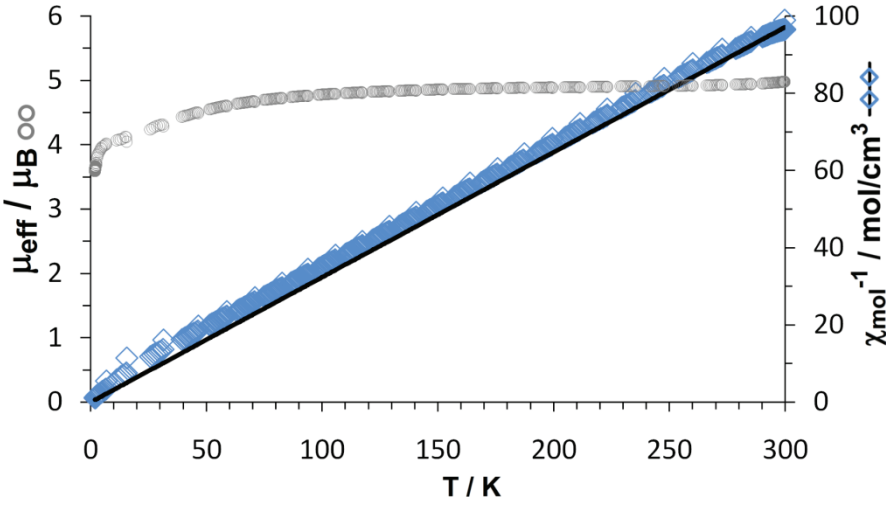

a)

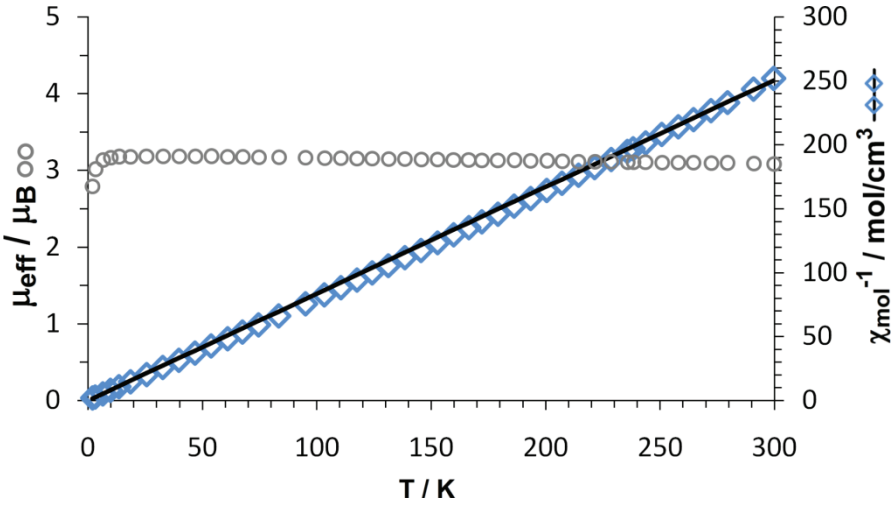

b)

Figure 4.2.8.1 Plots of inverse susceptibility $\chi^{-1}(T)$ and the effective magnetic moments μ_{eff} as function of temperature for the high-spin cobalt(II) **13tcp** complex **(a)** and nickel(II) complex **14tcp (b)** in a field of 10 kOe**.** The experimental data correspond to open square and circle points. The solid line represents the best fit to the Curie-Weiss model $\chi_{mol} = C/(T - \Theta)$ with $\Theta = 0$ K and C = 3.08 cm³K/mol for **13tcp** and $\chi_{mol} = C/(T - \Theta)$ with $\Theta = 0$ K and C = 1.20 cm³K/mol for **14tcp**. Agreement factor for the least-square fit: $R = 9.95 \cdot 10^{-3}$ for **13tcp** and $2.07 \cdot 10^{-3}$ For **14tcp.**

4.3 Conclusions

The study of the simple salts and mononuclear complexes with the tcp ligand led to synthesis and structural characterization of the first transition metal complexes of tcp anion. In two isotypic mononuclear discrete complexes $[Co(MeCN)_4(tcp)_2] \cdot 2$ MeCN **(13tcp)** $[Ni(MeCN)_4(tcp)_2] \cdot 2$ MeCN (**14tcp**) the tetracyanopyrrolide anion acts as a monodentate ligand towards the transition metal ions. Both complexes behave as diluted $S = 3/2$ (Co(II), **13tcp**) and S = 1 (Ni(II), **14tcp**) spin systems and obey the Curie-Weiss law. Only the η^1-*N*-σ coordination mode through the lone electron pair of the N atom of the pyrrolide ring was found. The other possible coordination mode, via the N atoms of the nitrile substituents were observed only in the structure of $[Na(tcp)H_2O] \cdot H_2O$ **(11tcp)** so far. The use of the Me_4N^+ cation yields mainly

isolated ions, which form parallel stacks within non-covalent π···π interactions between the aromatic rings in the crystal. In the presence of Cu^{2+} ions and even small amounts of water, tcp undergoes rapid mono-hydration under transformation of one cyano substituent to give a carboxamide group. The product 3,4,5-tricyanopyrrolide-2-carboxamide acts as a bidentate ligand as found in the complexes $[Cu(tcpc)_2(H_2O)_2] \cdot H_2O$ **(16tcpc)** and $[Cu(tcpc)_2(dmf)_2]$ **(17tcpc)**.

4.4 Experimental Section

Safety note: Sodium cyanide is highly poisonous and liberates volatile HCN when mixed with acids. Organic perchlorates like $[Me_4N]ClO_4$ have to be treated as potential explosives and must therefore be handled with precautions; only small amounts should be prepared. $Co(ClO_4)_2 \cdot 6 H_2O$, $Ni(ClO_4)_2 \cdot 6 H_2O$ and $Fe(ClO_4)_2 \cdot 6 H_2O$ and were dried under reduced pressure at 50 °C for about 5 hours. Acetonitrile and acetone were stirred overnight with dry K_2CO_3 and then destilled.

Tetramethylammonium tetracyanopyrrolide [Me_4N]tcp: The procedure mainly follows that given in [8] and with some modifications in [9].

Synthesis of tetramethylammonium tetracyanopyrrolide [Me_4N]tcp (12tcp): The procedure mainly follows that given in [8] and with some modifications in [9].
Finely powdered sodium cyanide NaCN (29.4 g, 0.6 mol) and 180 mL dmf were placed in a 1 L round-bottom flask and stirred. Then 47 mL (0.78 mol) of carbon disulfide CS_2 are added dropwise over 30 minutes. Stirring was continued overnight and a dark-brown mass was produced. To this mass, 250 mL of n-butanol was added and the mixture was heated to dissolve the product. The dark brown hot solution was filtrated to remove a residual of NaCN. From the filtrate dark brown crystal needles crystallized on cooling. After filtration, the wet crystalline solid was dissolved in 500 mL of distilled water and stirred for 24 hours. From the dark brown aqueous solution, sulphur precipitated and the solution became pale yellow. When dimerization was completed, sulphur was removed by filtration. Solid ammonium peroxodisulphate $(NH_4)_2S_2O_8$ (137 g, 0.6 mol) was added slowly over 2 hours. During this time, tetracyano-1,4-dithiine as a raw product precipitated from the aqueous solution. Yield: 18 g (55.5 %).
Tetracyanodithiine (10.8 g, 0.05 mol), sodium azide (3.25 g, 0.05 mol), and 200 mL EtOH were stirred over night at room temperature. The dark red reaction mixture was filtrated to remove elemental sulphur, and the filtrate was concentrated by removal of the solvent at reduced pressure using a rotary evaporator. The dark brown residual was dissolved in 200 mL of H_2O and treated with charcoal. After filtration, the volume of clear dark brown aqueous filtrate of raw product Na(tcp) was reduced on a rotary evaporator to about 40 ml and cooled down to 0 °C. A saturated solution of 11 g of tetramethlyammonium chloride $[Me_4N]Cl$ was added. Due to a moderate solubility of the final product in H_2O, a brown crystalline solid was obtained. This

was re-crystallized from a small amount of hot H_2O/acetone solution twice to give brown crystal needles of Me_4N(tcp) **(12tcp)** as a the pure product. Yield: 4.3 g (37 %); M.p. 280 °C; Elemental Analysis (%) $C_{12}H_{12}N_6$ (240.28 g/mol): C 59.05 (calc. 59.99); H 5.52 (5.03); N 34.39 (34.98) %; ^{1}H NMR (300 MHz, Me_2SO-D_6) δ 3.10 (s, CH_3, 12H) ppm; ^{13}C NMR (75 MHz, Me_2SO-D_6): δ 119.73 (s, C_{quat}, 2C), 114.50 (s, C_{quat}, 2C), 112.43 (s, C_{quat}, 2C), 101.94 (s C_{quat}, 2C), 54.38 (t, $J_{N,C}$ = 3.9 Hz, CH_3, 4 C) ppm.

Synthesis of Htcp (10tcp): The compound was prepared according to published procedure: A column containing 200 g a freshly regenerated ion exchanger Amberlite IR-120 (H^+-form) was washed first with acetone, then with acetonitrile. **(10tcp)** was prepared by passing 25 mL of an acetonitrile solution of 2 g of **12tcp** through the column of ion exchange resin. Obtained diluted solution of 10tcp was concentrated using a rotary evaporator to dryness. The brown residue was recrystallized twice from hot CH_2Cl_2 to give pale brown crystals. Yield: 0.16 g (12%) . M.p.: 200 °C. Elemental analysis (%) C_8N_5H (167.13 g/mol): calc. C57.50, H 0.60, N 41.90; found C 57.19, H 0.99, N41.20. ^{1}H NMR (300 MHz, Me_2SO-D_6) δ 7.78 (s, 1 H, NH) ppm. ^{13}C NMR (75 MHz, Me_2SO-D_6): δ 119.91 (s, C_{quat}, 2C), 114.49 (s, C_{quat}, 2C), 112.42 (s, C_{quat}, 2C), 101.94 (s C_{quat}, 2C) ppm.

Synthesis of [Na(tcp)H_2O] · H_2O (11tcp): The 200 mL of clear dark brown aqueous filtrate of raw product of Na(tcp) was applied to the top of a silica gel column. The column was eluted with $CHCl_3$/MeOH (v:v = 10:3.5). Three fractions were collected. Slowly evaporation of second fraction gave pale yellow crystals of **11tcp**. Yield: 23 %.

Crystallization of [Co(MeCN)$_4$(tcp)$_2$] · 2 MeCN (13tcp): 60 mg (0.25 mmol) of dry [Me_4N]tcp was dissolved in 10 mL dry acetone and mixed with a solution of 33 mg (12 mmol) of $Co(ClO_4)_2$ 10 mL dry acetone. [Me_4N]ClO_4 precipitated as a white solid, which was filtrated and discarded. The filtrate was evaporated to dryness and the solid residue was dissolved in dry acetonitrile. Slow evaporation of the solution (within about 6 days) produced orange crystals, which rapidly lost included solvent when taken out of the solution. Yield: 20 mg (20 %)**;** m.p. >420 °C under decomposition, analysis for $C_{24}H_{12}N_{14}Co$ (555.39 g/mol): C 46.17 (calc. 51.90); H 2.22 (2.18); N 32.63 (35.31) %.

Crystallization of [Ni(MeCN)$_4$(tcp)$_2$] · 2 MeCN (14tcp): The synthetic procedure follows that of **13tcp**, but with the use of $Ni(ClO_4)_2$. The product was obtained 33 % yield as air stable violet crystals. M.p. > 420 °C under decomposition. Elemental analysis $C_{28}H_{18}N_{16}Ni$ (637.27): C 52.02 (calc. 52.72); H 2.89 (2.84); N 34.98 (35.16) %

Crystallization of [Cu(tcpc)$_2$(H_2O)$_2$] · H_2O (16tcpc): $CuCl_2$ · $2H_2O$ (20 mg, 0.12 mmol) was disolved in 5 ml of H_2O. 5 mL of a solution of 30 mg (0.12 mmol) of 12tcp in acetone were added. After one day yellow-green crystals of **16tcpc** appeared.

Crystallization of [Cu(tcpc)$_2$(dmf)$_2$] (17tcpc): $Co(ClO_4)_2 \cdot 6\ H_2O$ (23 mg, 0.06 mmol) was dissolved in 10 mL of acetone. 5 mL of a solution of 30 mg (0.12 mmol) 12tcp in acetone were added. $[Me_4N]ClO_4$ precipitated as a white solid, which was filtered off and discarded. The filtrate was evaporated to dryness and dissolved in 3 mL of dmf. After four days, blue crystals in the shape of blocks appeared.

References:

[1] O. W. Webster, *J. Polymer Sci*. **2002**, *40*, 210.

[2] P. Johansson, H. Nilsson, P. Jabcobsson, M. Armand, *Phys. Chem.* **2004**, *6*, 895

[3] Rimarčík, V. Lukeš, E. Klein, M. Griesser, A. M. Kelterer, *Chem. Phys*. **2008**, *353*, 177.

[4] R. J. Less, M. McPartlin, J. M. Rawson, P. T. Wood, D. S. Wright, *Chem. Eur. J.* **2010**, *16*, 13723.

[5] R. J. Less, T. C. Wilson, M. McPartlin, P. T. Wood, D. S. Wright, *Chem. Commun.* **2011**, *47*, 10007.

[6] R. J. Less, B. Guan, N. M. Muresan, M. McPartlin, E. Reisner, T. C. Wilson D. S. Wright, *Dalton Trans.* **2012**, *41*, 5919.

[7] R. J. Less, T. C. Wilson, B. Guan, M. McPartlin, A. Steiner, P.T. Wood, D. S. Wright, *Eur. J. Inorg. Chem.* **2013**, *7*, 1161.

[8] H. E. Simmons, R. D. Vest, S. A. Vladuchick, O. W. Webster, *J. Org. Chem.* **1980**, *45*, 5113.

[9] M. Becker, J. Harloff, T. Jantz, A. Schulz, A. Villinger, *Eur. J. Inorg. Chem.* **2012**, *34*, 5658.

[10] K. Nasser. J. Thallaj, R. Przybilla, W. D. Mandon, *J. Am. Chem. Soc.* **2008**, *130*, 2414.

[11] J. Wang, *Analytical Electrochemistry*, Chapter 2, John Wiley & Sons, **2000**.

[12] R. S. Nicholson, I. Shain, *Anal. Chem.***1964**, *36*, 706.

[13] J. Bernstein, R. E. Davis, L. Shimoni, N. L. Chang, *Angew. Chem. Int. Ed. Engl.* **1995**, *34*, 1555.

[14] A. Holleman, E. Wiberg, *Lehrbuch der Anorganischen Chemie*, vol. 102, Walter de Gruyter, Berlin, **2007**.

[15] N. Kuhn, M. Köckerling, S. Stubenrauch, D. Bläser, R. Boese, *J. Chem. Soc., Chem. Commun.* **1991**, 1368.

[16] N. Kuhn, G. Henkel, J. Kreutzberg, S. Stubenrauch, *J. Organomet. Chem.* **1993**, 456, 97.

[16a] T. Astley, J. M Gulbis, M.A Hitchman, E. R. T. Tiekink, *J. Chem. Soc., Dalton Trans.* **1993**, 509.

[17] R. Grinter, *The Quantum in Chemistry: An Experimentalist's View*, Wiley Publishers, **2005**, p. 198.

[18] H. Lueken, *Magnetochemie*, Teubner Publishers, Stuttgart, Germany, **1999**.

[19] J. J. McGarvey, H. Toftlund, A. H. R. Al-Obaidi, K. P. Taylor, S. E. J. Bell, *Inorg. Chem.* **1993**, *32*, 2469.

[20] P. A. Anderson, T. Astley, M. A. Hitchman, R. F. Keene, B. Moubaraki, K. S. Murray, B. W. Skelton, E. R. T. Tiekink, H. Toftlund, A. H. White, *Dalton Trans.* **2000**, 3505.

[21] B. Moubaraki, B . A. Leita, G. J. Halder, S. R. Batten, P. Jensen, J. P. Smith, J. D. Cashion, C. J. Kepert, J. F. Létard, K. S. Murray, *Dalton Trans.*, **2007**, 4413.

[22] C. J. Schneider, B. Moubaraki, J. D. Cashion, D. R. Turner, B. A. Leita, S. R. Batten, K. S. Murray, *Dalton Trans.* **2011**, 40, 6939

PART 5

SPIN CROSSOVER IN THE MONONUCLEAR BIS-TRIPODAL IRON(II) COMPLEX CONTAINING TCP COUNTER-ION

Abstract

The mononuclear iron(II) complex $[Fe(tpm)_2](tcp)$ (**15tcp**) containing the neutral tripodal N_3-donor ligand tris(pyrazol-*1*-yl)methane (tpm) and the mononegative tetracyanopyrrolide (tcp) as counter-anion has been characterized by X-ray diffraction and investigated in the solid state by magnetical susceptibility measurements and differential scanning calorimetry. Comparisons are made with known analogous $[Fe(tpm)_2]^{2+}(X^-)_2$ compounds bearing different anions X, which display similar crossover behavior.

5.1 Introduction

Octahedrally coordinated iron(II) d^6 complexes exhibit a thermally induced spin transition called spin crossover (SCO).[1] The transition implies the reversible conversion between the low-spin (LS) and high-spin (HS) state associated with the rearrangement of 3d valence electrons in the octahedral ligand field: $t_{2g}^6 e_g^0 ({}^1A_{1g}, \mathrm{LS}) \leftrightarrow t_{2g}^4 e_g^2 ({}^5T_{2g}, \mathrm{HS})$.[2] In the thermal driven spin transition a sample usually behaves as paramagnetic (S = 2) at high temperatures, whereas upon cooling the diamagnetic state (S = 0) is present. The occurrence and course of SCO is mainly determined by the nature of the coordinating ligand, its field strength and interelectronic repulsion energy.[3,4] The spin state switching process is often controlled by external parameters such as temperature,[5] pressure,[6] magnetic field[7] or light irradiation.[8] Numerous mononuclear iron(II) spin crossover complexes possess an octahedral [FeN_6] coordination.[1] For them, the change in Fe–N distances is significant and usually observed around 0.2 Å (1.96 – 2.00 Å for the LS state and 2.15 – 2.20 Å for the HS state).[1,9] The cationic complex $[Fe(tpm)_2]^{2+}$ containing the neutral tripodal N_3-donor ligand tris(pyrazol-*1*-yl)methane (tpm) had already been examined for the thermal SCO effect with a small series of anions: BF_4^-,[10] PF_6^-,[11] ClO_4^-,[12] and NO_3^-.[13] Only the respective tetrafluoroborate and two polymorphs of the nitrate were structurally characterized. It is known that besides the coordinating ligand the type of the non-coordinating counter-anions of positively charged complexes, solvent molecules or formation of mixed crystals influence the electronic structure of the metal ion and consequently the SCO process.[14] Studies to investigate the influence of the counter-anion were recently published.[15]

In this report, the series of counter-ions is extended to the weakly coordinating mononegative tetracyanopyrrolide (tcp) anion, which represents a pyrrolide ring with four attached cyano groups. A detailed discussion of the magnetic properties, crystal structure, bonding, and the influence of the uncoordinated anion on the spin crossover of the new, air stable $[Fe(tpm)_2](tcp)_2$ complex salt (Scheme 5.1) is provided and compared to the known congeners.

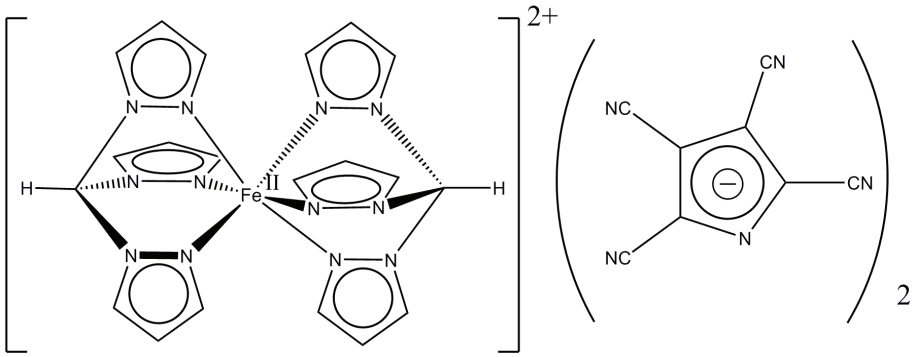

Scheme 5.1 The mononuclear cationic $[Fe(tpm)_2]^{2+}$ complex and the tetracyanopyrrolide anion tcp as the constituents of the complex salt **15tcp**.

5.2 Results and Discussion

The complex salt $[Fe(tpm)_2](tcp)_2$ (**15tcp**) was crystallized as long, red violet needle-shaped crystals from acetone solutions containing Fe^{2+}, the tripodal donor ligand tpm and tcp ions. For purification the samples were recrystallized from acetone. All crystals suitable for X-ray diffraction were found to be systematically twinned[4]. All inspected crystals showed signs of systematic, non-merohedral twinning. At first, the data integration was performed while ignoring the second twin domain. The structure was solved with the Patterson method and refined with anisotropic displacement parameters for all non-hydrogen atoms against F^2. Hydrogen atoms were refined using constraints. The two twin domains are related by a 180° rotation around the reciprocal c^*-axis, which results in the following superposition matrix between the two twin domain unit cells: $h_{TWIN} = -h, 0, 0$; $k_{TWIN} = 0, -k, 0$; $l_{TWIN} = 0.582\ h, 0.311\ k, l$. Refinement with a HKLF4 data set using TWIN and BASF instructions did not yield satisfactory R-values. So both twin domains were integrated[27] and treated with a semi-empirical absorption correction suitable for twinned crystals.[28] Refinement with the so generated HKLF5 data set was successful (Figure 5.2.1).

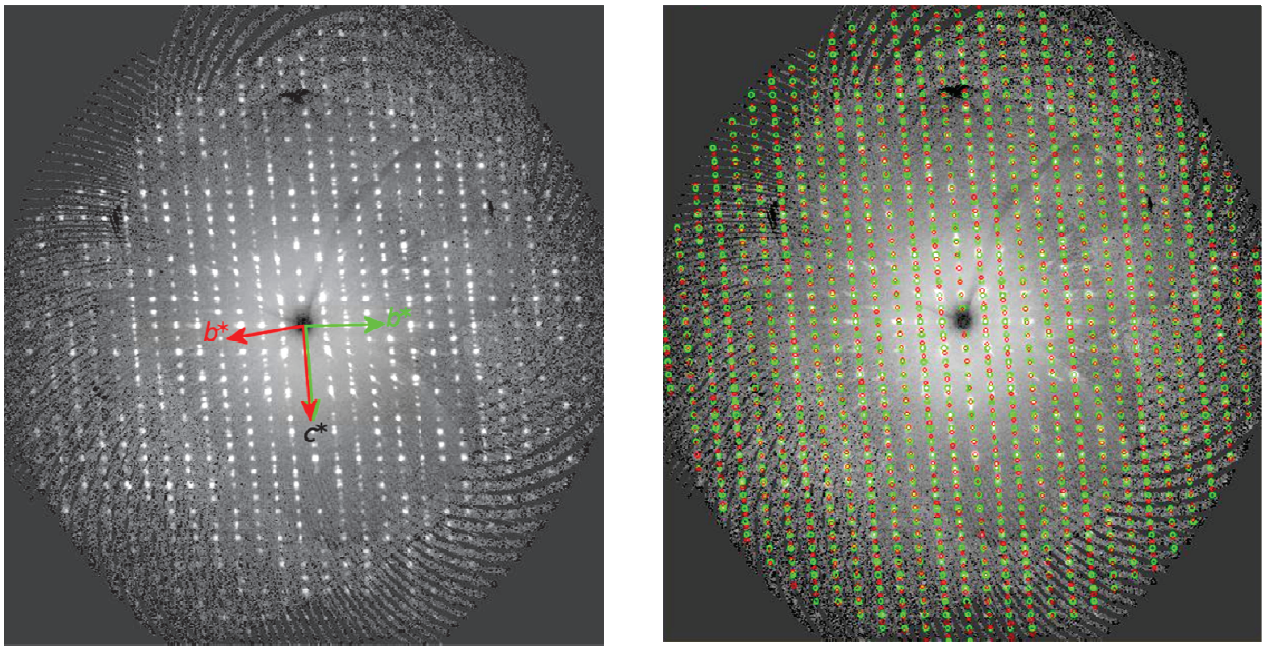

Figure 5.2.1 (a) The reconstructed reciprocal lattice plane (0*kl*) of **15tcp**. The green and red arrows indicate the reciprocal lattices vectors of the two twin domains. The twinning rotation axis is identical with the reciprocal c^*-axis of both domains. **(b)** The reconstructed reciprocal lattice plane (0*kl*) of **15tcp.** The green and red circles are predicted reflection positions for the first and the second twin domain.

[4] The crystallographic treatment of the twinning and the precession representations were performed by Christian Landvogt.

The crystal structure of **15tcp**, which crystallizes in the triclinic space group $P\bar{1}$, contains two crystallographic independent centrosymmetric $[Fe(tpm)_2]^{2+}$ cations located with the Fe positions in inversion centers and two independent tcp anions in the asymetric part of the unit cell. The reported congeners with the anions BF_4^-,[10] and the α and β polymorphs with NO_3^-[13] crystallize both in space group $P2_1/n$ but contain only one crystallographic independent complex cation located in an inversion center. In the structure of **15tcp**, the two independent Fe complexes and the two anions do not show significant differences in their structural parameters. The ions are each coordinated by two neutral tpm ligands, giving an almost regular octahedral coordination geometry that shows only small deviations from local D_{3d} symmetry. The $[Fe(tpm)_2]^{2+}$ cations adopt a staggered conformation with tpm ligands twisted about 60° (synclinal) and 180° (antiperiplanar) around the central Fe atom (Figure 5.2.2(a)). The Fe–N bond lengths are observed in the narrow range between 1.962(3) and 1.980(3) Å (at 123 K) (Appendix E), and are in the typical range reported for LS iron(II) complexes (Table 5.2.1). The difference between **15tcp** and the known cogeners concerns the anionic part. Here, tetracyanopyrrolide monoanions, located in general positions, balance the charge of the cationic complexes.

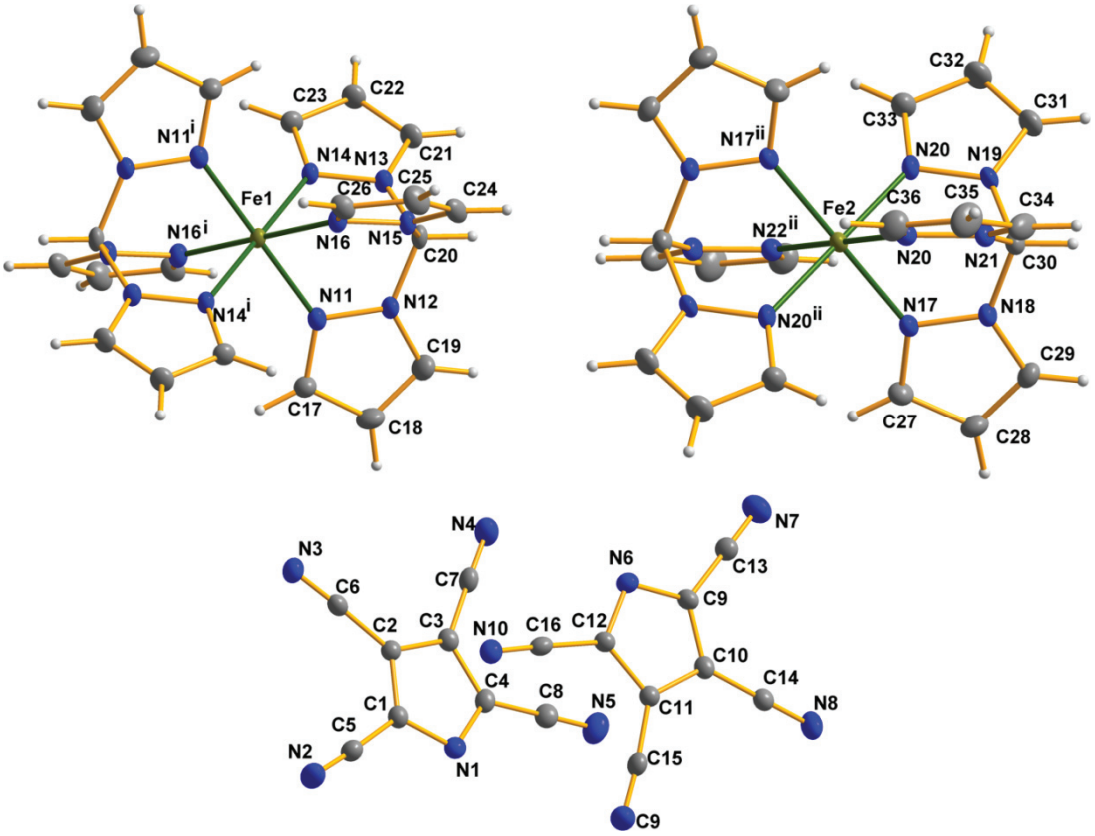

Figure 5.2.2 (a) The two indenpdent cationic $[Fe(tpm)_2]^{2+}$ complexes and the two independent tetracyanopyrrolide anions in the structure of $[Fe(tpm)_2](tcp)_2$. Thermal ellipsoids are scaled to include a probabitiliy density of 50 %. Symmetry codes: (i) $-x+2, -y+1, -z$; (ii) $-x+1, -y+1, -z+1$.

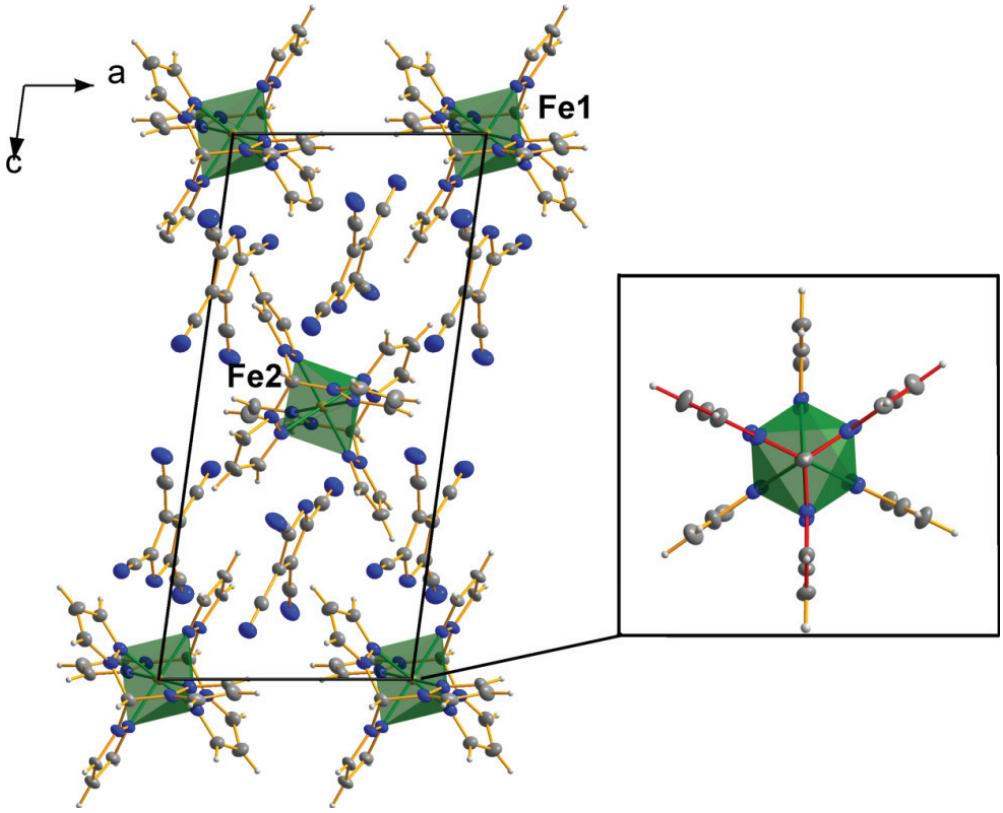

Figure 5.2.2 (b) Packing of the unit cell of **15tcp** in a view along the *b*-axis. The inset shows a projection of an individual $[Fe(tpm)_2]^{2+}$ complex along the nearly fulfilled C_3 axis. Displacement ellipsoids are drawn to enclose a 50 % probability.

The bigger size of the tpc anion, compared to the anions already used, results in an enlarged unit cell volume of 1857.62(6) Å^3 ($V_{(BF4-)}$ = 1315.4(2) Å^3, $V_{(\gamma\text{-}NO3-)}$ = 1272.6(7) Å^3, $V_{(\beta\text{-}NO3-)}$ =1220.6(7) Å^3). A remarkable structural feature is the arrangement of the planar anions in stacks running along the *a*-axis. Short intermolecular distances are present with the minimum of 3.164(4) Å between a ring carbon atom (C17) and terminal nitrogen of a nitrile group (N10) of a neighbouring anion. Although the tcp molecules are aligned in parallel arrangement and packed in columns, their centroids are about 4.6 Å apart, which excludes any significant π–π interactions of overlapping aromatic systems.[16] In the crystal, cations and anions are associated by weak electrostatic C···N interactions close to the sum of the van der Waals radii (3.25 Å),[17] which emerge in short intermolecular contacts between tpm ligands and the tcp anions.

Thermogravimetric analyses of **15tcp** were performed in order to investigate the limit of thermal stability and the course of thermal decomposition of the complex. **15tcp** is thermally stable up to 583 K (310 °C). Above this temperature, the complex salt starts to decompose (Figure 5.2.3). The DSC measurement was also performed in order to detect any caloric effects accompanied with the spin crossover. The thermal profile of **15tcp** does not show significant signs of a phase transition in heating/cooling cycles (Figure 5.2.4), which is common for gradual spin transition.[14] The continuous SCO process proceeds without considerable structural transformations, which was additionally proved by X-ray powder diffraction (see Experimental

Part). No significant changes were observed in the calculated X-ray powder diffraction pattern at 123 K compared to the experimental pattern recorded at room temperature. **15tcp** shows a distinct thermochromism, probably associated with the spin transition. The colour of the sample changes from pink at 77 K to dark red-violet at 425 K (Figure 5.2.5).

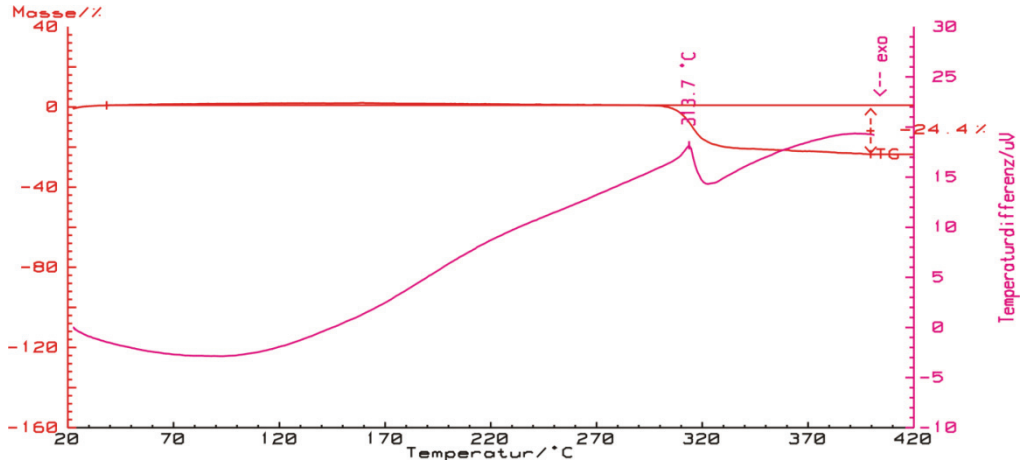

Figure 5.2.3 TG/DTA plot of crystalline **15tcp**. Red - TG curve, pink - DTA curve.

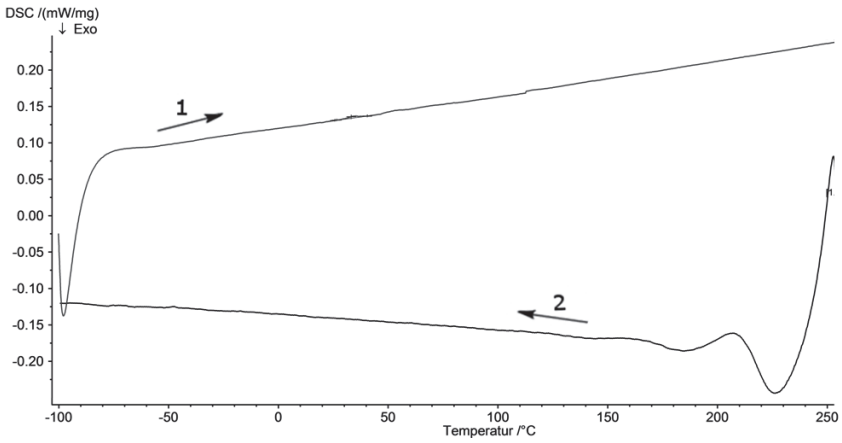

Figure 5.2.4 Differential scanning calorimetry plot of the **15tcp** complex, curve 1 – heating, curve 2 – cooling.

Temperature dependence of the magnetic susceptibility of **15tcp** was studied in heating and cooling modes in the temperature range 1.9-400 K. The dependence of $\chi_{mol}T$ on temperature displays a gradual, incomplete spin transition in the accessible temperature interval (Figure 5.2.5). As expected, at the lowest temperatures **15tcp** is in the diamagnetic low spin state (S = 0). On heating, $\chi_{mol}T$ slowly but constantly increases from 0.004 cm^3K/mol at 1.9 K to 0.30 cm^3K/mol at 250 K, likely indicative for some HS states trapped at lower temperatures. Above this point, $\chi_{mol}T$ increases rapidly to achieve the value of 1.42 cm^3K/mol at 400 K. The maximal experimental effective moment μ_{eff} at 400 K equals 3.29 μ_B, which is significantly lower than the spin-only value ($\mu_{eff} = 2[S(S + 1)]^{1/2}$) of 4.90 μ_B expected for a free Fe^{2+} ion with four unpaired electrons. Taking into account the spin-orbit coupling ($\mu_{eff} = [L(L + 1) + 4S(S + 1)]^{1/2}$) and full

occupation of the high-spin state gives 5.48 μ_B. The experimental results allow for the estimation that only about 60 % of the iron(II) centers populate the high-spin state at the highest temperature of measurement. The cooling-heating cycles show no thermal hysteresis of the magnetization. The previously described congeners $[Fe(tpm)_2](X)_2$ (X = BF_4^-, PF_6^-, ClO_4^- and NO_3^-) also show a comparable gradual and incomplete spin crossover.

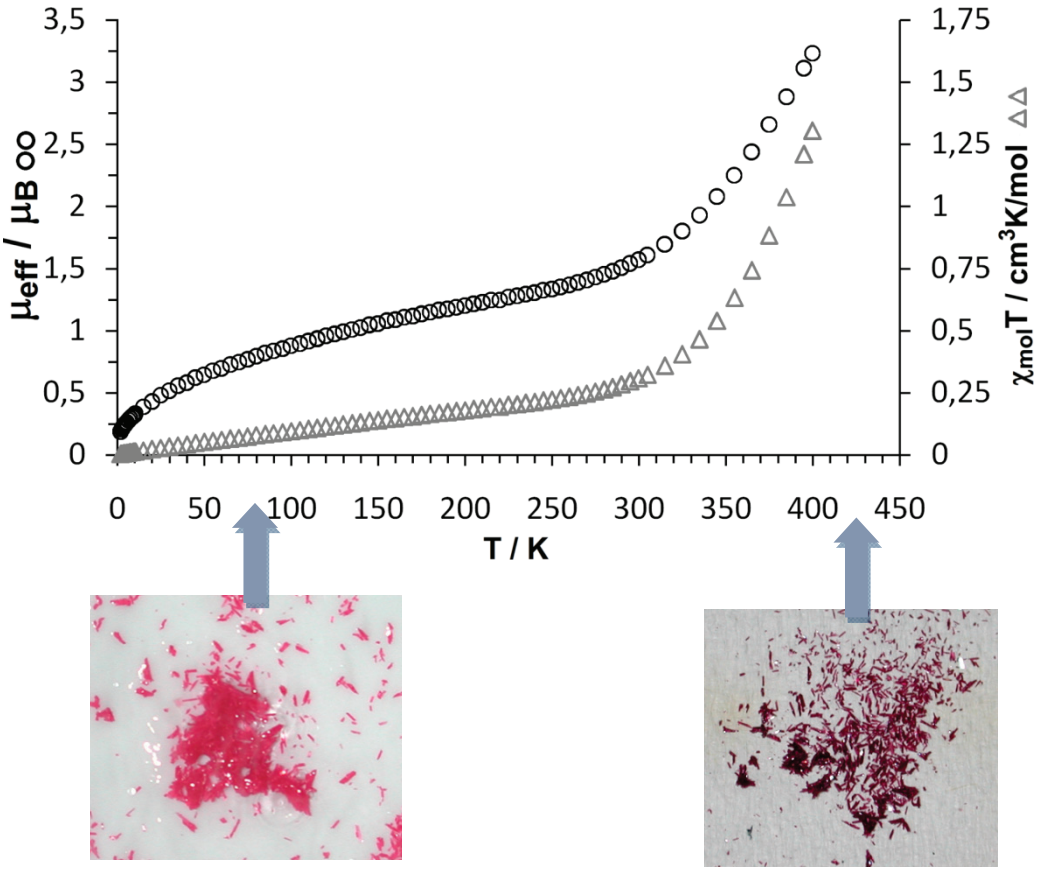

Figure 5.2.5 The incomplete gradual spin crossover of **15tcp** in a field of 10 kOe. The $\chi_{mol}T$ versus T plot is marked as triangles and the experimental effective moment μ_{eff} is marked as circles.

The obtained results for **15tcp** are closely related to the tetrafluoroborate salt, where the rapid increase of the effective moment starts at 320 K, rising to 3.24 μ_B at 400 K and reaching fully saturation of HS states at 470 K based on Mössbauer spectroscopy studies.[10]

It is known, that the course of spin crossover of positively charged complexes may depend on the nature of the counter-ion. Its exchange often influences the crystal structure resulting in slight but effective distortions of the complex moiety or even in a complete different structure.[18,19,20] Size and shape of the anion may shift the temperature of the spin transition.[21] Smaller anions imply shorter anion-metal distances, what can effect distortions of the $[FeN_6]$ coordination environment.[22] Indeed, the crystal field strength can be easily affected by only changing the crystal symmetry as observed for different polymorphs.[23,24] Therefore, the character of the SCO is not strictly molecular, but is also sensitive to the localization or different alignment of the active complexes in the crystal lattice.

Obviously the use of the tcp anion in the current study does not affect substantially the symmetry of the $[Fe(tpm)_2]^{2+}$ complex. The centrosymmetry of the $[Fe(tpm)_2]^{2+}$ cation and the almost ideal $[FeN_6]$ coordination sphere is still maintained. Despite there are differences in the crystal symmetry in comparison to the known congeners with other anions and there are two independent Fe(II) complexes present in the crystal, no significant differences in the course of the spin crossover was found for **15tcp**.

	LS [A] [13]	**LS [B] [13]**	**LS [C] [10]**	**HS [E] [29]**
Fe–N(11)*	1.975(3)	1.963(2)	1.966(3)	2.129(2)
Fe–N(21)*	1.966(3)	1.957(3)	1.977(3)	2.140(2)
Fe–N(31)*	1.963(3)	1.957(2)	1.972(7)	2.142(2)
N(11)–Fe–N(21)*	87.7(1)	87.1(1)	87.74(13)	84.34(9)
N(11)–Fe–N(31)*	87.1(1)	87.96(9)	86.83(13)	86.00(9)
N(21)–Fe–N(31)*	88.0(1)	87.7(1)	87.78(12)	95.06(9)

Table 5.2.1 Selected cation geometries, Fe–N bond lengths (A°), bond angles (°).* Due to different numeration of the atoms in the cif files, atoms were assigned as N11, N21, N31. The $[Fe^{II}(tcp)_2][NO_3]_2$ (α-form and β- form) and **15tcp** complexes were measured at 123 K, where $[Fe((H\text{-}pz)_3CH)((3,5\text{-}Me_2pz)_3CH)](BF_4)_2$ complex at 260 K. Foot note [A] - $[Fe^{II}(tpm)_2](NO_3)_2$ (α-form), [B] - $[Fe^{II}(tpm)_2](NO_3)_2$ (β-form), [C] - $[[Fe^{II}(tpm)_2](BF_4)_2$, [E] - $[Fe((H\text{-}pz)_3CH)((3,5Me_2pz)_3(CH)](BF_4)_2$. For selected cation geometries of **15tcp** see Appendix E.

5.3 Conclusions

In conclusion, the structural investigations on the mononuclear $[Fe(tpm)_2](tcp)_2$ complex at 123 K reveal Fe–N distances typical for low-spin d^6 iron(II) complex. **15tcp** undergoes a gradual, incomplete spin-crossover in the examined temperature range 1.9 – 400 K. The analysis of the crystal structure shows no larger influence of the tcp counter-ion on the symmetry of the cationic $[Fe(tpm)_2]^{2+}$ complex. Moreover, continuous LS↔HS spin switching process proceeds without detectable phase transition and structural changes.

5.4 Experimental Section

Tris(pyrazol-*1*-yl)methane, $HC(C_3H_3N_2)_3$ (tpm) was synthesised according to published procedures,[26] unreacted pyrazole was removed by sublimation under vacuum ($4 \cdot 10^{-3}$ mbar) at 90-95 °C; pale yellow solid. M.p.: found 98–99 °C, lit.[26] 102–104 °C.

Crystallization of $[Fe(tpm)_2](tcp)_2$ (15tcpc): Dry $Fe(ClO_4)_2$ (79 mg, 0.31 mmol) was added to 10 mL of a dry acetone solution containing 12tcp (150 mg, 0.62 mmol). $[Me_4N]ClO_4$ precipitated as a white solid, which was filtrated and discarded. The 5 mL of acetone solution containing tpm

(140 mg, 0.62 mmol) was added to the mixture. After 3 days clear pink crystals of the iron(II) complex were filtrated and washed with water:acetone mixture and recrystallized from acetone. Yield 81.5 mg (32 %). Elemental analysis $C_{36}H_{20}FeN_{22}$ (816.58 g/mol): C 52.98 (calc. 52.95); H 3.12 (2.47); N 37.76 (37.74); IR: 3134 (m), 3131(m), 3000 (m), 2994 (w), 2226 (s), 2216 (s),1413 (m), 1282 (w), 1093 (w), 875 (m), 742 (s) cm^{-1}.

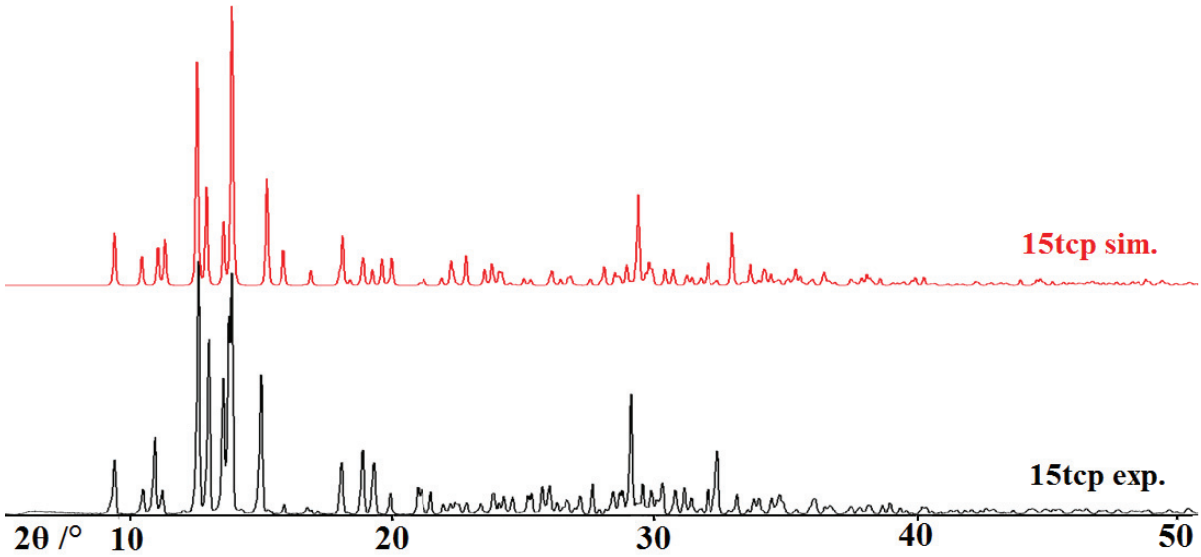

Figrue 5.4.1 Comparison of the simulated X-ray powder diffraction pattern (123 K, red) with the experimental pattern from the crystalline powder of $[Fe(tpm)_2](tcp)_2$ at room temperature (black). 2θ range 5 – 50 °, (Co-Kα radiation).

References

[1] M. A. Halcrow, *Polyhedron* **2007**, *26*, 3523.

[2] P. Gütlich, A. B. Gaspar, Y. Garcia, *Beilstein J. Org. Chem.* **2013**, *9*, 342.

[3] H. L. Schläfer, G. Gliemann, *Einführung in die Ligandenfeldtheorie*, Akademische Verlagsgesellschaft: Wiesbaden, Germany, **1980**.

[4] D. F. Shriver, P. W. Atkins, C. H. Langford, *Inorganic Chemistry*, 2nd ed.; Oxford University Press: Oxford, Melbourne, Tokyo, **1994**.

[5] P. Gütlich, H. A. Goodwin, *Spin Crossover in Transition Metal Compounds I, Topics in Current Chemistry*, Springer-Verlag, Berlin, **2004**, vol. 233.

[6] P. Gütlich, V. Ksenofontov, A. B. Gaspar, *Coord. Chem. Rev.* **2005**, *249*, 1811.

[7] A. Bousseksou, F. Varret, M. Goiran, K. Boukheddaden, J. P. Tuchagues, *Spin Crossover in Transition Metal Compounds III, Topics in Current Chemistry*, ed. P. Gütlich, H. A. Goodwin, Springer-Publishers, Berlin, **2004**, vol. 235, pp. 65.

[8] O. Sato, J. Tao, Y. Z. Zhang, *Angew. Chem., Int. Ed.* **2007**, *46*, 2152.

[9] **(a)** H. A. Goodwin, *Coord. Chem. Rev.* **1976**, *18*, 293; **(b)** L. Wiehl, G. Kiel, C. P. Köhler, H. Spiering, P. Gütlich, *Inorg. Chem.* **1986**, *25*, 1565; **(c)** K. Nakano, N. Suemura, K. Yoneda, S. Kawata, S. Kaizaki, *Dalton Trans.* **2005**, 740; **(d)** J. A. Kitchen, S. Brooker, *Coord. Chem. Rev.* **2008**, *252*, 2072; (e) K. S. Murray, *Eur. J. Inorg. Chem.* **2008**, 3101.

[10] L. D Reger, A. Little, *Inorg. Chem.* **2001**, *40*, 1508.

[11] H. Winkler, A. X. Trautwein, H. Toftlund, *Hyperfine Interact.* **1992**, *70*, 1083.
[12] J. J. McGarvey, H. Toftlund, A. H. R. Al-Obaidi, K. P. Taylor, S. J. Bell, *Inorg. Chem*. **1993**, *32*, 2469.
[13] P. A. Anderson, T. Astley, M. A. Hitchman, F. R. Keene, B. Moubaraki, K. S. Murray, B. W. Skelton, E. R. T. Tiekink, H. Toftlund, A. H. White, *J. Chem. Soc., Dalton Trans.* **2000**, 3505.
[14] P. Gütlich, A. Hauser, H. Spiering, *Angew. Chem. Int. Ed. Engl.* **1994**, *33*, 2024-
[15] J. Elhaik, C. A. Kilner, M. A. Halcrow, *Eur. J. Inorg. Chem*. **2014**, 4250-
[16] C. Janiak, *J. Chem. Soc., Dalton Trans.* **2000**, 3885-
[17] A. Holleman, E. Wiberg, N. Wiberg, *Lehrbuch der Anorganischen Chemie*, vol. 102, Berlin, **2007**.
[18] M. Quesada, F. Prins, E. Bill, H. Kooijman, P. Gamez, O. Roubeau, A. L. Spek, J. G. Haasnoot, J. Reedijk, *Chem. Eur. J.* **2008**, *14*, 8486.
[19] L. Wiehl, G. Kiel, C. P. Köhler, H. Spiering, P. Gütlich, *Inorg. Chem.* **1986**, *25*, 1565..
[20] G. A. Renovitch, W. A. Baker, *J. Am. Chem. Soc*. **1967**, *89*, 6377..
[21] O. Roubeau, J. M. A. Gomez, E. Balskus, J. J. A. Kolnaar, J. G. Haasnoot, J. Reedijk, *New J. Chem.* **2001**, *25*, 144.
[22] M.Yamada, M. Ooidemizu, Y. Ikuta, S. Osa, N. Matsumoto, S. Iijima, M. Kojima, F. Dahan, J. P. Tuchagues, *Inorg. Chem.* **2003**, *42*, 8406.
[23] J. Tao, R. J. Wei, R. B. Huang, L. S. Zheng, *Chem. Soc. Rev*. **2012**, *41*, 703.
[24] I. Salitros, O. Fuhr, A. Eichhöfer, R Kruk, J. Pavlik, L. Dlhan, R. Boca, M. Ruben, *Dalton Trans.* **2012**, *41*, 5163.
[25] H. E. Simmons, R. D. Vest, S. A. Vladuchick, O. W. Webster, *J. Org. Chem.* **1980**, *45*, 5113.
[26] D. L. Reger, T. C Grattan, K. J. Brown, C. A. Little, J. J. S. Lamba, A. L. Rheingold, R. D. Sommer, *J. Organomet. Chem.* **2000**, *607*, 120.
[27] A. J. M. Duisenberg, L. M. J. Kroon-Batenburg, A. M. M. Schreurs, *J. Appl. Cryst.* **2003**, *36*, 220.
[28] *TWINABS, Scaling and corrections for twinned crystals*, V1.05, Bruker Nonius, **2004**.
[29] B. Moubaraki, B. A. Leita, G. J. Halder, S. R. Batten, P. Jensen, J. P. Smith, J. D. Cashion, C. J. Kepert, J. F. Létard, K. S. Murray, *Dalton Trans*. **2007**, 4413.

PART 6

STRUCTURAL CHARACTERIZATION OF TWO NEW ORGANIC SALTS: TETRAETHYLAMMONIUM 2,4,5-TRICYANOIMIDAZOLATE AND TETRAPHENYLPHOSPHONIUM 4,5-DICYANO-1,2,3-TRIAZOLATE

Abstract

The new cyano-azolates 2,4,5-tircyanoimidazolate (**18tci**) and 4,5-dicyano-1,2,3-triazolate (**19*cis*-dct**) were synthesized and fully characterized as organic salts by X-ray diffraction.

6.1 Introduction

4,5-dicyano-1,2,3-triazolate anion (***cis*-dct**) represents a binary carbon-nitrogen derivative of the triazolate anion with high nitrogen content. Its composition $(C_4N_5)^-$, makes it a candidate for coordination chemistry, despite the fact that it may be a weakly coordinating ligand owing to the extensive negative charge delocalization across the anion's structure.[1] The *cis*-dct anion has been known for a long time,[2] but it was investigated by spectroscopic and theoretical studies only in 2003 by Johannson *et al.* and considered as a possible component of lithium battery electrolytes.[3] A few years later, these studies were explored in depth, giving insight in the crystal structure of lithium salts with the *cis*-dct anion.[4] However, the first structural reports and the full characterization of the *cis*-dct anion had been done by Klapötke *et al*.[5] in new nitrogen-rich materials, in sodium, silver salts and later complemented by the simple alkali and alkaline earth metal salts.[6] In addition to the previous studies, there is only one report of an uranium(VI) complex, showing a direct coordination of the *cis*-dct ligand via the central ring N atom to the metal centre as a new possibility.[7] Later, the studies of *cis*-dct were expanded to structural studies on its lithium salts, demonstrating the range of coordination modes of this ligand.[4]

Since the discovery of 4,5-dicyanoimidazole (**dci**) in 1950[8] (Scheme 6.1.1), this moiety has become a potentially π-conjugated linker in charge transfer chromophores used in organic materials.[9] Later the development its polycyano compounds was continued by Rasmussen *et al*..[10] The search for planar, conjugated molecules, capable of forming stacked molecules led to the investigations of the Y-shaped 2,4,5-tricyanoimidazolate anion (**tci**) as a possibly electron accepting moiety.[11] But to our best knowledge, a structural investigation of the tci anion had been never done, despite the fact, that its dci congener was thoroughly explored and successfully used in the construction of coordination polymers.[12]

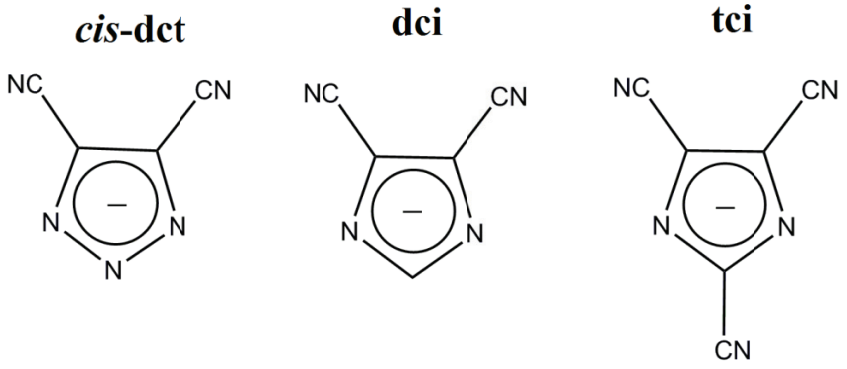

Scheme 6.1.1 Structural formulae for the *cis*-dct (4,5-dicyano-1,2,3-triazolate), dci (4,5-dicyanoimidazolate) and tci (2,4,5-tricyanoimidazolate) anions.

These two anions (*cis*-dct and tci) attracted our attention, not only because they are interesting N-donor ligands with up to five N coordination sites, but also because they are poorly investigated. Thus, we report here the first structural characterization of the 2,4,5-

tricyanoimidazolate anion as tetraethylammonium salt (**18tci**) and also a new salt of tetraphenylophosphonium 4,5-dicyano-1,2,3-triazolate (**19*cis*-dct**). Both substances can be easily deprotonated and potentially used as a bridging ligands for magnetically interesting transition metal complexes and coordination polymers.

6.2. Results and Discussion

The first synthesis of the protonated *cis*-Hdct was reported as early as in 1923 by diazotation of aminomalonoitrile with *in situ* generated HNO_2.[2] During the practical work of this thesis, *cis*-Hdct was obtained in the cyclization process of diaminomaleodinitrile with hydrochloric acid and sodium nitrite in water at 0 °C following the modified literature procedure (See Experimental Section).[5] After sublimation of the crude product, pure *cis*-Hdct was obtained as a white crystalline powder. **(19*cis*-dct)** was precipitated from aqueous solution on reaction of *cis*-Hdct with one equivalent of PPh_4Cl. Recrystallization from dmso gave big, pale yellowish transparent crystals suitable for X-ray analysis. For a detailed synthetic route see Appendix H.

Tetraethylammonium 2,4,5-tricyanoimidazolate (**18tci**) was prepared from commercially available 2-amino-4,5-dicyano-1*H*-imidazole under Sandmayer reaction conditions following the synthetic route given by Rasmussen *et al.*[11] (see Appendix H or Experimental Section). The substituted amine group quickly reacted with nitrite to form diazonium salt (unstable above 10 °C), which later decomposed in the presence of CuCN to form the sodium salt of Na(tci). The final product **18tci** was obtained in the reaction between the sodium salt of tci and tetraethylammonium bromide in aqueous solution. Extraction of the product into the organic phase, followed by recrystallization from hot water gave dark-yellow crystals of $[NEt_4]$tci suitable for X-ray analysis.

6.2.1 Crystal Structure of Tetraphenylphosphonium 4,5-dicyano-1,2,3-triazolate

The **19*cis*-dct** salt crystallizes in the orthorhombic space group *Pccb* with four molecular moieties in the unit cell. Both cations and anions are bisected by two-fold rotation axes. The two-fold axis parallel to the *b*-axis passes through the central phosphorous atom of the PPh_4^+ and the second one parallel to the *c*-axis passes through the central N atom of triazolate ring. The crystal structure can be explained by efficient packing of the PPh_4^+ cations and *cis*-dct anions, which are associated by weak inter-ion interactions (C–H···N) (Figure 6.2.1). The *cis*-dct anions are completely surrounded by the bulky cations, excluding any anion-anion interactions. For the anion, the N–N distance in the triazolate ring equals 1.338 Å, which is between N–N single bond (1.454 Å) and N=N double bonds (1.245 Å).[13] The C≡N bond length (1.152 Å) is comparable with those of 5-cyanotetrazolate and tetracyanopyrrolide anions. The inner ring C–N bond length equals 1.355 Å and is shorter than the average C–N single bond distance (1.47 Å),[14] appointing a highly delocalized electronic system.

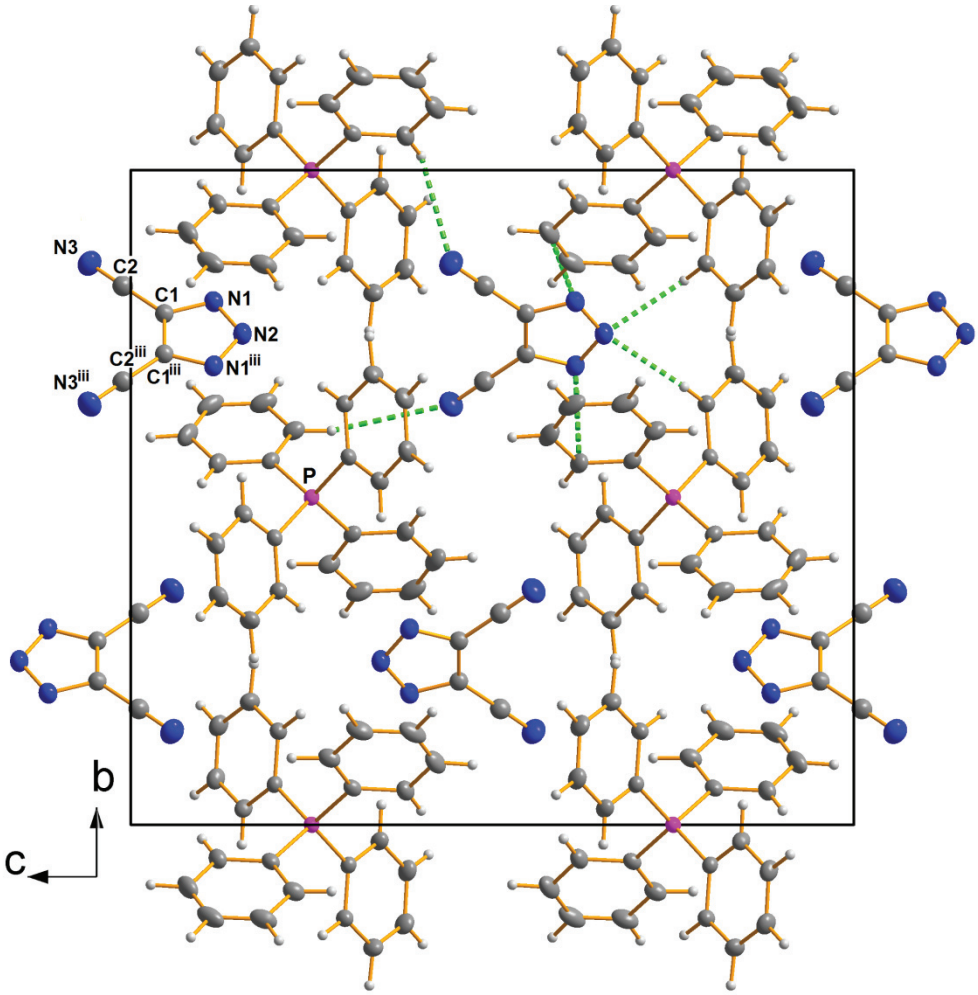

Figure 6.2.1 The packing of the unit cell of **19*cis*-dct**. Dotted green lines – short inter-ion interactions. Displacement ellipsoids are drawn in 40 % probability level. Symmetry code: (iii) $-x+1$, $-y+1/2$, z.

6.2.2 Crystal Structure of Tetraethylammonium 2,4,5-tricyanoimidazolate

The crystal structure of **18tci**, refined in the centrosymmetric space group *C*2/*m* consists of mononegative tci anions, which are balanced by positively charged tetraethylammonium ions. Both cations and anions are bisected by the crystallographic mirror planes, passing through the nitrogen atom of the tetraethylammonium moiety and through one cyano arm of the anion. As a result, the tci anions are planar and the cationic parts are disordered over this special position (Figure 6.2.2.1). The anions are arranged in stacked columns, the shortest anion···anion distances equal about 3.80 Å and 4.31 Å, excluding significant interactions. The $[NEt_4]^+$ cations, located between the stacked anionic columns, form the motif of a hexagonal rod packing along *c*-axis (Figure 6.2.2.1). For the anion, the C–N bond lengths in the aromatic ring were found to be 1.346 Å and 1.360 Å. They are shorter than the average C–N single bond distance (1.47 Å),[14] but significantly longer than C=N double bond (1.22 Å), suggesting a bond order 1.5. A similar trend is observed for the C–C bond length (1.392 Å), which is significantly shorter than a single C–C bond length (1.54 Å) but longer than a double bond length (1.33 Å).[14]

The C≡N distance of 1.15 Å are comparable with those of 5-cyanotetrazolate, tetracyanopyrrolide and 4,5-dicyano-1,2,3-triazolate anions, indicating the bond order 3.

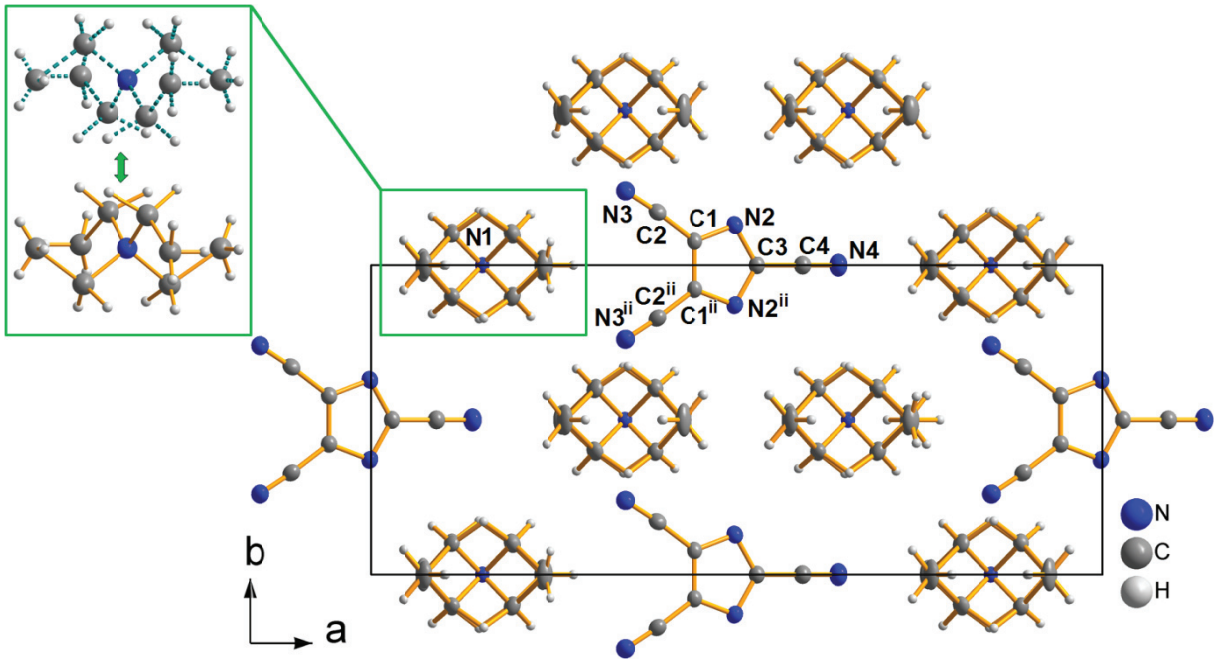

Figure 6.2.2.1 The view of the unit of **18tci** cell along the *a*-axis, showing a hexagonal packing of the cationic moiety. Displacement ellipsoids are drawn at the 50 % probability level. The N atoms of the tetraethylammonium moiety are located in a special position in mirror planes, thus the spatial cation is disordered in 0.5/0.5 ratio (see green box). Symmetry code: (ii) *x*, −*y*+1, *z*.

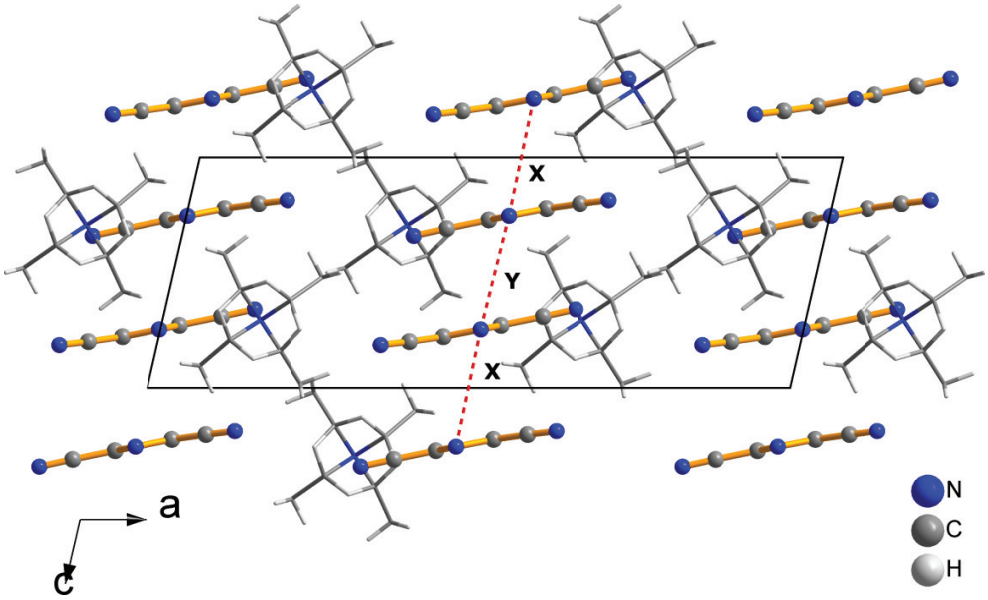

Figure 6.2.2.2 The view of the unit cell of **18tci** along the *b*-axis. The stacked columns of the anions are extended along the *c*-axis (anion···anion distances: X = 3.80 Å and Y = 4.31 Å).

6.3 Conclusions

Two new salts bearing 2,4,5-tricyanoimidazolate and 4,5-dicyano-1,2,3-triazolate anions were synthesized in a good yield from commercially available materials. The structure of **18tci** is discussed for first time and appoints for a highly delocalized π-electronic system. Both substances **18tci** and **19*cis*-dct** can be easily deprotonated and potentially used as bridging ligands for magnetically interesting transition metal complexes and coordination polymers.

6.4. Experimental section

Safety note: Sodium cyanide is highly poisonous and liberates volatile HCN when mixed with acids. The diazonium zwitterion is extremely shock- and heat-sensitive. It should be prepared in small quantities only and handled while moist.

Synthesis of PPh_4(*cis*-dct) 19*cis*-dct: The procedure follows that given in [5] Diaminomaleodinitrile (10.81 g, 100.0 mmol) was dissolved in 125 mL of water and acidified with hydrochloric acid (1M, 100 mL). At 0 °C, sodium nitrite (6.89 g, 100.0 mmol) was added portion wise, while maintaining the reaction temperature below 4 °C. The reaction mixture was then allowed to warm up to room temperature and stirred for 1 h. After filtration, the brownish solution was extracted five times with a total of 600 mL of diethylether. After removal of the solvent of the combined ether extracts under reduced pressure, a pale light brown solid was obtained. Yield of crude product 10.6 g (89 %). Analytically pure **19cis-dct** was obtained by subliming the crude product at 90°C under vacuum to yield white crystals of *cis*-Hdct. The PPh_4(*cis*-dct) compound was precipitated quantitatively from aqueous solution when the *cis*-Hdct was reacted with one equivalent of PPh_4Cl. Elemental Analysis $C_{28}H_{20}N_5P$ (475.47): C 72.63 (calc. 73.51), H 4.57 (calc. 4.4), N 16.14 (calc. 15.31) (%).^{1}H NMR (300 MHz, Me_2SO-D_6) δ: 8.0-7.7 (m, 20*H*, Ar*H*) ppm; ^{13}C NMR (75 MHz, Me_2SO-D_6) δ: 135.5 (d, $^4J_{PC}$ = 2.6 Hz, Ph_{para}), 134.5 (d, $^2J_{PC}$ = 10.3 Hz, Ph_{ortho}), 130.4 (d, $^3J_{PC}$ = 12.9 Hz, Ph_{meta}), 117.7 (s, ***C***-CN), 120 (d, $^1J_{PC}$ = 89.2 Hz, Ph_{ipso}), 113.83 (s, C-***C***N).

Synthesis of [NEt_4]tci 18tci: The procedure follows that given in [11]. To a mixture of 1.44 g (10.8 mmol) of 2-amino-4,5-imidazoledicarbonitrile in 30 ml of water were added 12 ml of concentrated HC1 and 0.84 g (12.2 mmol) of $NaNO_2$. The 2-diazo-4,5- imidazoledicarbonitrile zwitterion precipitated and was isolated by filtration. The zwitterion was added to a solution of 1.11 g (22.7 mmol) of NaCN and 1.30 g {14.5 mmol) of CuCN in 100 ml of water. Nitrogen gas evolved immediately. The mixture was stirred for 3 h. 8.41 g (40 mmol) of tetraethylammonium bromide were then added. The dark reaction mixture was filtered and extracted with dichloromethane (10 × 50 ml). The organic extracts were combined and the solvent was evaporated to give 1.63 g of the tetraethylammonium salt (58%). The salt was recrystallized

from water to give a yellow-orange solid. $C_{14}H_{20}N_6$ (272.35): C 61.56 (calc. 61.74), H 7.2 (calc. 7.4), N 30.80 (calc. 30.86) (%). Melting point 95 °C. ^{1}H NMR (300 MHz, Me_2SO-D_6) δ: 3.21 (8H *J*= 7.3 Hz), 1.17 (tt, 12H J_{H-H} = 7.3 Hz, J_{H-N} = 1.8 Hz) ppm. ^{13}C NMR (75 MHz, Me_2SO-D_6) δ: δ 131.91 (s, NC-***C***N), 119.74 (s, N***C***-CN), 115.56 (s, C***C***-CN), 114.31 (s,CC-***C***N), 51.38 (t, ***C***H_3, J ^{14}N= 3.20 Hz), 7.02 ppm (s, ***C***H_2).

References

[1] C. Herriot, S, Khatun, E. T. Fox, P. Judeinstein, M. Armand, W. A. Henderson, S. Greenbaum, *J. Phys. Chem. Lett.* **2012**, *3*, 441.

[2] E. Gryszkiewicz-Trochimowski, *Chem. Zent. Bl.* **1923**, *94*, 1366.

[3] P. Johansson, S. Beranger, M. Armand, H. Nilsson, P. Jacobsson, *Solid State Ionics* **2003**, *156*, 129.

[4] D. W. McOwen, S. A. Delp, E. Paillard, C. Herriot, S. D. Han, P. D. Boyle, R. D. Sommer, W. A. Henderson, *Phys. Chem. C* **2014**, *118*, 7781.

[5] M. J. Crawford, K. Karaghiosoff, T. M. Klapötke, F. Martin, *Inorg. Chem.* **2009**, *48*, 1731.

[6] C. M. Sabaté, E. Jeanneau, H. Delalua, *Dalton Trans.* **2012**, *41*, 3817.

[7] M. J. Crawford, A. Ellern, K. Karaghiosoff, F. Martin, P. Mayer, *Inorg. Chem.* **2010**, *49*, 2674.

[8] D. W. Woodward, U.S. Patent 2,534,331, Dec *19*, 1950.

[9] Kulhánek, F. Bureš, *Beilstein J. Org. Chem.* **2012**, *8*, 25.

[10] **(a)** J. B. Wright *Chem. Rev.* **1951**, 48, 397; **(b)** C. G. Densmore, P. G. Rasmussen, *Macromolecules* **2004**, *37*,5900; **(c)** P. G. Apen, P. G. Rasmussen, *Heterocycles* **1989**, *29*, 1325; **(d)** R. P. Subrayan, J. W. Kampf, P. G. Rasmussen, *J. Org. Chem.* **1994**, *59*, 4341; **(e)** R. P. Subrayan, P. G. Rasmussen, *Tetrahedron* **1995**, *51*, 6167; **(f)** R. P. Subrayan, P. G. Rasmussen, P. G. *Tetrahedron* **1999**, *55*, 353; **(g)** T. Jang, P. G. Rasmussen, *J. Polym. Sci., Part A: Polym. Chem.* **1998**, *36*, 2619; **(h)** P. G. Apen, P. G. Rasmussen, *J. Polym. Sci., Part A: Polym. Chem.* **1992**, *30*, 203; **(i)** T. Jang, P. G. Rasmussen, *J. Polym. Sci., Part A: Polym. Chem.* **2000**, *38*, 3828; **(j)** P. G. Rasmussen, R. L. Hough, J. E. Anderson, O. H. Bailey, J. C. Bayon, *J. Am. Chem. Soc.* **1982**, *104*, 6155.

[11] D. S. Allan, D. F. Bergstrom, P. G. Rasmussen, *Synth. Met.* **1988**, *25*, 139.

[12] **(a)** J. X. Li, Z. X. Du, J. G. Wang, Tao Wang, J. N. Lv, *Inorg. Chem. Commun.* **2012**, *15*, 243; **(b)** J. X. Li, Z. X. Du, J. Zhou, H. Q. An, B. L. Zhu, S. R. Wang, S. M. Zhang, S. H. Wu, W. P. Huang, *Inorg. Chem. Commun.* **2010**, *13*, 127.

[13] **(a)** M. Ebespächer, T. M. Klapötke and C. Miró Sabaté, *New J. Chem.* **2009**, *33*, 517.; **(b)** K. Karaghiosoff, T. M. Klapötke and C. Miró Sabaté, *Eur. J. Inorg. Chem.* **2009**, *4*, 238.

[14] A. F. Holleman, E. Wiberg and N. Wiberg, *Lehrbuch der Anorganischen Chemie*, Walter de Gruyter, Berlin, Germany, 101st edn, **1995**.

PART 7

COORDINATION POLYMERS OF THE *N,N´,N´´*-TRICYANOGUANIDINATE DIANION $(C_4N_6)^{2-}$

Abstract

This part concerns of a new series of 2D and 3D coordination polymers incorporating the binary dianion *N,N´,N´´*-tricyanoguanidinate (tcg, $(C_4N_6)^{2-}$). Five complexes, namely *mer*-[Cu(tcg)$(py)_3$]· py **(20tcg)**, two supramolecular isomers *fac*-[Co(tcg)$(dmf)_2(H_2O)$] **(21a-tcg)** and **(21b-tcg)**, *fac*-[Mn(tcg)$(dmf)_2(H_2O)$] **(22tcg)** and [Co(tcg)$(dmf)_4$Co(tcg)] · 3dmf **(23tcg)** have been synthesized and structurally characterized. Magnetic studies indicate that the tcg dianion provides only a weak ferromagnetic spin coupling via the *[-NCNCNCN-]* bridge in the **21a-tcg** complex, while antiferromagnetic exchange is mediated through H-bonds of adjacent layers in **22tcg**. The room temperature effective moments of the examined complexes indicate the presence of the high-spin form complexes with tcg acting as a weak-field ligand.

7.1 Introduction

The class of compounds based on guanidine-type molecules containing the Y-shaped CN_3 core moiety has attracted considerable attention in coordination and organometalic chemistry.[1] The *N*-donor strength of the guanidine core is controlled by introduction of various substituents on the nitrogen atoms, that influence the properties of the molecule.[2] In particular, with the addition of groups having an electron-withdrawing effect (NO_2, CN, NH_2, OH, OCH_3, aryl, acyl or sulfonyl) the high basicity of the guanidine backbone can be reduced from pK_a 13.6[3l] to pK_a values around ~ 7 – 8.[4] Among this family, *N,N´,N´´*-tri-substituted guanidinates can act as *N*-donor ligands in both monoanionic and dianionic form when one or two active N–H amine nitrogen atoms are deprotonated. Very often, the CN_3 backbone is directly bound to the metal ion in chelating or bridging bidentate mode[1] but the introduction of additional donor atoms can change its binding tendency and the guanidine CN_3 moiety is not more engaged in a metal coordination sphere.[5]

The well investigated complexes that contain the cyanoguanidinate ligand bearing only one CN functional group are examples where ligating abilities depends mainly on substituent moiety.[6] Keeping this in mind, we extended the coordination chemistry of the guanidinates to the *N,N´,N´´*-tricyanoguanidinate dianion (tcg), early characterized only as the disodium salt $Na_2(tcg) \cdot H_2O$, the monoguanidinium monosodium salt $[Na(C(NH_2)_3)(tcg)]$[7] or as the metallic cation-radical $(BEDO–TTF)_4[tcg] \cdot H_2O$ salt.[8] Owing to the lone electron pairs on its nitrogen atoms of three cyano groups, tcg can be potentially a planar, trigonal 3-connected organic linker in metal complexes. Thus, we have prepared new coordination polymeric networks composed of paramagnetic M(II) transition metal ions that are bridged through the diamagnetic tcg linkers and have determined their structures with a particular focus on the magnetic properties of the new polymeric materials.

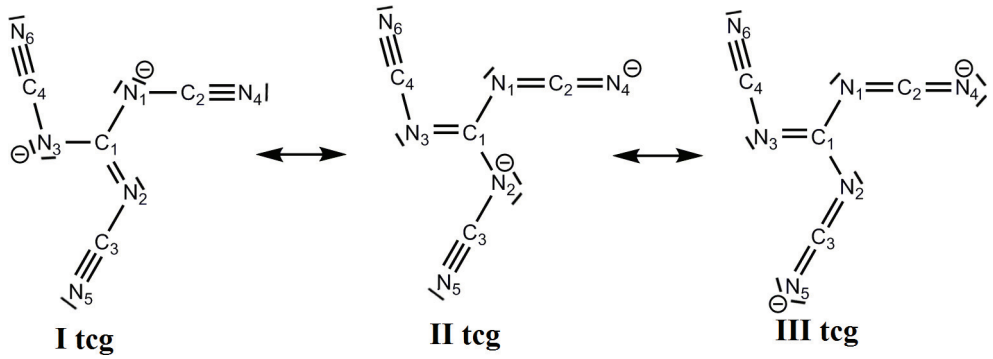

Scheme 7.1 Some Lewis resonance forms and atom numbering scheme of tcg dianion.

7.2 Results and Discussion

7.2.1 Description of the Crystal Structures

The shape of the tcg dianion, depicted in Scheme 7.1 is similar in the all described coordination polymers (**20tcg**, **21a-tcg, 21b-tcg, 22tcg** and **23tcg)** and deviates only to a small extent. As expected, the dianion consists of a central sp^2 carbon centre to which three N atoms are covalently bound. Originally, in the guanidine $(NH_2)_2C{=}NH$ molecule, the CN_3 core consists of two amino C–N single bonds and one shorter imino C=N bond, but in its protonated derivative the six π-electrons are delocalised over symmetric CN_3 unit in the guanininium cation and therefore called Y-aromatic.[9] The differences in the bond length between the central carbon atom and the imino or amino nitrogen atoms referred to the bond order in the tcg dianion. In a fully localized system (retaining C–N amine (1.38 Å) and C=N imine (1.28 Å) groups) the calculated length difference between the double imine and the single amine C–N bond would be 0.10 Å.[10] In the other hand, in a fully delocalised system this difference should be negligible, with all three C–N bond distances close to 1.33 Å, which is consistent with the bond order 1.5. In all crystal structures (**20tcg**, **21a-tcg, 21b-tcg, 22tcg** and **23tcg)** the difference between longest and shortest C–N bond in the CN_3 core (C1–N1, C1–N2 and C1–N3) is only about 0.02 Å (Appendix E), so there is no evidence for any localised double bond in contrast to other *N,N´,N´´*-trisubstituted guanidinates[11] or to the guanidine.[12]

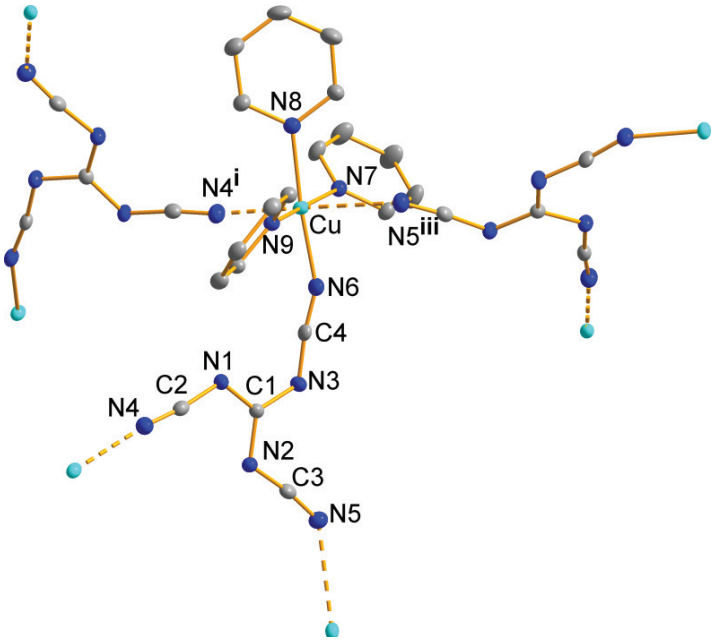

Figure 7.2.1.1 The numbering scheme in the local coordination geometry of Cu^{2+} ions in the coordination polymer **20tcg**. Displacement ellipsoids are drawn in 50 % probability level. Symmetry codes: (i) $x-1/2, -y+1/2, -z$; (iii) $-x, y+1/2, -1/2-z$.

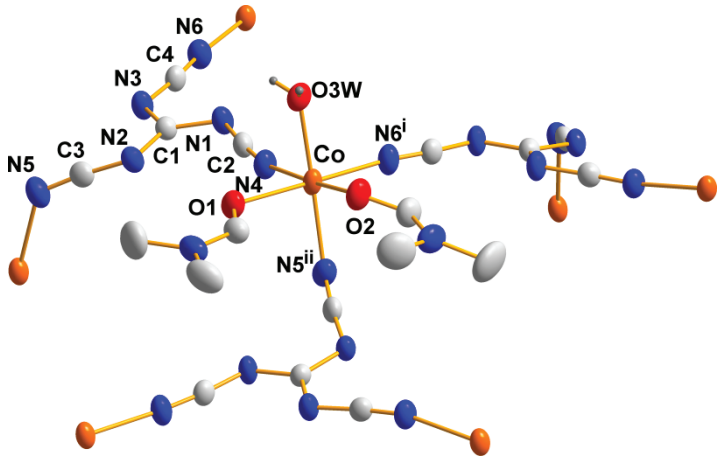

Figure 7.2.1.2 The numbering scheme in the local coordination geometry of Co^{2+} ions in the coordination polymer **21a-tcg**. Displacement ellipsoids are drawn in 50 % probability level. Symmetry codes: (i) *x*−1/2, *y*, −*z*+1/2; (ii) *x*, −*y*+1/2, *z*+1/2.

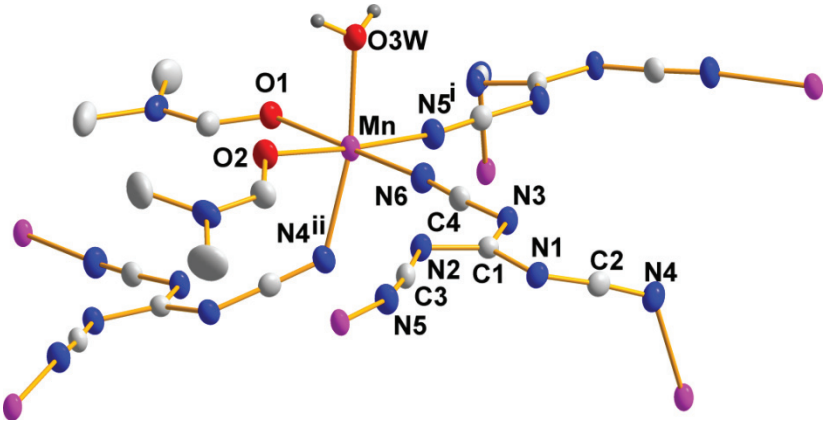

Figure 7.2.1.3 The numbering scheme in the local coordination geometry of Mn^{2+} ions in the coordination polymer **22tcg**. Displacement ellipsoids are drawn in 30 % probability level. Symmetry codes: (i) *x*−1/2, *y*, −*z*+1/2; (ii) *x*, −*y*+3/2, *z*−1/2.

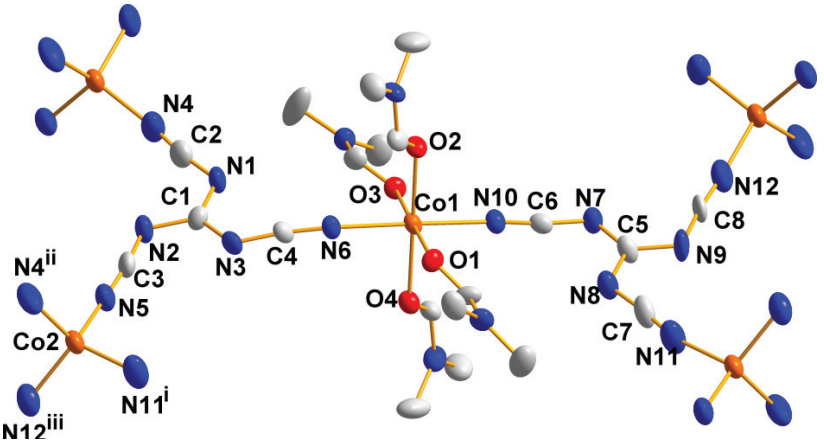

Figure 7.2.1.4 The numbering scheme in the local coordination geometry of Co^{2+} ions in the coordination polymer **23tcg**. Displacement ellipsoids are drawn in 50 % probability level. Symmetry codes: (i) −*x*+2, −*y*+2, −*z*; (ii) −*x*+2, *y*+1/2, −*z*+1/2; (iii) *x*+1, −*y*+3/2, *z*+1/2.

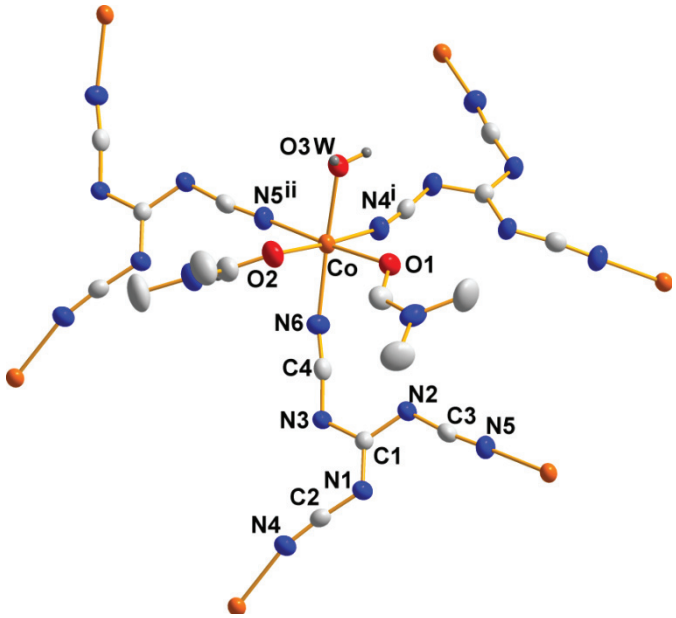

Figure 7.2.1.5 The numbering scheme in the local coordination geometry of Co^{2+} ions in the coordination polymer **21b-tcg**. Displacement ellipsoids are drawn in 50 % probability level. Symmetry codes: Symmetry codes: (i) $-x+3/2, y-1/2, -z+1/2$; (ii) $x-1, y, z$.

All dianions adopt only one conformation of approximate C_{3h} symmetry with the N2—C1—N1, N1—C1—N3 and N2—C1—N3 angles of the CN_3 unit close to 120°. The angles C1—N3—C4, C1—N1—C2 and C1—N2—C3 are also close to 120°, which defines the propeller-like shape of the molecules (Appendix E). Moreover, the Y-shaped tcg molecules are entirely planar, as is evident from the sum of three N2—C1—N1, N2—C1—N3 and N2—C1—N3 angles of the CN_3 core, which gives the value of approximately 360° (Appendix E) and therefore implying a significant π-conjugation around the central carbon atom.

The presence of three widely separated cyano N coordination sites makes tcg a bridging ligand, capable to bind up to three metal centres. The crystal structures of the M(II) transition metal series containing the tcg ligand represent novel 2D **(21a-tcg**, **21b-tcg** and **22tcg)** or 3D coordination polymers (**20tcg** and **23tcg**) with the metal ions bridged through the tcg dianions. Each divalent metal atom (exception Co^{2+} from **23tcg**) is surrounded by three solvent molecules (**20tcg**: three pyridine molecules, **21a-tcg**, **21b-tcg** and **22tcg**: two dmf molecules and one water molecule) and three tcg dianions to from two stereoisomers in the *fac*- and *mer*-$\{M^{II}(tcg)_3(solv)_3\}$ octahedral coordination environment (Figure 7.2.1.1-7.2.1.5).

In pyridine as solvent, the 3D *mer*-isomer **20tcg** is formed, which involves three tcg ligands situated in one plane including the metal centre (Figure 7.2.1.1). The *mer*-$[Cu(tcg)(py)_3] \cdot py$ complex is the best described in the orthorhombic space group $P2_12_12_1$ and features a complicated three dimensional chiral net as shown in Figure 7.2.1.7. Each crystallographically equivalent Cu centre is surrounded by three tcg units, adopting a T-shaped arrangement. Accordingly, the remaining three equatorial places are reserved for pyridine molecules. A significant elongation of *trans*-positioned Cu–N bonds manifests in their enlarged lengths (Cu–$N5^{iii}$ 2.736 Å and Cu–$N4^{i}$ 2.258 Å) and indicates a Jahn-Teller distortion. In this three

dimensional net, the tcg dianion bridges up to three metal ions in comparably large separation to form a triangle with Cu···Cu distances of 8.902 Å, 8.493 Å and 10.461 Å (Figure 7.2.1.1).
The *facial* geometry, in which three tcg ligands occupy one face of the octahedron are restricted to the layered structures **21a-tcg, 21b-tcg** and **22tcg**. Two supramolecular isomers[13] formulated as *fac*-[Co(tcg)(dmf)$_2$(H_2O)] and denoted as **21a-tcg** and **21b-tcg** have this same composition, local geometries and the same ligand-linker combinations but different 2D networks (Figure 7.2.1.8 and 7.2.1.9). In the local geometry both isomers posses crystallographically equivalent Co atoms. Each is coordinated by three tcg ligands, one water moleculeand two dmf molecules to form a slightly distorted octahedron. The Co–N and Co–O bond lengths fall in the range of 2.0637(7) – 2.1874(5) Å.

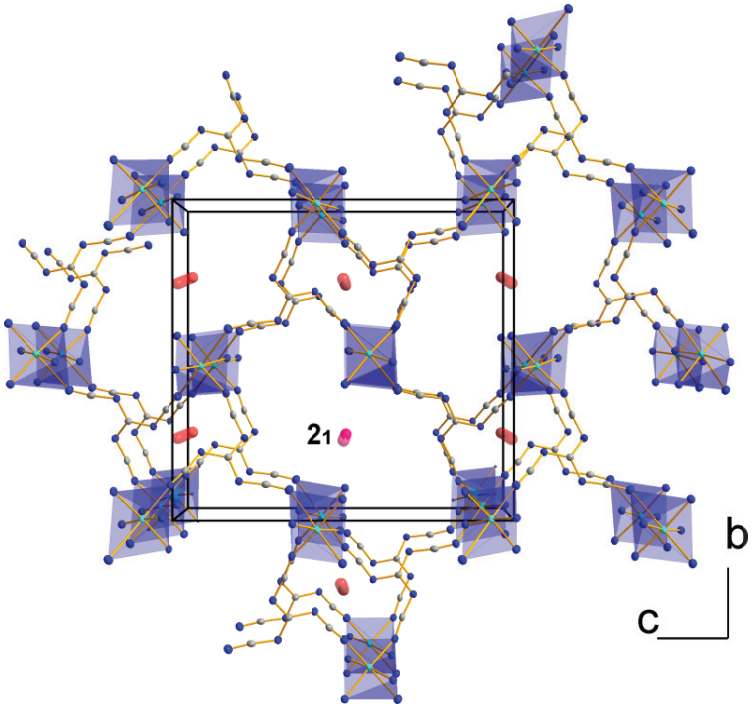

Figure 7.2.1.6 Projection of the unit cell of the 3D coordination polymer **20tcg** along the *a*-axis. Six 2_1 screw axes are marked as red sticks. The big channels are filled by pyridine molecules, here omitted for clarity. Displacement ellipsoids are drawn at the 50 % probability level.

As can be seen on Figure 7.2.1.8 and 7.2.1.9 , the metal-to-ligand connectivity is the same but the distinct orientation of the tcg ligands causes different topologies of the layers in **21a-tcg** and **21b-tcg**. In the isomer **21a-tcg**, equatorial tcg dianions are coplanar with the equatorial plane with defined angles of 174.70° for Co–N6^{i}–C3^{i} and 167.60° Co–N4–C2. One axially positioned tcg dianion coordinates to the Co atom with the defined Co–N5^{ii}–C3^{ii} angle of 129.50° and thus it is bound in a 'bend' way in respect to the axial direction. In the isomer **21b-tcg**, both equatorial dianions and dmf molecules are twisted out of the equatorial plane and the axially positioned tcg dianion is approximately parallel to the axial axis and defined by Co–N6–C4 angle of 157.00°. The axially positioned water molecules stay unchanged in both isomers.

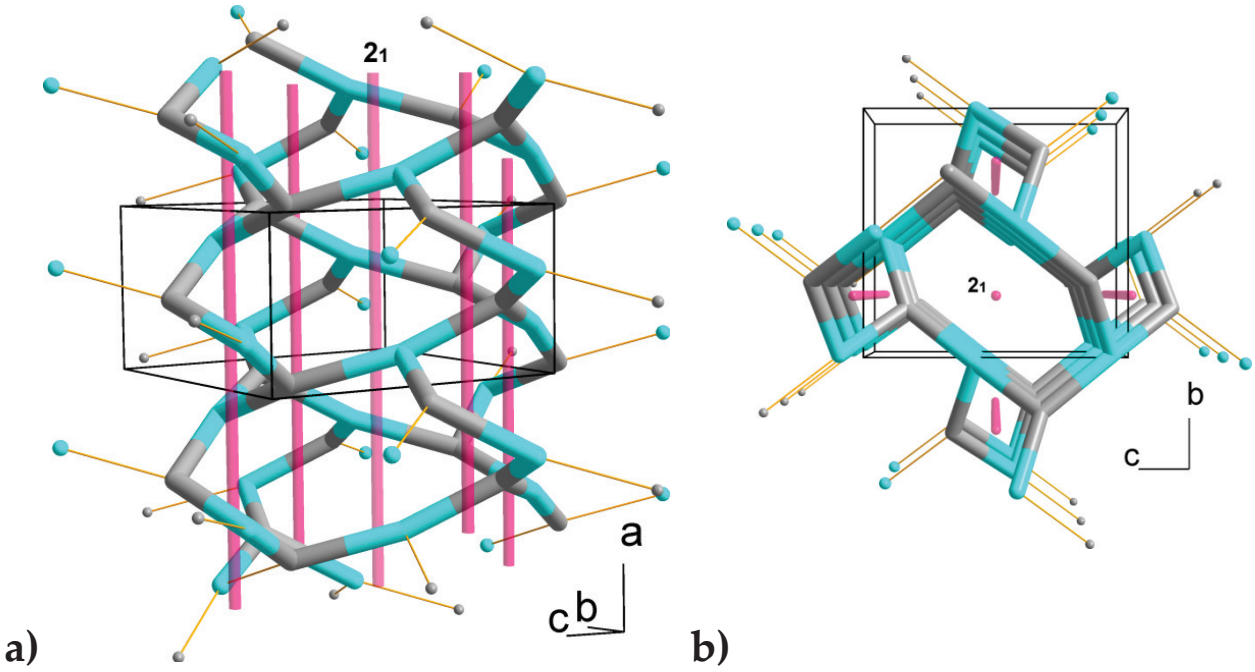

Figure 7.2.1.7 (a) A section of the topological network in the structure of **20tcg** shown along the *a*-axis. The molecules are simplified to points (balls), gray – tcg molecules, blue – three-connected Cu nodes, py molecules are omitted for clarity. The bold wireframe-styled part shows a section of a chiral network **(b)** The topological network shown along *a*-axis.

While both 2D arrays seem to be similar, the different zigzag layers in the complexes **21a-tcg** and **21b-tcg** are obvious and caused by the conformational freedom of tcg the ligands (Figure 7.2.1.8 and 7.2.1.9). Owing to propensity to bind to three different metal sites, the tcg dianion separates Co ion centres in the distance of 8.532 Å, 8.682 Å and 9.298 Å within the layers in the isomer **21a-tcg** and on the distance of 8.704 Å, 9.150 Å and 9.542 Å within the layers in the isomer **21b-tcg**. In both crystal structures, the layers are superimposed on each other and connected through hydrogen bonds between terminally coordinated water molecules (donors) and tcg or dmf molecules (acceptors) of adjacent sheets (Figures 7.2.1.8 and 7.2.1.9).
In both packing motifs, edge-to-edge aggregation is sustained by O–H···$O_{(dmf)}$ and O–H···$N_{(tcg)}$ interactions, defined by O···O and O···N distances of 2.908(5)–2.938(2) Å (Appendix E). Accordingly, the nearest Co···Co distances in the adjacent sheets are shorter than in the layers and amount to 5.185 Å for **21a-tcg** and 5.261 Å for **21b-tcg**. The coordination polymer **22tcg** is isostructural to the topological isomer **21a-tcg**, exhibiting the same topological network, thus only structure **21a-tcg** was representatively described here. The nearest Mn···Mn distances in the layers are 8.641 Å, 8.783 Å and 9.408 Å and 5.295 Å in the adjacent layers.

The crystal structure of $[Co(tcg)(dmf)_4Co(tcg)] \cdot 3dmf$ **(23tcg)** consists of a three dimensional network, composed from four- and six-coordinated cobalt(II) sites denoted as Co(1) and Co(2), both located in general positions. Co(2) exhibits a slightly distorted tetrahedral $\{CoN_4\}$ coordination, ligated by four tcg dianions with average Co(2)–N bond length of ca. 1.95 Å. Each tcg ligand binds two Co(2) centres on the distance of ca. 8.49 Å, generating a layer parallel to the

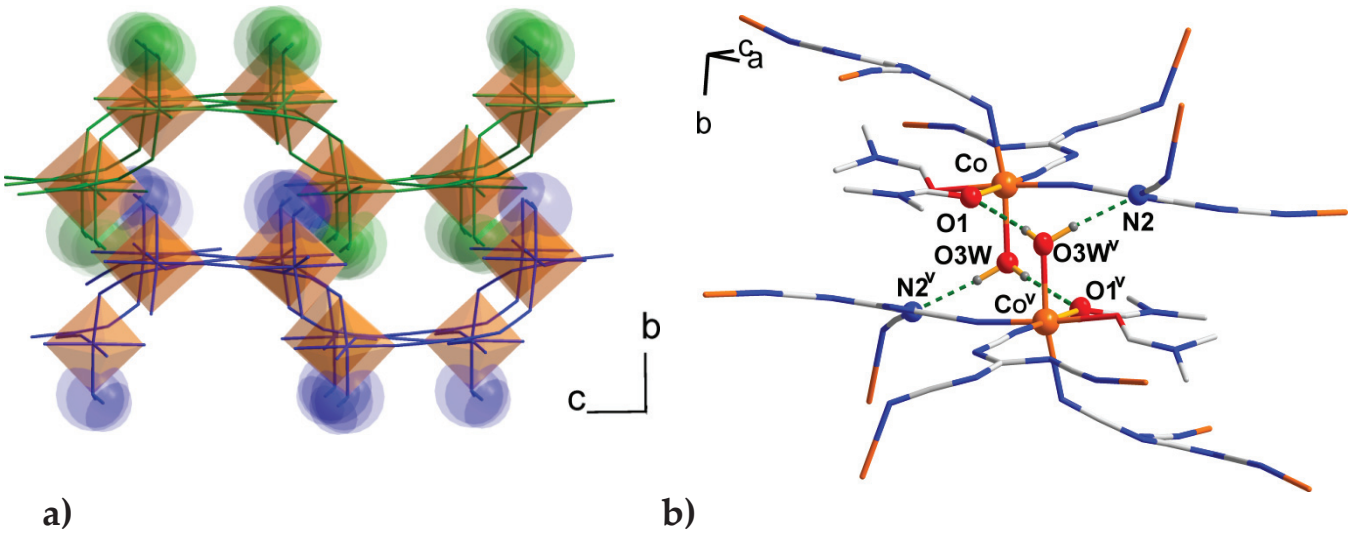

Figure 7.2.1.8 (a) The zigzag shape of two superimposed sheets (green and blue) of the coordination polymer **21a-tcg**. Characteristic ..AAA.. arragement is shown. Coordinated water molecules are drawn in the space-filling fashion to detail the H-bonding between the layers. The rest of the structure is drawn using the wireframe diagram. Dmf molecules are omitted for clarity. **(b)** The H-bonding situation between the crystallographically dependent Co atoms between the layers in **21a-tcg.** Symmetry codes: (v) $-x, -y, -z+1$.

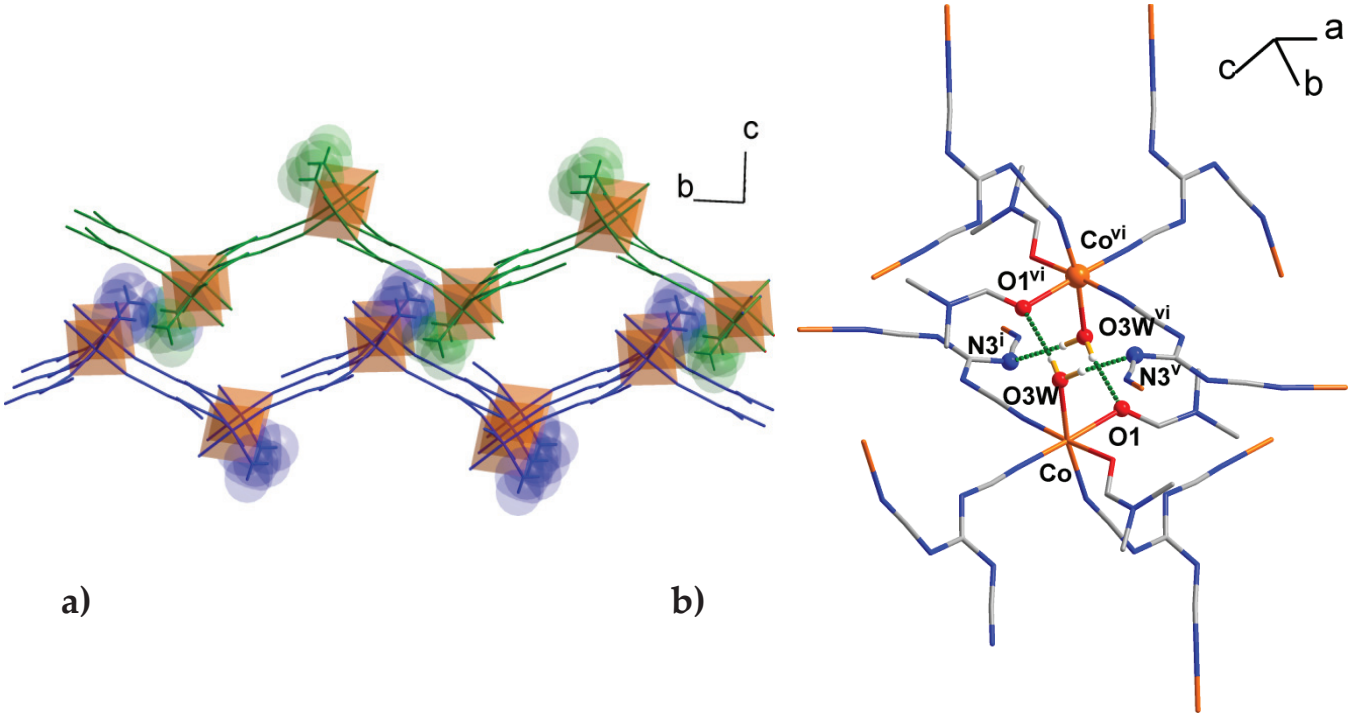

Figure 7.2.1.9 (a) The zigzag shape of two superimposed sheets (green and blue) of the coordination polymer **21b-tcg**. Characteristic ..ABA.. arragement is shown. Coordinated water molecules are drawn in the space-filling fashion to detail the H-bonding between the layers. The rest of the structure is drawn using the wireframe diagram. Dmf molecules are omitted for clarity. **(b)** The H-bonding situation between the crystallographically dependent Co atoms between the layers in the **21b-tcg.** Symmetry codes: (i) $-x+3/2, y-1/2$, (v) $x-1/2, -y+1/2, z-1/2$; (vi) $-x+1, -y, -z$.

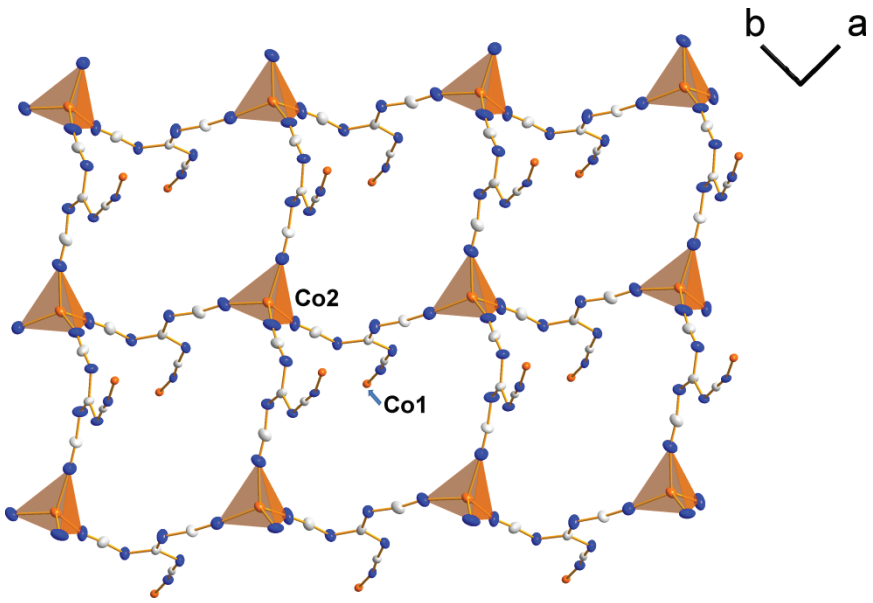

Figure 7.2.1.10 A section of the 2D layer of thecoordination polymer **23tcg** extending parallel to the *ab*-plane. Displacement ellipsoids are drawn at 40% probability level. Dmf molecules are omitted for clarity.

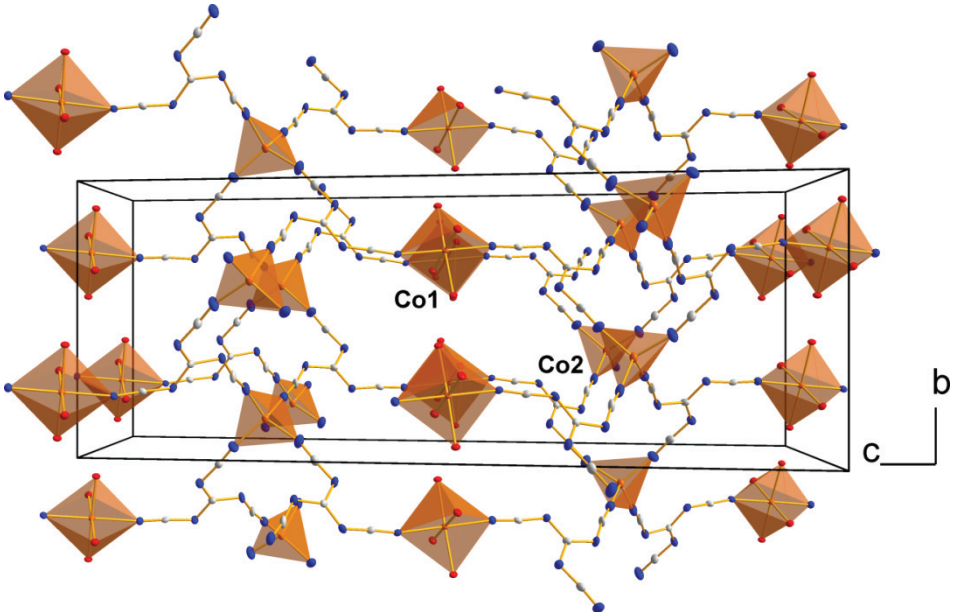

Figure 7.2.1.11 Perspective view of the 3D structure of coordination polymer **23tcg** along the *a*-axis. Dmf molecules are omitted for clarity.

ab-plane (Figure 7.2.1.10). The 2D layered network is aided by the propeller-like shape of the ligands and results in a square-grid sheet structure containing Co2 atoms.

While two CN groups of each tcg ligand join the Co(2) tetrahedra, the third cyano arm coordinates to the Co(1) atom. Co(1) atoms reside between the layers, interlinking them on the quite long distance of ca. 16.19 Å. Each Co(1) centre has a slightly distorted octahedral environment and is coordinated by four dmf molecules that occupy the equatorial plane and by

two tcg ligands that reside in the *trans* positions. The Co(1)–N(≡C) bond lengths (2.102 Å and 2.076 Å) are comparable to the Co(1)–$O_{(dmf)}$ bond lengths (~ 2.09 Å).

7.2.2 Thermal Behaviour of the tcg Coordination Polymers

Thermogravimetric analyses (TGA) were performed for **20tcg**, **23tcg**, **21a-tcg** and **22tcg** to verify the thermal stability and desolvation of the new compounds. The released volatile matter was identified through the characteristic mass loss and compared to the calculated mass from the molecular formula of the investigated compounds. The thermal decomposition of [Cu(tcg)py_3] · py **(20tcg)** compound occurs in two stages in the temperature range 20 – 420 °C. The first mass loss of 29.7 % occurs between 80 – 130 °C with an endothermic DTA peak at 132 °C assigned to the release of two pyridine molecules (calculated 30.6 %) per unit formula. The second mass loss of 33.5 % is attributed to the loss of next two pyridine molecules per formula unit, which is in agreement with the corresponding crystal structure of **20tcg** (Figure 7.2.2.1).

The TG curve of [Co(tcg)$(dmf)_4$Co(tcg)] · 3dmf **(23tcg)** displays a weight loss of 36.1 % from 90 to 170 °C corresponding to the progressive loss of three dmf molecules (calculated 33 %) per unit formula (endothermic DTA peak at 166 °C). Increasing the temperature up to 370 °C results in the decomposition of the sample to the black powder (Figure 7.2.2.2).

The thermogravimetric analysis of *fac*-[Mn(tcg)$(dmf)_2(H_2O)$] **(22tcg)** indicates that two solvent molecules, water and dmf are lost in two events between 80 – 320 °C. First mass loss occurs in 80 – 140 °C, corresponds to 8.84 % mass loss due to the removal of one coordinated water molecule (calculated 5.12 %) per unit formula. Than the weight decreases until ca. 320 °C, with the loss of 25.7 %, which approximately corresponds to the release of one dmf molecule per unit formula (calculated 20.8 %). At higher temperatures (420 °C) the **22tcg** complex decomposes to a black powder (Figure 7.2.2.3).

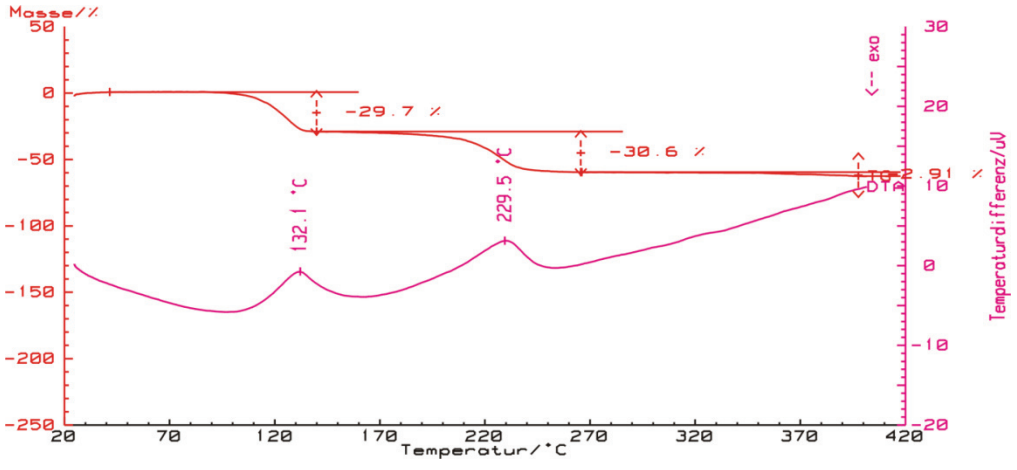

Figure 7.2.2.1 TG/DTA curves of **20tcg** measured under argon-gas flow at a heating rate of 7 °C/min. Red - TG curve, pink - DTA curve.

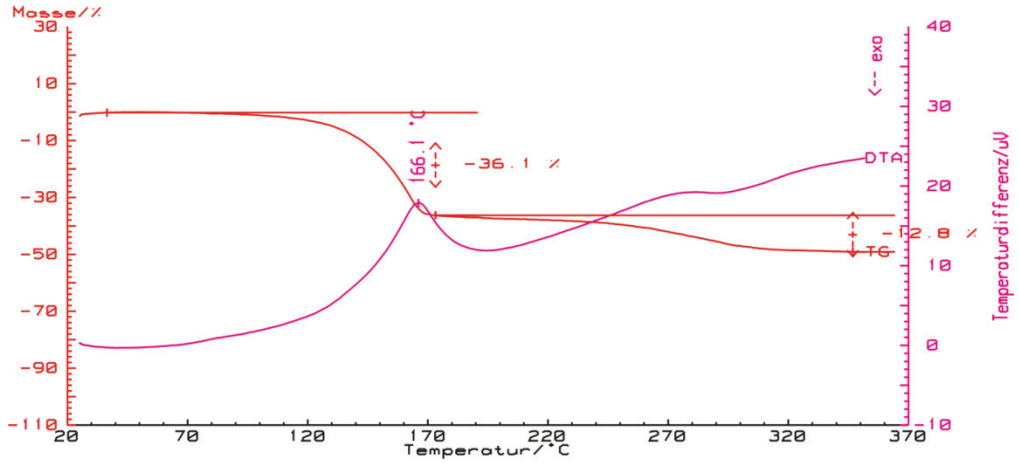

Figure 7.2.2.2 TG/DTA curves of **23tcg** measured under argon-gas flow at a heating rate of 7 °C/min. Red - TG curve, pink - DTA curve.

In the pink coordination polymer [Co(tcg)(dmf)$_2$(H_2O)] **(21a-tcg)** which is isostructural to the compound **22tcg**, the degradation starts at higher temperatures, around 120 °C up to 160 °C with the mass loss of 25.8 % (endothermic DTA peak at 137 °C), attributed to the release of one water molecule (calculated 5.1 %), directly followed by the release of one dmf molecule (calculated 20.6 %). The resultant blue [Co(tcg)dmf] residue is stable up to 220 °C. In higher temperatures it decomposes irreversibly to a black powder. If the heating of the sample is stopped at 160 °C (Figure 7.2.2.4), cooled to room temperature and being exposed to water vapour, the sample slowly absorbs water and becomes pink.

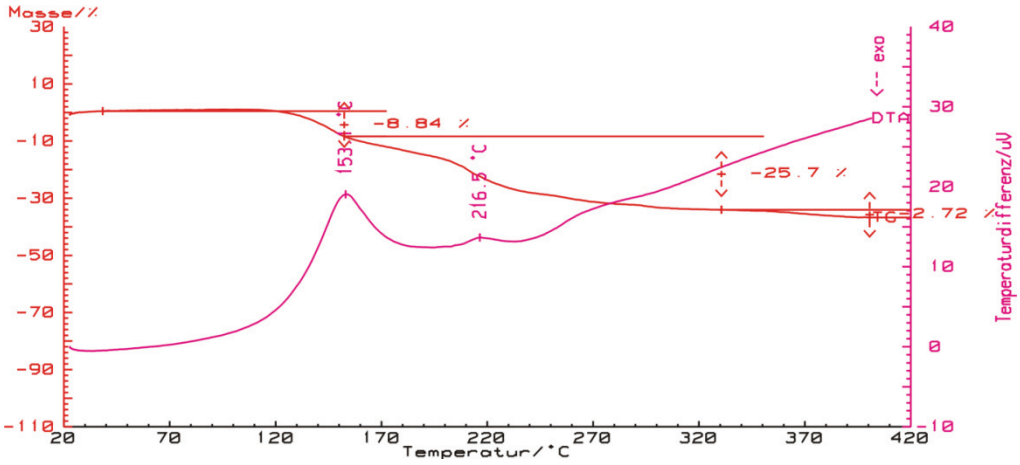

Figure 7.2.2.3 TG/DTA curves of **22tcg** measured under argon-gas flow at a heating rate of 7 °C/min. Red - TG curve, pink - DTA curve.

If the new pink material is once again slowly heated up to 160 °C, a new smooth weight loss of 10.9 % is attributed to the dehydration of two absorbed water molecules (calculated 12 %) per unit formula resulting in a stable, water-free environment blue [Co(tcg)dmf] residue (Scheme 7.2.2.1).

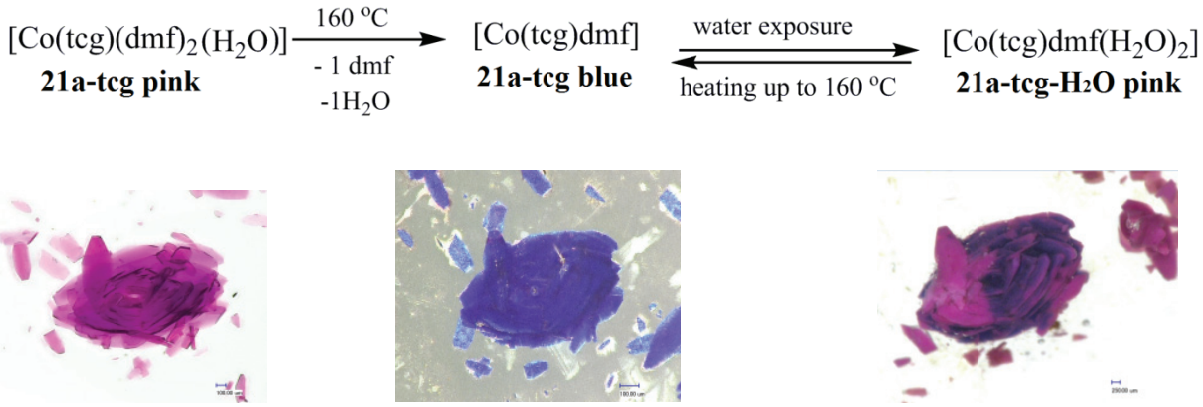

Scheme 7.2.2.1 Reaction scheme summarizing the thermal stability of **21a-tcg pink** and the partly desolvation and rehydration process of **21a-tcg blue/21a-tcg-H₂O pink** coordination polymers. The substances shown in photos are immersed in oil. Due to protection from the moisture, substance on the right only partly absorbed water.

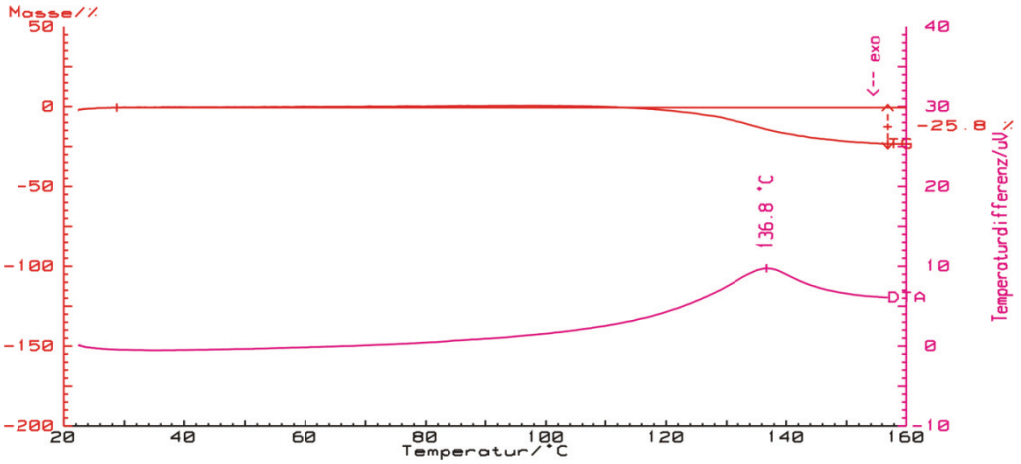

a)

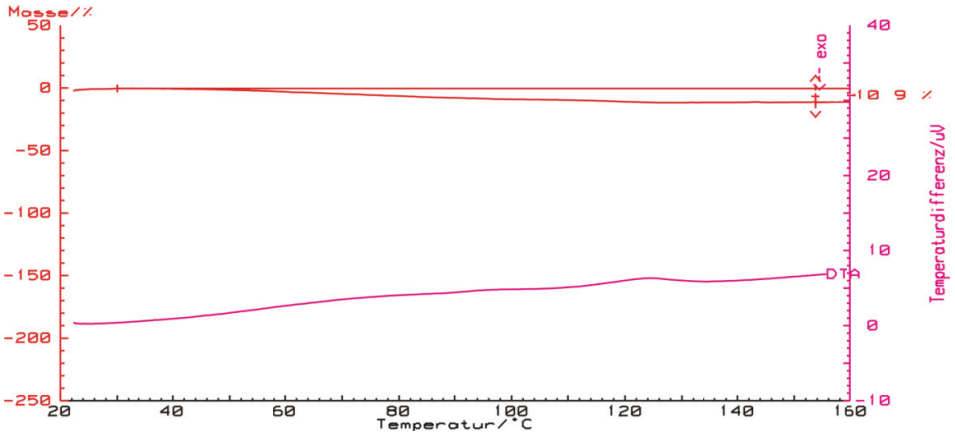

b)

Figure 7.2.2.4 TG/DTA curves of **21a-tcg** compound measured under argon-gas flow at a heating rate of 7 °C/min. **(a)** Partly desolvation of $[Co(tcg)(dmf)_2(H_2O)]$ to [Co(tcg)dmf] in the temperature range 20 – 160 °C. **(b)** Reversible dehydration of $[Co(tcg)dmf(H_2O)_2]$ to [Co(tcg)dmf] in the temperature range 20-160 °C. Red - TG curve, pink - DTA curve.

It is noteworthy to mention that the material **21a-tcg-H_2O pink** starts to lose weight at lower temperatures when heated, compared to initial [Co(tcg)(dmf)$_2$(H_2O)] material. The partly desolvation and rehydration process is associated with the pink-to-blue reversible colour change upon heating up to 220 °C and water exposure.

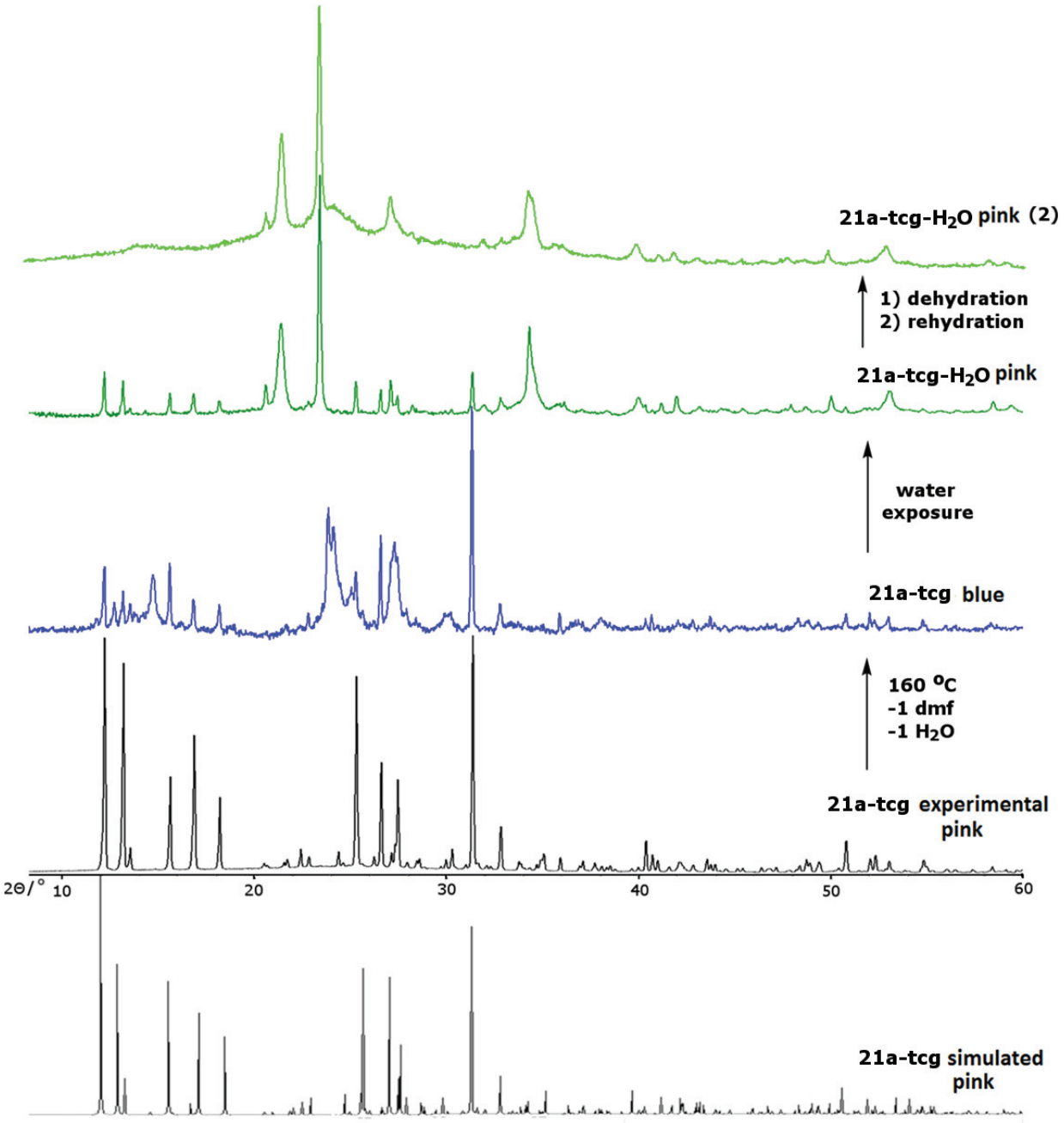

Figure 7.2.2.5 Conversion of **21a-tcg** to **21a-tcg-H_2O pink** on loss of dmf and water monitored using X-ray powder diffraction, the samples were recorded at room temperature in a sealed glass capillary. Description explained in text, (Co-Kα radiation).

The powder X-ray diffraction patterns of the blue and pink materials show that during heating up to 160 °C and cooling to room temperature crystallinity is partly retained in the first cycle. The de-/rehydration process exhibits a good reversible performance. In second cycle the pink

[Co(tcg)(dmf)$(H_2O)_2$] substance suffers from poor crystallinity (Figure 7.2.2.5). changes in the PXRD patterns of **21a-tcg pink**, **21a-tcg blue** and **21a-tcg-H_2O pink**, suggest the presence of three different compounds [Co(tcg)$(dmf)_2(H_2O)$], [Co(tcg)dmf], and [Co(tcg)dmf$(H_2O)_2$]. This assumption is supported by TG/DTA analyses. Unfortunately, X-ray single diffraction analysis of the **21a-tcg blue** substance failed due to very poor crystallinity of examined crystals.

7.2.3 Magnetic Properties of the tcg Coordination Polymers

Magnetic properties of **20tcg** (Figures 7.2.3.1), **21a-tcg** (Figures 7.2.3.3)**, 22tcg** (Figures 7.2.3.2) and **21a-tcg blue** (Figure 7.2.3.4) are displayed as the thermal dependence of χ_{mol}^{-1} and $\chi_{mol}T$. The $\chi_{mol}^{-1}(T)$ function of **20tcg** is essentially linear in the full range of temperature and obeys the Curie-Weiss law $\chi_{mol} = C/(T-\Theta)$ (Eqn. 1.8, Part 1) with C = 0.45 cm^3 K mol^{-1} and Θ = –0.12 K, giving a paramagnetic moment of 1.89 μ_B at 298 K per Cu(II) ion. Although the Cu^{2+} ions are bridged by the tcg dianions, they are widely separated by a distance of more than 8.3 Å, thus the magnetic interactions between the paramagnetic centres are negligible.

The magnetic behaviour of the coordination polymer **22tcg** follows the Curie-Weiss law with Θ = –0.81 K and results in a Curie constant of C = 4.27 cm^{3}Kmol^{-1}. From the equation $\mu_{eff} = 2.828(\chi_{mol}T)^{1/2}$ the calculated effective magnetic moment per Mn^{2+} ion in the complex is 5.84 μ_B at 300 K, which is consistent with an uncoupled high-spin S = 5/2 Mn(II) ion (expected spin-only value is 5.92 μ_B). Upon cooling, the $\chi_{mol}T$ product is constant and amounts to about 4.24 cm^{3}Kmol^{-1}. Below 25 K the $\chi_{mol}T$ drops down to 2.41 cm^{3}Kmol^{-1} clearly indicating very weak antiferromagnetic coupling of Mn(II) ions. The best fit to the experimental data could be achieved by using the van Vleck equation (Eq. 1.15, Part 1) for two interacting spins centers with S = 5/2.

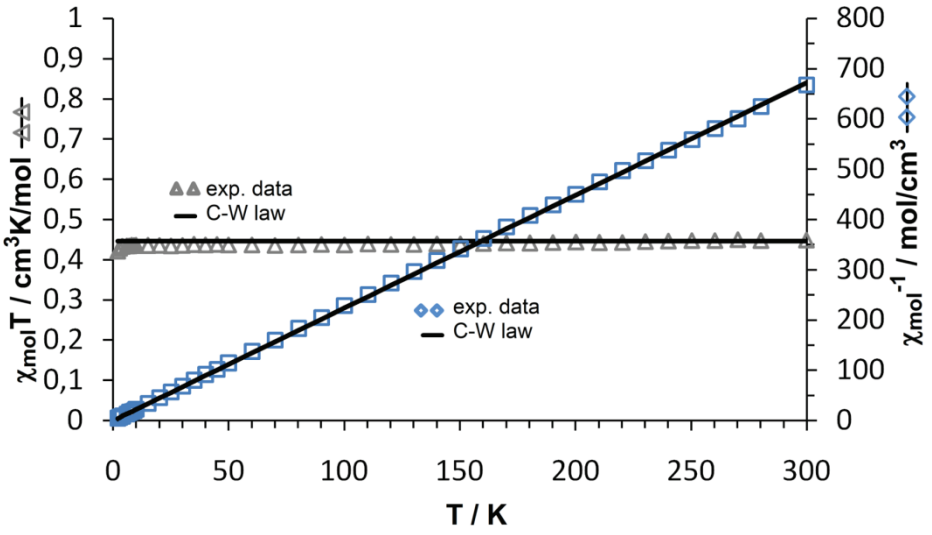

Figure 7.2.3.1 Plots of $\chi^{-1}(T)$ and the $\chi T(T)$ of **20tcg** in a field of 10 kOe. The solid line represents the best fit for Curie-Weiss model $\chi_{mol} = C/(T - \Theta)$ with Θ = 0 K. Agreement factor for the least-square fit: $R = 4.38 \cdot 10^{-4}$.

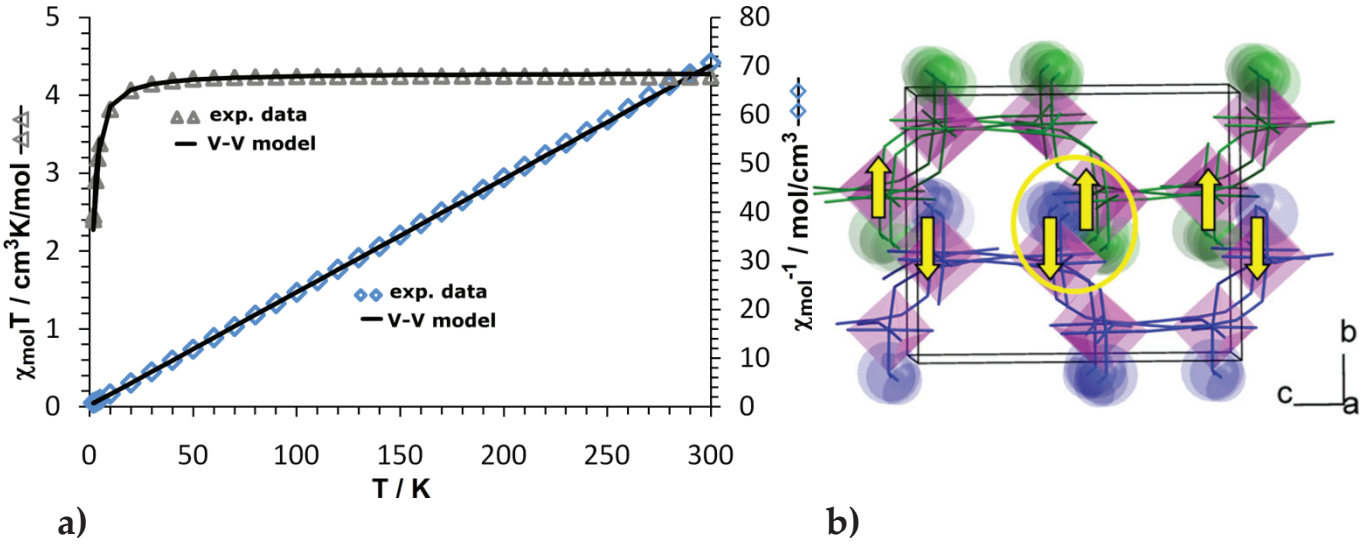

Figure 7.2.3.2 (a) Plots of $\chi^{-1}(T)$ and $\chi T(T)$ for **22tcg** in a field of 10 kOe**. (b)** The solid line represents the best fit for the van Vleck model. **(b)** Schematic representation of the spin coupling model. Agreement factor for the least-square fit: $R = 7.9 \cdot 10^{-5}$.

Due to a very weak magnetic response, the J coupling constant was roughly estimated to be –0.12 cm^{-1} with the g parameter of 1.98. The crystal structure of **22tcg** suggests that this antiferromagnetic exchange could be mediated through the O–H···O$_{(dmf)}$ and O–H···N$_{(tcg)}$ hydrogen bonds that join the layers (Figure 7.2.3.8) due to the shortest Mn···Mn distances (about 5.30 Å).

The 2D coordination polymer **21a-tcg** shows a different linear dependence of χ_{mol}^{-1} vs. T. Taking into account the Curie-Weiss relationship, $\chi_{mol} = C/(T-\Theta)$ yields a paramagnetic Curie-Weiss temperature of θ_P= –29.4 K and μ_{eff} = 4.95 μ_B per cobalt atom at 300 K. This effective moment fall in the range of 4.8-5.1 μ_B for an independent, octahedral high-spin Co^{2+} centre with three unpaired electrons. However, below 60 K the $\chi^{-1}(T)$ product is quenched, suggesting the presence of two magnetically different Co sites. The temperature function of the experimental susceptibility can be fitted quite accurately with the parameters C = 3.38 cm^3 K mol^{-1}, θ_P= –29.4 K, θ' = –15 K, ζ = 130 K using the Néel model (Eq.1.10, Part 1). The relation of the parameters (negative θ_P and positive ζ) to the crystal structure allows for the roughly assumption of an existence of two magnetic sublattices in low temperatures. The magnetic behaviour of the isostructural manganese complex **22tcg** suggests that in the cobalt complex **21a-tcg** this same antifrerromagnetic spin-coupling mediated through H-bonds could be present. Thus, it was assumed that a very weak ferromagnetic exchange could be mediated through the diamagnetic tcg linkers within the layers.

Partial loss of coordinated solvent molecules of the **21a-tcg** polymer is accompanied by the changes in the coordination environment of the Co^{2+} centres and leads to the new blue [Co(tcg)dmf] species. The magnetic behaviour of this new produced substance is slightly different from this of [Co(tcg)(dmf)$_2$(H_2O)] owing to the absence of the essential H-bonds that

join the adjacent layers and mediate information about spin alignment of neighbouring paramagnetic centre

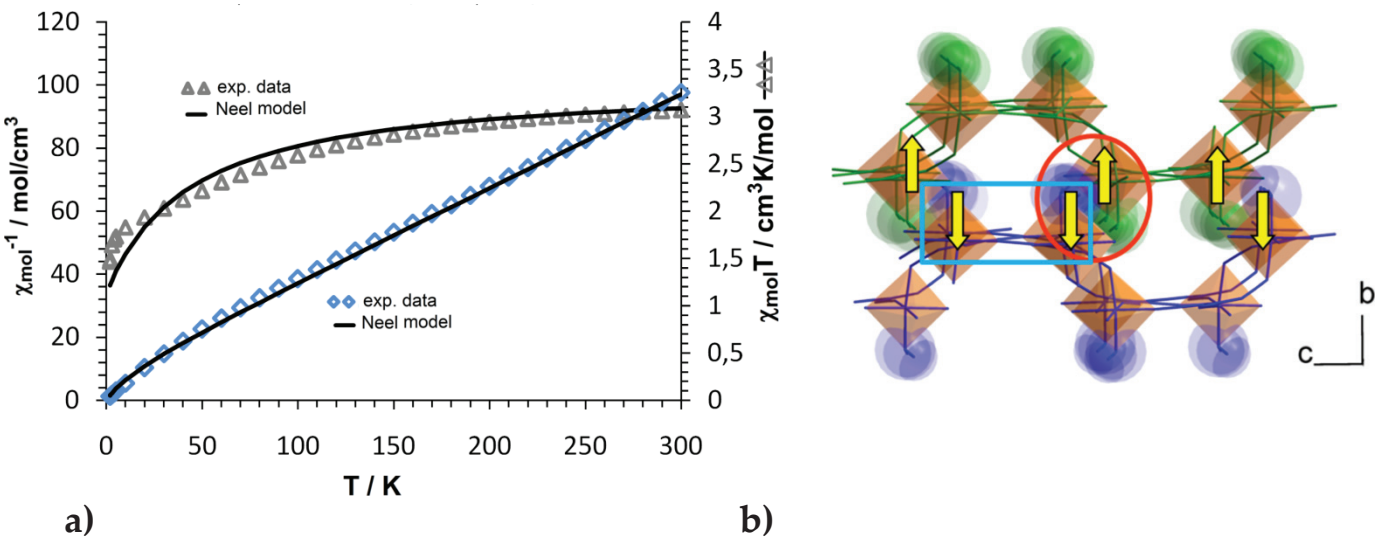

Figure 7.2.3.3 (a) Plot of $\chi^{-1}(T)$ and the $\chi T(T)$ of 21a-tcg in a field of 10 kOe. The solid black line represents the best fit to the Néel model with the following parameters θ_P= –29.4 K, θ' = –15 K, ζ = 130 K. Agreement factor for the least-square fit: $R = 2.3 \cdot 10^{-3}$. (b) Schematic representation of the spin coupling model.

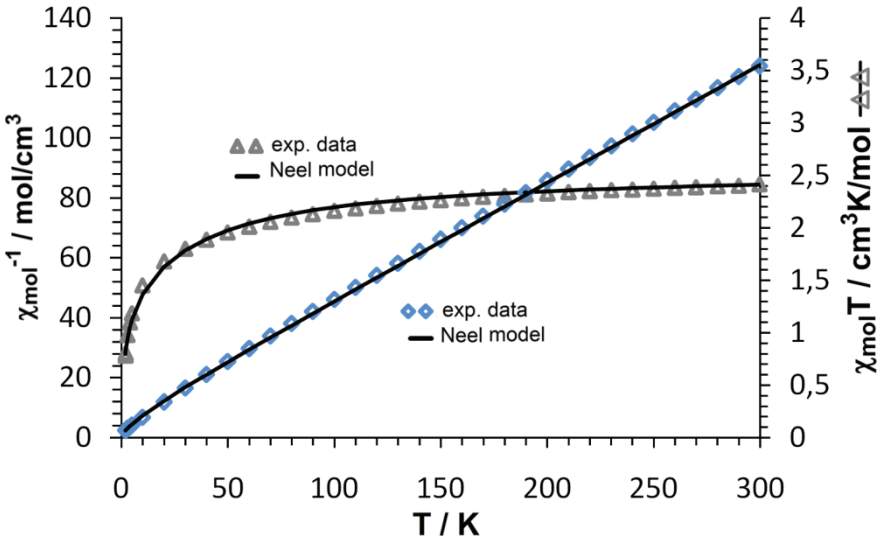

Figure 7.2.3.4 Plots of $\chi^{-1}(T)$ and the $\chi T(T)$ for **21a-tcg blue** in a field of 10 kOe. The solid black line shows the best fit to the Néel model with the following parameters: θ_P= –18.0 K, θ' = –15 K, ζ = 92 K. Agreement factor for the least-square fit: $R = 4.5 \cdot 10^{-4}$.

As it is shown in the Figure 7.2.3.4 the fitting of the χ_{mol}^{-1}(T) experimental data to Curie-Weiss law above 50 K a gives an enlarged θ_P = –18.0 K and a reduced C = 2.55 cm^3 $Kmol^{-1}$. The experimental effective moment is also lowered and equals 4.40 μ_B per cobalt atom at 300 K. The change of the Curie-Weiss temperature from –29.4 K (**21a-tcg**) to –18.0 K (**21a-tcg blue**) could be

related with the absence of H-bonds between the layers, which are responsible for the antiferromagnetic coupling between "pseudo-dimers". Thus, the magnetic effect is weaker compared to the parent **21a-tcg** material.

7.2.4 UV/Vis/NIR Investigations of 21a-tcg pink and 21a-tcg blue Complexes

Tetrahedral and octahedral coordinations are most typical for cobalt(II) complexes. The color of the substance is very often indicative for the geometry (usually octahedral Co(II) complexes are pink and tetrahedral blue or greenish-blue). Classification of the complexes based on the color alone is not sufficient. That is why studies of electronic spectra of the complexes provide an information about the identity of the cation and its oxidation state, local structure, coordination number and the character of the ligands.[14] Energies of electronic transitions result in characteristic spectral patterns which are a consequence of the excitation of valence electrons (for example d or f electrons). Very useful during interpretation of the experimental spectra of transition metal complexes are Tanabe-Sugano diagrams (Appendix I). These diagrams include important parameters like the crystal-field splitting parameter Δ, which reflects energy separation of two sets of d-orbitals splitted in a perfect octahedral field. They contain also the Racah parameter *B* related to the repulsion energies between individual d-electrons and containing the information about metal-ligand covalency.

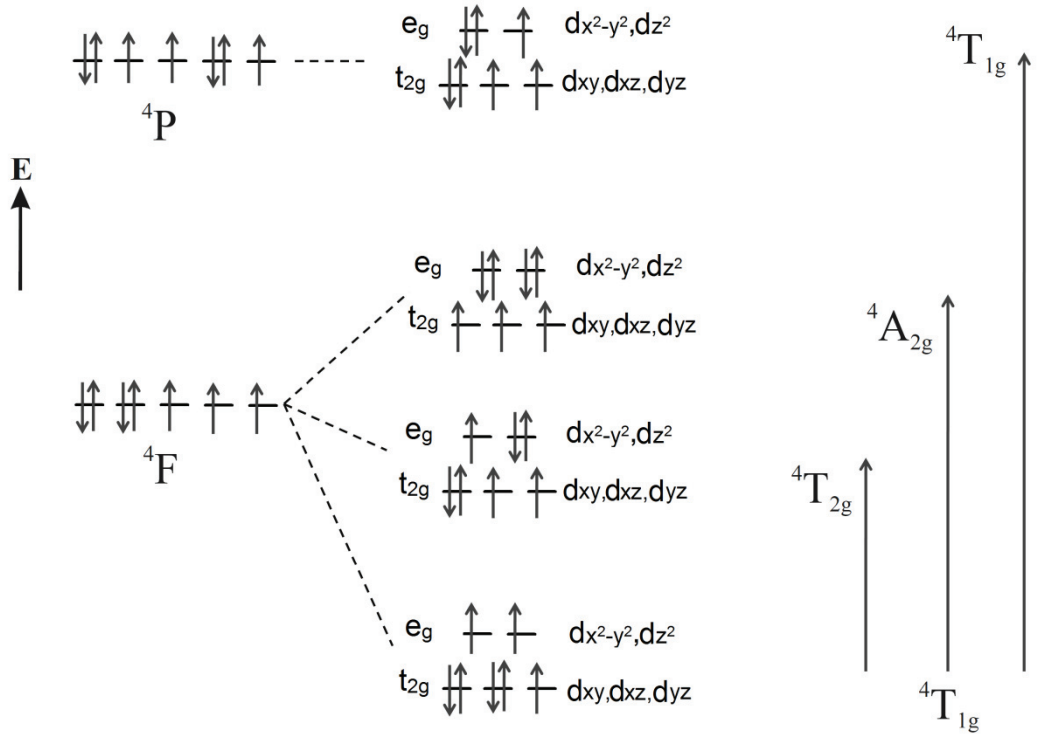

Figure 7.2.4.1 Crystal field splitting diagrams of the d-orbitals of a free ion Co^{2+} (left) and in octahedral field (middle) including the possible electron transitions in the Co(II) high-spin complexes.

Generally speaking, the absorption spectra of high-spin octahedral Co(II) complexes are predicted to show three spin allowed d-d transitions stated in Figure 7.2.4.1.[15] The first band $\tilde{\nu}_1$ corresponds to the $^4T_{1g}(F) \rightarrow {}^4T_{2g}(F)$ transition experimentally seen in the near-IR region (about 8000 – 10000 cm^{-1} range). The second band $\tilde{\nu}_2$ corresponds to the $^4T_{1g}(F) \rightarrow {}^4A_{2g}(F)$ transition, which is expected to be weak because it represents a two-electron jump. The third band $\tilde{\nu}_3$ corresponding to the $^4T_{1g}(F) \rightarrow {}^4T_{1g}(P)$ transition, is seen in the visible region (about 20000 cm^{-1}), giving rise to the characteristic pink color.[16] In the absorption spectra of tetrahedral coordinated cobalt(II) complexes the ground state is $^4A_2(F)$ with the configuration $(e^4)(t_2^3)$. From crystal-field theory, three transitions are predicted: rarely observed band $\tilde{\nu}_1$ corresponds to the $^4A_2(F) \rightarrow {}^4T_2(F)$ transition, the second band $\tilde{\nu}_2$ corresponds to the $^4A_2(F) \rightarrow {}^4T_1(F)$ transition and the third band $\tilde{\nu}_3$ corresponds to the $^4A_2(F) \rightarrow {}^4T_1(P)$ transition occurring in the visible region (about 15000 cm^{-1}). In the tetrahedral coordination there are only four ligands, which show a distinct orientation to the d-orbitals in regards to an octahedral coordination. The cumulative effect of these two amount to about 4/9 of the octahedral crystal field splitting (Δ_o). As a result the tetrahedral bands are shifted towards the infrared region.[14,17]

In the theoretical description of spectroscopic properties of metal complexes, the **angular overlap model (AOM**) has become a useful tool to perform accurate ligand-field analyses.[18] Basically, within this model the d-orbital energies in a complex are obtained by considering the geometry of chromophores derived from the crystal structure analysis. The earlier crystal-field approach used the global parameter Δ (=10Dq) to describe the contribution of all six ligands to the ligand-field potential in an octahedrally coordinated d-system. In the AOM model, each metal-ligand interaction is described by a set of parameters (e_σ, $e_{\pi x}$ and $e_{\pi y}$) and used for the fitting between calculated and observed transition energies in a chromophore. Based on the geometry of the $\{CoN_3O_3\}$ chromophore of the **21a-tcg** complex, the σ-interactions were assumed to be proportionally to the −5th power of the metal-ligand distance $(d(M–L)^{-5} \approx e_\sigma)$.[19] The π-interactions between p-orbitals of the ligands and d-orbitals of the central ion were assumed to be $e_\pi \approx {}^1/_4\, e_\sigma$. The isotropic interactions were assumed to be: $e_{\pi x} \approx e_{\pi y}$. In the simple case the 18 interaction parameters were reduced to only one independent parameter $e_{\sigma,max}$ for the shortest metal-ligand distance (d(M−L)). Moreover, the Racah parameters *B* and *C* (cm^{-1}) and the spin-orbit coupling ζ (cm^{-1}) were introduced to the angular overlap modelling.

The AOM calculations were carried out for the $\{CoN_3O_3\}$ chromophore of the **21a-tcg** complex using the CAMMAG program[20] and later compared to the experimental electronic spectrum of the single crystal of **21a-tcg.** During the calculations, the transition energies were matched to the experimental bands using the variable AOM parameters like $e_{\sigma,max}$, B, C, the energies e_σ and e_π (6 x e_σ and 12 x e_π) and the spin-orbit coupling ζ (cm^{-1}).

The electronic absorption spectra of the single-crystal of the $[Co(tcg)(dmf)_2(H_2O)]$ **21a-tcg** were measured at room temperature in the UV/Vis/NIR region using a modified CARY 17 microcrystal spectrophotometer. The examined crystal shows polarization dependence varying

from pink to light-pink in the horizontal and vertical direction (hpol and vpol) due to the chromophore {CoN_3O_3} (Figure 7.2.4.2). Crystal faces were not indexed. The attempts to model observed d-d transition energies in **21a-tcg** using CAMMAG program, led to the following parameters: $e_{\sigma,max}$ = 3500 cm^{-1}, k = 0.835, B = 826.0 cm^{-1}, C = 3551.8 cm^{-1} and ζ = 430.1 cm^{-1}. Unfortunately, the calculated spectrum does not predict one experimental band, that should occur at about 12800 cm^{-1} (Figure 7.2.4.2).

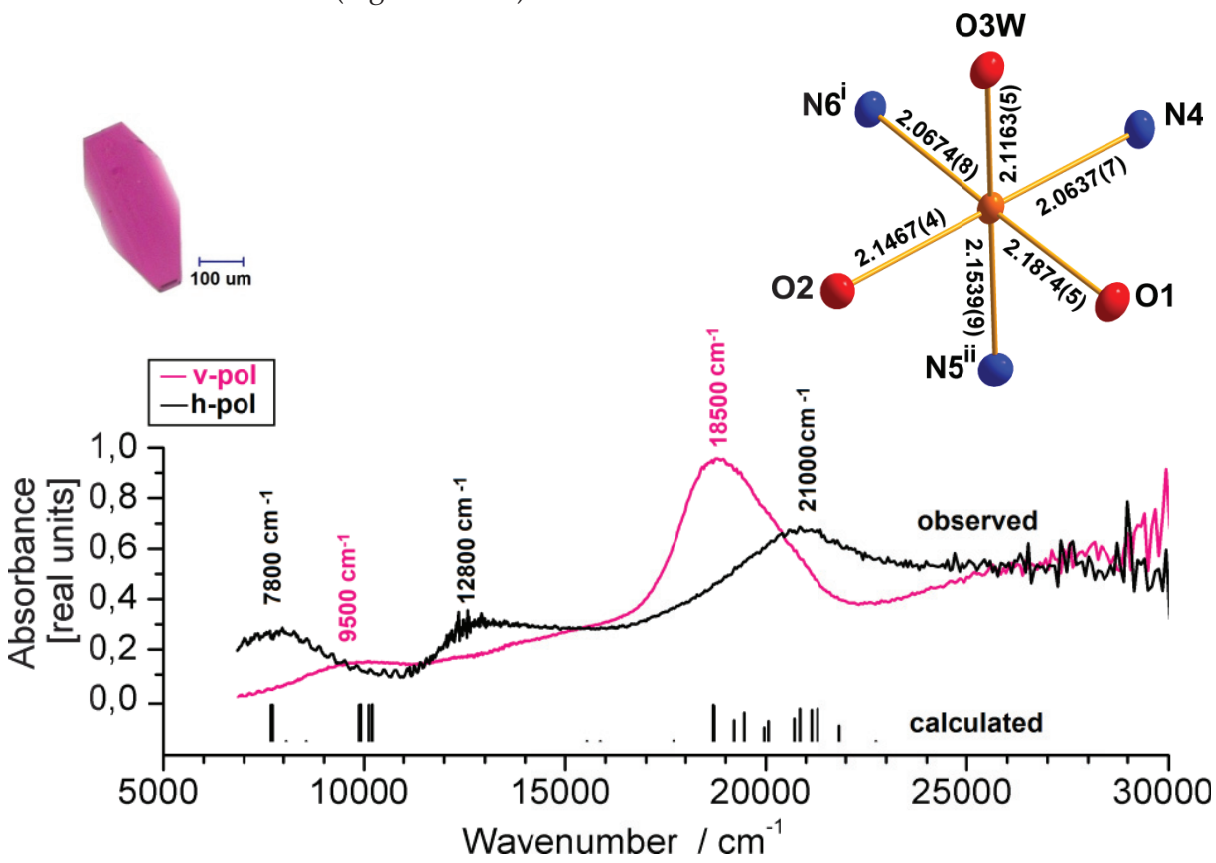

Figure 7.2.4.2 Polarized single-crystal electronic absorption spectra of **21a-tcg** compared to the calculated bands obtained using CAMMAG program. On top - the geometry of the {CoN_3O_3} chromophore in the **21a-tcg**. The respective distances are given in Å. For the detailed description of the crystal structure of the **21a-tcg** complex see chapter 7.2.1, for the selected bond distances and angles see Appendix E.

The detailed assignment of these transitions, was not possible on the basis of the AOM treatment and on the simple Tanabe-Sugano approach. In this particular case, the electronic situation of the Co^{2+} in the **21a-tcg** complex is quite complex, since there are three different kinds of ligands (H_2O, dmf and tcg) and chemically different donor atoms. Detailed insight into the crystal structure of **21a-tcg** reveals two tcg ligands linearly bound to the Co ion. One axially positioned tcg dianion coordinates in a bent fashion to the cobalt centre, the Co–N5^{ii}–C3^{ii} angle strongly deviates from 180 °, thereby indicating a contribution of metal-ligand π-back bonding. Moreover, the introduction of a strongly anisotropic π-overlap in the AOM for some N and O atoms allowed for a reasonable fit to the observed transition bands (see Appendix I).

Nevertheless, the observed energy of the electronic transitions results in a characteristic spectral pattern, very similar to those reported in the literature spectra of octahedral cobalt(II)

complexes.[14,17]

Due to the missing crystal structure of **21a-tcg blue,** the spectroscopic investigations were limited only to the interpretation using Tanabe-Sugano diagrams. In contrast to **21a-tcg**, [Co(tcg)dmf] **(21a-tcg blue)** reveals a substantially different electronic spectrum (Figure 7.2.4.3). The observed d–d transitions are characteristic for tetrahedral Co^{2+} complexes.[14,17,21] The spectrum shown in Figure 7.2.4.3 is interpreted using the Tanabe-Sugano diagram for d^3 configuration in an octahedral field (Appendix I), which suggests the transition from the ground term $^4A_2$(F) to the excited states $^4T_1(F)$ and $^4T_1(P)$:

band	observed wavenumber [cm^{-1}] hpol, vpol	observed average wavenumber [cm^{-1}]	transition (term symbol for T_d symmetry)
$\tilde{\nu}_1$ (E_1)	–	–	$^4A_2(F) \rightarrow {}^4T_2(F)$
$\tilde{\nu}_2$ (E_2)	7500	7500	$^4A_2(F) \rightarrow {}^4T_1(F)$
$\tilde{\nu}_3$ (E_3)	15500 15800	15650	$^4A_2(F) \rightarrow {}^4T_1(P)$

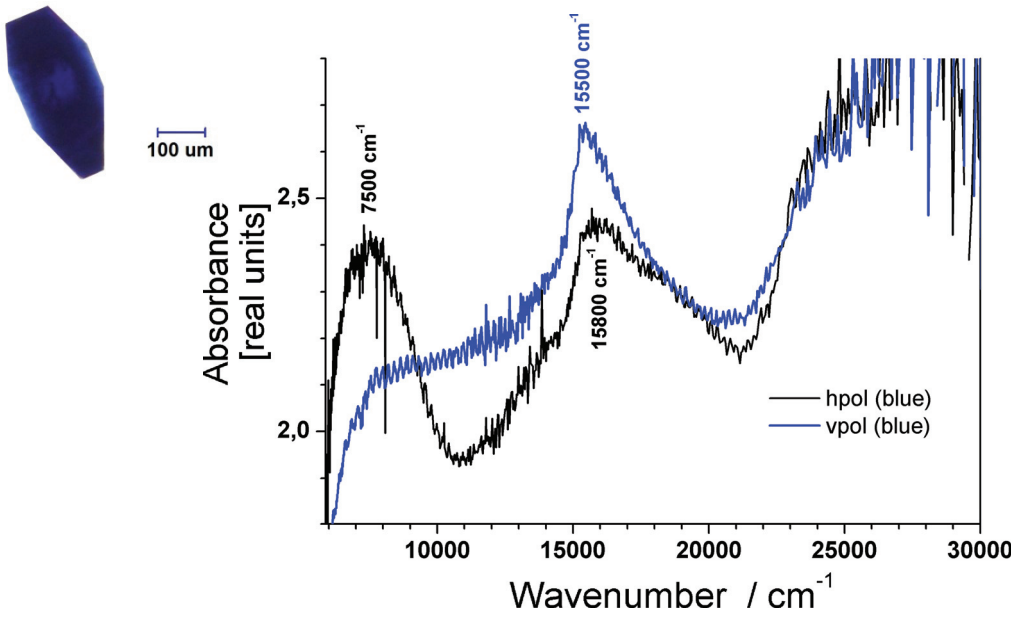

Figure 7.2.4.3 UV-Vis/NIR absorption spectrum of single crystal of [Co(tcg)dmf] **(21a-tcg blue)**. Left - Upon heating up to 160 °C, the single crystal of **21a-tcg** complex changes its color from pink to blue.

The ratio of the average energies of the two transitions ($(^{E_3}/_{E_2}) \approx 2.1$) fits the Tanabe-Sugano diagram at $\Delta/B \approx 6.5$. This suggests that the $^4A_2(F) \rightarrow {}^4T_1(P)$ transition occurs at $^{E_3}/_B \approx 23$, yielding the Racah parameter B ≈ 680 cm^{-1}, corresponding to 69 % of the free ion value of 989 cm^{-1}. This gives the estimated Δ ≈ 4420 cm^{-1} for the tetrahedral cobalt(II) ion. According to the calculations, the band corresponding to the $^4A_2(F) \rightarrow {}^4T_2(F)$ transition is expected to occur at about 4420 cm^{-1}. The ligand field splitting parameter is compared with other Co(II) complexes in

tetrahedral field and consistent with the crystal-field theory.[14, 17]

7.2.5 Diffuse X-ray Scattering in Disordered $Na_2(tcg) \cdot H_2O$ Single Crystal

During X-ray single crystal data collection of disodium $Na_2(tcg) \cdot H_2O$ salt in our laboratory, using the 4-circle diffractometer with 95 mm CCD camera equipped with molybdenum radiation type, a diffuse X-ray scattering pattern was observed on the some precession photos (Figure 7.2.5.1). The diffraction data suggested a hexagonal lattice with the following cell parameters: a, b = 15.4758 Å, c = 6.2458 Å, α = 90.00 °, β = 90.00 °, γ = 120.00 °. Unfortunately, the attempts to solve the crystal structure of $Na_2(tcg) \cdot H_2O$ salt was unsuccessful due to advanced disorder of the structure.

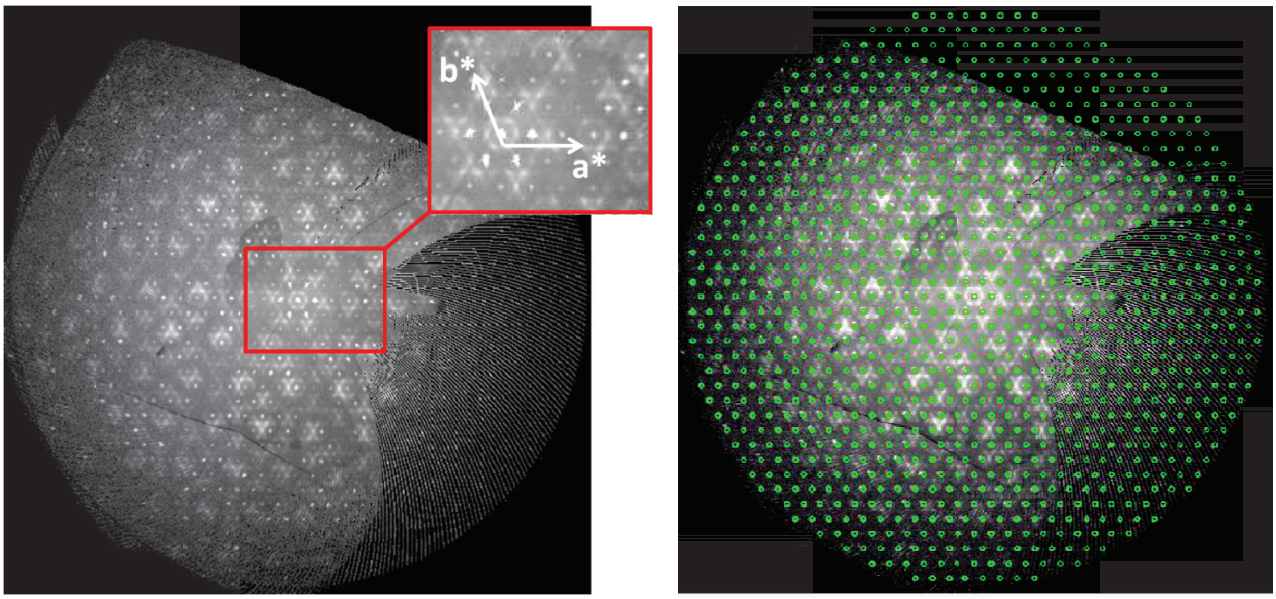

Figure 7.2.5.1 (a) The precession photo of the *hk2* reciprocal plane of $Na_2(tcg) \cdot H_2O$ single crystal reveals a diffuse scattering pattern as a weak "spheres" around ordinary Bragg peaks. This phenomenon originates from structural disorder (description see text). **(b)** The reconstructed hexagonal reciprocal lattice plane (*hk2*) of the single crystal of $Na_2(tcg) \cdot H_2O$ measured by dr. J. Daniels. The diffuse scattering pattern is not taken into account in the unit cell determination.

A correct structural model can be derived only by taking into account the diffuse scattering, which appears as a weak "spheres" around the ordinary Bragg peaks. The data collection requires the newest X-ray and neutron sources equipped with special area detectors.[22] Moreover, a structure refinement against the diffuse data requires complicated "Monte Carlo" algorithms, which lead to detailed insight into the structure of the compound.[23] The presence of the diffuse intensity and the location around ordinary reflections can be interpreted by a some spherical modulation.[24] In several recent studies, diffuse X-ray scattering was observed among wide variety of materials and usually contained the information about deviations from average

structures (different type of disorders, short-range order).[21] In this particular case the disorder of $Na_2(tcg) \cdot H_2O$ salt affects the electronic environment of the compound and it is essential for a physical property like the second harmonic generation.[25]

7.3 Conclusions

The current study shows that the tcg dianion was successfully used as a Lewis-base in the construction of coordination polymers of Cu^{2+}, Mn^{2+}, Co^{2+} transition metal ions. The tcg dianion acts as a trigonal, 3-connected linker adopting C_{3h} symmetry in the examined compounds. In spite of the fact that tcg ligand reveals strong electron delocalization, which was proved by detailed structural analysis of the dianion, the larger size of the ligand makes coordination networks more spacious, thus only a very weak ferromagnetic spin coupling via a seven atom bridge was observed in the complex **21a-tcg**. The effective magnetic moments at room temperature correspond to high-spin complexes in **22tcg** (5.84 μ_B) and **21a-tcg** (4.95 μ_B) with S=5/2 and S=3/2, respectively. Removal of strongly hydrogen-bonding molecules (H_2O, dmf) during heating of the cobalt complex **21a-tcg** slightly affects the magnetic properties, suggesting antiferromagnetic coupling between the Co layers and tetrahedral coordination around metal centers.

7.4 Experimental Section

Potassium Cyanodithioimididocarbonate[26]: to a stirred solution containing 84 g (1.0 mole) of 50% aqueous cyanamide, 200ml of ethanol, and 84 g (1.1 mole) of carbon disulfide, 126 g (2.0 moles) of 90% potassium hydroxide in 500 ml of ethanol was added slowly at 0-15 ˚C over a 15 min period. After stirring at 25-30 ˚C for 1 hour, the precipitate was collected by filtration, washed with 500 ml of ethanol, and air dried at 45-50 ˚C. The product was obtained in 87 % yield and was used without any further purification.

Potassium Methyl Cyanodithioimidocarbonate[27]: A solution of 150.0 g (0.77 mole) of dipotassium cyanodithioimidocarbonate in 615 ml of acetone and 690 ml of water was cooled below 0˚C, and 109.2 g (0.77 mole) of methyl iodide in 310 ml of acetone was added dropwise with rapid stirring below 0 ˚C under argon atmosphere. After completion of the addition, the reaction mixture was stirred for another 0.5 hour in the ice bath and for 3.5 hour at ambient temperature. The solution was evaporated and the product was dried at 50 ˚C to give 271.0 g of solid. This was stirred with 1625 ml of acetone and filtered. The filtrate was evaporated and the residue was washed with two 650ml portions of ether to yield 124.5 g of crude product (mp 215.5–218.0 ˚C). The product was further purified by dissolving in 2050 ml of ethyl acetate and reprecipitating with an equal volume of ligroin (bp 60-90 ˚C) to give 61.7 g of pure product. mp 214–216 ˚C.

Dimethyl Cyanodithioimidocarbonate[27]: A solution of 12.8 g (0.075 mole) of potassium methyl cyanodithioimidocarbonate in 64 ml of acetone was cooled below 10 °C in a argon atmosphere and 12.8 g (0.090 mole) of methyl iodide was added dropwise (mildly exothermic). The ice bath was removed, and the reaction mixture was stirred for 2.5 hours at room temperature. The acetone was removed in a rotary evaporator to leave a solid which was purified by twice dissolving in acetone and precipitating with water. The product weighed 6.4 g (58 %), mp.: 51-52.5 °C.

Disodium *N',N'',N'''*-Tricyanoguanidinate Monohydrate, $Na_2(tcg) \cdot H_2O$[7]: To a suspension of disodium cyanamide (4.400 g, 0.005 mol) in *N,N*-dimethylacetamide (DMAc, 10 mL) was added in 2 mL portions (20 minutes each 2 mL) the solution of dimethyl cyaniminodithiocarbonate (3.9 g, 0.027 mol) dissolved in 8 mL of DMAc, and the reaction mixture was heated to 120-140 °C. After each addition a brownish foam was produced, which disappeared after addition of the last portion of dimethyl cyaniminodithiocarbonate. When the last portion of solution was added, the stirring and heating was continued for next 3 hours, and then left stirring over night in room temperature. After filtration, the solid was recrystallized from hot water to gave a white crystalline product. Yield: 0.7 g (12 %). Mp >400 °C. ^{1}H NMR (300 MHz, Me_2SO-D_6) δ 3.32 (H_2O) ppm. ^{13}C NMR (75 MHz, Me_2SO-D_6): δ 175.61 (s *C*N_3), 122.03 (s, *C*N) ppm.

Tetraphenylphosphonium *N',N'',N'''*-Tricyanoguanidinate ($PPh_4)_2$tcg: ($PPh_4)_2$tcg was prepared by combining aqueous solutions in 2:1 molar ratio of PPh_4Cl: $Na_2tcg \cdot H_2O$. ($PPh_4)_2$tcg precipitated as a white crystalline solid, which was filtered and dried in vacuo. IR (KBr disc): 3100-2900, 2169, 2136, 1603, 1047, 1214, 1103, 1072, 1060, 1042, 753, 721, 694 cm^{-1}.

Crystallization of $[Cu(tcg)py_3]\cdot$ py (20tcg): 100 mg (0.21 mmol) of ($PPh_4)_2$tcg was disolved in 15 mL of pyridine and mixed with 5 mL solution of pyridine that contains of 37 mg (0.21 mmol) of $CuCl_2 \cdot 2H_2O$. Slow evaporation of the solvent yielded after 3 days greenish long needle-shaped crystals of **20tcg**. Yield 66 mg (61 %). Analysis for $C_{24}H_{20}CuN_{10}$ (512.04 g/mol): N 26.63 (calc. 27.35), C 56.30 (55.82), H 4.27 (3.94) %.

Crystallization of $[Co(tcg)(dmf)_4Co(tcg)] \cdot 3dmf$ (23tcg): 100 mg (0.51 mmol) of $Na_2(tcg) \cdot H_2O$ was completely dissolved in 40 mL of hot dmf and mixed with a 5 mL solution that contains 180 mg (0.51 mmol) of $Co(ClO_4)_2 \cdot 6H_2O$. A blue precipitate formed immediately during cooling of the mixture. Additional portion of the dmf solvent (10 mL) was added to speed up the process of crystallization. After one day, the small blue crystals were collected in 26 % yield (120 mg), washed with dmf solution and dried in air. The blue crystals were unstable in the presence of moisture and decomposed to **21a-tcg**. Thus storage in the dmf solution was necessary.

Crystallization of *fac*-$[Co(tcg)(dmf)_2(H_2O)]$ (21a-tcg): Crystallization follows that for $[Co(tcg)(dmf)_4Co(tcg)] \cdot 3dmf$. During formation of blue precipitate small portions of water were added until the blue crystals were dissolved and solution became pink. Slow evaporation

of the solvents yielded pink plates. The pink crystals were collected and washed with a mixture dmf/water, then dried in air.

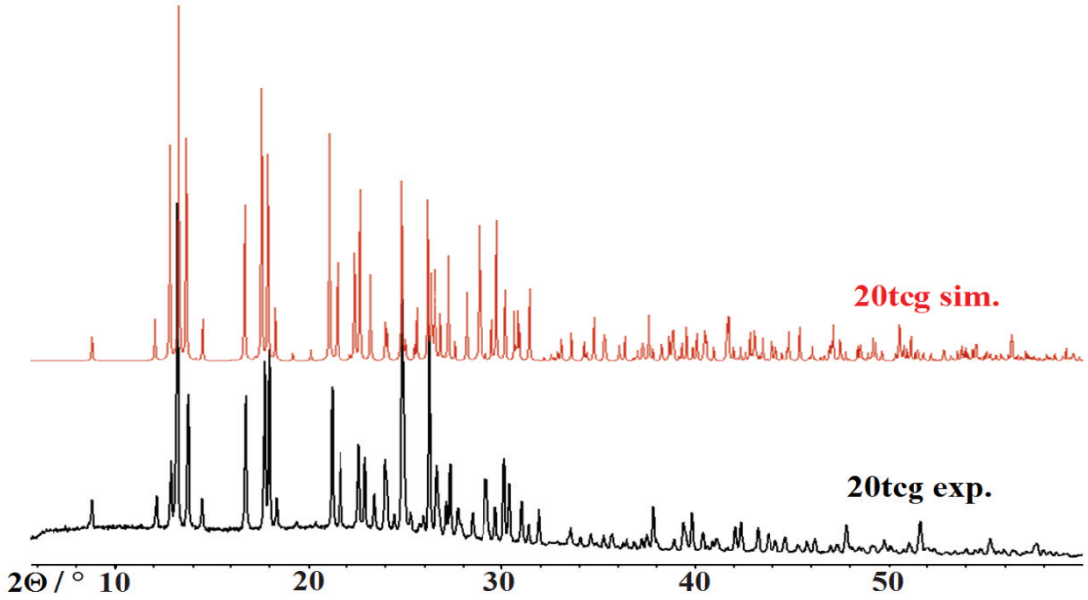

Figure 7.4.1 The simulated and experimental X-ray powder diffraction patterns of **20tcg** are shown (Co-Kα radiation).

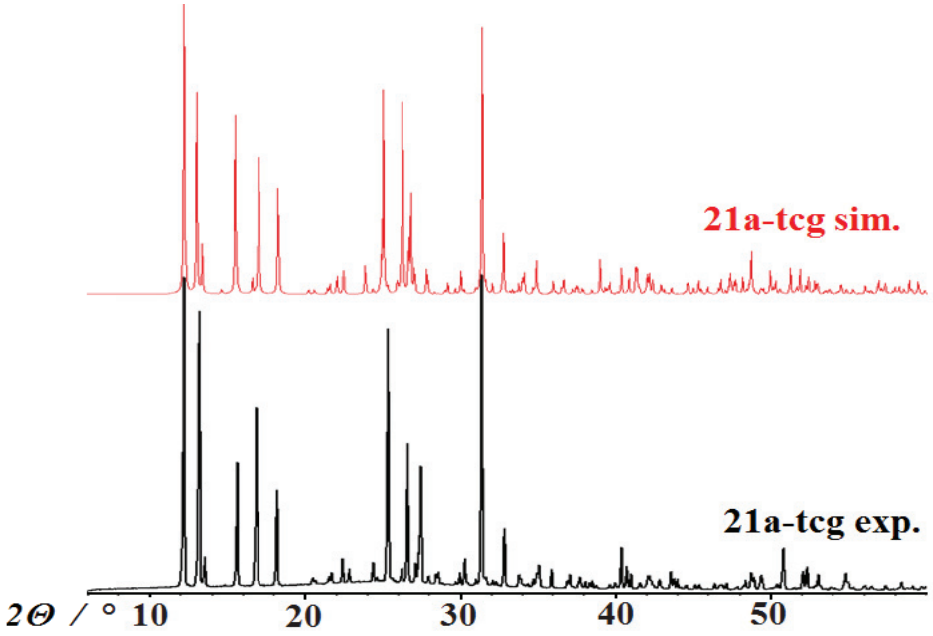

Figure 7.4.2 The simulated and experimental X-ray powder diffraction patterns of **21a-tcg** isolated as a pure phase (Co-Kα radiation).

Crystallization of 21b-tcg: Crystals of the **21a-tcg** isomer were obtained only once. 50 mg (0.25 mmol) of $Na_2(tcg) \cdot H_2O$ was completely dissolved in 40 mL of hot dmf and mixed with a 40 mL solution that contains 90 mg (0.25 mmol) of $Co(ClO_4)_2 \cdot 6H_2O$. Very slow evaporation of the solvent gave reddish block-shaped crystals suitable for X-ray analysis (Yield 19 %). The repetition of this procedure produced the isomer **21a-tcg** in all following attempts, which was proved by X-ray powder diffraction pattern analysis.

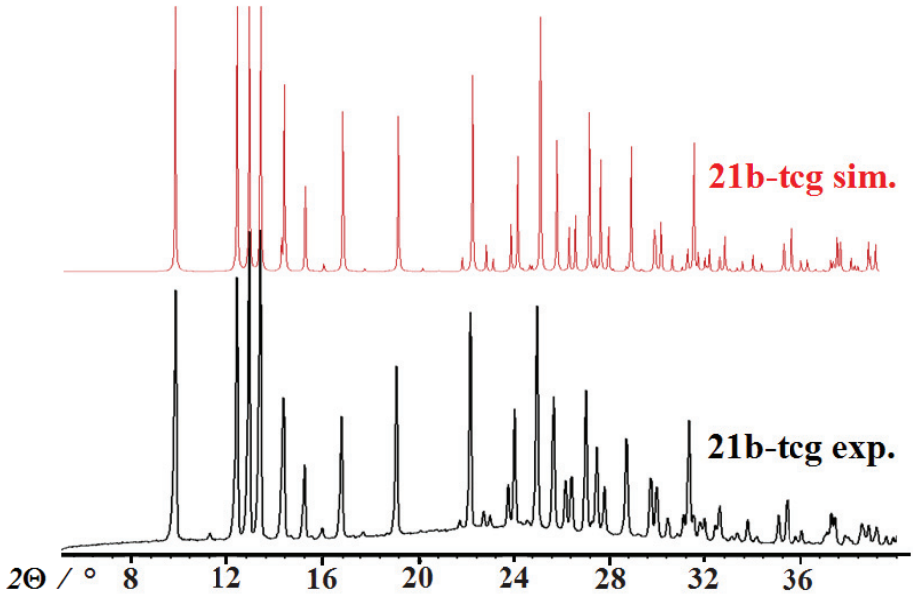

Figure 7.4.3 The simulated and experimental X-ray powder diffraction patterns of **21b-tcg** isolated as a pure phase (Co-Kα radiation).

Crystallization of *fac*-[Mn(tcg) (dmf)$_2$(H$_2$O)] (22tcg): 150 mg (0.76 mmol) of $Na_2(tcg) \cdot H_2O$ was completely dissolved in 40 mL of hot dmf and mixed with 15 mL solution that contains 277 mg (0.76 mmol) of $Mn(ClO_4)_2 \cdot 6H_2O$. Slow evaporation of the solvent gave colourless block-shaped crystals (yield 37 %).

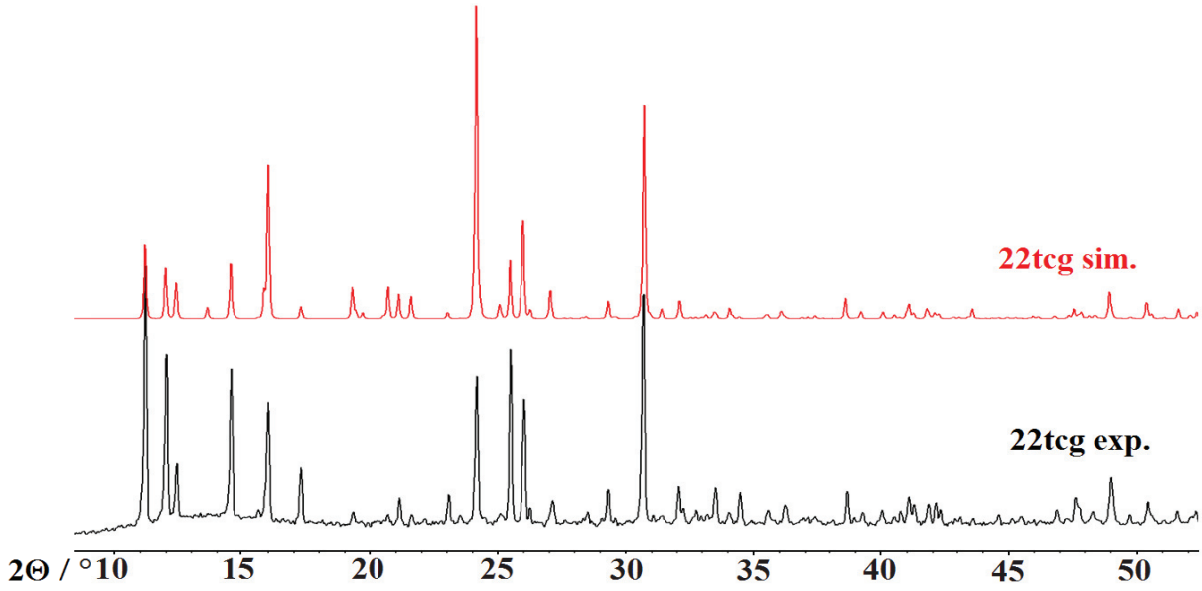

Figure 7.4.4 The simulated and experimental X-ray powder diffraction patterns of **22tcg** are shown (Co-Kα radiation).

References

[1] **(a)** P. J. Bailey, S. Pace, *Coord. Chem. Rev*. **2001**, *214*, 91; **(b)** C. Alonso-Moreno, A. Antinolo, F. Carrillo-Hermosilla, A. Otero, *Chem. Soc. Rev.* **2014**, *43*, 3406.

[2] M. P. Coles, Dalton Trans., **2006**, 985.

[3] S. J. Angyal, W. K. Warburton, *J. Chem. Soc.* **1951**, 2492.

[4] F. Saczewski, L. Balewski, *Expert. Opin. Ther. Patents* **2009**, *19*, 1417.

[5] **(a)** K. E. Besslera, A.T. de Sousaa, V. M. Deflona, E. Niquetb, *Z. Anorg. Allg. Chem.* **2003**, *629*, 1091; **(b)** A. S. Batsanov, P. Hubberstey, C. E. Russell, P. H. Walton, *J. Chem. Soc., Dalton Trans.* **1997**, 2667; **(c)** A. G. Tskhovrebov, N. A. Bokach, M. Haukka, V. Y. Kukushkin, *Inorg. Chem.* **2009**, *48*, 8678.

[6] **(a)** A. S. Batsanov, P. Hubberstey, C. E. Russell, P. H. Walton, *J. Chem. Soc., Dalton Trans.* **1997**, 2667; **(b)** K. E. Bessler, A. Torres de Sousa, V. M. Deflon, E. Niquet, *Z. Anorg. Allg. Chem.* **2003**, *629*, 1091; **(c)** L. Coghi, A. Mangia, N. Nardelli, G. Pelizzi, L. Sozzi, *Chem. Commun.* **1968**, 1475; **(d)** A. Chiesi-Villa, L. Coghi, A. Mangia, N. Nardelli, G. Pelizzi, *Acta Crystallogr., Sect. B*, **1971**, *27*, 192; **(e)** A. S. Batsanov, P. Hubberstey, C. E. Russell, *J. Chem. Soc.,Dalton Trans.* **1994**, 3189.

[7] R. P. Subrayan, A. H. Francis, J. W. Kampf, P. G. Rasmussen, *Chem. Mater.* **1995,** *7*, 2213.

[8] B. H .Ward, G. E. Granroth, J. B. Walden, K. A. Abboud, M. W. Meisel, *J. Mater. Chem.* **1998**, *8*, 1373.

[9] **(a)** A. Dworkin, R. Naumann, C. Seigfred, J. M. Karty, *J. Org. Chem.* **2005**, *70*, 7605; **(b)** A. Gobbi, G. Frenking, *J. Am. Chem. Soc.* **1993**, *115*, 2362.

[10] **(a)** A. Gobbi, G. Frenking, *J. Am. Chem. Soc.* **1993**, *115*, 2362; **(b)** K. B. Wiberg, *J. Am. Chem. Soc.* **1990**, *112*, 4177; **(c)** R. Caminiti, A. Pieretti, L. Bencivenni, F. Ramondo, N. Sanna, *J. Phys. Chem.* **1996**, *100*, 10928.

[11] K. Gopi, B. Rathi, N. Thirupathi, *J. Chem. Sci.* **2010**, *122*, 157.

[12]T. Yamada, X. Liu, U. Englert, H. Yamane, R. Dronskowski, *Chem. Eur. J.* **2009**, *15*, 5651.

[13] A. J. Blake, N. R. Brooks, N. R. Champness, M. Crew, A. Deveson, D. Fenske, D. H. Gregory, L. R. Hanton, P. Hubberstey, M. Schröder, *Chem. Commun.* **2001**, 1432.

[14] B. N. Figgis, M. A Hitchman, *Ligand Field Theory and Its Applications*, Wiley-VCH, **2000**

[15] A. B. P Lever, *Inorganic Electronic Spectroscopy*, ELESEVIER, 2nd Edition, Amsterdam, Oxford, New York, Tokyo **1984**.

[16] B. Scrosati, *Applications of Electroactive Polymers*, Springer Science & Business Media, **1993**.

[17] D. N. Sathyanarayana, *Electronic Absorption Spectroscopy and Related Techniques*, Universities Press, **2001**, p. 266.

[18] **(a)** E. Larsen, G. N. La Mar, *J. Chem. Ed. 51*, **1974**, 633; **(b)** C. K. Jørgensen, R. Pappalardo, H. H. Schmidtke, *J. Chem. Phys.* **1963**, *39*, 1422; **(c)** D. E. Richardson, *J. Chem. Educ.* **1993**, *70,* 372.

[19] R. Glaum, M. Hitchman, *Aust. J. Chem.* **1996**, *49*, 1221.

[20] M. Gerloch, *Cam. Univ. Press,* **1983**; D. A. Cruse, J. E. Davies, J. H. Harding, M. Gerloch, D. J. Mackey, R. F. McMeeking,„CAMMAG, a FORTRAN programm", Cambridge, 1980.

[21] I. E. Uflyand, A. G. Starikov, *Transition Met. Chem.* **1991**, *16*, 126.

[22] **(a)** T. R. Welberry, D. J. Goossens, *Acta Cryst.* 2008, *A64,* 23; **(b)** T. R. Welberry, A. P. Heerdegen, D. C. Goldstone, I. A. Taylor, *Acta Cryst.* **2011,** *B67,* 516; **(c)** O. Oeckler, T. Weber, L. Kienle, H. Mattausch, A. Simon .*Angew. Chem. Int. Ed.* **2005,** *44,* 3917*;* **(d)** T. Welberry, M. Paściak, *Metall. Mater. Trans. A* **2011**, *42, 6*; **(e)** T. R. Welberry, E. J. Chan, D. J. Goossens, A. P. Heerdegen, *Metall. Mater. Trans. A* **2012**, *43,* 1434; **(f)** T. Welberry, E. Chan, D. Goossens, A. Heerdegen, *Phase Transitions,* **2010,** *83,* 80;

[23] (a) H.Weber, B. Brgi, *Acta Cryst. A* **2002**, *58*, 526; (b) T. Proffen, T. R. Welberry, *Acta Cryst. A* **1997**, *53*, 202; (c) T. R. Welberry, T. Proffen, M. Bown, *Acta Cryst. A* **1998**, *54*, 661.

[24] T. R. Welberry *Acta Cryst. A* **2001**, *57*, 244.

[45] J. M. Cole, C. C Wilson, J. A. K. Howard, F. R. Cruickshank, *Acta Cryst. B* **2000**, 56, 1085.

[26] J. J. D'Amico , R.Henry Campbell, *J. Org. Chem.* **1967**, *32*, 2567.

[27] R. J. Timmons , L. S. Wittenbrook, *J. Org. Chem.* **1967**, *32*, 1566

Final Conclusions

This thesis provides the successful syntheses and crystal structure characterization four of six possible cyano-azolates, obtained as organic salts: PPh_4(ctz), $[Me_4N]$tcp, PPh_4(*cis*-dct) and $[NEt_4]$tci.

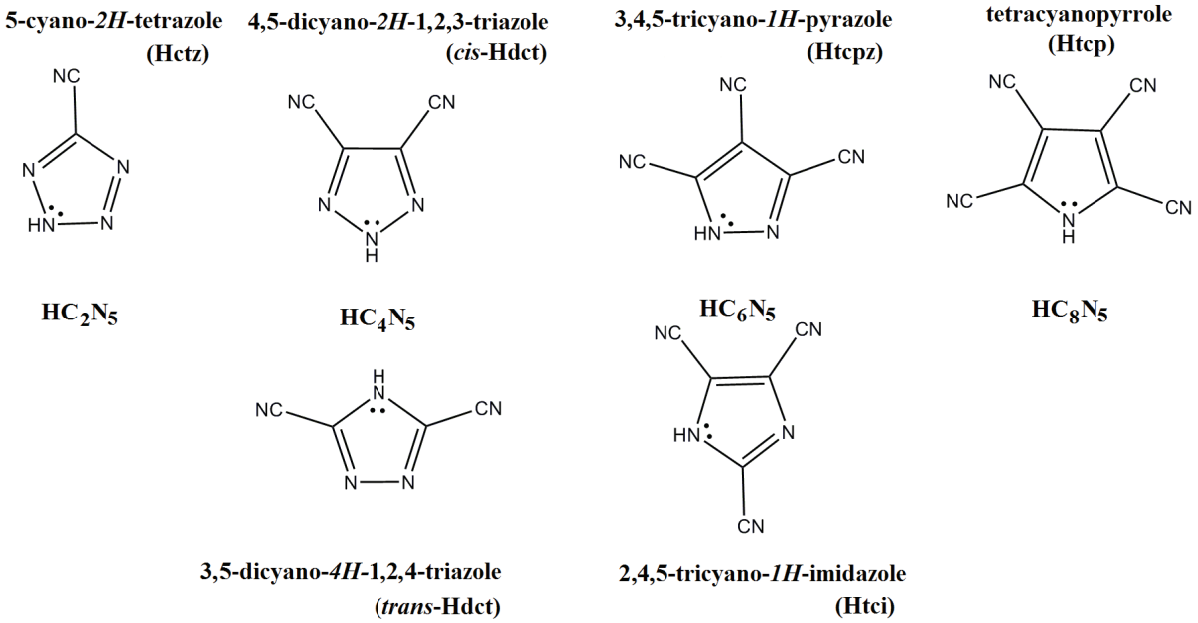

Structural formulae of the series of cyano-substituted neutral azoles. The conjugate bases are readily formed upon deprotonation.

5-Cyanotetrazole (HC_2N_5) is known to be readily formed from $(CN)_2$ and HN_3. The coordination abilities of the anion 5-cyanotetrazolate (ctz) towards Cu(II) ions were examined and a series of complexes and coordination polymers were synthesized and characterized by single-crystal structure analyses: $PPh_4[Cu(ctz)_3]$ (**1ctz**), $[Cu(ctz)_2(bipy)]$ (**2ctz**), $[CuCl(py)_4](ctz) \cdot 2py$ (**3ctz**), $[Cu_2(ctz)_6Cu(CH_3CN)_2(H_2O)_2] \cdot 2CH_3CN$ (**4a-ctz**), $[Cu_2(ctz)_6Cu(H_2O)_3\{(CH_3)_2CO\}] \cdot 3(CH_3)_2CO$ (**4b-ctz**), $[Cu(ctz)_2(py)_4]$ (**5ctz**), $[Cu_2(ctz)_4(bipy)_2]$ (**6ctz**), $[Cu_2(ctz)_2(tpm)_2(NO_3)]NO_3$ (**7ctz**). Only copper complexes of ctz were investigated, since the crystallization together with neutral co-ligands (py, bidentate 2,2′-bipy, and tridentate tpm) provided suitable single crystals for X-ray diffraction studies. Other transition metal complexes (Ni^{2+}, Co^{2+}, Fe^{2+}) of 5-cyanotetrazolate formed highly insoluble polycrystalline, intractable products, which limited their structural characterization within the scope of this thesis. The structures of compounds **1ctz**-**7ctz** reflect the versatile coordination abilities of ctz by the various types of coordination environments of the Cu(II) ions and dimensionalities of linking. The structures represent 1D chain motifs (**1ctz, 2ctz, 3ctz**), 2D layered structures (**4a-ctz**, **4b-ctz**), mononuclear (**5ctz**) and dinuclear complexes

(**6ctz, 7ctz**). Magnetic coupling phenomena were detected by susceptibility measurements of **1ctz**, **4a-ctz**, **6ctz** and **7ctz**, which were fitted to the magnetic models according to antiferromagnetic spin-pairing of two S = 1/2 systems (Bleaney-Bowers) for **6ctz** (J = –0.53 cm^{-1}) and **7ctz** (J = −2.91 cm^{-1}), to the ferromagnetic high-temperature series expansion based on the Baker 1D (S = 1/2) chain model for **1ctz** (J = +6.5 cm^{-1}) and to the Néel model of ferrimagnetism for **4a-ctz**. The diverse magnetic interactions between the Cu^{2+} sites are communicated by the bridging ctz anions.

Two isotypic mononuclear discrete complexes $[Co(MeCN)_4(tcp)_2]\cdot 2MeCN$ (**13tcp**) and $[Ni(MeCN)_4(tcp)_2]\cdot 2MeCN$ (**14tcp**) containing the **tetracyanopyrrolide anion** $(C_8N_5)^-$ were synthesized from [Me4N]tcp and the respective metal perchlorates in acetone/acetonitrile. Tcp coordinates to the transition metal atoms in η^1-N-σ fashion via the nitrogen atom of the pyrrole ring. No coordination via the cyano groups is observed for these complexes. This other possible coordination mode, via the N atoms of the CN substituents, is observed only in the crystal structure of $[Na(tcp)H_2O] \cdot H_2O$ **(11tcp**) so far. Magnetic investigations reveal that both transition metal complexes show nearly ideal paramagnetic behavior according to the Curie law with magnetic moments of 4.98 μ_B for **13tcp** and 3.09 μ_B for **14tcp** at 300 K. It was also possible to crystallize the mononuclear complex $[Fe(tpm)_2](tcp)_2$ (**15tcp**), in which each metal centre is enclosed by two „scorpionate" tris(pyrazol-*1*-yl)methane ligands to form the $[Fe(tpm)_2]^{2+}$ cation, charge-balanced by the mononegative tcp counter ions. The structural investigations on this complex at 123 K reveal Fe−N distances typical for low-spin d^6 iron(II). In the examined temperature range 1.9–400 K **15tcp** undergoes a gradual, incomplete spin crossover.
Unsuccessful attempts were undertaken to crystallize other transition metal complexes of thetcp anion (Mn^{2+}, Co^{2+} and Ni^{2+}). Various methods like precipitating organic perchlorates, adding neutral co-ligands (py, 2,2´-bipy, tpm) or using various of crystallization techniques (especially vapor diffusion) were tested. The desired complexes tend to oil out on removal of the solvent even when crystallized at low temperatures (–15 °C).

In the presence of water, the cyano groups of cyanotetrazolate and cyanopyrrolides undergo hydrolytic transformation forming the $C(O)NH_2$ carboxamide. Tetrazolate-5-carboxamide and 3,4,5-tricyanopyrrole-2-carboxamide trapped as copper(II) complexes, were accidentally obtained and model for the catalytical role of Cu(II) has been set up.

The ***N,N´,N´´*-tricyanoguanidinate** dianion (tcg) $(C_4N_6)^{2-}$ was successfully used in construction of 2D and 3D coordination polymers incorporating Cu^{2+}, Co^{2+} and Mn^{2+} paramagnetic centres.

***N,N′,N″*-tricyanoguanidinate (tcg)**

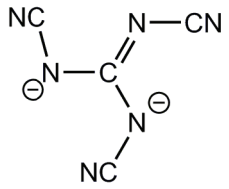

$(C_4N_6)^{2-}$

Structural formula of the tcg anion

In five complexes, namely *mer*-[Cu(tcg)(py)$_3$]· py **(20tcg)**, two topological isomers *fac*-[Co(tcg)(dmf)$_2$(H$_2$O)] **(21a-tcg)** and **(21b-tcg)**, *fac*-[Mn(tcg)(dmf)$_2$(H$_2$O)] **(22tcg)** and [Co(tcg)(dmf)$_4$Co(tcg)] · 3dmf **(23tcg)** the tcg anion acts as 3-connected linker adopting C_{3h} symmetry. Magnetic susceptibility measurements between 1.9 and 300 K were analysed with physical models according to antiferromagnetic spin-pairing of two S=5/2 systems (Van Vleck Model) for **22tcg** (J = −0.12 cm^{-1}), to the Néel model of ferrimagnetism for **21a-tcg** and to the Curie-Weiss law for **20tcg.** The results indicate that the tcg dianion provides only a weak ferromagnetic spin coupling via the *[-NCNCNCN-]* bridge in the **21a-tcg** complex, while antiferromagnetic exchange is mediated through H-bonds of adjacent layers in **22tcg**. The room temperature effective moments of the examined complexes indicate the presence of the high-spin form complexes with tcg acting as a weak-field ligand. Other transition metal complexes (Fe^{2+} or Ni^{2+}) with tcg anion were obtained only as very small and highly insoluble crystals, which limited their structural characterization within the scope of these studies.

In general conclusion, so far 16 coordination complexes and networks with cyano-substituted azolates and 5 coordination polymers based on *N,N´,N´´*-tricyanoguanidinate dianion were synthesized and structurally characterized, demonstrating a large diversity of coordination modes and the general σ-N donor nature of the used ligands. In 11 cases magnetic investigations were undertaken, providing a large variety of cooperative magnetic effects. The schematic spin coupling models proposed in this thesis are only suggestions based on the magnetic parameters such as the exchange energy coupling constant J and the Curie-Weiss temperature θ and invite for confirmation by neutron diffraction experiments.

APPENDIX

APPENDIX A: USED CHEMICALS AND PURIFICATION

All chemicals were obtained commercially and were used as received without further purification from main suppliers: Sigma-Aldrich, Fluka, Alfa Aesar and Merck with purity 97–99 %. $Fe(ClO_4)_2 \cdot 6\ H_2O$ was dried *in vacuo* at 50 °C for about 5 hours. Acetone was dried over 3 Å molecular sieves. $Co(ClO_4)_2 \cdot 6H_2O$ and $Ni(ClO_4)_2 \cdot 6H_2O$ were dried under reduced pressure at 50 °C for about 5 h. Acetonitrile and acetone were stirred overnight with dry K_2CO_3 and then distilled.

List of reagents used in the work:

Name	Formula	Molecular weight / gmol^{-1}
pyrazole	$C_3H_3N_2H$	68.08
sodium carbonate	Na_2CO_3	105.98
tetra-*n*-butylammonium bromide	$C_{16}H_{36}BrN$	322.36
tetramethylammonium chloride	$C_4H_{12}NCl$	109.60
potasium carbonate	K_2CO_3	138.20
sodium sulfate	Na_2SO_4	142.04
activated charcoal	C	12
sodium azide	NaN_3	65.01
sodium cyanide	NaCN	49.01
copper (I) cyanide	CuCN	89.563
copper(II) sulfate	$CuSO_4$	159.60
tetraphenylphosphonium chloride	PPh_4Cl	374.84
cyanamide	CH_2N_2	42.04
disodium cyanamide	CN_2Na_2	86.00
N.N-dimethylacetamide	$CH_3CN(CH_3)_2$	87.12
potassium hydroxide	KOH	56.10
methyl iodide	CH_3I	141.94
ethyl acetate	$C_4H_8O_2$	88.11
copper (II) nitrate trihydrate	$CuNO_3 \cdot 3H_2O$	241.60
2,2′-bipyridine	$C_{10}H_8N_2$	156.18
acetic acid	CH_3COOH	60.05
cobalt (II) perchlorate hexahydrate	$Co(ClO_4)_2 \cdot 6\ H_2O$	365.92
nickel (II) perchlorate hexahydrate	$Ni(ClO_4)_2 \cdot 6\ H_2O$	365.68
iron (II) perchlorate hexahydrate	$Fe(ClO_4)_2 \cdot 6\ H_2O$	362.83
manganese (II) perchlorate hexahydrate	$Mn(ClO_4)_2 \cdot 6\ H_2O$	361.93
copper (II) perchlorate hexahydrate	$Cu(ClO_4)_2 \cdot 6\ H_2O$	370.53
carbon disulfide	CS_2	76.14
ammonium peroxodisulphate	$(NH_4)_2S_2O_8$	228.20
copper(II) chloride	$CuCl_2 \cdot 2H_2O$	170.48
diaminomaleodinitrile	$NCC(NH_2)=C(NH_2)CN$	108.10
sodium nitrite	$NaNO_2$	68.99
2-amino-4,5-imidazoledicarbonitrile	$C_5H_3N_5$	133.11
hydrochloric acid	HCl	36.46
chloroform	$CHCl_3$	119.38
pyridine	C_5H_5N	79.10
ethanol	EtOH	46.07

acetonitrile	CH_3CN	41.05
diethyl ether	$(C_2H_5)_2O$	74.12
dimethylformamide	C_3H_7NO	73.09
n-butanol	$C_4H_{10}O$	74.12
dichloromethane	CH_2Cl_2	84.93

APPENDIX B: EXPERIMENTAL METHODS[5]

Single-crystal X-ray Diffraction (XRD)

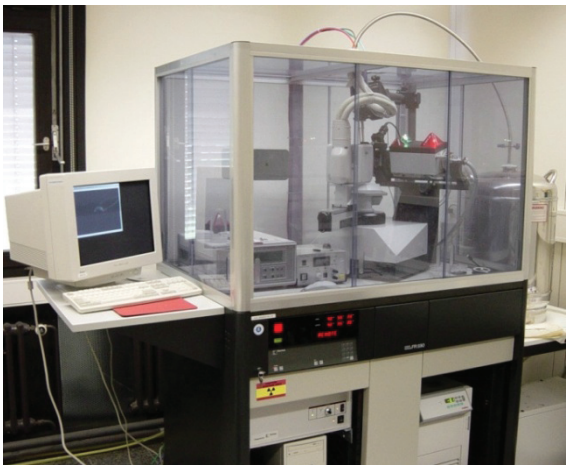

Single crystals were examined using a Bruker-Nonius kappa-CCD four circle diffractometer equipped with graphite monochromatized Mo-Kα radiation (λ = 0.71073 Å). Data collection was performed at -150 °C (123 K) using an external Oxford Cryosystems 600 Series cooling device.

The crystals were selected immersed in perfluorinated oil and transferred in this medium into the cold nitrogen stream of the crystal cooling device. The crystal structures were solved by Direct Methods and refined using the SHELX97 program suite [G. M. Sheldrick, SHELX2013 (includes SHELXS 2013,SHELXL2013, CIFTAB) – Programs for Crystal Structure Analysis (release 2013), University of Göttingen, Germany, 2013; Programs for Crystal Structure Analysis, University of Göttingen, Germany, **1998**]. Analytical absorption corrections were applied to all data sets [**N**. W. Alcock, *Cryst. Computing* **1977**, 271]. Hydrogen atoms were refined in idealized positions as riding on their attached carbon atoms with isotropic displacement factors fixed to the value 1.5 of the respective carbon atoms or found from the electron density map. Graphical representations were made using the program DIAMOND [*DIAMOND*, Program for Crystal Structure Visualisation, Crystal Impact Corp., Bonn, Germany, **2005**].

[5] The photos of presented instruments were taken from: http://anorganik.chemie.unibonn.de/akbkhome/

Powder X-ray Diffraction (PXRD)

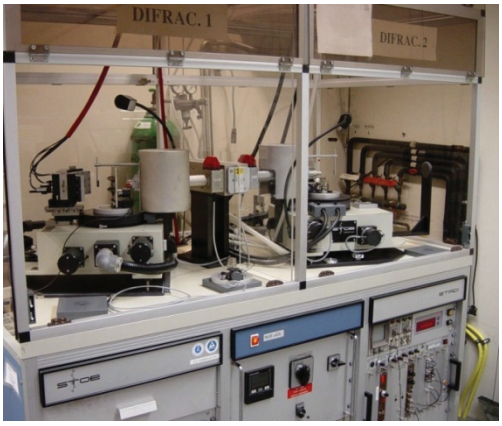

X-ray Powder diffraction patterns were recorded at room temperature using a STOE Stadi P diffractometer equipped with Co-Kα radiation and a position sensitive detector. Simulated powder patterns were based on single-crystal data and calculated using the STOE Win XPOW software package or using the PLATON program.

Magnetic Measurements

The magnetic susceptibility measurements were performed with a Quantum Design PPMS vibrating sample magnetometer (VSM) in the usual temperature range 1.9–300 K, an applied magnetic field of 20 kOe for **1ctz**, **4a-ctz**, **7ctz** and a magnetic field of 10 kOe was used for **6ctz**, **13tcp**, **14tcp**, **15tcp** (temperature range for 1.9–400 K), **20tcg**, **21a-tcg**, **21b-tcg**, **22tcg**. Samples of weights between 1.5 and 12 mg were used.

Thermoanalytical measurements

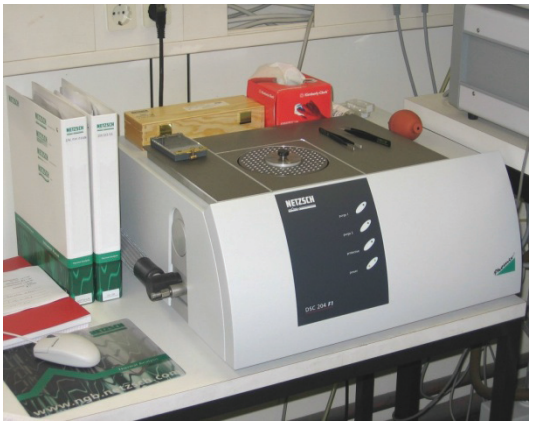

DSC measurements were perfomed using a DSC 204 Phoenix instrument (Netzsch Inc.).

TG-DTA analyses were performed using a thermoanalyzer STA 429 (Netzsch) under argon atmosphere.

NMR Spektroscopy

^{1}H and ^{13}C NMR spectra were recorded using 300 MHz multi nuclei NMR. Samples were dissolved in deuterated solvents.

IR spectroscopy

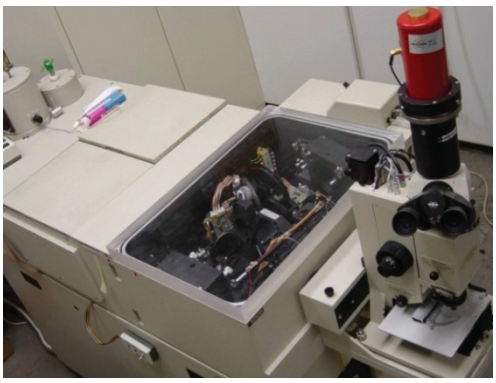

FT–IR spectra were detected from KBr disks (Aldrich, 99%+, FT–IR grade) and measured on Bruker IFS 113v spectrometer.

Elemental analysis

Elemental analysis for C, H and N was measured using a CHNS-932 Elemental Analyser and performed in the Microanalysis Laboratory at the Department of Organic Chemistry, University of Bonn.

Single crystal UV/Vis/NIR Spectroscopy

Single crystal UV/Vis/NIR spectra were recorded at ambient temperature by modified CARY 17 microcrystal spectrophotometer (spectral service, ANU Canberra, Australia). The CARY 17 enables to measure the whole spectrum (5800–36000 cm^{-1}) of single crystal with dimension down to 0.1 mm edge length using a halogen lamp as light source. From 280 to 900 nm (Vis region) the intensity data was recorded by a PMT detector system with slit width of 0.08 mm, respectively whereas from 600 to 1700 nm (NIR region). Ge semiconductor detector cooled with liquid nitrogen was used to record the intensity data with the same slit width. In Vis and NIR region the step widths were 1 and 2 nm respectively which corresponds to 621 and 550 data points are collected, accordingly.

APPENDIX C: CRYSTALLOGRAPHIC DATA

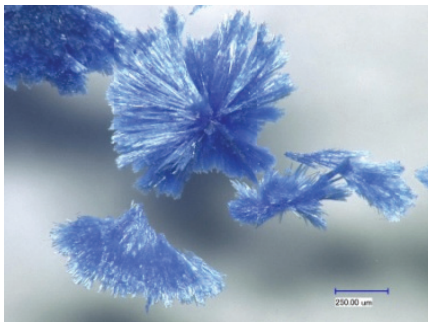

	$PPh_4[Cu(ctz)_3]$ (1ctz)	**$[Cu(ctz)_2(bipy)]$ (2ctz)**
Formula	$C_{30}H_{20}CuN_{15}P$	$C_{14}H_8CuN_{12}$
***Mr* / g·mol^{-1}**	685.12	407.86
Crystal system	monoclinic	monoclinic
Space group	$P2_1/c$	$P2_1/c$
***a* / Å**	7.5389(3)	13.0387(8)
***b* / Å**	15.0865(6)	8.6569(3)
***c* /Å**	27.3257(9)	17.6482(8)
α / °	90	90
β / °	93.637(2)	126.492
γ / °	90	90
***V* / Å^3**	3101.6(2)	1601.48(13)
D_{calc} / mg·m^{-3}	1.467	1.692
Z	4	4
μ / mm^{-1}	0.81	1.39
crystal size / mm	0.23 × 0.04 × 0.03	0.33 × 0.30 × 0.03, 0.15 (radius)
Measured refl.	20135	13251
Independent refl.	5633	3643
Data averaging R_{int}	0.123	0.075
Refined parameters	428	245
R [$F^2 > 2\sigma(F^2)$]	0.055	0.045
R(F^2) all refl.	0.106	0.090
***wR*(F^2)**	0.122	0.098
goodness of fit, S	1.05	1.05
$\Delta\varrho_{max}$/ $\Delta\varrho_{min}$ e· Å^{-3}	0.39 / −0.44	0.39 / −0.48
Flack Parameter	–	–

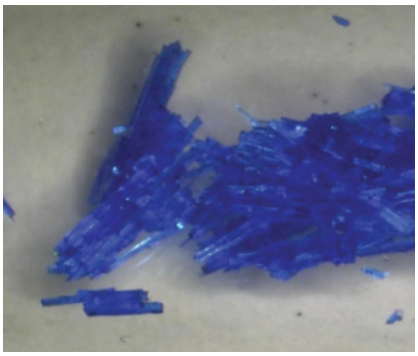

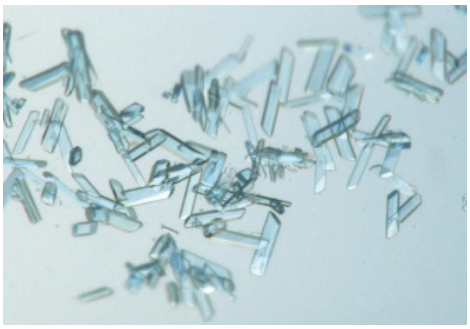

	[CuCl(py)$_4$](ctz) · 2py (3ctz)	[Cu$_2$(ctz)$_6$Cu(CH$_3$CN)$_2$(H$_2$O)$_2$] · 2CH$_3$CN (4a-ctz)
Formula	$C_{32}H_{20}ClCuN_{30}$	$C_{20}H_{16}Cu_3N_{34}O_2$
***Mr* / g·mol^{-1}**	667.66	955.29
Crystal system	monoclinic	triclinic
Space group	*Cc*	$P\bar{1}$
***a* / Å**	19.318(1)	7.6953(3)
***b* / Å**	16.550(1)	11.0073(5)
***c* /Å**	11.436(1)	11.7836(6)
α / °	90	102.715(2)
β / °	119.503(1)	100.109(3)
γ / °	90	95.054(3)
***V* / Å^3**	3182.1(4)	950.15(7)
***D$_{calc}$* / mg·m^{-3}**	1.394	1.670
Z	4	1
***μ* / mm^{-1}**	0.81	1.74
crystal size / mm	0.26 × 0.13 × 0.12	0.14 × 0.10 × 0.03, 0.07 (radius)
Measured refl.	64413	30883
Independent refl.	9279	4359
Data averaging R$_{int}$	0.113	0.107
Refined parameters	406	280
R [$F^2 > 2\sigma(F^2)$]	0.028	0.044
R(F^2) all refl.	0.034	0.087
***wR*(F^2)**	0.066	0.089
goodness of fit, S	1.04	1.05
Δϱ$_{max}$/ Δϱ$_{min}$ e· Å^{-3}	0.28 / −0.56	1.08 / −0.50
Flack Parameter	−0.001 (5)	

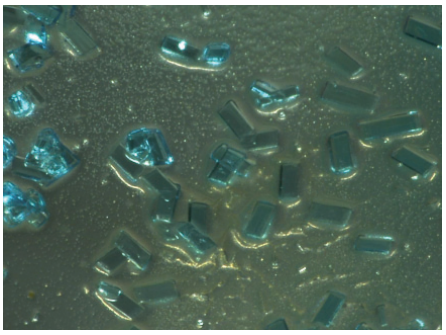

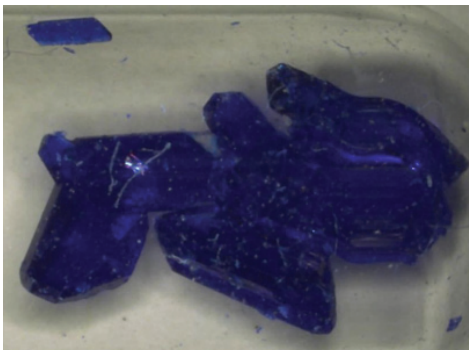

	$[Cu_2(ctz)_6Cu(H_2O)_3\{(CH_3)_2CO\}] \cdot 3(CH_3)_2CO$ (4b-ctz)	$[Cu(ctz)_2(py)_4]$ (5ctz)
Formula	$C_{24}H_{30}Cu_3N_{30}O_7$	$C_{24}H_{20}CuN_{14}$
***Mr* / g·mol^{-1}**	1041.40	568.08
Crystal system	triclinic	triclinic
Space group	$P\bar{1}$	$P\bar{1}$
***a* / Å**	12.918(1)	9.2140(1)
***b* / Å**	13.452(1)	9.7424(2)
***c* /Å**	14.518(1)	14.8033(3)
α / °	112.180(1)	106.9547(8)
β / °	115.315(1)	93.4679(11)
γ / °	92.626(1)	91.3533(10)
***V* / Å^3**	2046.1(3)	1267.57(4)
***D*$_{calc}$ / mg·m^{-3}**	1.690	1.488
Z	2	2
μ / mm^{-1}	1.63	0.91
crystal size / mm	0.13 × 0.10 × 0.06	0.25 × 0.22 × 0.02
Measured refl.	72841	38444
Independent refl.	11966	5816
Data averaging R$_{int}$	0.059	0.040
Refined parameters	606	352
R [$F^2 > 2\sigma(F^2)$]	0.035	0.032
R(F^2) all refl.	0.053	0.042
***wR*(F^2)**	0.087	0.073
goodness of fit, S	1.01	1.03
$\Delta\varrho_{max}$/ $\Delta\varrho_{min}$ e· Å^{-3}	0.71 / -0.81	0.30 / -0.46
Flack Parameter		

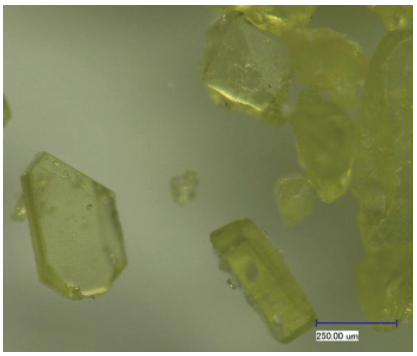

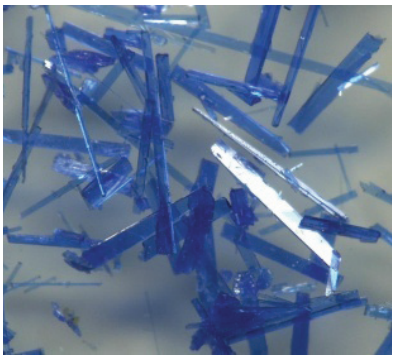

	[Mn(ctz)$_2$(bipy)$_2$] (5a-ctz)	[Cu$_2$(ctz)$_4$(bipy)$_2$] (6ctz)
Formula	$C_{24}H_{20}MnN_{14}$	$C_{28}H_{16}Cu_2N_{24}$
***Mr* / g·mol^{-1}**	555.45	815.73
Crystal system	Monoclinic	triclinic
Space group	$P2_1/c$	$P\bar{1}$
***a* / Å**	9.5023(2)	7.6353(3)
***b* / Å**	14.3992(3)	10.5980(6)
***c* /Å**	18.3220(4)	21.0646(10)
α / °	90	99.683(2)
β / °	103.693(1)	98.429(3)
γ / °	90	100.126(3)
***V* / Å^3**	2435.67(9)	1626.59(14)
***D$_{calc}$* / mg·m^{-3}**	1.515	1.666
Z	4	2
μ / mm^{-1}	0.59	1.37
crystal size / mm	0.23 × 0.21 × 0.10	0.19 × 0.10 × 0.04
Measured refl.	73574	33258
Independent refl.	7098	7155
Data averaging R$_{int}$	0.073	0.093
Refined parameters	416	487
R [$F^2 > 2\sigma(F^2)$]	0.038	0.066
R(F^2) all refl.	0.0681	0.135
***wR*(F^2)**	0.0883	0.160
goodness of fit, S	1.02	1.05
$\Delta\varrho_{max}$/ $\Delta\varrho_{min}$ e· Å^{-3}	0.32 /–0.44	1.80 / –0.58
Flack Parameter	–	–

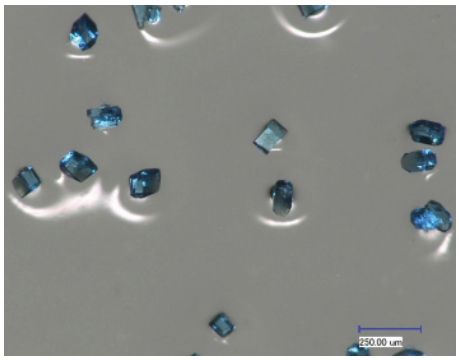

	$[Cu_2(ctz)_2(tpm)_2(NO_3)]NO_3$ (7ctz)	$[Cu(tca)_2(bipy)] \cdot H_2O$ (8tca)
Formula	$C_{24}H_{20}Cu_2N_{24}O_6$	$C_{10}H_{12}CuN_{10}$
***Mr* / g·mol^{-1}**	867.72	921.07
Crystal system	orthorhombic	triclinic
Space group	*Pmmn*	$P\bar{1}$
***a* / Å**	12.9376(2)	8.6520(17)
***b* / Å**	16.9821(2)	10.493(2)
***c* /Å**	7.3954(1)	11.914(2)
α / °	90	63.96(3)
β / °	90	79.35(3)
γ / °	90	73.79(3)
***V* / Å^3**	1624.83(4)	930.8(4)
D_{calc} / mg·m^{-3}	1.806	1.643
Z	2	1
μ / mm^{-1}	1.39	1.22
crystal size / mm	0.20 × 0.17 × 0.10, 0.07 (radius)	0.21 × 0.13 × 0.11
Measured refl.	47046	33824
Independent refl.	2011	4291
Data averaging R_{int}	0.034	0.054
Refined parameters	147	339
R [$F^2 > 2\sigma(F^2)$]	0.034	0.033
R(F^2) all refl.	0.047	0.0387
***wR*(F^2)**	0.131	0.082
goodness of fit, S	1.06	1.00
$\Delta\varrho_{max}$/ $\Delta\varrho_{min}$ e· Å^{-3}	2.30 / –1.59	0.51/ –0.68
Flack Parameter	–	–

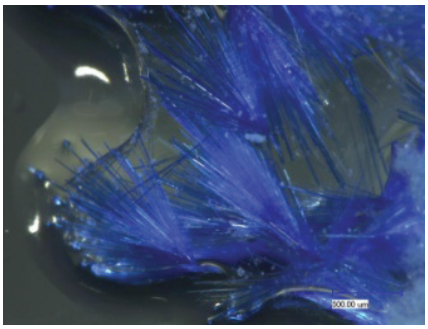

	[Cu(ctz)(tca)(bipy)]$_{0.5}$[Cu(ctz)$_2$(bipy)]$_{0.5}$ 8a-tca	Cu(tca)$_2$ · 2H$_2$O (9tca)
Formula	$C_{28}H_{16}Cu_2N_{24}O$	$C_4CuN_{10}O_3H_4$
***Mr* / g·mol^{-1}**	831.73	623.42
Crystal system	triclinic	orthorhombic
Space group	$P\bar{1}$	*Iba*2
***a* / Å**	8.0561(11)	8.2588(2)
***b* / Å**	10.5883(11)	16.0521(5)
***c* /Å**	10.7370(14)	17.2156(5)
α / °	94.192(7)	90
β / °	99.761(7)	90
γ / °	111.756(7)	90
***V* / Å^3**	829.02(18)	2282.29(11)
***D$_{calc}$* / mg·m^{-3}**	1.666	1.814
Z	*1*	4
μ / mm^{-1}	1.35	1.94
crystal size / mm	0.41 × 0.11 × 0.09	0.52 × 0.06 × 0.03
Measured refl.	6560	16981
Independent refl.	2188	2617
Data averaging R$_{int}$	0.134	0.068
Refined parameters	297	167
R [$F^2 > 2\sigma(F^2)$]	0.052	0.043
R(F^2) all refl.	0.0886	0.100
***wR*(F^2)**	0.105	0.130
goodness of fit, S	1.15	1.09
Δϱ$_{max}$/ Δϱ$_{min}$ e· Å^{-3}	0.32/ −0.39	0.58/ −0.55
Flack Parameter	–	0.060 (14)

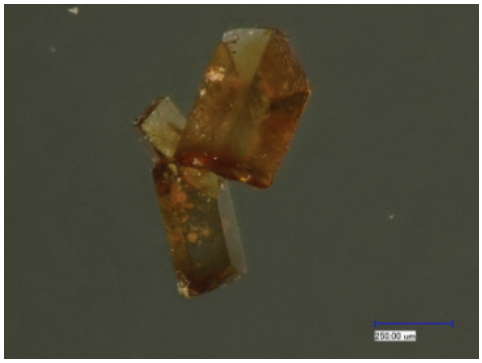

	Htcp (10tcp)	[Na(tcp)H$_2$O] · H$_2$O (11tcp)
Formula	C_8HN_5	$C_{12}H_{12}N_6$
***Mr* / g·mol^{-1}**	1.328	225.15
Crystal system	orthorhombic	monoclinic
Space group	*Pna*2$_1$	*C*2/*c*
***a* / Å**	11.398(2)	31.859(3)
***b* / Å**	7.5864(15)	3.7429(2)
***c* /Å**	9.6680(19)	23.3758(19)
α / °	90	90
β / °	90	129.552(2)
γ / °	90	90
***V* / Å^3**	836.0(3)	2149.2(3)
***D$_{calc}$* / mg·m^{-3}**	1.328	1.392
Z	4	8
μ / mm^{-1}	1.19	0.14
crystal size / mm	0.31 × 0.21 × 0.99	0.42 × 0.09 × 0.06
Measured refl.	4859	7161
Independent refl.	2150	2450
Data averaging R$_{int}$	0.028	0.056
Refined parameters	122	158
R [$F^2 > 2\sigma(F^2)$]	0.030	0.051
R(F^2) all refl.	0.0362	0.10
***wR*(F^2)**	0.062	0.138
goodness of fit, S	1.00	1.07
Δϱ$_{max}$/ Δϱ$_{min}$ e· Å^{-3}	0.14/ −0.17	0.21/ −0.28
Flack Parameter	0 (2) Refined as an inversion twin.)	–

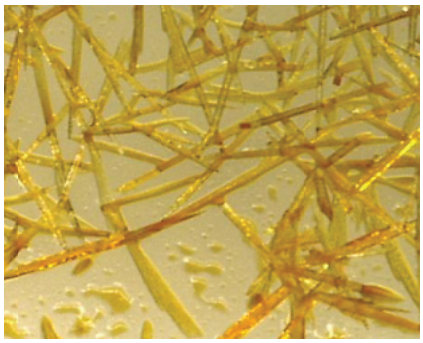

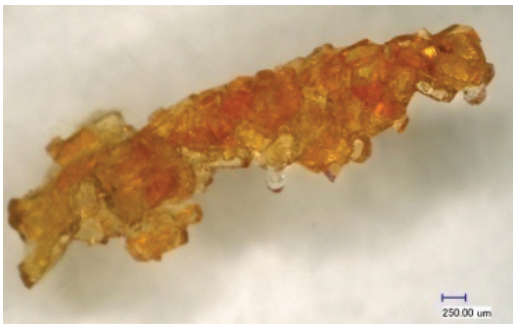

	$Me_4N(tcp)$ (12tcp)	**$[Co(MeCN)_4(tcp)_2] \cdot 2\ MeCN$ (13tcp)**
Formula	$C_{15}H_{18}N_6O$	$C_{24}H_{12}CoN_{14}\cdot 2(C_2H_3N)$
***Mr* / g·mol^{-1}**	240.28	637.51
Crystal system	orthorhombic	triclinic
Space group	*Cmca*	$P\bar{1}$
***a* / Å**	6.8107(2)	7.8693(2)
***b* / Å**	21.4694(10)	9.9411(3)
***c* /Å**	19.7556(9)	10.4822(3)
α / °	90	96.171(2)
β / °	90	102.334(2)
γ / °	90	90.110(1)
***V* / Å^3**	2888.7(2)	796.19(4)
***D_{calc}* / mg·m^{-3}**	1.105	1.330
Z	8	1
***μ* / mm^{-1}**	0.07	0.59
crystal size / mm	0.45 × 0.72 × 0.32 mm	0.13 × 0.10 × 0.10
Measured refl.	26211	27031
Independent refl.	1313	3664
Data averaging R_{int}	0.107	0.071
Refined parameters	110	208
R [$F^2 > 2\sigma(F^2)$]	0.117	0.037
R(F^2) all refl.	0.2258	0.0551
***wR*(F^2)**	0.410	0.077
goodness of fit, S	1.29	1.06
$\Delta\varrho_{max}$/ $\Delta\varrho_{min}$ e· Å^{-3}	0.48, −0.19	0.27, −0.52
Flack Parameter	–	–

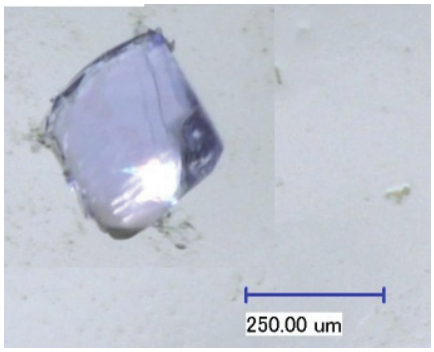

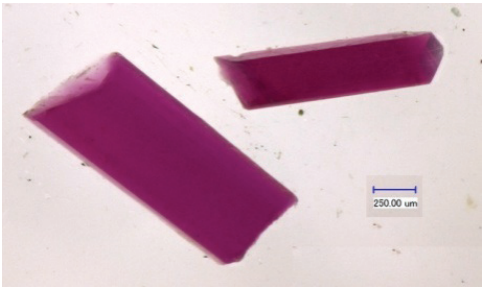

	[Ni(MeCN)$_4$(tcp)$_2$] · 2 MeCN (14tcp)	**[Fe(tpm)$_2$](tcp)$_2$ (15tcp)**
Formula	$C_{24}H_{12}N_{14}Ni{\cdot}2(C_2H_3N)$	$C_{20}H_{20}FeN_{12}{\cdot}2(C_8N_5)$
***Mr* / g·mol^{-1}**	637.29	816.59
Crystal system	triclinic	triclinic
Space group	$P\bar{1}$	$P\bar{1}$
***a* / Å**	7.8384(1)	9.2671(2)
***b* / Å**	9.9108(1)	11.7990(2)
***c* /Å**	10.4508(1)	18.6007(3)
α / °	83.9247(7)	92.440(1)
β / °	77.8296(7)	96.224(1)
γ / °	89.8964(6)	112.679(1)
***V* / Å^3**	788.99(2)	1857.62(6)
***D$_{calc}$* / mg·m^{-3}**	1.341	1.46
Z	*1*	2
μ / mm^{-1}	0.66	0.47
crystal size / mm	0.16 × 0.11 × 0.09	0.40 × 0.14 × 0.10
Measured refl.	29462	9052
Independent refl.	4614	9052
Data averaging R$_{int}$	0.039	0.0991
Refined parameters	208	536
R [$F^2 > 2\sigma(F^2)$]	0.030	0.050
R(F^2) all refl.	0.0365	0.106
***wR*(F^2)**	0.073	0.099
goodness of fit, S	1.05	1.09
Δϱ$_{max}$/ Δϱ$_{min}$ e· Å^{-3}	0.34, −0.59	0.394/−0.495
Flack Parameter	–	–

	$[Cu(tcpc)_2(H_2O)_2] \cdot H_2O$ (16tcpc)	**$[Cu(tcpc)_2(dmf)_2]$ (17tcpc)**
Formula	$C_{16}H_8CuN_{10}O_4 \cdot H_2O$	$C_{22}H_{18}CuN_{12}O_4$
Mr / g·mol^{-1}	503.9	578.02
Crystal system	monoclinic	triclinic
Space group	$P2_1/c$	$P\bar{1}$
a / Å	9.2488(3)	6.4860(3)
b / Å	13.9242(6)	9.9804(5)
c /Å	7.8802(3)	10.5548(6)
α / °	90	109.265(2)
β / °	98.363(2)	94.697(4)
γ / °	90	101.619(4)
V / Å^3	1004.04(7)	623.58(6)
D_{calc} / mg·m^{-3}	1.667	1.539
Z	2	1
μ / mm^{-1}	1.15	0.93
crystal size / mm	0.44 × 0.12 × 0.01	0.16 × 0.07 × 0.04
Measured refl.	23314	8797
Independent refl.	2302	2672
Data averaging R_{int}	0.162	0.075
Refined parameters	170	180
R [$F^2 > 2\sigma(F^2)$]	0.054	0.044
R(F^2) all refl.	0.098	0.0666
wR(F^2)	0.126	0.097
goodness of fit, S	1.03	1.04
$\Delta\varrho_{max}$/ $\Delta\varrho_{min}$ e· Å^{-3}	0.97, −0.54	0.46, −0.72
Flack Parameter	–	–

	Et_4N(tci) (18tci)	PPh_4(*cis*-dct) (19*cis*-dct)
Formula	$C_{14}H_{20}N_6$	$C_{32}H_{20}N_5P$
Mr / g·mol^{-1}	272.36	M_r = 457.46
Crystal system	monoclinic	orthorhombic
Space group	*C*2/*m*	*Pccb*
a / Å	21.6913(5)	7.2210(2)
b / Å	8.9289(3)	17.1037(4)
c /Å	7.9689(2)	18.8986(5)
α / °	90	2334.09(10)
β / °	102.900(2)	90
γ / °	90	90
V / Å^3	1504.46(7)	90
D_{calc} / mg·m^{-3}	1.202	1.302
Z	4	4
μ / mm^{-1}	0.08	0.14
crystal size / mm	0.28 × 0.26 × 0.08	0.17 × 0.32 × 0.29
Measured refl.	7604	68057
Independent refl.	1736	5115
Data averaging R_{int}	0.033	0.097
Refined parameters	153	156
R [$F^2 > 2\sigma(F^2)$]	0.051	0.042
R(F^2) all refl.	0.0605	0.0581
wR(F^2)	0.153	0.117
goodness of fit, S	1.08	1.07
$\Delta\varrho_{max}$/ $\Delta\varrho_{min}$ e· Å^{-3}	0.43 / −0.36	0.36 / −0.37
Flack Parameter	–	–

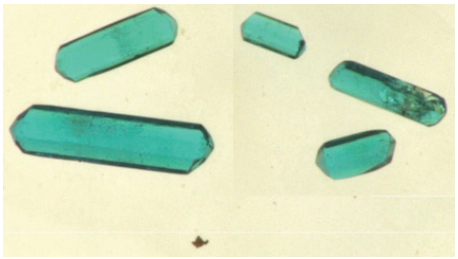

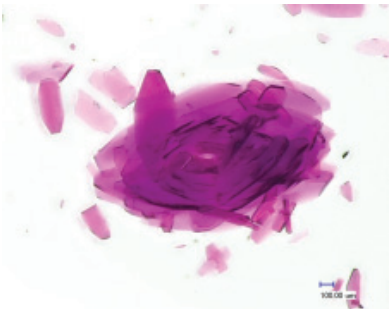

	mer-[Cu(tcg)(py)$_3$] · py (20tcg)	*fac*-[Co(tcg)(dmf)$_2$(H$_2$O)] (21a-tcg)
Formula	$C_{19}CuN_9H_5$	$C_{10}CoN_8O_3H_{16}$
Mr / g·mol^{-1}	512.04	355.24
Crystal system	orthorhombic	orthorhombic
Space group	$P2_12_12_1$	*Pbca*
a / Å	8.7498(17)	15.126(3)
b / Å	15.857(3)	13.214(3)
c /Å	16.836(3)	15.544(3)
α / °	90	90
β / °	90	90
γ / °	90	90
V / Å^3	2335.9(8)	3106.9(11)
D_{calc} / mg·m^{-3}	1.456	1.519
Z	4	8
μ / mm^{-1}	0.97	1.13
crystal size / mm	0.96 × 0.28 × 0.05 mm	0.142 × 0.19× 0.015
Measured refl.	34817	32103
Independent refl.	5345	3549
Data averaging R_{int}	0.062	0.059
Refined parameters	318	204
R [$F^2 > 2\sigma(F^2)$]	0.033	0.033
R(F^2) all refl.	0.0399	0.089
wR(F^2)	0.081	0.079
goodness of fit, S	1.04	1.00
$\Delta\varrho_{max}$/ $\Delta\varrho_{min}$ e· Å^{-3}	0.40 / −0.48	0.38 / −0.33
Flack Parameter	−0.009 (14) (Refined as an inversion twin.)	−

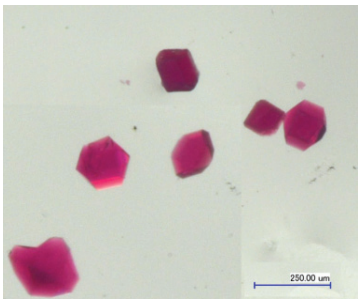

	fac-[Co(tcg)(dmf)$_2$(H$_2$O)] (21b-tcg)	[Mn(tcg)(dmf)$_2$(H$_2$O)] (22tcg)
Formula	$C_{10}CoN_8O_3H_{16}$	$C_{10}MnN_8O_3H_{16}$
Mr / g·mol^{-1}	355.24	351.25
Crystal system	monoclinic	orthorhombic
Space group	$P2_1/n$	*Pbca*
a / Å	8.7040(17)	15.369(3)
b / Å	14.290(3)	13.107(3)
c /Å	12.805(3)	15.849(3)
α / °	90	90
β / °	98.22(3)	90
γ / °	90	90
V / Å^3	1576.3(6)	3192.6(11)
D$_{calc}$ / mg·m^{-3}	1.497	1.14
Z	4	8
μ / mm^{-1}	1.11	0.85
crystal size / mm	0.055 × 0.058 × 0.093	0.130 × 0.126 × 0.112
Measured refl.	17834	28657
Independent refl.	3619	3659
Data averaging R$_{int}$	R_{int} = 0.042	0.048
Refined parameters	203	210
R [F^2 > 2σ(F^2)]	0.033	0.030
R(F^2) all refl.	0.0493	0.0554
wR(F^2)	0.089	0.083
goodness of fit, S	1.01	1.02
Δϱ$_{max}$/ Δϱ$_{min}$ e· Å^{-3}	0.32, −0.58	0.24, −0.28
Flack Parameter	-	–

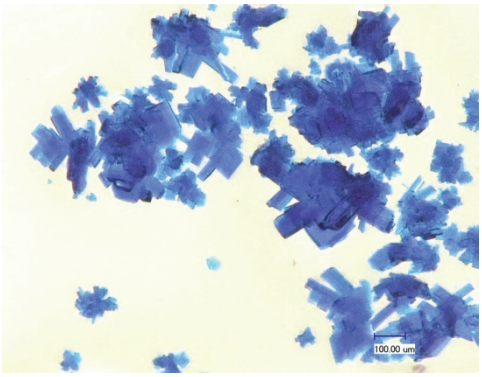

	[Co(tcg)(dmf)$_4$Co(tcg)] · 3dmf (23tcg)
Formula	$C_{29}H_{49}Co_2N_{19}O_7$
Mr / g·mol^{-1}	893.73
Crystal system	monoclinic
Space group	$P2_1/c$
a / Å	12.547(3)
b / Å	11.688(2)
c /Å	31.752(6)
α / °	90
β / °	100.98(3)
γ / °	90
V / Å^3	4571.2(17)
D_{calc} / mg·m^{-3}	1.299
Z	4
μ / mm^{-1}	0.79
crystal size / mm	0.21 × 0.20 × 0.06
Measured refl.	18013
Independent refl.	9081
Data averaging R_{int}	0.092
Refined parameters	528
R [$F^2 > 2\sigma(F^2)$]	0.122
R(F^2) all refl.	0.2345
wR(F^2)	0.366
goodness of fit, S	1.07
$\Delta\varrho_{max}$/ $\Delta\varrho_{min}$ e· Å^{-3}	1.67 / −1.07
Flack Parameter	–

APPENDIX E: SELECTED BOND DISTANCES, ANGLES AND HYDROGN BONDS

Selected bond distances (Å) and angles (°) for ctz geometry in complexes **1ctz-7ctz:**

	calculated geometry of ctz[12]	**ctz[12]**	**1ctz**	**2ctz**
Bonds				
N1—N2	1.326	1.333(6)	1.334(4)	1.333(4)
N2—N3	1.324	1.303(11)	1.328(4)	1.331(4)
N3—N4	1.326	1.333(6)	1.342(5)	1.339(4)
N1—C1	1.344	1.325(5)	1.341 (5)	1.345(4)
N4—C1	1.344	1.325(5)	1.333(5)	1.335(4)
C1—C2	1.417	1.430(9)	1.422(6)	1.427(5)
N5—C2	1.159	1.137(10)	1.148(6)	1.139(4)
Angles				
N3—N2—N1	110.1	109.8(3)	111.4(3)	107.5(3)
N2—N3—N4	110.1	109.8(3)	108.1(3)	112.0(2)
N4—C1—C2	123.7	123.8(3)	122.5(4)	122.0(3)
N5—C2—C1	180	180.0	177.4(5)	178.1(4)
N2—N1—C1	103.7	103.8(4)	102.7(3)	105.1(3)
C1—N4—N3			104.6(3)	102.5(3)
Torsion angles				
C1—N1—N2—N3			0.3(4)	0.2(3)
N1—N2—N3—N4			0.3(4)	−0.3(3)
N2—N3—N4—C1			−0.6(5)	0.3(3)
N3—N4—C1—N1			0.8(5)	−0.2(3)

Bonds	**3ctz**	**4a-ctz**	**4b-ctz**	**5ctz**
N1—N2	1.338(2)	1.341(4)	1.339(2)	1.345(2)
N2—N3	1.312(3)	1.328(4)	1.311(2)	1.327(2)
N3—N4	1.345(2)	1.333(4)	1.338(2)	1.333(2)
N1—C1	1.330(2)	1.328(4)	1.342(2)	1.336(2)
N4—C1	1.336(2)	1.344(4)	1.342(2)	1.337(2)
C1—C2	1.427(2)	1.439(5)	1.434(3)	1.435(3)
N5—C2	1.150(3)	1.145(4)	1.139(3)	1.146(3)
Angles				
N3—N2—N1	110.30(15)	111.0(3)	111.74(14)	109.88(14)
N2—N3—N4	109.85(16)	108.5(3)	107.60(14)	109.89(14)
N4—C1—C2	121.85(17)	123.2(3)	124.88(17)	122.47(16)
N5—C2—C1	177.0(2)	178.1(4)	179.0(2)	178.5(2)
N2—N1—C1	103.19(16)	102.9(3)	103.40(15)	103.03(14)
C1—N4—N3	102.91(16)	104.3(3)	105.62(15)	103.58(14)
Torsion angles				

C1—N1—N2—N3	0.5(2)	0.2(4)	−0.5(2)	−0.07(18)
N1—N2—N3—N4	−0.3(2)	−0.4(4)	0.2(2)	0.33(19)
N2—N3—N4—C1	−0.1(2)	0.4(4)	0.1(2)	−0.43(19)
N3—N4—C1—N1	0.5(2)	−0.4(4)	−0.4(2)	0.4(2)

Bonds	**6ctz**	**7ctz**
N1—N2	1.337(6)	1.325(3)
N2—N3	1.323(6)	1.333(4)
N3—N4	1.332(6)	1.325(3)
N1—C1	1.323(6)	1.339(3)
N4—C1	1.317(7)	1.339(3)
C1—C2	1.417(8)	1.433(5)
N5—C2	1.137(8)	1.149(5)
Angles		
N3—N2—N1	108.7(4)	110.15(12)
N2—N3—N4	110.4(4)	110.15(12)
N4—C1—C2	123.7(5)	122.99(15)
N5—C2—C1	179.0(8)	176.5(5)
N2—N1—C1	103.8(4)	102.9(2)
C1—N4—N3	103.6(4)	102.9(2)
Torsion angles		
C1—N1—N2—N3	0.3(6)	0.1(2)
N1—N2—N3—N4	−0.7(6)	0.00
N2—N3—N4—C1	0.7(6)	0.1(2)
N3—N4—C1—N1	−0.5(7)	−0.2(4)

Coordination environment of transition metal atoms in complexes **1ctz-7ctz.** Selected bond distances (in Å) and angles (in °):

$PPh_4[Cu(ctz)_3]$ (1ctz)			
Cu1—$N2^{i}$	2.001(3)	$N2^{i}$—Cu1—$N2^{ii}$	180.00(15)
Cu1—$N2^{ii}$	2.001(3)	$N2^{i}$—Cu1—$N8^{ii}$	90.11(13)
Cu1—$N8^{ii}$	2.044(3)	$N2^{ii}$—Cu1—$N8^{ii}$	89.89(13)
Cu1—$N8^{i}$	2.044(3)	$N2^{i}$—Cu1—$N8^{i}$	89.89(13)
Cu1—$N11^{iii}$	2.365(3)	$N2^{ii}$—Cu1—$N8^{i}$	90.11(13)
Cu1—N11	2.365(3)	$N8^{ii}$—Cu1—$N8^{i}$	180.0
Cu2—$N12^{i}$	2.012(3)	$N2^{i}$—Cu1—$N11^{iii}$	90.48(12)
Cu2—N12	2.012(3)	$N2^{ii}$—Cu1—$N11^{iii}$	89.52(12)
Cu2—N7	2.036(3)	$N8^{ii}$—Cu1—$N11^{iii}$	89.38(12)
Cu2—$N7^{i}$	2.036(3)	$N8^{i}$—Cu1—$N11^{iii}$	90.62(12)
Cu2—$N1^{i}$	2.327(3)	$N2^{i}$—Cu1—N11	89.53(12)
Cu2—N1	2.327(3)	$N2^{ii}$—Cu1—N11	90.47(12)

N7—Cu2—N7^{i}	180.0	N8^{ii}—Cu1—N11	90.62(12)
N12^{i}—Cu2—N1^{i}	89.33(12)	N8^{i}—Cu1—N11	89.38(12)
N12—Cu2—N1^{i}	90.67(12)	N11^{iii}—Cu1—N11	180.0
N7—Cu2—N1^{i}	90.26(12)	N12^{i}—Cu2—N12	180.0
N7^{i}—Cu2—N1^{i}	89.74(12)	N12^{i}—Cu2—N7	90.15(13)
N7—Cu2—N7^{i}	180.0	N12—Cu2—N7	89.85(13)
N12^{i}—Cu2—N1^{i}	89.33(12)	N12^{i}—Cu2—N7^{i}	89.85(13)
N12—Cu2—N1^{i}	90.67(12)	N12—Cu2—N7^{i}	90.16(13)

Symmetry codes: (i) −*x*+2, −*y*+1, −*z*; (ii) *x*−1, *y*, *z*; (iii) −*x*+1, −*y*+1, −*z*; (iv) *x*+1, *y*, *z*

[Cu(ctz)$_2$(bipy)] (2ctz)

Cu—N3^{i}	2.000(3)	N3^{i}—Cu—N12	172.40(11)
Cu—N12	2.003(3)	N3^{i}—Cu—N6	87.78(11)
Cu—N6	2.016(3)	N12—Cu—N6	96.96(11)
Cu—N11	2.023(3)	N3^{i}—Cu—N11	92.95(11)
Cu—N1	2.279(3)	N12—Cu—N11	80.87(11)
N12—Cu—N1	91.53(10)	N6—Cu—N11	164.16(11)
N6—Cu—N1	97.54(11)	N3^{i}—Cu—N1	93.74(10)
N11—Cu—N1	98.19(10)		

Symmetry codes: (i) −*x*+1, *y*−1/2, −*z*+3/2; (ii) −*x*+1, *y*+1/2, −*z*+3/2.

[CuCl(py)$_4$](ctz) · 2py (3ctz)

Cu—N9	2.0257(13)	N9—Cu—N7	173.08(5)
Cu—N7	2.0340(13)	N9—Cu—N6	89.97(5)
Cu—N6	2.0356(12)	N7—Cu—N6	89.71(5)
Cu—N8	2.0399(12)	N9—Cu—N8	89.83(5)
Cu—Cl	2.6226(4)	N7—Cu—N8	89.73(5)
Cu—Cl^{i}	3.1075(4)	N6—Cu—N8	173.68(6)
N6—Cu—Cl	95.92(4)	N9—Cu—Cl	93.60(4)
N8—Cu—Cl	90.40(4)	Cu—Cl—Cu^{i}	176.502(17)

Symmetry codes: (i) x, −y+1, z−1/2.

[Cu$_2$(ctz)$_6$Cu(CH$_3$CN)$_2$(H$_2$O)$_2$] · 2CH$_3$CN (4a-ctz)

Cu1—N7	2.017(3)	N7—Cu1—N7^{i}	180.0
Cu1—N7^{i}	2.017(3)	N7—Cu1—N12^{i}	88.66(10)
Cu1—N12^{i}	2.030(3)	N7^{i}—Cu1—N12^{i}	91.34(10)
Cu1—N12	2.030(3)	N7—Cu1—N12	91.34(10)
Cu1—N1^{i}	2.353(3)	N7^{i}—Cu1—N12	88.65(10)
Cu1—N1	2.353(3)	N12^{i}—Cu1—N12	180.0
Cu2—N2^{ii}	1.998(3)	N7—Cu1—N1^{i}	89.25(10)
Cu2—N2	1.998(3)	N7^{i}—Cu1—N1^{i}	90.75(10)
Cu2—N13	2.050(3)	N12^{i}—Cu1—N1^{i}	85.72(10)
Cu2—N13^{ii}	2.050(3)	N12—Cu1—N1^{i}	94.28(10)
Cu2—N6^{ii}	2.353(3)	N7—Cu1—N1	90.75(10)

Cu2—N6	2.353(3)	$N7^{i}$—Cu1—N1	89.25(10)
$Cu3—O1W^{iii}$	1.950(2)	$N12^{i}$—Cu1—N1	94.28(10)
Cu3—O1W	1.950(2)	N12—Cu1—N1	85.72(10)
Cu3—N9	2.013(3)	$N1^{i}$—Cu1—N1	180.0
$Cu3—N9^{iii}$	2.013(3)	$N2^{ii}$—Cu2—N2	180.0
Cu3—N16	2.380(3)	$N2^{ii}$—Cu2—N13	90.07(10)
$Cu3—N16^{iii}$	2.380(3)	N2—Cu2—N13	89.93(10)
$N6^{ii}$—Cu2—N6	179.999(1)	$N2^{ii}$—Cu2—$N13^{ii}$	89.93(10)
$O1W^{iii}$—Cu3—O1W	180.0	N2—Cu2—$N13^{ii}$	90.07(10)
$O1W^{iii}$—Cu3—N9	88.89(11)	N13—Cu2—$N13^{ii}$	180.0
O1W—Cu3—N9	91.11(11)	$N2^{ii}$—Cu2—$N6^{ii}$	89.91(10)
N9—Cu3—$N9^{iii}$	180.00(16)	$N13^{ii}$—Cu2—$N6^{ii}$	86.73(10)
$O1W^{iii}$—Cu3—N16	89.37(11)	$N2^{ii}$—Cu2—N6	90.09(10)
O1W—Cu3—N16	90.63(11)	N2—Cu2—N6	89.91(10)
N9—Cu3—N16	88.29(11)	N13—Cu2—N6	86.73(10)
$N9^{iii}$—Cu3—N16	91.71(11)	$N13^{ii}$—Cu2—N6	93.27(10)
$O1W^{iii}$—Cu3—$N16^{iii}$	90.63(11)	N9—Cu3—$N16^{iii}$	91.71(11)
O1W—Cu3—$N16^{iii}$	89.37(11)	$N9^{iii}$—Cu3—$N16^{iii}$	88.29(11)

Symmetry codes: (i) −x+1, −y, −z; (ii) −x, −y, −z; (iii) −x+1, −y, −z+1.

$[Cu_2(ctz)_6Cu(H_2O)_3\{(CH_3)_2CO\}] \cdot 3(CH_3)_2CO$ (4b-ctz)

Cu2—N7	1.9973(17)	N7—Cu2—N22	177.70(6)
Cu2—N22	2.0232(17)	N7—Cu2—N28	94.49(7)
Cu2—N28	2.0453(16)	N22—Cu2—N28	87.67(6)
Cu2—N13	2.0586(16)	N7—Cu2—N13	89.61(6)
Cu2—N16	2.3108(16)	N22—Cu2—N13	88.19(6)
Cu2—N1	2.4084(16)	N28—Cu2—N13	174.66(6)
$Cu3—N27^{i}$	2.0258(16)	N7—Cu2—N16	90.39(6)
Cu3—N27	2.0258(16)	N22—Cu2—N16	90.38(6)
Cu3—N21	2.0521(16)	N28—Cu2—N16	90.67(6)
$Cu3—N21^{i}$	2.0521(16)	N13—Cu2—N16	92.73(6)
$Cu3—N17^{i}$	2.3023(16)	N7—Cu2—N1	89.52(6)
Cu3—N17	2.3023(16)	N22—Cu2—N1	89.64(6)
$Cu1—N12^{ii}$	2.0242(16)	N28—Cu2—N1	91.23(6)
Cu1—N12	2.0242(16)	N13—Cu2—N1	85.38(6)
$Cu1—N2^{ii}$	2.0514(15)	N16—Cu2—N1	178.11(5)
Cu1—N2	2.0514(15)	$N27^{i}$—Cu3—N27	180.0
Cu1—N6	2.3733(17)	$N27^{i}$—Cu3—N21	91.25(6)
$Cu1—N6^{ii}$	2.3733(17)	N27—Cu3—N21	88.75(6)
Cu4—O1W	1.9695(14)	$N27^{i}$—Cu3—$N21^{i}$	88.75(6)
Cu4—O3W	1.9866(14)	N27—Cu3—$N21^{i}$	91.25(6)
$Cu4—N19^{iii}$	2.0059(15)	N21—Cu3—$N21^{i}$	180.0
Cu4—N4	2.0156(15)	$N27^{i}$—Cu3—$N17^{i}$	89.50(6)
Cu4—O2W	2.2648(16)	N27—Cu3—$N17^{i}$	90.50(6)
Cu4—O4	2.3885(16)	N21—Cu3—$N17^{i}$	89.55(6)
$N12^{ii}$—Cu1—N2	90.04(6)	$N21^{i}$—Cu3—$N17^{i}$	90.45(6)
N12—Cu1—N2	89.96(6)	$N27^{i}$—Cu3—N17	90.50(6)

$N2^{ii}$—Cu1—N2	179.99(1)	N27—Cu3—N17	89.50(6)
$N12^{ii}$—Cu1—N6	93.82(6)	N21—Cu3—N17	90.45(6)
N12—Cu1—N6	86.18(6)	$N21^{i}$—Cu3—N17	89.55(6)
N12—Cu1—$N6^{ii}$	93.82(6)	N12—Cu1—$N2^{ii}$	90.04(6)
$N2^{ii}$—Cu1—$N6^{ii}$	89.74(6)		
N2—Cu1—$N6^{ii}$	90.26(6)		
N6—Cu1—$N6^{ii}$	180.0		

Symmetry codes: (i) $-x, -y, -z$; (ii) $-x+1, -y+1, -z+1$; (iii) $x+1, y, z$; (iv) $x-1, y, z$.

$[Mn(ctz)_2(bipy)_2]$ (5a-ctz)

Mn—N5	2.2211(14)	Mn—N5	2.2211(14)
Mn—N7	2.2378(14)	Mn—N7	2.2378(14)
Mn—N9	2.2716(14)	Mn—N9	2.2716(14)
Mn—N10	2.2800(14)	Mn—N10	2.2800(14)
Mn—N1	2.2845(13)	Mn—N1	2.2845(13)
Mn—N2	2.2900(13)	Mn—N2	2.2900(13)
N4—N7	1.3380(19)	N4—N7	1.3380(19)
N5—N11	1.320(2)	N5—N11	1.320(2)
N1—C12	1.344(2)	N1—C2	1.355(2)
N2—C17	1.342(2)	N2—C7	1.352(2)
N3—N6	1.331(2)	N3—C10	1.341(2)
N4—C10	1.336(2)	N7—Mn—N2	94.45(5)
N5—N12	1.337(2)	N9—Mn—N2	93.25(5)
N5—Mn—N1	98.03(5)	N10—Mn—N2	71.93(5)
N5—Mn—N2	96.23(5)		

$[Cu(ctz)_2(py)_4]$ (5ctz)

Cu—N2	2.6266(15)	N14—Cu—N12	176.01(6)
Cu—N7	2.6151(15)	N14—Cu—N13	92.62(5)
Cu—N11	2.0449(14)	N12—Cu—N13	86.38(5)
Cu—N12	2.0283(14)	N14—Cu—N11	92.25(5)
Cu—N13	2.0369(14)	N12—Cu—N11	89.02(6)
Cu — N14	2.027(10)	N13—Cu—N11	173.76(6)
N14—Cu—N2	86.30(5)	N14—Cu—N7	83.54(5)
N12—Cu—N2	97.59(5)	N12—Cu—N7	92.68(5)
N13—Cu—N2	92.26(5)	N13—Cu—N7	94.29(5)
N11—Cu—N2	84.17(5)	N11—Cu—N7	90.13(5)
N7—Cu—N2	168.14(5)		

$[Cu_2(ctz)_4(bipy)_2]$ (6ctz)

CuA—$N3A^{i}$	2.002(4)	CuB—$N2B^{ii}$	1.988(4)
CuA—N7A	2.008(5)	CuB—N7B	2.004(4)
CuA—N11A	2.013(4)	CuB—N11B	2.005(4)
CuA—N12A	2.037(5)	CuB—N12B	2.016(4)

CuA—N2A	2.264(4)	CuB—N3B	2.370(5)
N3Ai—CuA—N7A	87.17(18)	N2B^{ii}—CuB—N7B	88.79(18)
N3Ai—CuA—N11A	164.30(18)	N2B^{ii}—CuB—N11B	170.07(18)
N7A—CuA—N11A	97.69(19)	N7B—CuB—N11B	96.73(18)
N3Ai—CuA—N12A	91.70(18)	N2B^{ii}—CuB—N12B	92.81(18)
N7A—CuA—N12A	168.32(18)	N7B—CuB—N12B	176.39(18)
N11A—CuA—N12A	80.51(18)	N11B—CuB—N12B	81.23(18)
N3Ai—CuA—N2A	99.05(16)	N2B^{ii}—CuB—N3B	97.96(17)
N7A—CuA—N2A	88.02(17)	N7B—CuB—N3B	89.69(18)
N11A—CuA—N2A	96.04(17)	N11B—CuB—N3B	90.34(16)
N12A—CuA—N2A	103.64(17)	N12B—CuB—N3B	93.30(17)

Symmetry codes: (i) −x+1, −y+2, −z+1; (ii) −x+1, −y+1, −z.

$[Cu_2(ctz)_2(tpm)_2(NO_3)]NO_3$ (7ctz)

Cu—N6	2.011(2)	N6—Cu—N6^{i}	87.20(13)
Cu—N6^{i}	2.011(2)	N6—Cu—N2^{i}	179.10(10)
Cu—N2^{i}	2.023(2)	N6^{i}—Cu—N2^{i}	92.41(10)
Cu—N2	2.023(2)	N6—Cu—N2	92.41(10)
Cu—O1	2.335(4)	N6^{i}—Cu—N2	179.10(10)
Cu—N4	2.376(3)	N2^{i}—Cu—N2	87.96(13)
N2—Cu—O1	84.54(10)	N6—Cu—O1	94.68(10)
N6—Cu—N4	83.17(9)	N6^{i}—Cu—O1	94.68(11)
N6^{i}—Cu—N4	83.17(9)	N2^{i}—Cu—O1	84.54(10)
N2^{i}—Cu—N4	97.59(9)	N2—Cu—N4	97.59(9)

Symmetry code: (i) −x+1/2, y, z.

$[Cu(tca)_2(bipy)] \cdot H_2O$ (8tca)

Cu—N4B	1.9995(17)	N4B—Cu—N2A	164.62(7)
Cu—N2A	2.0137(17)	N4B—Cu—N3C	86.58(7)
Cu—N3C	2.0271(19)	N2A—Cu—N3C	97.02(7)
Cu—N1A	2.027(2)	N4B—Cu—N1A	93.36(7)
Cu—N3B^{i}	2.2992(19)	N2A—Cu—N1A	80.67(7)
Cu—O1B	2.522(7)	N3C—Cu—N1A	170.62(7)
C2B —N5B	1.311(7)	N3C—Cu—N3B^{i}	92.32(7)
C2B—O1B	1.246(9)	N4B—Cu—N3B^{i}	100.33(6)
C2C—O1C	1.343(9)	N1A—Cu—N3B^{i}	96.84(7)
C2C—N5C	1.324(9)	O1B—Cu —N3B^{i}	174.22(7)
		N2A—Cu—N3B^{i}	94.48(7)

Symmetry code: (i) −x+1, −y+1, −z+1.

$[Cu(ctz)(tca)(bipy)]_{0.5}[Cu(ctz)_2(bipy)]_{0.5}$ (8a-tca)

Cu—N3	1.981(5)	N3—Cu1—N4	175.4(2)
Cu—N4	1.999(4)	N3—Cu1—N1	88.55(18)
Cu—N1	2.014(4)	N4—Cu1—N1	93.09(17)

Cu—N9	2.019(4)	N3—Cu1—N9	95.54(18)
Cu—N7^{i}	2.250(5)	N4—Cu1—N9	81.38(18)
Cu—O2	2.491(4)	N1—Cu1—N9	158.64(19)
C15—N11	1.162(2)	N3—Cu1—N7^{i}	95.0(2)
C15—N12	1.117(2)	N9—Cu1—N7^{i}	100.08(19)
C15—O2	1.484(2)	O2— Cu1—N7^{i}	174.13(3)

Symmetry code: (i) $-x, -y, -z+2$.

$Cu(tca)_2 \cdot 2H_2O$ (9tca)			
Cu—N3^{i}	1.976(7)	Cu—O2	2.574(2)
Cu—N6	1.987(6)	N3^{i}—Cu1—N6	172.0(3)
Cu—N5	2.012(7)	N3^{i}—Cu1—N5	92.2(3)
Cu—N4	2.022(7)	N6—Cu1—N5	91.8(3)
Cu—O4	2.362(5)	N3^{i}—Cu1—N4	86.4(3)
C4 —N9	1.325(7)	N6—Cu1—N4	92.0(3)
C1—N10	1.327(6)	N5—Cu1—N4	161.6(3)
C1—O2	1.226(10)	N4—Cu1—O4	100.6(3)
C4—O4	1.262(9)		

Symmetry codes: (i) $x, -y-1, z+1/2$.

Selected bond lengths (in Å) and angles (in °) in compounds:

Htcp (10tcp)			
N1—C1	1.353(2)	C3—C5	1.414(2)
N1—C7	1.354(2)	C3—C4	1.431(2)
N1—H1	0.88(2)	C4—N3	1.141(2)
N2—C2	1.146(2)	C4—C3	1.431(2)
N3—C4	1.141(2)	C5—C7	1.385(2)
N4—C6	1.151(2)	C5—C6	1.422(2)
N5—C8	1.147(2)	C6—N4	1.151(2)
C1—N1	1.353(2)	C7—C5	1.385(2)
C1—C3	1.384(2)	C7—C8	1.426(2)
C1—C2	1.426(2)	C8—N5	1.147(2)
C2—C1	1.426(2)		
C1—N1—C7	109.38(14)	N3—C4—C3	179.8(3)
C1—N1—H1	128.2(13)	C7—C5—C3	106.29(14)
C7—N1—H1	122.3(13)	C7—C5—C6	124.77(15)
N1—C1—C3	108.41(14)	C3—C5—C6	128.80(14)
N1—C1—C2	123.61(15)	N4—C6—C5	177.62(19)
C3—C1—C2	127.95(16)	N1—C7—C5	108.83(14)
N2—C2—C1	175.89(19)	N1—C7—C8	123.56(15)
C1—C3—C5	107.08(14)	C5—C7—C8	127.59(15)
C1—C3—C4	125.78(15)	N5—C8—C7	177.11(19)
C5—C3—C4	127.13(16)		
N1—C1—C3—C5	0.2(2)	C4—C3—C5—C7	−179.59(18)
C2—C1—C3—C5	−177.92(17)	C1—C3—C5—C6	175.37(17)

N1—C1—C3—C4	179.31(18)	C4—C3—C5—C6	−3.8(3)
C2—C1—C3—C4	1.2(3)	C1—N1—C7—C5	0.51(19)
C1—C3—C5—C7	−0.46(19)	C1—N1—C7—C8	179.09(17)

[Na(tcp)H$_2$O] · H$_2$O (11tcp)			
Na—O1	2.370(2)	N5—C8	1.140(3)
Na—O1^{i}	2.407(2)	C1—C3	1.398(3)
Na—N3	2.424(2)	C1—C2	1.430(4)
Na—N4^{ii}	2.505(2)	C3—C5	1.415(3)
Na—N5^{iii}	2.508(2)	C3—C4	1.424(3)
Na—N4^{iv}	2.802(2)	C5—C6	1.420(3)
Na^{v}—Na^{vi}	3.7429(2)	C7—C8	1.423(3)
N1—C1	1.354(3)	N1—C1—C3	112.0(2)
N1—C7	1.362(3)	N1—C1—C2	119.6(2)
C5—C7	1.399(3)	C3—C1—C2	128.5(2)
N2—C2	1.130(3)	N2—C2—C1	176.5(3)
N3—C4	1.131(3)	C1—C3—C5	105.35(19)
N4—C6	1.140(3)	C5—C3—C4	126.3(2)
O1—Na—O1^{i}	103.17(7)	N3—C4—C3	178.4(3)
O1—Na—N3	90.74(8)	C7—C5—C3	105.66(19)
O1^{i}—Na—N3	84.76(8)	C7—C5—C6	127.1(2)
O1—Na—N4^{ii}	87.25(7)	C3—C5—C6	127.2(2)
O1^{i}—Na—N4^{ii}	169.56(8)	N3—Na—N5^{iii}	169.36(9)
N3—Na—N4^{ii}	96.00(8)	N4^{ii}—Na—N5^{iii}	88.61(8)
O1—Na—N5^{iii}	99.07(8)	O1—Na—N4^{iv}	176.71(7)
O1^{i}—Na—N5^{iii}	88.98(8)	N3—Na—N4^{iv}	90.23(8)
		N4^{ii}—Na—N4^{iv}	89.52(7)

Symmetry codes: (i) *x*, *y*−1, *z*; (ii) −*x*, *y*+1, −*z*−1/2; (iii) *x*, −*y*, *z*−1/2; (iv) −*x*, *y*, −*z*−1/2; (v) *x*, *y*+1, *z*; (vi) −*x*, *y*−1, −*z*−1/2

[Me$_4$N]tcp (12tcp)			
N1—C7	1.309(10)	C7—N1—C1	105.3(8)
N1—C1	1.367(10)	N1—C1—C2	121.0(11)
N2—C2	1.161(12)	N1—C1—C3	111.5(7)
N3—C4	1.176(13)	C2—C1—C3	127.5(11)
N4—C6	1.143(9)	N2—C2—C1	177.4(15)
N5—C8	1.099(12)	C5—C3—C4	128.6(8)
C1—C2	1.420(13)	C5—C3—C1	104.6(8)
C1—C3	1.420(11)	C4—C3—C1	126.7(9)
C3—C5	1.348(9)	N3—C4—C3	176.7(12)
C3—C4	1.387(13)	C3—C5—C7	107.1(7)
C5—C7	1.428(10)	C3—C5—C6	128.2(8)
C5—C6	1.438(11)	C7—C5—C6	124.6(7)
C7—C8	1.404(13)	N4—C6—C5	178.7(9)

[Co(MeCN)$_4$(tcp)$_2$] · 2 MeCN (13tcp)			
Co—N7^i	2.1158(15)	C2—C3	1.409(2)
Co—N7	2.1158(15)	C2—C6	1.428(2)
Co—N6	2.1240(14)	C3—C4	1.393(2)
Co—N6^i	2.1241(14)	C3—C7	1.423(3)
Co—N1	2.1471(14)	C4—C8	1.436(2)
Co—N1^i	2.1471(14)	C9—C10	1.456(2)
Co—N7^i	2.1158(15)	C2—C3	1.409(2)
N1—C4	1.362(2)	N7^i—Co—N7	180.00(12)
N1—C1	1.368(2)	N7^i—Co—N6	90.44(6)
N2—C5	1.149(2)	N7—Co—N6	89.56(5)
N3—C6	1.146(2)	N7^i—Co—N6^i	89.56(6)
N4—C7	1.144(2)	N7—Co—N6^i	90.45(6)
N5—C8	1.147(2)	N6—Co—N6^i	180.0
N6—C9	1.138(2)	N7^i—Co—N1	89.93(5)
N7—C11	1.140(2)	N7—Co—N1	90.07(5)
N8—C13	1.134(3)	N6—Co—N1	89.65(5)
C1—C2	1.393(2)	N6^i—Co—N1	90.35(5)
C1—C5	1.430(2)	N7^i—Co—N1^i	90.07(5)
N6—Co—N1^i	90.35(5)	N7—Co—N1^i	89.93(5)
N6^i—Co—N1^i	89.65(5)		
N1—Co—N1^i	180.00(8)		
Symmetry codes: (i) $-x$+1, $-y$+1, $-z$+1.			

[Ni(MeCN)$_4$(tcp)$_2$] · 2 MeCN (14tcp)			
Ni—N6^i	2.0688(10)	C2—C3	1.4067(16)
Ni—N6	2.0688(10)	C2—C6	1.4252 (17)
Ni—N7	2.0754(10)	C3—C4	1.3961(16)
Ni—N7^i	2.0754(10)	C3—C7	1.4266(16)
Ni—N1^i	2.1132(10)	C4—C8	1.4317(17)
Ni—N1	2.1132(10)	C9—C10	1.4536(17)
N1—C1	1.3632(14)	N1—C4—C3	111.67(10)
N1—C4	1.3666(15)	N1—C4—C8	123.92(11)
N2—C5	1.1485(16)	C3—C4—C8	124.39(11)
N3—C6	1.1446(17)	N1—C4—C3	111.67(10)
N4—C7	1.1465 17)	N1—C4—C8	123.92(11)
N5—C8	1.1494(17)	N2—C5—C1	175.62(13)
N7—C11	1.1408(16)	N4—C7—C3	179.08(13)
N8—C13	1.136(2)	N2—C5—C1	175.62(13)
C1—C2	1.3964(16)	N3—C6—C2	178.70(15)
C1—C5	1.4319(16)	N6^i—Ni—N6	180.0
N6—Ni—N7	90.37(4)	N6^i—Ni—N7	89.63(4)
Symmetry codes: (i) $-x$, $-y$, $-z$+2.			

[Fe(tpm)$_2$](tcp)$_2$ (15tcp)			
Fe1—N16^{i}	1.962(3)	Fe2—N22	1.958(3)
Fe1—N16	1.962(3)	Fe2—N22^{ii}	1.958(3)
Fe1—N14	1.969(2)	Fe2—N17^{ii}	1.969(2)
Fe1—N14^{i}	1.969(2)	Fe2—N17	1.969(2)
Fe1—N11^{i}	1.980(3)	Fe2—N20	1.976(3)
Fe1—N11	1.980(3)	Fe2—N20^{ii}	1.976(3)
N16^{i}—Fe1—N16	180	N22—Fe2—N22^{ii}	180
N16^{i}—Fe1—N14	92.45(10)	N22—Fe2—N17^{ii}	92.12(11)
N16—Fe1—N14	87.55(10)	N22^{ii}—Fe2—N17^{ii}	87.88(11)
N16^{i}—Fe1—N14^{i}	87.55(10)	N22—Fe2—N17	87.88(11)
N16—Fe1—N14^{i}	92.45(10)	N22^{ii}—Fe2—N17	92.12(11)
N14—Fe1—N14^{i}	180	N17^{ii}—Fe2—N17	180
N16^{i}—Fe1—N11^{i}	87.47(11)	N22—Fe2—N20	87.94(11)
N16—Fe1—N11^{i}	92.53(11)	N22^{ii}—Fe2—N20	92.06 (11)
N14—Fe1—N11^{i}	93.61(10)	N17^{ii}—Fe2—N20	93.13(10)
N14^{i}—Fe1—N11^{i}	86.39(10)	N17—Fe2—N20	86.87(11)
N16^{i}—Fe1—N11	92.53(11)	N22—Fe2—N20^{ii}	92.06(11)
N16—Fe1—N11	87.47(11)	N22^{ii}—Fe2—N20^{ii}	87.94(11)
N14—Fe1—N11	86.39(10)	N17^{ii}—Fe2—N20^{ii}	86.87(11)
N14^{i}—Fe1—N11	93.61(10)	N17—Fe2—N20^{ii}	93.13(10)
N11^{i}—Fe1—N11	180	N20—Fe2—N20^{ii}	180
Symmetry codes: (i) −*x*+2, −*y*+1, −*z*; (ii) −*x*+1, −*y*+1, −*z*+1.			

[Cu(tcpc)$_2$(H$_2$O)$_2$] · H$_2$O (16tcpc)			
Cu—O1	1.968(2)	N3—C8	1.140(5)
Cu—O2	2.500(2)	N4—C7	1.145(5)
Cu—N1^{i}	1.969(3)	N5—C5	1.156(5)
O1—C3	1.265(4)	C1—C2	1.398(5)
N1—C4	1.355(5)	C1—C6	1.412(5)
N1—C2	1.361(4)	C1—C8	1.434(5)
N2—C3	1.316 (4)	C2—C3	1.468(5)
C6—C7	1.431 (6)	C4—C6	1.396(5)
		C4—C5	1.422(5)
O1—Cu—O1^{i}	180	O1—Cu—N1	82.72(11)
O1—Cu—N1^{i}	97.28(11)	O1^{i}—Cu—N1	97.28(11)
O1^{i}—Cu—N1^{i}	82.72(11)	N1^{i}—Cu—N1	180
O1—Cu—O1^{i}	180	O1—Cu—N1	82.72(11)
O1—Cu—N1^{i}	97.28(11)	O1^{i}—Cu—N1	97.28(11)
O1^{i}—Cu—N1^{i}	82.72(11)	N1^{i}—Cu—N1	180
Symmetry codes: (i) −*x*+1, −*y*−1, −*z*+1.			

[Cu(tcpc)$_2$(dmf)$_2$] (17tcpc)			
Cu—N1	1.9649(19)	C1—C2	1.395(3)
Cu—O2	2.559(19)	C1—C5	1.434(3)
Cu—O1	1.9675(16)	C2—C3	1.408(3)
O1—C8	1.269(3)	C2—C6	1.430(4)
O2—C9	1.243(3)	C3—C4	1.389(3)
N1—C1	1.360(3)	C3—C7	1.434(3)
N1—C4	1.362(3)	C4—C8	1.473(3)
N2—C5	1.149(3)	N1—Cu—N1^{i}	180
N3—C6	1.146(3)	N1—Cu—O1	83.28(7)
N4—C7	1.145(3)	N1^{i}—Cu—O1^{i}	83.28(7)
N5—C8	1.316(3)	O1—Cu—O1^{i}	180
Symmetry codes: (i) $-x$, $-y$, $-z$.			

Et$_4$N(tci) (18tci)			
N1—C12	1.513(3)	N2—C3	1.3462(15)
N1—C12^{i}	1.513(3)	N2—C1	1.3602(16)
N1—C9^{i}	1.518(3)	N3—C2	1.1520(19)
N1—C9	1.518(3)	N4—C4	1.142(3)
N1—C11^{i}	1.533(3)	C1—C1^{ii}	1.392(3)
N1—C11	1.533(3)	C1—C2	1.4249(19)
N1—C10	1.534(3)	C3—N2^{ii}	1.3462(15)
N1—C10^{i}	1.534(3)	C3—C4	1.444(3)
C3—N2—C1	101.42(12)	N2—C1—C1^{ii}	109.64(8)
N2—C1—C2	124.55(13)	C1^{ii}—C1—C2	125.74(8)
N3—C2—C1	176.12(15)	N2—C3—N2^{ii}	117.87(17)
N2—C3—C4	121.06(9)	N2^{ii}—C3—C4	121.06(9)
N4—C4—C3	179.3(2)		
Symmetry codes: (i) x, $-y$, z; (ii) x, $-y+1$, z.			

PPh$_4$(*cis*-dct) (19*cis*-dct)			
N1—N2	1.3387(12)	C3—C4	1.4041(14)
N1—C1	1.3549(13)	C4—C5	1.3890(15)
N2—N1^{iii}	1.3387(12)	C5—C6	1.388(2)
N3—C2	1.1515(15)	C6—C7	1.379(2)
C1—C1^{iii}	1.3901(19)	C7—C8	1.3984(15)
C1—C2	1.4267(14)	C9—C10	1.3943(13)
C3—C8	1.3918(14)	C9—C14	1.4035(13)
N2—N1—C1	106.33(9)	N1—C1—C2	121.81(9)
N1—N2—N1^{iii}	111.80(12)	C1^{iii}—C1—C2	130.40(6)
N1—C1—C1^{iii}	107.77(6)	N3—C2—C1	179.39(13)
Symmetry codes: (i) x, $-y$, $-z+1/2$; (ii) $-x+1$, $y-1/2$, $-z+1/2$; (iii) $-x+1$, $-y+1/2$, z; (iv) x, $y-1/2$, $-z$; (v) x, $y+1/2$, $-z$			

mer-[Cu(tcg)(py)$_3$] · py (20tcg)			
Cu—N6	1.988(3)	N6—C4	1.163(4)
Cu— N5^{iii}	2.736(3)	N6—Cu—N7	91.15(11)
Cu—N7	2.043(3)	N6—Cu—N9	90.50(11)
Cu—N9	2.043(3)	N7—Cu—N9	172.85(11)
Cu—N8	2.046(3)	N6—Cu—N8	175.06(12)
Cu—N4^{i}	2.258(3)	N7—Cu—N8	88.41(11)
N1—C1	1.343(4)	N9—Cu—N8	89.35(11)
N2—C1	1.342(4)	N6—Cu—N4^{i}	92.84(11)
N3—C1	1.359(4)	N7—Cu—N4^{i}	94.30(11)
N1—C2	1.319(4)	N9—Cu—N4^{i}	92.58(11)
N2—C3	1.320(4)	N8—Cu—N4^{i}	92.09(11)
N3—C4	1.307(4)	C2—N1—C1	118.5(3)
N4—C2	1.146(4)	C4—N3—C1	116.5(3)
N6—C4	1.163(4)	N2—C1—N1	121.1(3)
N5—C3	1.161(5)	N2—C1—N3	120.1(3)
N5—C3—N2	172.4(4)	N1—C1—N3	118.7(3)
N6—C4—N3	172.3(3)	N4—C2—N1	172.9(4)
C3—N2—C1—N1	−175.9(3)	C4—N3—C1—N2	−175.4(3)
C3—N2—C1—N3	7.2(5)	C4—N3—C1—N1	7.7(5)
C2—N1—C1—N2	4.2(5)	C9—N7—C5—C6	0.8(6)
C2—N1—C1—N3	−178.9(3)	C4—N3—C1—N2	−175.4(3)
Cu—N7—C5—C6	−176.7(3)		
Symmetry codes: (i) *x*−1/2, −*y*+1/2, −*z*; (ii) *x*+1/2, −*y*+1/2, −*z*; (iii) −*x*, *y*+1/2, −1/2 −*z*			

fac-[Co(tcg)(dmf)$_2$(H$_2$O)] (21a-tcg)			
Co—N4	2.0637(7)	N1—C2	1.308(3)
Co—N6^{i}	2.0674(8)	N1—C1	1.350(2)
Co—O3W	2.1163(5)	N2—C3	1.312(2)
Co—O2	2.1467(4)	N2—C1	1.358(3)
Co—N5^{ii}	2.1539(9)	N3—C4	1.304(3)
Co—O1	2.1874(5)	N3—C1	1.342(2)
O1—C10	1.245(3)	N4—C2	1.151(3)
O2—C7	1.238(3)	N5—C3	1.159(2)
N4—Co—N6^{i}	91.53(7)	C2—N1—C1	117.29(17)
N4—Co—O3W	90.62(6)	C3—N2—C1	115.59(15)
N6^{i}—Co—O3W	92.39(6)	C4—N3—C1	118.91(16)
N4—Co—O2	175.46(7)	Co–N4–C2	167.60(6)
N6^{i}—Co—O2	90.09(6)	Co–N6^{i}–C3^{i}	174.70(7)
O3W—Co—O2	85.08(6)	Co–N5^{ii}–C3^{ii}	129.50(5)
N4—Co—N5^{ii}	97.14(7)	C2—N1—C1—N2	1.2(3)
N6^{i}—Co—N5^{ii}	93.41(7)	C3—N2—C1—N3	13.4(3)
O3W—Co—N5^{ii}	170.18(6)	C3—N2—C1—N1	−166.83(18)
O2—Co—N5^{ii}	86.99(7)	C4—N3—C1—N1	4.9(3)
N4—Co—O1	89.84(6)	C2—N1—C1—N3	−179.10(18)
N6^{i}—Co—O1	178.30(6)		

O3W—Co—O1	86.59(5)	C4—N3—C1—N2	−175.38(18)
O2—Co—O1	88.46(6)	N6^{i}—Co—N5^{ii}	93.41(7)
N5^{ii}—Co—O1	87.42(6)	O3W—Co—N5^{ii}	170.18(6)
O3W—Co—O2	85.08(6)	O2—Co—N5^{ii}	86.99(7)
N6^{i}—Co—O1	178.30(6)	N4—Co—O1	89.84 (6)

Symmetry codes: (i) *x*−1/2, *y*, −*z*+3/2; (ii) *x*−1/2, −*y*+1/2, −*z*+1; (iii) *x*+1/2, −*y*+1/2, −*z*+1; (iv) *x*+1/2, *y*, −*z*+3/2.

***fac*-[Co(tcg)(dmf)$_2$(H$_2$O)] (21b-tcg)**			
Co—N4^{i}	2.0642 (16)	N1—C2	1.308(2)
Co—N5^{ii}	2.0828 (17)	N1—C1	1.343(2)
Co—N6	2.1078(16)	N2—C3	1.305(2)
Co—O3W	2.1382(13)	N2—C1	1.343(2)
Co—O2	2.1571(14)	N3—C4	1.310(2)
Co—O1	2.1593(14)	N3—C1	1.357(2)
O1—C5	1.241(2)	N4—C2	1.156(2)
O2—C8	1.234(2)	N6—C4	1.157(2)
N4^{i}—Co—N5^{ii}	91.57(7)	C2—N1—C1	117.75(16)
N4^{i}—Co—N6	96.83(7)	C3—N2—C1	117.91(15)
N5^{ii}—Co—N6	97.23(7)	C4—N3—C1	117.02(15)
N4^{i}—Co—O3w	89.06(6)	N2—C1—N3	119.56(15)
N5^{ii}—Co—O3w	90.14(6)	N4—C2—N1	174.38(19)
N6—Co—O3w	170.41(6)	N5—C3—N2	173.16(19)
N4^{i}—Co—O2	175.94(6)	N6—C4—N3	173.76(19)
N5^{ii}—Co—O2	88.46(6)	N1—C1—N2	120.44(16)
N6—Co—O2	87.19(6)	N1—C1—N3	120.00(15)
		Co–N6–C4	157.00(12)
O3—Co—O2	86.88(5)	C2—N1—C1—N2	−177.74(17)
N4^{i}—Co—O1	91.50(6)	C2—N1—C1—N3	3.2(3)
N5^{ii}—Co—O1	174.26(6)	C3—N2—C1—N1	2.7(3)
N6—Co—O1	87.21(6)	C3—N2—C1—N3	−178.30(16)
O3—Co—O1	85.06(5)	C4—N3—C1—N1	168.96(17)
O2—Co—O1	88.13(6)	C4—N3—C1—N2	−10.1(3)

Symmetry codes: (i) −*x*+3/2, *y*−1/2, −*z*+1/2; (ii) *x*−1, *y*, *z*; (iii) −*x*+3/2, *y*+1/2, −*z*+1/2; (iv) *x*+1, *y*, *z*.

[Mn(tcg)(dmf)$_2$(H$_2$O)] (22tcg)			
Mn—N5^{i}	2.1491(15)	N5^{i}—Mn—N6	91.78(6)
Mn—N6	2.1691(15)	N5^{i}—Mn—O2	175.79(6)
Mn—O2	2.2037(13)	N6—Mn—O2	89.31(5)
Mn—O3W	2.2149(15)	N5^{i}—Mn—O3W	91.05(6)
Mn—O1	2.2643(12)	N6—Mn—O3W	92.44(5)
Mn—N4^{ii}	2.2661(17)	O2—Mn—O3W	84.84(5)
N1—C2	1.314(2)	N5^{i}—Mn—O1	90.89(5)
N1—C1	1.356(2)	N6—Mn—O1	176.96(6)
N2—C3	1.305(2)	O2—Mn—O1	87.93(5)

N2—C1	1.351(2)	O3W—Mn—O1	86.05(4)
N3—C4	1.305(2)	N5^{i}—Mn—N4^{ii}	97.60(6)
N3—C1	1.338(2)	N6—Mn—N4^{ii}	93.70(5)
N4—C2	1.162(2)	O2—Mn—N4^{ii}	86.39(6)
N5—C3	1.153(2)	O3W—Mn—N4^{ii}	169.22(5)
N6—C4	1.153(2)	C2—N1—C1	115.55(13)
N3—C1—N2	120.57(14)	C3—N2—C1	117.33(14)
N3—C1—N1	119.13(14)	C4—N3—C1	118.88(14)
N2—C1—N1	120.30(14)	C4—N3—C1—N2	−4.4(2)
N4—C2—N1	173.98(18)	C4—N3—C1—N1	175.28(15)
N5—C3—N2	174.19(17)	C3—N2—C1—N3	178.73(16)
N6—C4—N3	172.98(18)	C3—N2—C1—N1	−0.9(2)
		C2—N1—C1—N3	−11.4(2)
		C2—N1—C1—N2	168.25(16)

Symmetry codes: (i) *x*−1/2, *y*, −*z*+1/2; (ii) *x*, −*y*+3/2, *z*−1/2.

[Co(tcg)(dmf)4Co(tcg)] · 3dmf (23tcg)

Co1—N6	2.076(7)	C1—N3	1.343(12)
Co1—O2	2.084(7)	C1—N2	1.347(12)
Co1—O3	2.091(6)	C1—N1	1.353(13)
Co1—O1	2.096(6)	C2—N4	1.154(15)
Co1—N10	2.102(7)	C2—N1	1.309(15)
Co1—O4	2.118(7)	C3—N5	1.150(15)
Co2—N11^{i}	1.932(11)	C3—N2	1.290(15)
Co2—N4^{ii}	1.935(11)	C4—N6	1.180(11)
Co2—N12^{iii}	1.951(10)	C4—N3	1.288(11)
Co2—N5	1.958(10)	C5—N9	1.332(12)
C6—N10	1.134(12)	C5—N7	1.350(13)
C6—N7	1.301(12)	C5—N8	1.364(13)
C7—N11	1.145(14)	C7—N8	1.324(14)
C8—N9	1.290(13)	C8—N12	1.161(14)
N6—Co1—O2	88.1(3)	N3—C1—N2	121.4(9)
N6—Co1—O3	92.4(3)	N3—C1—N1	119.3(9)
O2—Co1—O3	90.5(3)	N2—C1—N1	119.3(9)
N6—Co1—O1	88.9(3)	N4—C2—N1	173.3(13)
O2—Co1—O1	90.3(3)	N5—C3—N2	169.7(14)
O3—Co1—O1	178.5(3)	N6—C4—N3	173.9(11)
N6—Co1—N10	178.9(3)	N9—C5—N7	121.9(9)
O2—Co1—N10	93.0(3)	N9—C5—N8	118.2(10)
O3—Co1—N10	87.6(3)	N7—C5—N8	119.9(9)
O1—Co1—N10	91.1(3)	N10—C6—N7	172.7(11)
N6—Co1—O4	91.5(3)	N11—C7—N8	174.2(12)
O2—Co1—O4	179.0(3)	N12—C8—N9	171.7(12)
O3—Co1—O4	90.3(3)	N3—C1—N1—C2	−174.4(10)
O1—Co1—O4	88.8(3)	N2—C1—N1—C2	3.6(16)
N10—Co1—O4	87.4(3)	N5—C3—N2—C1	−154 .2(7)
N11^{i}—Co2—N4^{ii}	109.7(5)	N3—C1—N2—C3	−0.2(6)

N11^{i}—Co2—N12^{iii}	111.1(5)	N1—C1—N2—C3	−178.2(11)
N4^{ii}—Co2—N12^{iii}	106.7(4)	N2—C1—N3—C4	177.5(10)
N11^{i}—Co2—N5	106.9(4)	N1—C1—N3—C4	−4.5(15)
N4^{ii}—Co2—N5	111.0(5)	N2—C3—N5—Co2	−144(6)
N12^{iii}—Co2—N5	111.4(5)	N9—C5—N7—C6	−175.1(11)
N9—C5—N8—C7	2.5(16)	N8—C5—N7—C6	7.6(16)
N7—C5—N8—C7	179.9(10)	N7—C5—N9—C8	7.5(17)
		N8—C5—N9—C8	−175.1(11)

Symmetry codes: (i) −x+2, −y+2, −z; (ii) −x+2, y+1/2, −z+1/2; (iii) x+1, −y+3/2, z+1/2; (iv) −x+2, y−1/2, −z+1/2; (v) x−1, −y+3/2, z−1/2.

HYDROGEN BONDS

Hydrogen-bond geometry given in Å and in °:

[Cu_2(ctz)$_6$Cu(CH_3CN)$_2$(H_2O)$_2$] · 2CH_3CN (4a-ctz)

D—H···*A*	*D*—H	H···*A*	*D*···*A*	*D*—H···*A*
O1W—H1W···N10^{iv}	0.840(2)	1.953(5)	2.788(4)	174.1(3)
O1W—H2W···N17^{v}	0.840(2)	1.914(13)	2.728(5)	163.2(4)

Symmetry codes: (iv) −*x*, −*y*, −*z*+1; (v) *x*, *y*−1, *z*.

[Cu_2(ctz)$_6$Cu(H_2O)$_3${(CH_3)$_2$CO}] · 3(CH_3)$_2$CO (4b-ctz)

D—H···*A*	*D*—H	H···*A*	*D*···*A*	*D*—H···*A*
O1W—H1W···O6	0.840(2)	1.857(3)	2.696(2)	177.1(2)
O1W—H2W···N20^{ii}	0.840(2)	2.025(7)	2.843(2)	165.5(2)
O2W—H3W···N5^{v}	0.840(2)	2.152(10)	2.947(2)	158.6(2)
O2W—H4W···O5^{vi}	0.840(2)	1.981(7)	2.796(2)	163.7(2)
O3W—H5W···O5^{vii}	0.840(2)	2.205(16)	2.885(2)	138.8(2)
O3W—H6W···O7	0.840(2)	1.793(5)	2.627(2)	172.8(3)

Symmetry codes: (ii) −*x*+1, −*y*+1, −*z*+1; (v) −*x*+1, −*y*, −*z*; (vi) −*x*+1, −*y*+1, −*z*; (vii) *x*, *y*−1, *z*.

[Cu(tca)$_2$(bipy)] · H_2O (8tca)

D—H···*A*	*D*—H	H···*A*	*D*···*A*	*D*—H···*A*
N5B—H1B···O1CA^{ii}	0.81(3)	2.46(3)	3.041(5)	130.2(3)
N5B—H1B···N4C^{ii}	0.81(3)	2.51(3)	3.118(3)	133.2(3)
N5B—H2B···O1WA	0.88(3)	2.06(3)	2.938(6)	172.7(3)
N5B—H2B···O1W	0.88(3)	2.08(3)	2.885(4)	152.9(3)
N5C—H1C···N1C^{iii}	0.91(3)	2.18(3)	3.051(3)	158.5(2)
N5C—H2C···O1CA^{iv}	0.80(4)	2.17(4)	2.910(5)	155.1(4)
N5C—H2C···O1C^{iv}	0.80(4)	2.17 (4)	2.906(4)	153.4(4)

Symmetry codes: (ii) *x*−1, *y*, *z*; (iii) −*x*+1, −*y*, −*z*+2; (iv) −*x*+2, −*y*, −*z*+2.

Cu(tca)$_2$ · H2O (9tca)				
D—H···*A*	*D*—H	H···*A*	*D*···*A*	*D*—H···*A*
N9—H9A···O3A	0.88(3)	2.1(3)	2.920(14)	154.2(3)
N9—H9A···O3B	0.88(3)	2.16(4)	3.010(18)	162.1(3)
N9—H9B···O2^{v}	0.88(3)	2.22(4)	3.032(8)	153.2(3)
N10^{vi}—H10A^{vi}···N7	0.88(3)	2.07(3)	2.924(9)	163.1(3)
Symmetry codes: (v) *x*, *y*−1/2, −*z*+3/2; (vi) *x*−1/2, −*y*+2, *z*				

Htcp (10tcp)				
D—H···A	D—H	H···A	D···A	D—H···A
N1—H1···N3^{i}	0.887(20)	2.053(18)	2.894(3)	157.7(3)
Symmetry code: (i) *x*-0.5, *y*, -*z*+1.				

[Na(tcp)H$_2$O] · H$_2$O (11tcp)				
D—H···*A*	*D*—H	H···*A*	*D*···*A*	*D*—H···*A*
O1—H1···O2^{viii}	0.84(2)	1.91(2)	2.732(3)	167.1(3)
O1—H2···N2^{ix}	0.83(2)	2.23(2)	3.040(3)	164.4(2)
O2—H3···N1	0.90(2)	1.87(2)	2.762(3)	168.1(4)
O2—H4···O2^{x}	0.87(2)	1.76(2)	2.623(4)	173.2(5)
Symmetry codes: (viii) *x*, −*y*+1, *z*−1/2; (ix) −*x*+1/2, −*y*+3/2, −*z*; (x) −*x*+1/2, *y*+1/2, −*z*+1/2.				

[Cu(tcpc)$_2$(H$_2$O)$_2$] · H$_2$O (16tcpc)				
D—H···*A*	*D*—H	H···*A*	*D*···*A*	*D*—H···*A*
N2—H6···N3^{i}	0.90(2)	2.29(3)	3.04 (4)	140.1(3)
O3^{iv}—H5··· N2	0.89(2)	2.05(2)	2.94(5)	168.2(4)
O2^{ii} —H4W··· O3^{v}	0.83(2)	1.96(2)	2.79(4)	171.9(4)
N5—H5···O3^{iv}	0.88(2)	2.06(4)	2.94 (4)	171.2(4)
Symmetry codes: : (i) −x,-y, −z+1; (ii) −x+1,y+1/2, −z+1/2; (iii) −x+1, −y, −z; (iv) x ,y, 1−z.				

[Cu(tcpc)$_2$(dmf)$_2$] (17tcpc)				
D—H···*A*	*D*—H	H···*A*	*D*···*A*	*D*—H···*A*
N5—H5A···N4^{ii}	0.79	2.37(2)	3.010(3)	139.1(5)
N5—H5B···O2^{iii}	0.96	1.89(2)	2.798(3)	155.7(5)
Symmetry codes: (i) −*x*+1, −*y*, −*z*; (ii) −*x*−1, −*y*+1, −*z*; (iii) −*x*−1, −*y*, −*z*.				

fac-[Co(tcg)(dmf)$_2$(H$_2$O)] (21a-tcg)				
D—H···*A*	*D*—H	H···*A*	*D*···*A*	*D*—H···*A*
O3W—H1W···O1^{v}	0.76(2)	0.76(2)	2.908(5)	1745(5)
O3W—H2W···N2^{v}	0.94(2)	1.97(2)	2.910(5)	175.9(7)
Symmetry codes: (v) −*x*, −*y*, −*z*+1; (vi) −*x*+1/2, −*y*, *z*+1/2.				

***fac*-[Co(tcg)(dmf)2(H2O)] (21b-tcg)**				
D—H···*A*	*D*—H	H···*A*	*D*···*A*	*D*—H···*A*
O3W—H3W···N3^{v}	0.84(4)	2.10(3)	2.938(2)	174.6(1)
O3W—H4W···O1^{vi}	0.82(4)	2.12(3)	2.938(2)	172.3(1)
Symmetry codes: (v) *x*−1/2, −*y*+1/2, *z*−1/2; (vi) −*x*+1, −*y*, −*z*.				

[Mn(tcg)(dmf)$_2$(H$_2$O)] (22tcg)				
D—H···*A*	*D*—H	H···*A*	*D*···*A*	*D*—H···*A*
O3W—H1W···N3^{v}	0.838(2)	2.082(2)	2.91(2)	176.1(2)
O3W—H2W···O1^{vi}	0.810 (2)	2.122(2)	2.93(2)	174.4(2)
Symmetry codes: (i) -*x*+3/2, -*y*+1, *z*-1/2; (ii) -*x*+1, -*y*+1, -*z*.				

APPENDIX G: PHYSICAL CONSTANTS, UNITS AND CONVERSION USED IN CALCULATIONS

	SI system	***cgs emu* system**
μ_B Bohr magneton	$9.27401549 \cdot 10^{-24}$ J/K	$9.27401549 \cdot 10^{-21}$ erg/K
k Boltzman constant	$1.3806580 \cdot 10^{-23}$ J/K	$1.3806580 \cdot 10^{-16}$ erg/K
N number of Avogadro	$6.022 \cdot 10^{23}$ mol^{-1}	
g factor for free electron	2.0023	
1K = 6.95039 · 10^{-1} cm^{-1}		

APPENDIX H: NMR SPECTRA AND SYNTHETIC ROUTES

Part 3: Synthetic route for Hctz (E. Oliveri-Mandala, T. Passalaqua, *Gazz. Chim. Ital.* **1912**, *41*,430–35):

$$2CuSO_4 + 4NaCN \longrightarrow 2Na_2SO_4 + 2Cu(CN)_2 \quad (1)$$

$$2Cu(CN)_2 \longrightarrow 2\,CuCN + C_2N_2 \quad (2)$$

$$C_2N_2 + HN_3 \longrightarrow HC_2N_5 \quad (3)$$

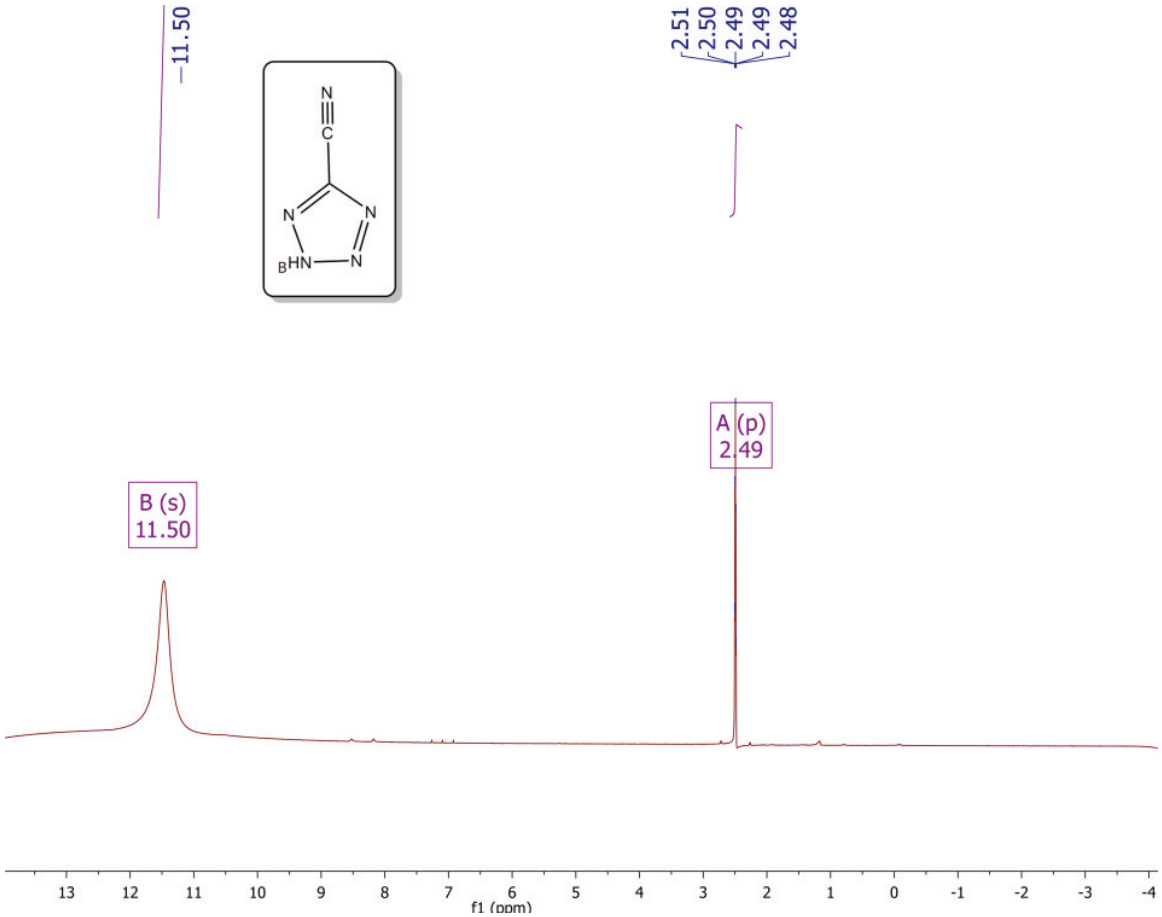

^{1}H NMR Hctz (300 MHz, DMSO-d$_6$)

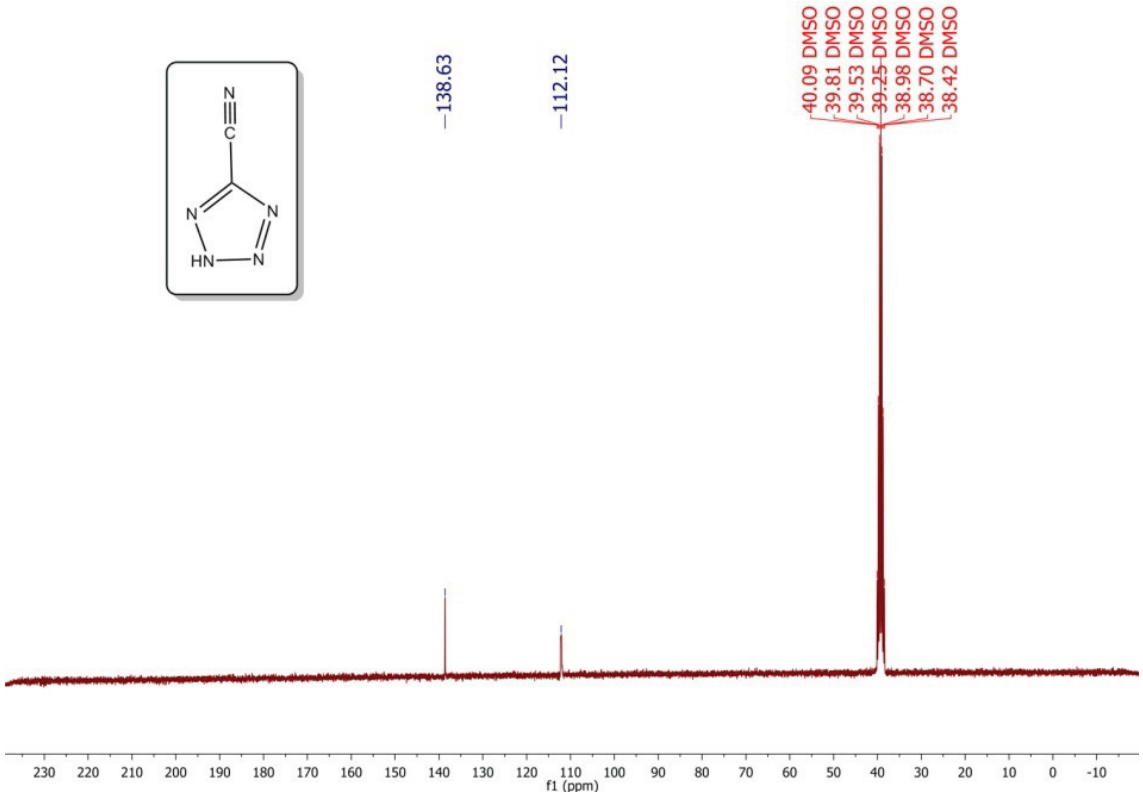

^{13}C NMR Hctz (75 MHz, DMSO-d$_6$)

Part 4: Synthetic route for [Me4N]tcp (H.E. Simmons, R.D Vest, S.A. Vladuchick, O.W. Webster, *J. Org. Chem.* **1980**, *45*, 5113–5121):

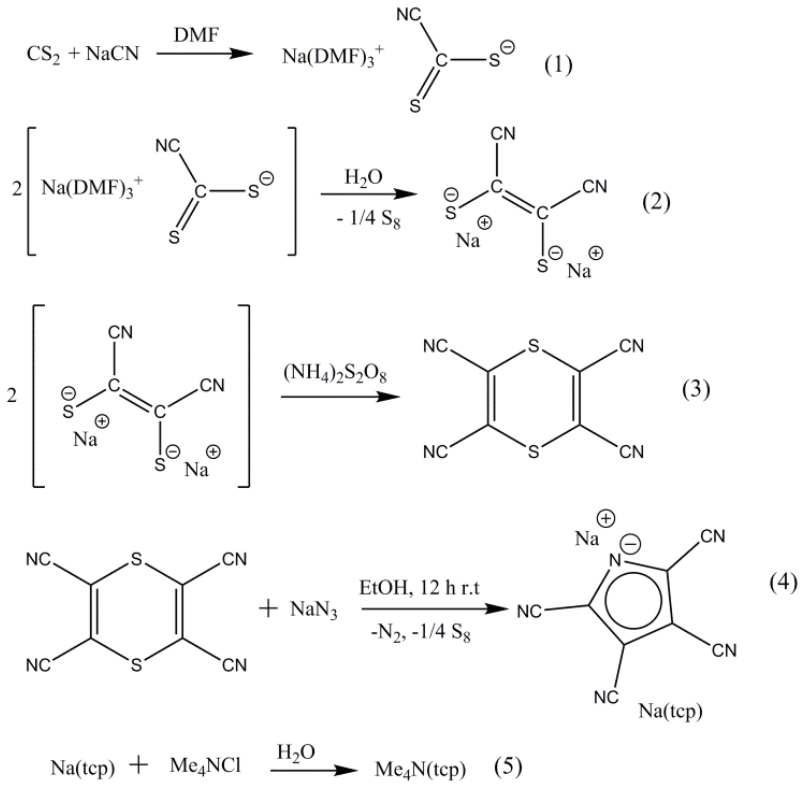

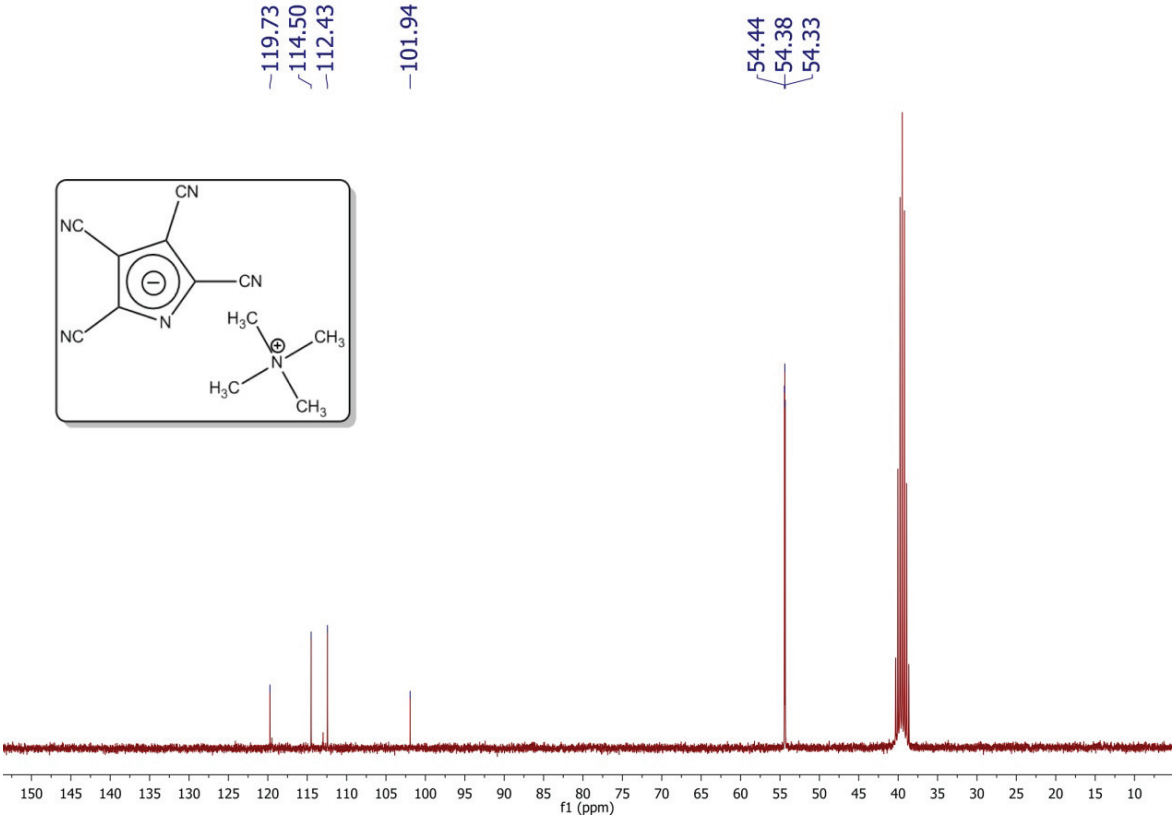

^{13}C NMR **[Me4N]tcp** (75 MHz, DMSO-d6)

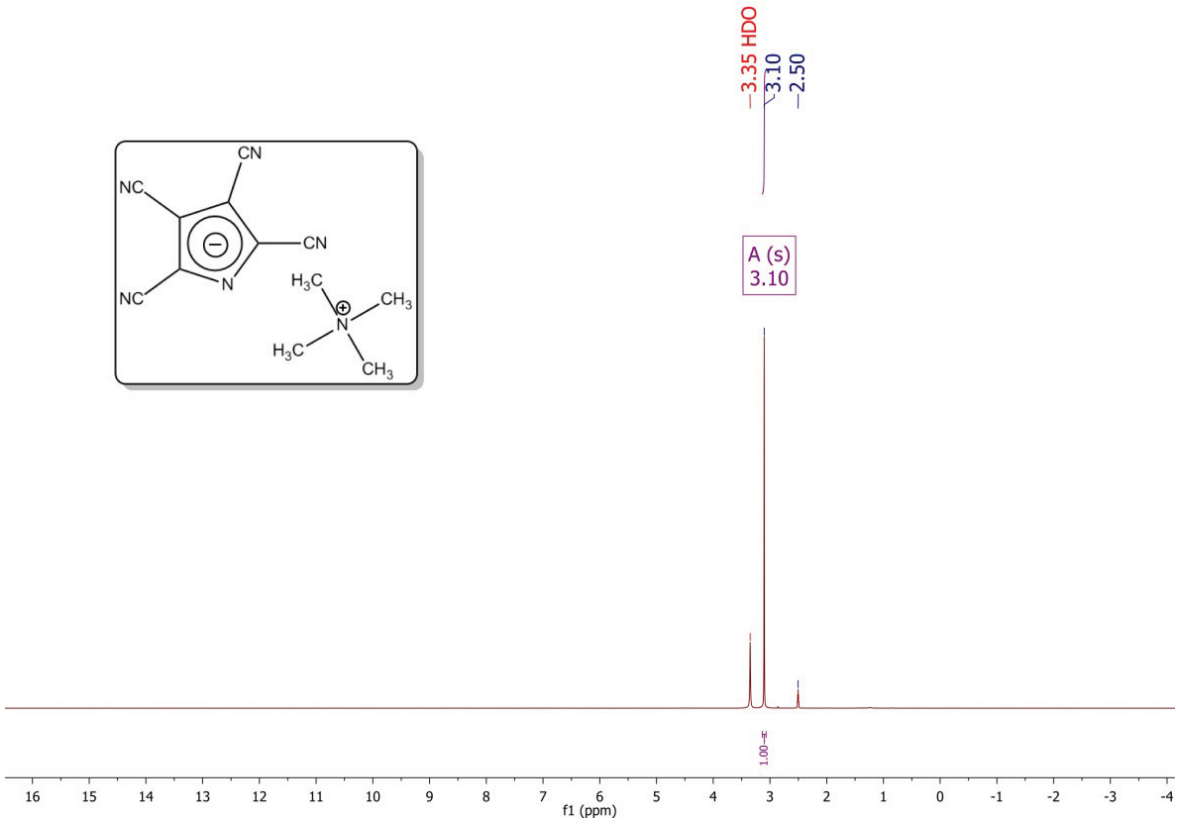

^{1}H NMR **[Me$_4$N]tcp** (300 MHz, DMSO-d$_6$)

Part 6: Synthetic route for [PPh$_4$]*cis*-dct (E. Gryszkiewicz-Trochimowski, *Chem. Zent. bl.* **1923**, *94*, 136):

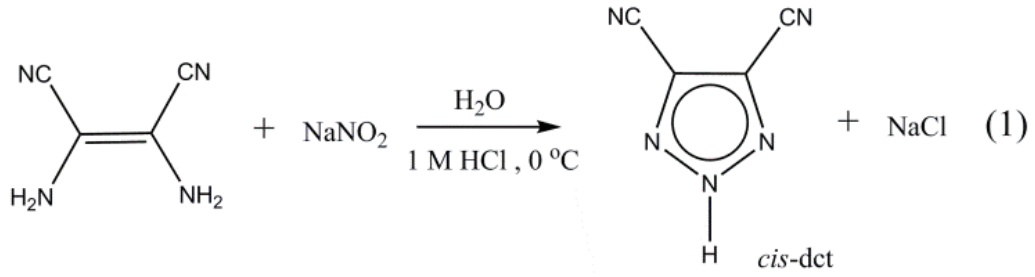

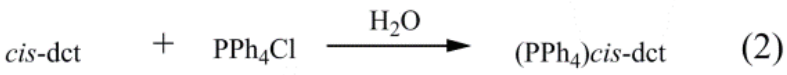

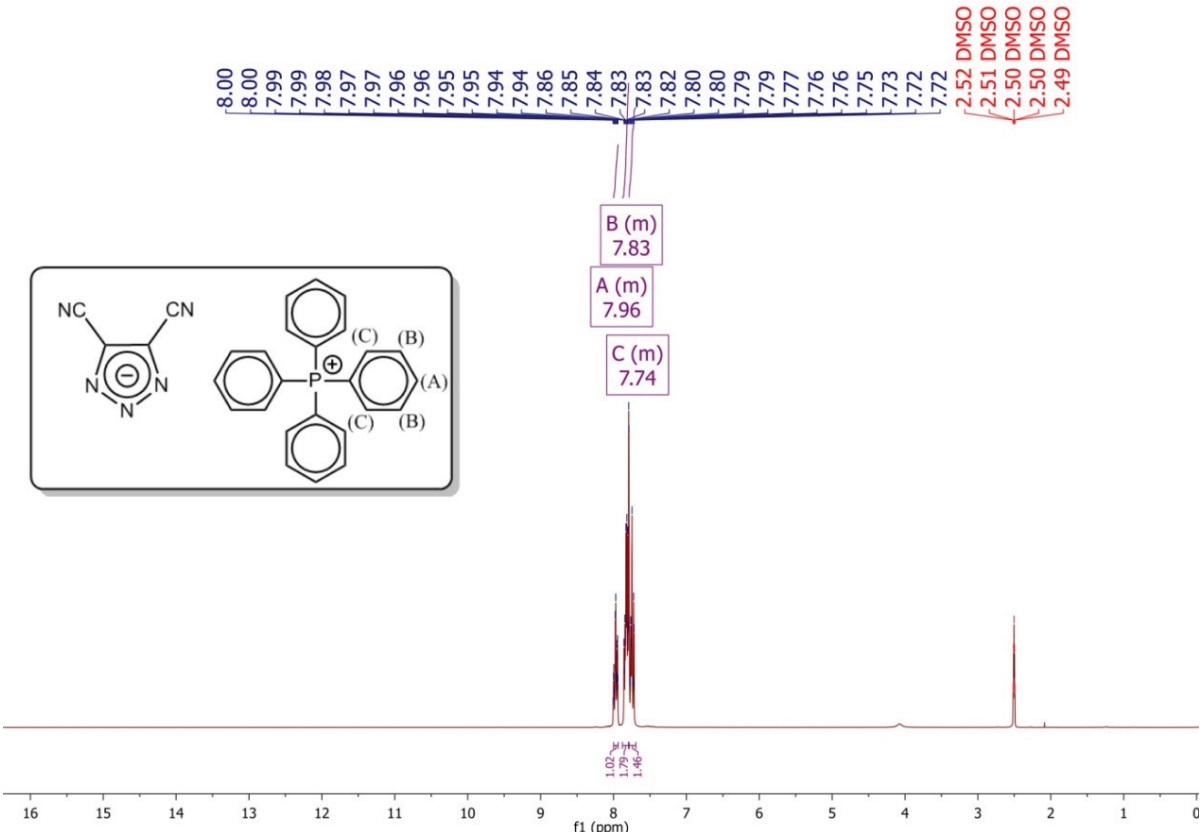

^{1}H NMR **[PPh$_4$]*cis*-dct** (300 MHz, DMSO-d$_6$)

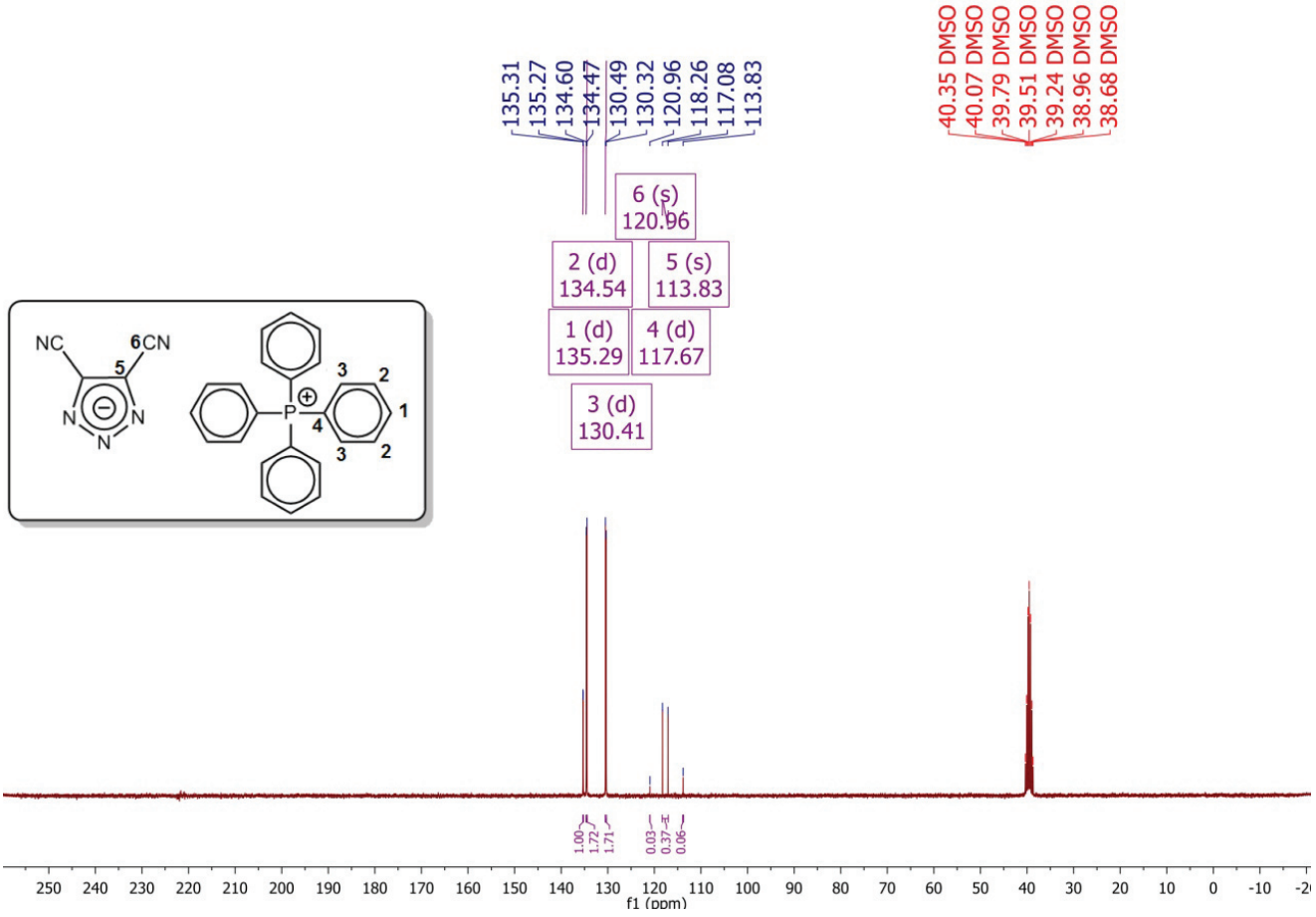

^{13}C NMR **[PPh$_4$]*cis*-dct** (75 MHz, DMSO-d$_6$)

Synthetic route for [Et4N]tci (S.D. Allan, D.F Bergstorm,P.G. Rasmussen, *Synthetic Metals* **1988**, *25*, 139-155):

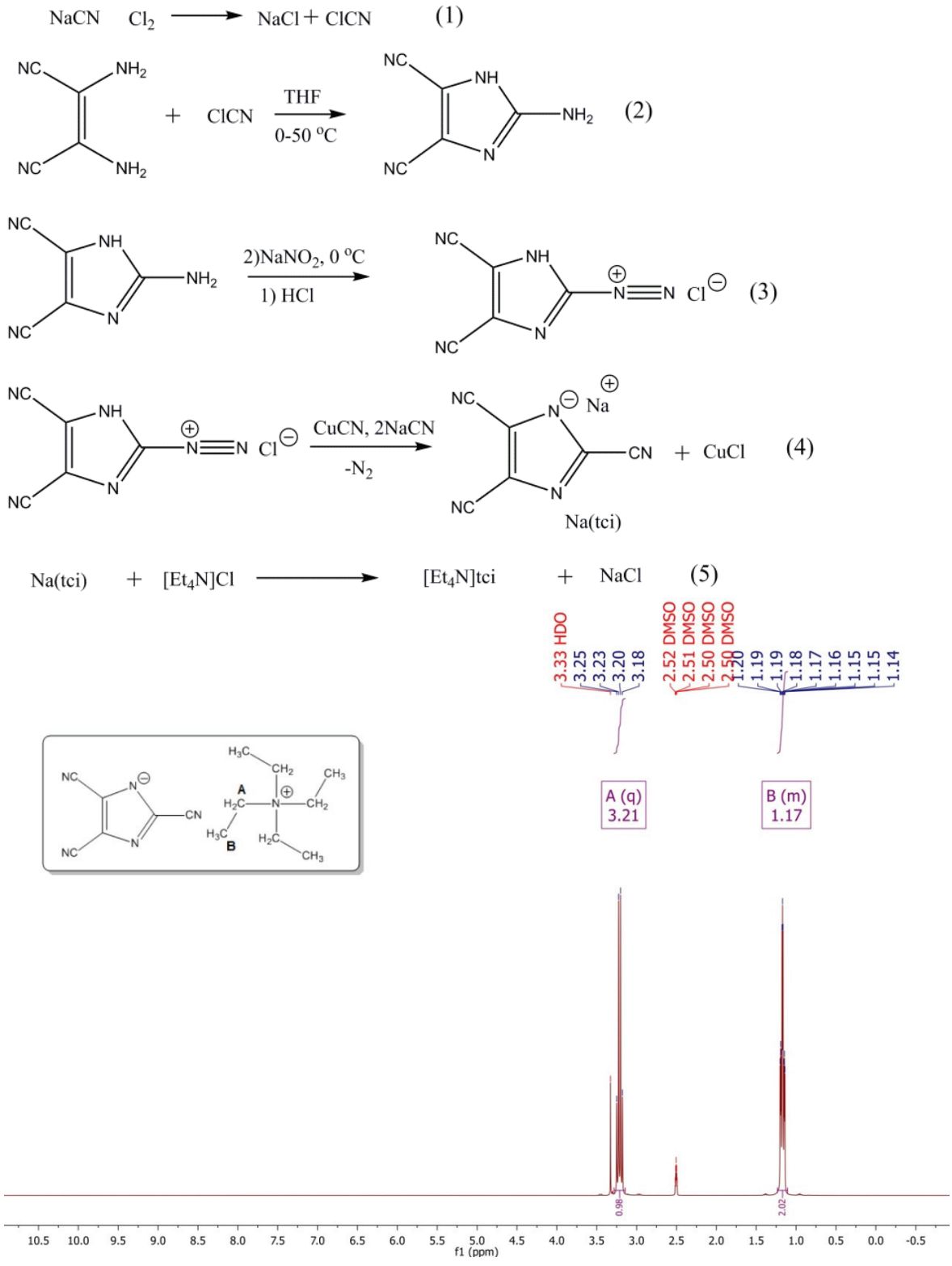

^{1}H NMR **[Et4N]tci** (300 MHz, DMSO-d6)

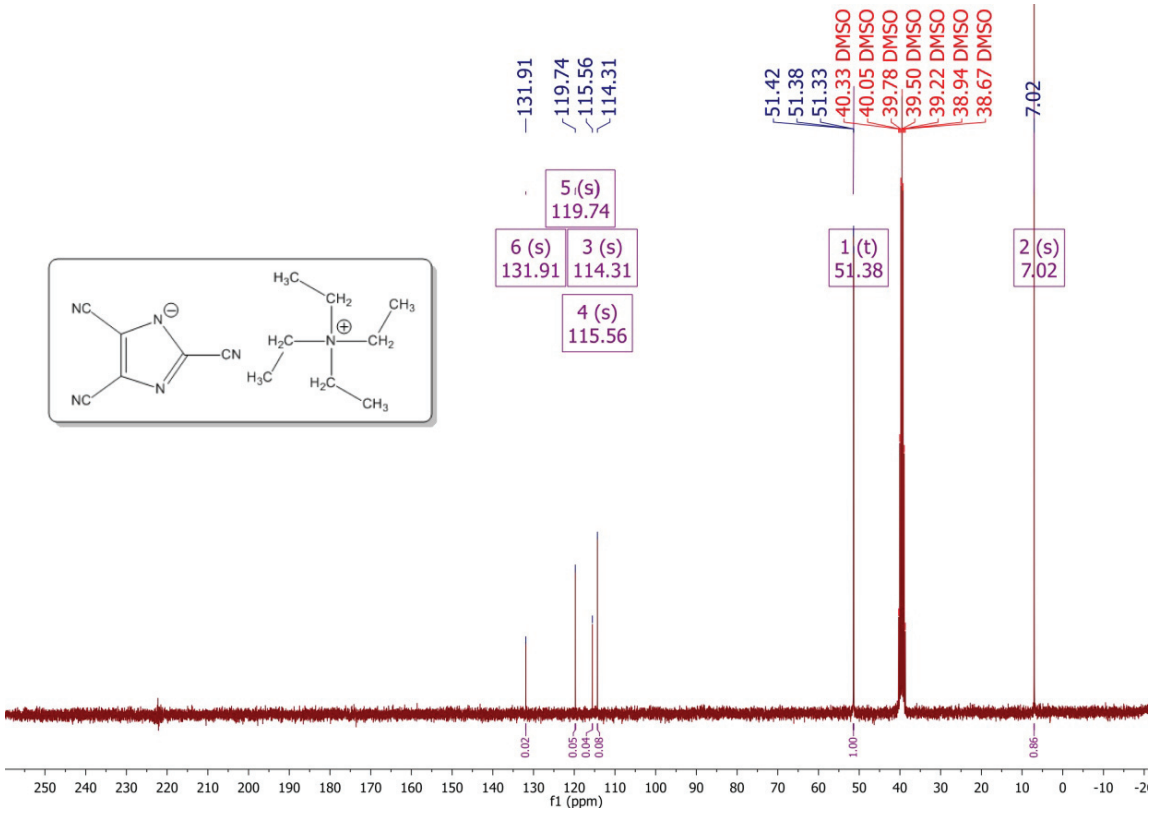

^{13}C NMR **[Et$_4$N]tci** (75 MHz, DMSO-d$_6$)

Part 7: Synthetic route for Na$_2$(tcg) · H$_2$O (J. J. D'Amico , R.Henry Campbell, *J. Org. Chem.*, **1967**, 32 (8), pp 2567–2570, R. J. Timmons , L. S. Wittenbrook, *J. Org. Chem.* **1967**, 32 (5), 1566–1572, R. P. Subrayan, A. H. Francis, J. W. Kampf and P. G. Rasmussen, *Chem. Mater.* 1995, 7, 2213-2216).

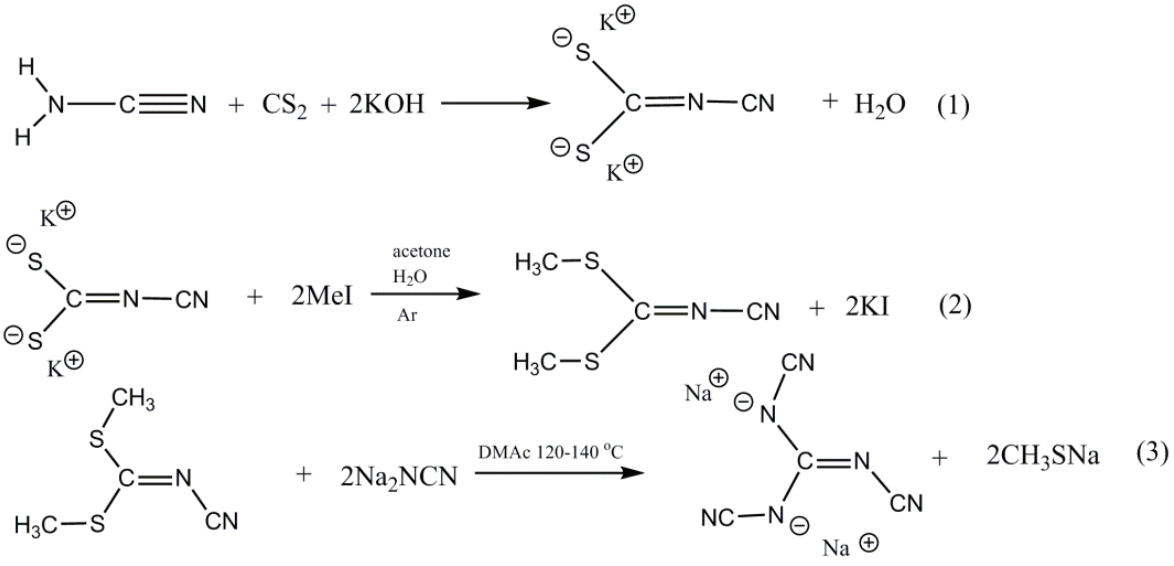

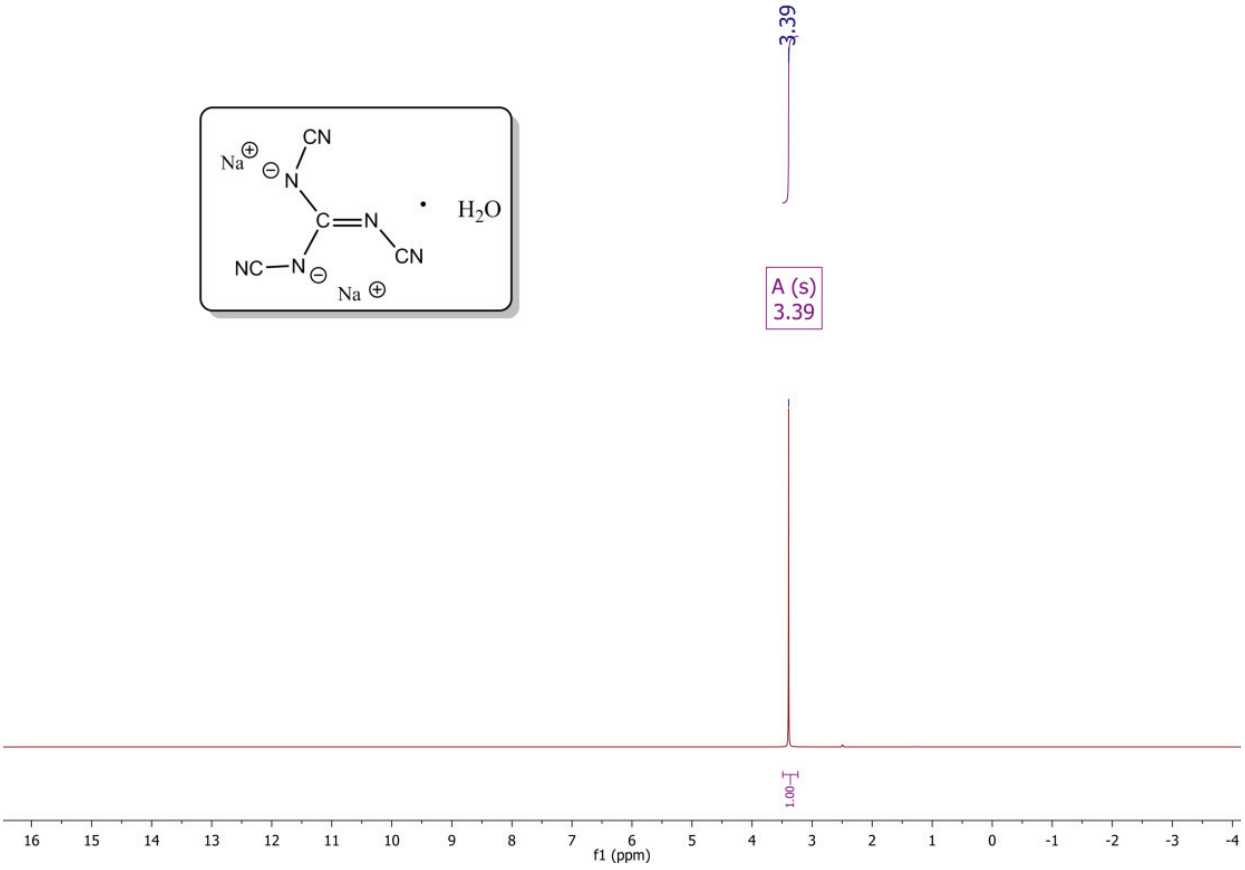

^{1}H NMR **$Na_2(tcg) \cdot H_2O$** (300 MHz, DMSO-d_6)

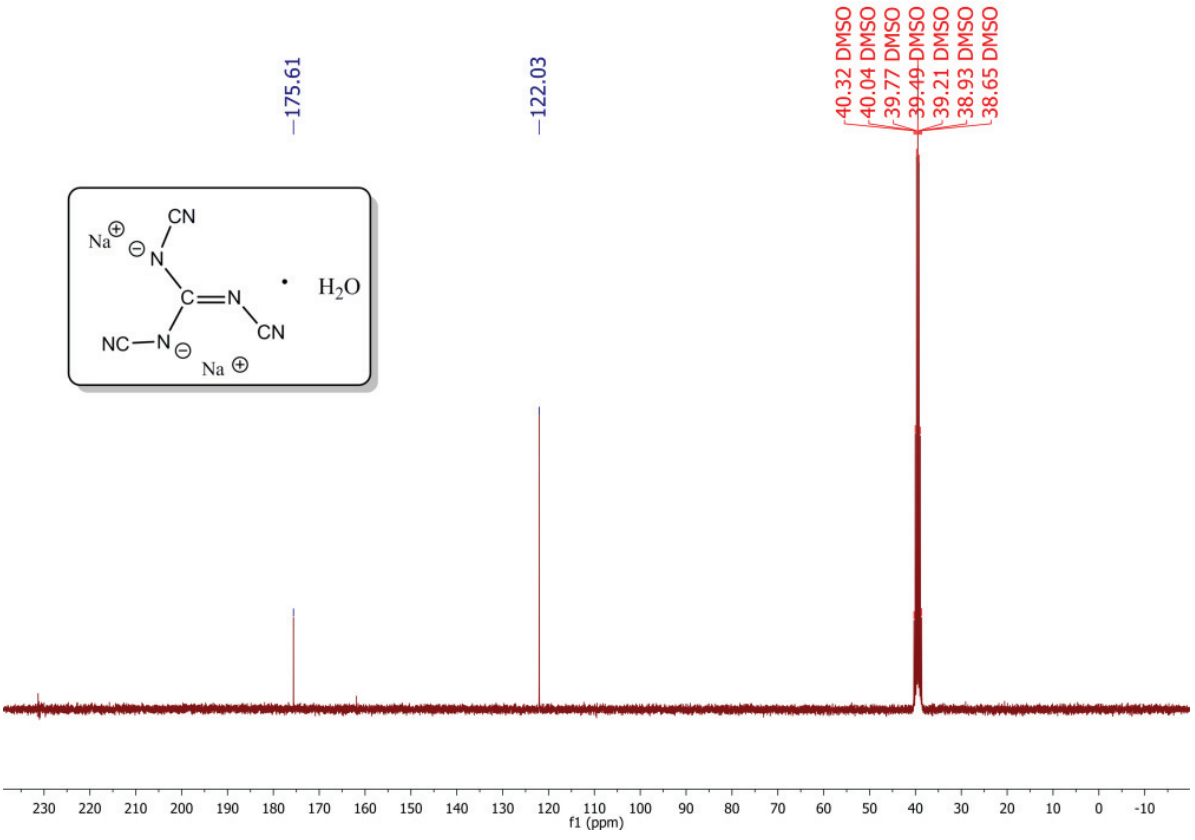

^{13}C NMR (75 MHz, DMSO-d_6)

APPENDIX I

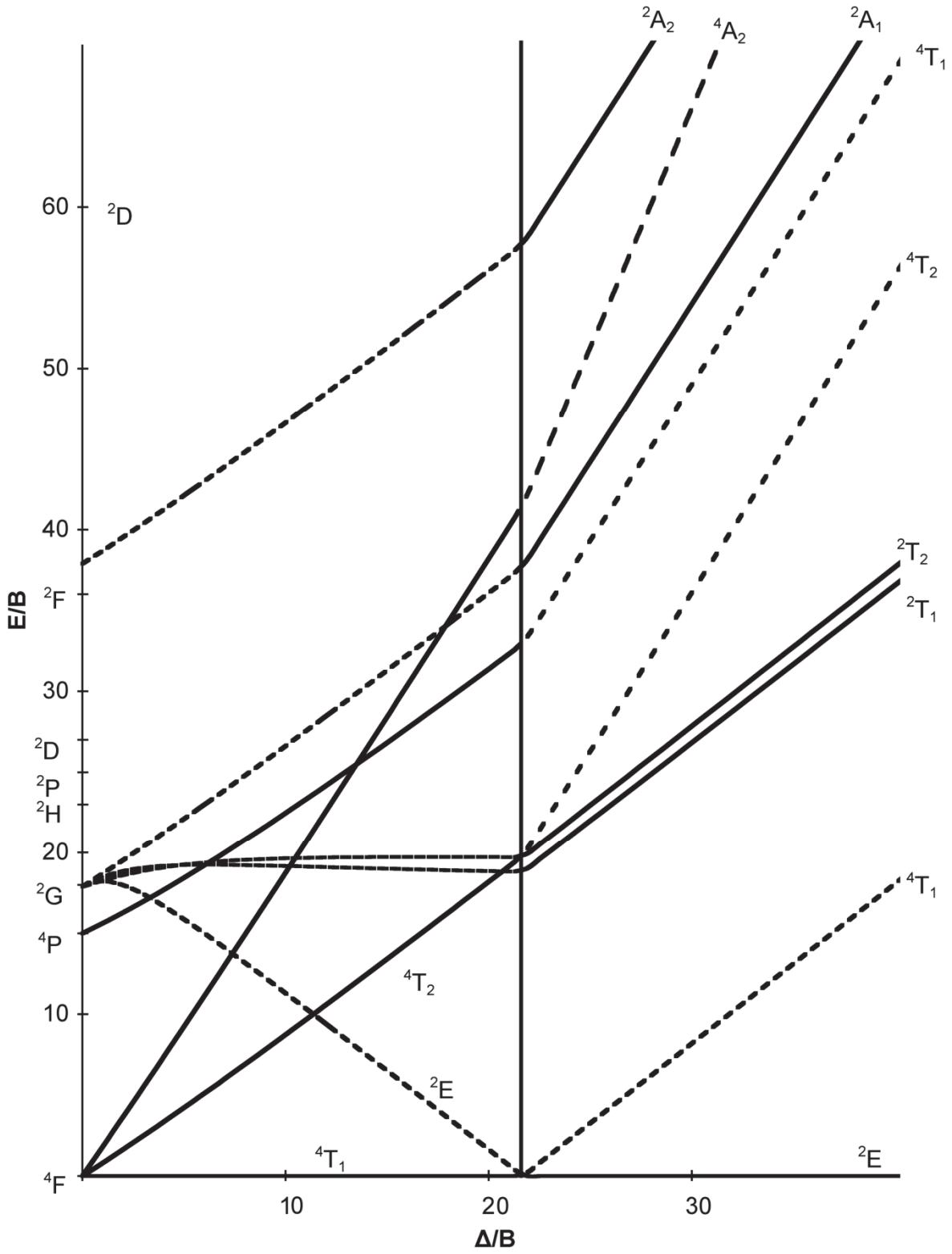

Figure A.I. 1 The Tanabe-Sugano diagram for the d^7 configuration in an octahedral field.

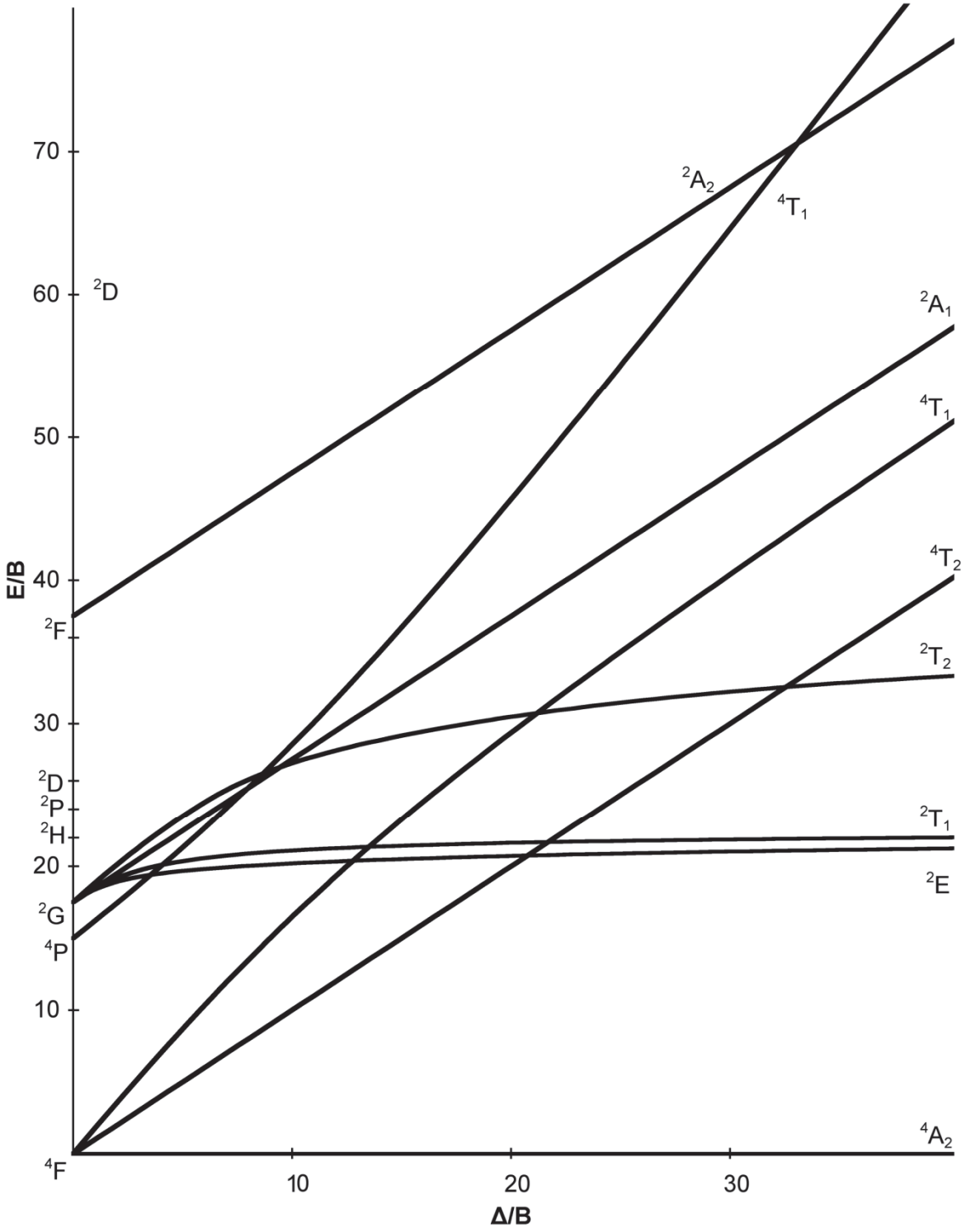

Figure A.I. 2 The Tanabe-Sugano diagram for the d^3 configuration in an octahedral field.

Input file for SETUP used in CAMMAG program

```
** SETUP 4.0 ** (11.11.93)  CAMMAG CAMMAG
CAMMAG CAMMAG  ** SETUP 4.0 **

 TITL Co(tcg)3(dmf)2(H2O) [CoN3O3] /
18.02.2015 /
 CELL 15.153,12.883,15.567,90.,90.,90.

 CONF 2 7


BASE 4F 4P 2P 2D1 2D2 2F 2G 2H

 CO      0.116550 0.114370 0.423130
 N5      -0.01500     0.13740     0.39580
 N4       0.14870     0.11660     0.29450
 N6       0.15040     0.27490     0.44060
 O3W      0.09640    -0.04760     0.42210
 O1       0.25030     0.07950     0.45440
 O3       0.08520     0.10850     0.55903
 C10      0.3142      0.1112      0.4116
 C7       0.1478      0.1116      0.6124
 C4       0.2074      0.3089      0.4825

 MULT 1


 XREF 1 4 2




 LGND 1 2 1 4
 LGND 2 3 1 4
 LGND 3 4 1 10
 LGND 4 5 1 2
 LGND 5 6 1 8
 LGND 6 7 1 9

 END
```

Comments

CELL defines the crystallographic unit cell.

CONF defines the configuration (here $3d^7$ for cobalt ion).
BASE- Specifies spin-triplet free electron state.

Fractional coordinates for atoms.

MULT 1 - Specifies that no two ligands are centro-symmetrically related.

XREF defines a global reference frame. Here z lies parallel to the vector from the 4st and 2th atoms.

The first integer following the keyword LGND specifies the ligand type: this number is referred to when choosing parameter values in the subsequent RUN part of the program. The last three integers define the local ligand axes in the same way as the XREF axes are defined.

Input file for RUN program

```
** RUN 4.0 (18.01.95) ** CAMMAG CAMMAG
CAMMAG CAMMAG  ** RUN 4.0 **
 SETUP: Co(tcg)3(dmf)2(H2O) [CoN3O3] /
18.02.2015 /
 INPUT DATA for RUN :
 TITL Co(tcg)3(dmf)2(H2O) [CoN3O3] /
18.02.2015 /

 CALC 2


 LATT 2
```

CALC - Determines that Eigenvalues, Eigenvectors and susceptibilities will be calculated.

LATT 2 - Indicates that the crystal symmetry is orthorhombic.

```
 B    826.0
 C    3551.8
```

The Racah parameters *B* and *C*.

```
 ZETA 430.1
```

ZETA - The one-electron spin-orbit coupling.

```
LIST 1 1 0 0 0 1 1 0 0 0 0
```

LIST - Determines those calculated quantities to be output on the lineprinter: Here parameter values, Eigenvalues and crystal susceptibilities.

```
K    0.835
```

K - Values for Stevens' orbital reduction factor.

```
 ESIG 1  3500
 EPIX 1  0
 EPIY 1  0
 ESIG 2  0
 EPIX 2  0
 EPIY 2  0
 ESIG 3  0
 EPIX 3  0
 EPIY 3  0
 ESIG 4  0
 EPIX 4  0
 EPIY 4  0
 ESIG 5  0
 EPIX 5  0
 EPIY 5  0
 ESIG 6  0
 EPIX 6  0
 EPIY 6  0
```

e_σ, $e_{\pi x}$ and $e_{\pi y}$ parameters for the ligands 1 to 6. In those calculations only e_σ of ligand 1 (=$e_{\sigma,\max}$) is independly varied. All other interaction parameters e_σ, $e_{\pi x}$ and $e_{\pi y}$ are through $e_\sigma(1)$ linked through command LINK.

```
 LINK 9  8    -0.25  0.0
 LINK 10 8    -0.25  0.0
 LINK 13 8    0.997 0.0
 LINK 14 8    -0.25  0.0
 LINK 15 8    -0.25  0.0
 LINK 18 8    0.811 0.0
 LINK 19 8    0.202 0.0
 LINK 20 8    0.202 0.0
 LINK 23 8    0.889 0.0
 LINK 24 8    0.000 0.0
 LINK 25 8    0.000 0.0
 LINK 28 8    0.841 0.0
 LINK 29 8    0.000 0.0
 LINK 30 8    0.210 0.0
 LINK 33 8    0.771 0.0
 LINK 34 8    0.000 0.0
 LINK 35 8    0.192 0.0
```

The parameter 9, ($e_{\pi x}(1)$), results from parameter 8, $e_\sigma(1)$ by multiplying -0.25 according to the ralation $e_{\pi x} \approx e_{\pi y} \approx {}^1/_4\, e_\sigma$. The values of other ligands are additionally reduced by the condition $e_\sigma \approx d^{-5}$.

```
 TEMP 500 450 400 350 300 250 200 150
100 80 60 50 40 30 20 10 5
```

TEMP - The temperature (in Kelvin) at which the susceptibility calculations will be made.

```
 END
```

Declaration of Originality

I hereby declare that this thesis, entiteld “Coordination Complexes and Networks with Cyano-Substituted Azolates” represents my original work and that I have used no other sources except those indicated by footnotes and citations. All data, tables, figures and textcitations, which have been reproduced from any other source, including the internet, have been explicitly acknowledged as such.

Barbara Szafranowska